Atmospheric Circulation in Antarctica: Analysis of Synoptic Structures via Measurement and Regional Climate Model

Dissertation zur Erlangung des Akademischen Grades Dr. rer. nat.

eingereicht von

Diplom-Physikerin Connie Walther

Geboren am 19.10.1984 in Schmölln

**an der Fakultät Umweltwissenschaften
der Technischen Universität Dresden**

Verteidigt am

20.11.2015

Gutachter

Prof. Christian Bernhofer
TU Dresden, Institut für Hydrologie und Meteorologie

Prof. Martin Horwath
TU Dresden, Institut für Planetare Geodäsie

Prof. Johannes Quaas
Universität Leipzig, Institut für Meteorologie

Erklärung des Promovenden:

Das vorliegende Exemplar entspricht einer leicht überarbeiteten, ergänzten und von dem betreuenden Hochschullehrer genehmigten Version der Originaldissertation:

"Atmospheric Circulation in Antarctica: Analysis of Synoptic Structures via Measurement and Regional Climate Model"

Abstract

Concerning climate change Antarctica is a very sensitive region. Those changes are relevant for synoptic systems, the humidity coupled with them and precipitation. In this study measurements of relevant climatic variables like mean sea level pressure, temperature and humidity are analysed together with results of the regional climate model HIRHAM. The objectives of this study are a validation of the model from the comparision with measurements with a special emphasis on humidity measurements, an analysis of synoptic structures based on mean sea level pressure, 2m-temperature and total water vapour, where typical pattern in different seasons will be analysed and the comparison of the different precipitation minus evaporation budgets in different phases of the Antarctic Oscillation. HIRHAM is a regional climate model consisting of model dynamics from HIRLAM and model physics from ECHAM. It is run with boundary conditions from ERA40 (1994 to 1999) and ERAinterim (1996 to 2009). Measurements are provided by radiosondes and GPS-retrieval. HIRHAM data has been compared to reanalyses and measurements at station sites. It shows that the steep antarctic orography leads to differences between measurements and model. Nevertheless HIRHAM provides a good performance simulating the relevant variables on decadal time scales in general but also concerning the specialities of the continent like for example katabatic winds. The systemic differences between both measurement methods GPS-retireval and radiosonding have been analysed. While GPS measures humidity in a volume of air, the radiosonde integrates humidity on a path, which leads to different results in total water vapour.

After the validation of the model, its data has been analysed concerning synoptical patterns. It could be shown, that in the HIRHAM grid area the most active region is the Ross- and Amundsen-Sea region. The MSLP standard deviation shows that the main cylone tracks are north of the East Antarctic Coast stations. This is one reason for the humidity being lower in this region. In Antarctica the humidity is low and has a strong humidity gradient around the coast. This is because of the different humidities over land and over and the steep orography in Antarctica. For a finer analysis of pressure patterns, a filter tool developed at the HZ Geesthacht has been used. Over the continent there is a high pressure zone, over the seas around it, especially in latitudes of ca. 60° mostly low pressure structures can be found. These patterns, reaching from Ross Sea to Amundsen Sea and the Peninsula, are synoptically active.

To find AAO-positive and AAO-negative seasons for an analysis of the synoptical behaviour in different AAO-phases, the first EOF of the Antarctic region has been calculated with ERA-interim data of the years 1996 to 2009. In AAO-positive phases the pressure is lower than in AAO-negative phases, especially in the region around West Antarctica. This effect is coupled to a higher humidity in this region on AAO-positive seasons. For a seasonal mean of daily P-E-budgets, the precipitation is stronger in AAO-positive phases. which is also consistent with the higher humidity and stronger lows in these seasons.

Die Antarktis ist bezüglich des Klimawandels eine sehr empfindliche Region. Die Änderungen haben Auswirkungen auf synoptische Systeme, Feuchte und Niederschlag. In dieser Studie werden Messwerte wichtiger Klimavariablen wie Druck, Temperatur und Feuchte zusammen mit den Ergebnissen des Regionalen Klimamodells HIRHAM analysiert. Die Ziele dieser Studie sind eine Validierung des Modells durch einen Vergleich mit Messwerten, wobei sich speziell auf Feuchtemessungen konzentriert wird, die Analyse synoptischer Strukturen basierend auf Bodendruck, 2m-Temperatur und Feuchte, wobei typische Muster in verschiedenen Jahreszeiten analysiert werden und der Vergleich der unterschiedlichen Niederschlag minus Verdunstung Budgets in verschiedenen Phasen der Antarktischen Oszillation.

HIRHAM ist ein regionales Klimamodell, welches auf der Dynamik von HIRLAM basiert und die Physik von ECHAM nutzt. Es wird in zwei Läufen mit Randbedingen von ERA40 (1994 bis 1999) und ERAinterim (1996 bis 2006) angetrieben. Messwerte wurden vor allem durch Radiosonden und GPS-Messungen gewonnen. Das Modell wurde zunächst mit Daten aus Reanalysen und Stationsmesswerten verglichen. Dabei zeigten sich Unterschiede zwischen Messung und Modell, die die durch die in der Antaktis typische steile Orografie entstehen. Dennoch zeigt HIRHAM eine gute Performance bei relevanten Klimadaten auf dekadischen Skalen allgemein und bezüglich der Besonderheiten des Kontinents, wie den katabatischen Winden. Zudem sind die systemischen Unterschiede der beiden Messmethoden GPS und Radiosonden untersucht worden. Da GPS die Feuchte in einem Luftvolumen vermisst, die Radiosonden dagegen auf einem Pfad, entstehen unterschiedliche Ergebnisse bei der integrierten Feuchte.

Nach der Validierung des Modells wurden seine Daten hinsichtlich synoptischer Strukturen analysiert. Es konnte gezeigt werden, dass im Modellgebiet die aktivsten Zonen in Ross- und Amundsensee liegen. Die Standardabweichung des Bodendrucks zeigt, dass sich die Zyklonentracks hauptsächlich nördlich der Küstenstationen der Ostantarktis befinden. Dies ist ein Grund für die niedrigere Feuchte in dieser Region. In der Antarktis ist die Feuchte sehr gering und hat einen starken Gradienten im Küstenbereich. Das liegt einerseits an unterschiedlichen Feuchte über Land und See, andererseits an der steilen Orografie des Kontinents. Um die Drucksysteme genauer zu analysieren wurde ein Filtertool, welches am HZ Geesthacht entwickelt worden ist, verwendet. Über dem Kontinent befindet sich ein Hochdruckgebiet, während über dem Meer, speziell auf 60° Breite meist Tiefdruckgebiete sind. Diese Strukturen, welche von Ross- über Amundsensee bis zur Halbinsel reichen, sind synoptisch aktiv.

Um das synoptische Verhalten in AAO-positiven und AAO-negativen Jahreszeiten zu analysieren, wurde die erste EOF der Antarktis mit ERA-interim-Daten der Jahre 1999 bis 2009 berechnet. In AAO-positiven Phasen ist der Druck geringer als in AAO-negativen Phasen, speziell in der Westantarktis. Dieser Effekt ist an das Auftreten einer höheren Feuchte während AAO-positiver Phasen in dieser Region gekoppelt. Im Jahreszeitenmittel täglicher Niederschlagsbudgets zeigt sich, dass der Niederschlag in AAO-positiven Phasen höher ist, was konsistent ist mit der entsprechend höheren Feuchte und intensiveren Tiefdruckgebieten.

Contents

Chapter 1

Introduction

The Antarctic Continent is influenced by recent climate changes. Although precipitation over the continent is increasing, especially the West-Antarctic glaciers are melting and such adding to an increased sea level (c.f. Horwath and Dietrich (2009) and Rignot et al. (2008)). Additionally Antarctica is connected to global climate via teleconnections, for example the coupling between El Niño and Southern Oscillation (ENSO) and the Antarctic Oscillation (AAO) as shown by Fogt and Bromwich (2006). On the Antarctic continent, there are only a few stations that provide all-year measurements, some of them are Automatic Weather Stations (AMS). So measurements from this climatically important region are rare.

Global Climate Models (here referred to as GCM) can help to close this gap. These models calculate atmospheric variables with physical equations from values provided by measurements, such as station data, sounding data or data from satellite retrieval amongst others. Regional climate models (RCM) have a finer resolution and a specialised parametrisation. Nowadays the most useful tool are RCMs that are driven by global climate models. In this case, RCMs have a boundary region which is fed with values from the GCMs. This provides climate data with a fine resolution and comparably low computing time. At the Utrecht University the RCM RACMO2.1/ANT is used to simulate snow drift in Antarctica Lenaerts and van den Broeke (2012), Monaghan et al. (2006) analysed recent trends in Antarctic snow accumulation with their model Polar MM5 and found that the trends are small.

In this thesis the Synoptic Structures around the continent will be analysed on decadal time scales. For this purpose RCM runs with different setups have been conducted. The first covers the time period from 1994 to 1999 and is driven by ERA40 boundary conditions (ERA40 run). The second run covers the years 1996 to 2009 and uses ERA-interim boundary data (ERAint run).

The first part of this study concentrates on the comparison of RCM data from the HIRHAM model with reanalyses (ERA and NCEP) and measurements, especially Radiosounding and Global Positioning System (GPS) retrieval. The most important variables in this study are: total water vapor (TWV), which is vertically integrated specific humidity, mean sea level pressure (MSLP), temperature, as well as wind speed and direction. A validation of the RCM, concerning temperature, humidity and wind, ensures a good model performance

and comparability with measurements. Other studies have compared global models with measurement. For example Genthon et al. (2010) compared atmospheric boundary layer measurements via tower with the global model ECMWF. They found that ECMWF has a warm bias of 3 to 4 K and that the model overestimated relative humidity because its absolute humidity was too small. A good parametrisation of the stable boundary layer has an influence on model performance on synoptical scale.

In a first step, the model setup was optimised with several sensitivity studies, concerning vertical resolution and sea ice thickness. King et al. (2001) showed in a sensitivity study for the climate model HadAM2 the sensitivity of the modelled climate to changes in parametrisations of surface and boundary layer fluxes, Holland et al. (2006) analysed the influence of subgrid-scale sea ice thickness distribution parametrisation for the model CCSM3 and found larger ice growth rates and thicker sea ice as a result of the parametrisation. For HIRHAM the variation of the sea ice thickness should show how much influence the changed surface has on the results of the modelled climate. Then the RCM was validated against measurements from radiosondes and weather stations around the coast of the Antarctic continent. From this study information on synoptical behaviour in the grid region around the stations could be retrieved. Grid regions means the four surrounding grid points of each station, an area of 50×50 m^2. Also different humidity measurement methods, sounding and GPS retrieval, have been compared.

The main question of this thesis is the analysis of Synoptic Structures and their coupling to teleconnection patterns. To do so, a filter especially developed for RCMs, developed at HZ Geesthaacht (c.f. Feser and von Storch (2005)), has been used to highlight synoptical patterns. With this tool, structures of different wave-lenghts can be analysed seperately. This study concentrates on wavelengths between 500 to 1000 km. Synoptical patterns are analysed for both runs seperately for each season over the whole integration period (1994 to 1999 and 1996 to 2009 respectively) and for every single year.

The synoptical patterns change significantly during different AAO-Phases. Glushak (2007) analysed AAO-phases with a duration of sevaral years, here the AAO-Phases are also analysed seperately for single seasons, namely summer and winter, in the time period from 1996 to 2009 (ERAint run). This thesis concentrates on MSLP as the main variable to show synoptical patterns, but also precipitation minus evaporation (P-E) is analysed to show the influences of different AAO-Phases on mass changes of the Antarctic glaciers.

Chapter 2 (atmospheric circulation, the climate of Antarctica and the influence of Antarctica on global climate) describes the objectives and the state of the art. Chapters 3 (the RCM HIRHAM), 4 (reanalyses of ERA and NCEP), 5 (measurement methods) and 6 (analysis methods) describe data and methods. The results are shown in chapters 7 (ERA40 run and its comparison with the measurements and comparison between the ERA40run and die ERAint run), 8 (filtered data concerning Synoptic Structures) and 9 (analyses according to the AAO-phases). The summary and conclusions can be found in chapter 10.

Chapter 2

Atmospheric Circulation and Synoptic Structures

2.1 Atmospheric Circulation

Atmospheric Circulation decribes the interaction of the main pressure regimes in the Earth's atmosphere and their connection with temperature, wind and humidity. An important field of study concerning atmospheric circulation are teleconnections. Teleconnection means the linkage of weather phenomena over great distances, mostly recognised via statistical analysis.
On the southern hemisphere, the most important are El Niño and Southern Oscillation (SO), viewed combined as ENSO. The SO is a coupling or a see-saw between pressure pattern in the western and southeastern Pacific, which are called Walker Circulation. In the standandised approach the Southern Oscillation Index (SOI) is usually calculated from differences of sea level pressure anomalies between Tahiti and Darwin in Australia (Troup (1965)). El Niño describes the event of warm water invasion into the eastern Pacific, which leads to heavy rain in the Andes and a decrease in fish population near the western South American coast. Both teleconnections show strong linkage to sea surface temperature (SST) in the Pacific Ocean. ENSO conditions are not only distinguished by a positive or a negative phase, but are more commonly called El-Nino (negative SO-Index) or La-Nina (positive SO-Index), depending on the circulation regimes. A normal ENSO pattern, that means neither an El-Nino or a La-Nina condition, would be a warm pool in the western Pacific and cool surface water in the eastern Pacific, enhanced by trade wind patterns. At the coast of Peru and Equador flow southern or southeastern winds that produce via Coriolis force an ocean current that leads away from the coast and thus produces upwelling cold water (Kraus (2004)). In developing an El Niño event SST anomalies first occur in Eastern Pacific, at the South American coast and spread westward afterwards. During such events, the upwelling of cold Pacific water on the coast decreases, circulation patterns change and precipitation in this region is also enhanced. The processes behind the ENSO teleconnection are still not understood in detail and are subject to research.

Another important teleconnection on the southern hemisphere is the Antarctic Oscillation (AAO). The AAO is a leading Empirical Orthogonal Function (EOF) in the southern hemispheres, analysed on different geopotential heights (Thompson and Wallace (2000)), for instance 700 hPa or 850 hPa. The CPC (CPC (2011)) uses 700 hPa height anomalies poleward of 20° on a daily basis. A positive phase means an EOF that is higher than the standard deviation of the time series CPC (2011). This means that usual pressure patterns are strengthened in positive years and weakened in negative years. In Antarcticas case the lows around the continent should be stronger in positive years and weaker in negative years.
According to Fogt and Bromwich (2006) ENSO and AAO are positively coupled in times of strong teleconnections, especially in spring and summer. So in strong El Niño phases, the AAO index would be positive, leading to stronger lows around the Antarctic Continent.

2.2   Climate of Antarctica

Antarctica as the southern continent has a special climate. As the Arctic, it is a region with low net radiation, even in the sunny season, due to the high radiative losses which are caused by the high albedo. But in contrast to the northern pole region, the land mass here is concentrated around the pole, leading to a circulation of air mass and ocean around the continent. This circulation isolates Antarctica, leaving it to develop a very cold and dry climate.

Sea ice and Polynyas

Most sea ice is first year ice and thus relatively thin. This has an effect on its albedo and insulation. Thin ice provides a lower insulation than thicker ice, so there is an easier heat exchange between ocean and atmosphere. Addionally younger sea ice has a lower albedo than snow-covered pack ice (Weiss et al. (2011)). In the marginal ice zone with its broken ice the surface conditions are complicated. Andreas et al. (1984) launched radiosondes along a track through the marginal ice zone. They found that with the increasing roughness of the surface and the higher drag coefficient the wind flow was decelerated and thus the inversion layer was lifted. Additionally they calculated a sensible heat flux of about $200W/m^2$ because of melting ice. Due to katabatic flow (a seaward downslope wind), polynyas can open up. A polynya is a zone of open water in otherwise closed sea ice, which often forms under the influence of katabatic winds. Bromwich and Kurtz (1984) analysed the formation of a polynya in Terra Nova bay and calculated freezing rates of new ice to be about 20cm/day. Massom et al. (1998) examined ice concentration derived from a microwave imager from July 1987 to August 1994. They defined polynyas as zones with an ice concentration of less than 75% and this way found 28 polynyas with their maximum extent from June to October at area sizes of several 1000 km^2. They stated that most polynyas formed under the combined influence of bathymetry, topography and wind, with only very few polynyas forming solely under the influence of katabatic winds.

In 20 locations anchored ice bergs or other barriers lead to a removal of ice in the lee of these barriers, thus forming a polynya. They also found that larger polynyas have a lower ice concentration and are more stable. Polynyas have an influence on Antarctic flora and fauna. The active sea ice production in Polynyas leads to the formation of Antactic Bottom Water, Tamura et al. (2008) calculated the heat flux in these zones with satellite-derived ice-thickness data. They stated that 10% of the antarctic sea ice is produced in Polynyas, although they cover only 1% of the maximum ice area. The Ross Ice Shelf Polynya showed the highest sea ice producion in this analysis. Polynyas lead to an early onset of phytoplankton productivity (Smith Jr and Gordon (1997)) and many penguin rookeries are located near polynyas (Massom et al. (1998)).

Radiation

Although the radiation income in the sunny season is approximately in the same range as in the mid-latitudes, due to the high albedo the radiation income per area and the radiative energy absorption is low in Antarctica. The net radiation losses are smaller in inner Antarctica than around the coast, because of the low temperature over the plateau. Still the radiative cooling is more important than warming through entrainment. The strong cooling leads to a superadiabatic environment and stable atmosphere (King and Turner (1997)). Typical albedo values over snow are 0.97 to 0.98 according to Carroll (1982). The ozone decrease in the stratosphere over Antarctica increases the amount of UV radiation reaching the ground (Budd (1991)). The ozone layer recovers only slowly, especially in Antarctica (Weatherhead and Andersen (2006)).

Temperature

Mean temperature is very low due to radiative losses and high albedo. On the Peninsula, there is a devision between the relative warm and humid western coast and the cool and dry eastern coast, because of the western flow cyclonic structures. The temperature variation is very low in winter and has only a small maximum peak in summer. Phillpot and Zillman (1970) found a strong inversion on the plateau of around 25 K, due to the radiative behavior (see above). van den Broeke et al. (2002) found that only 15 to 20 % of the shortwave radiation are absorbed and longwave radiation is emitted nearly as a blackbody. Thus, through extract of sensible heat from overlying air, an inversion of 15 to 30 K can develop. Whereas in January the surface cooling is weak and large scale pressure dominates the atmospheric boundary layer, in July the surface cooling is strong and a shallow katabatic jet over the interior will develop (King and Turner (1997)).

Pressure systems

Turner et al. (1998) found a synoptical active zone at about 64°S, with the greatest number of cyclogenesis in Bellingshausen Sea and in the Lee of the Antarctic Peninsula, whereas the greatest cyclolysis was found in the west of the Antarctic Peninsula. Sim-

monds et al. (2003) found the greatest cyclone system density in the Indian Ocean and south of Australia at a latitude of about 60°S . The highest cyclonicity according to them is in the coastal region of Antarctica, as well as the northern part of the Peninsula and the Drake Passage, whereas Cyclolysis is confined to the near-coastal region. Carrasco et al. (2003) analysed mesoscale cyclones around Antarctica. They showed that most deep vortices occur over Bellingshausen Sea and assumed that the genesis of mesocyclones in Antarctica is strongly coupled to catabatic winds, assuming that they also need boundary layer fronts and baroclonic processes for their development. Bromwich (1991) found a very active mesoscale cyclogenesis for two discharge locations of boundary layer air, namely Terra Nova Bay / Franklin Island and Byrd Glacier. These events were also linked to baroclinicity and cyclonic vorticity in the boundary layer and they have been influenced by synoptic forcing. The Antarctic Peninsula is a barrier over which only few systems can cross, although many cyclones form in its lee (Turner et al. (1998)) Over the continent, there is a weak surface anticyclone. Above 500 hPa, which is the first geopotential level that is entirely above the continental surface, there is a weak cyclonic vortex. The extreme elevation of the Antarctic continent leads to problems with the reduction of station level pressure to mean sea level pressure. Further details are given in King and Turner (1997).

Katabatic winds

On the Antarctic Plateau, where long wave net radiation losses cool the air, a high pressure system is developing (Hoinkes (1960)). Temperature inversion and katabatic wind are coupled, the force of the catabatic winds depends on the strenght of the inversion and the magnitude of the surface slope (van den Broeke et al. (2002)). A good description of katabatic winds can be found in King and Turner (1997): 'Strong cooling over the surface of the dome-shaped ice sheets generates a persistent katabatic circulation, with cold surface air flowing out from the interior towards the coast.' As they flow from the plateau they turn left due to Coriolis force and have a high directional constancy. Over the continent they are only persistent surface winds, but katabatic winds lie downstream of cold air convergence zones. Katabatic winds lead to a warming and drying of the air while it flows downhill. Thus the frequency and strength of katabatic wind influences average temperatures and humidities. Bromwich (1989a) stated, that usually katabatic winds are of the bora-type. Even if they seem to be foehn-like, their signatures do not vanish while propagating several km over the Ross Sea (Bromwich (1989b)). They assumed that due to the turbulent flow of the katabatic jet, warmer air is mixed to the surface. Also katabatic winds are strongly turbulent, since their wind speed exeeds the propagation speed of a katabatic front (Nylen et al. (2004)). When reaching the ice shelf and the sea ice, the air is thickening and piling up, which acts as opposing force to the katabatic jet and leads to a rising motion in the coastal zone as explained in van den Broeke et al. (2002). Still the flow can persist over substantial distances in certain region, for example at Terra Nova Bay, as found by Bromwich (1989a). Not every wind of a certain strenght and direction is indeed a katabatic wind. Renfrew and Anderson (2002) stated that in Coats Land, around Halley Station, in 40% to 50% of the time the wind was indeed katabatic, whereas

it seemed katabatic in 60% to 70% of the time (leading to ca. 20% of not katabatic, but only seemingly katabatic winds). They suggested that katabatic seeming winds can be associated with synoptic-scale low-pressure systems. The strongest katabatic winds occur on Adelie Land. Wendler et al. (1997) stated, that the annual mean wind speed at Cape Denison (near Dumont- D'Urville) is 19.1 m/s.

Surface mass balance, clouds and precipitation

In spite of difficulties in measuring Antarctic mass balance, Wingham et al. (2006) showed that 72% of the Antarctic ice sheet is gaining 27 ± 29 Gt per year. For the Ross Ice Stream Joughin and Tulaczyk (2006) found a growth rate of 26.8 Gt per year through measurements of the ice flow velocity. Rignot et al. (2008) calculated the mass balance via flux measurement from satellite inferometric radar and snow accumulation from a regional climate model and found mostly ice losses (-4 ± 61 Gt per year for West Antarctica, -132 ± 50 Gt per year for West Antarctica and -60 ± 46 Gt per year for the Peninsula), which shows the high uncertainties in the estimation of ice mass balance in Antarctica. According to Krinner et al. (2007), who modelled surface mass balance, the Antarctic surface mass balance is increasing by 32 mm per year in the next 100 years, which is equivalent to a sea level decrease of 1.2 mm per year. They assumed that increasing air temperature is leading to an increased moisture transport to the interior of Antarctica. Bintanja (2001) stated that snowdrift sublimation is an important factor to mass balance. Dery et al. (1998) showed in their study of blowing snow in Canada with their model PIEKTUK that sublimation of blowing snow can lead to temperature decreases of 0.5K and water vapour increases near the surface and is thus a sink of sensible heat and a source of moisture. The sublimation is a self-limiting process and strongest about 1km downstream. Most clouds in Antarctica are in regions with many active weather systems, with mostly synoptical precipitation. Through an onshore airstream and the according orographic lifting and adiabatic cooling, coastal region have a high amount of orographically induced precipitation. In inner Antarctica, clouds are rare and clear sky precipitation such as diamond dust plays an important role. In the whole Antarctic region most precipitation is solid (King and Turner (1997)).

2.3 Influence of Antarctica on Global Climate

Antarctica is a very important continent for global climate, as stated by Budd (1991). Its iceshield is a huge freshwater reservoir and has an influence on sea level increase or decrease. Goldner et al. (2013) analysed via simulations the influence of the antarctic ice shield on the temperature. In their simulations they added the modern antarctic ice shield to the eocene world and ran a modern world simulation without the ice shield. They found temperature anomalies ranging from -1.22K to -0.18K depending on background CO_2-levels for the modern world and -0.25K for the eocene world. Both values are influenced by cloud feedback. With rising temperature, Antarcticas glaciers are melting faster, as it happend in West Antarctica with the Larsen ice shelf. Observations show a decreasing

ice mass in West Antarctica (c.f. Horwath and Dietrich (2009)). In Antarctica increasing precipitation, which is especially the case on the Peninsula, as shown in Rignot et al. (2008), could lead to an increasing ice mass. Nevertheless, ice flow velocity has a huge influence on mass balance. So fast flowing West Antarctic glaciers lead to a mass loss and slow flowing glaciers, that flow into large ice shelfs are balanced or thickening (Rignot et al. (2008)). The albedo of the icesheet and the sea ice, that is surrounding Antarctica, can add to global cooling through radiative losses, but is very sensitive to the conditions of the ice, whether it is old, young, snow covered, melting or else. Brandt et al. (2005) measured albedos varying from 0.07 for young ice to 0.87 for snow covered ice. They also stated that the albedo of a certain region is dependent on ice concentration, ice type and its snow cover. The development of sea ice leads to the rejection of salt water which influences the ocean currents. Meredith and King (2005) stated, that due to the rise of the temperature by 3K in West Antarctica since 1951, also the ocean surface temperature in summer is rising by 1K and the salinity in the upper layers is getting stronger. This leads to a reduction of the sea ice extent and an atmospheric warming in winter. On the other hand side, Turner et al. (2009) showed that the sea ice extent has increased since the late 70s. They found the largest increase in autumn in Ross Sea due to a stronger atmospheric flow. The trend to a stronger atmospheric flow is related to stratospheric ozone depletion which strengthens the autumn wind and deepens the Amundsen Sea Low. The climate of the continent itself partitially cut of from global climate through the circumpolar circulation in the ocean as well as in the atmosphere. Still there are teleconnections to the global climate. Harangozo (2000) stated that El Niño / Southern Oscillation (ENSO) had an influence on the winter temperature in West Antarctica and the Peninsula. This is explained by an ENSO-related seasonal meridional flow that modifies the surface temperature due to changes in the local sea ice extent. Yuan (2004) found the strongest sea-ice-teleconnection between ENSO and the Antarctic Dipole. The Antarctic Dipole is sea ice and surface temperature anomalies in the Southern Pacific and South Atlantic which are persisting 3 to 4 seasons and are triggered bei ENSO. The mechanism behind that is the meridional flow of the Ferrel Cell and stationary eddies in the atmosphere. In a study by Kwok and Comiso (2002b) it is shown that the Southern Oscillation is related to anomalies in polar climate especially in Bellingshausen-, Ross- and Amundsen-Sea. They showed that in positive phases of the southern oscillation the sea level pressure is lower and the surface air temperature and sea surface temperature are cooler and vice versa in negative SO-phases. Peterson and White (1998) conducted a case study where they showed that in the western subtropical South Pacific is a major source for the Antarctic Circumpolar Wave, due to anomalies in sea surface temperature and precipitable water. Those anomalies are actively branching northward and reach the South Atlantic and Indian Oceans 6 to 8 years after occurring in the Pacific Ocean. This shows how the Southern Ocean around Antarctica is linking different Oceans around the world.

Chapter 3

Regional Climate Model HIRHAM

The regional climate model HIRHAM is composed of the HIRLAM (High-Resolution Limited Area Model) regional model dynamics and ECHAM parametrisations. Its outer and lower boundary values can be derived from global reanalyses or global climate scenario runs. Up to now it has mostly been used for the Arctic region Matthes et al. (2010). Polanski et al. (2010) used it for Monsoon research in the Himalaya region and Glushak (2007) was the first to apply it on Antarctica.

HIRHAM4 is a hydrostatic regional atmospheric climate model developed by Christensen et al. (1996). It is dynamically based on HIRLAM described by Machenbauer (1988) and the physical parametrisation from ECHAM4 in Roeckner et al. (1996). It was adapted for climate simulations of Antarctica by Glushak (2007) and used for an analysis of accumulation changes in Antarctica by Dethloff et al. (2010).

3.1   Prognostic and diagnostic equations

For horizontal discretisation, HIRHAM has an Arakawa-C-grid. Wind, temperature, specific humidity and linearised geopotential height are defined at full vertical levels. Pressure, geopotential height and vertical velocity are defined at half levels.

The hybrid coordinate is defined as follows:

$$p_{k+1/2} = A_{k+1/2}(\eta) + B_{k+1/2}(\eta)p_s(\lambda, \theta) \tag{3.1}$$

where k denotes the number of the level, p is the pressure, p_s is the surface pressure at the horizontal position (λ, θ) and A and B are the parameters for the vertical coordinates and can be found in Table C.4.

The continuity equation is:

$$\left(\frac{d_H}{dt} + D\right)\frac{\partial p}{\partial \eta} + \frac{\partial}{\partial \eta}\left(\dot{\eta}\frac{\partial p}{\partial \eta}\right) = 0 \tag{3.2}$$

with

$$D = \nabla_H \cdot \vec{v}_H \tag{3.3}$$

and

$$\frac{d_H}{dt} = \frac{\partial}{\partial t} + \vec{v}_H \cdot \nabla_H \tag{3.4}$$

The temperature equation is:

$$\frac{dT_k}{dt_k} = \left[\frac{\kappa T_v}{1 + (\delta - 1)q} \right]_k \left(\frac{\omega}{p} \right)_k + (P_T + K_T)_k \tag{3.5}$$

with

$$(T_v)_k = \left[1 + \left(\frac{1}{e} - 1 \right) q_k \right] T_k \tag{3.6}$$

and P_T and K_T represent physical and diffusion processes.

The momentum equations are:

$$\frac{d\vec{v}_k}{dt_k} = [-f\vec{k} \times \vec{v} - \nabla\phi - R_d T_v \nabla \ln p]_k + (\vec{P}_u + \vec{K}_u)_k \tag{3.7}$$

Specific humidity:

$$\left(\frac{dq}{dt} \right)_h = (P_q + K_q)_k \tag{3.8}$$

and cloud water equation:

$$\left(\frac{dm}{dt} \right)_h = (P_m + K_m)_k \tag{3.9}$$

c.f. Machenbauer (1988).

The equations are solved numerically with a semi-implicit so called 'Leap Frog' method:

$$\psi^{n+1} = \psi^{n-1} + 2\Delta t \cdot (f^n - S_\psi) \tag{3.10}$$

Here, ψ is a variable, $n-1$ and $n+1$ are the time step before and after n. f^n is the local temporal change of ψ at n. S_ψ denotes the semi-implicit correction and depends an ψ.

c.f. Dorn (2001).

3.2 Parametrisations

Radiation

In HIRHAM there is a distinction between clear-sky and cloudy-sky parametrisation:

- Clear-sky shortwave includes: Rayleigh scattering, Aerosol scattering and absorption and different gases, such as water vapour and ozone.

- Clear-sky longwave includes: Aerosols, water vapour, dicarbonate, ozone and other gases.

- Cloudy-sky shortwave includes: Droplet absorption and scattering and gas absorption.

- Cloudy-sky longwave includes: Droplet and gas absorption.

c.f. Christensen et al. (1996)

Soil Temperature

Soil Temperature is calculated with a five-layer soil model plus a possible snow layer. The following equation calculates the heat diffusion for the top soil layer (Christensen et al.

(1996)):

$$\frac{\partial T_1}{\partial t} = \frac{F_S}{\rho_s C_s \Delta z_1} + \frac{\kappa(T_2 - T_1)}{\Delta z_1 (\Delta z_1 + \Delta z_2)/2} \qquad (3.11)$$

If the snow layer exceeds 9 m, the surface is considered to be covered with ice and surface processes are calculated according to its properties (Christensen et al. (1996)):

$$\rho_i C_i = 2.09 \times 10^6 \, Jm^{-3}K^{-1} \qquad (3.12)$$

$$\kappa_i = 1.2 \times 10^{-6} m^2 s^{-1} \qquad (3.13)$$

Since the heat capacity of ice is sinking with sinking temperature, the heat capacity in the model is likely to be to high for antarctic conditions. Wexler et al. (2013) found a heat diffusivity of about $1.5 \times 10^{-6} m^2 s^{-1}$, which is nearly the value used in the model. With less then 0.025 m of snow the soil is considered to be bare. In the snow layer, temperature is calculated according to the properties of snow.

Hydrology

In HIRHAM there is a distinction between three water fields: Snow, water in vegetation and soil water. For Antarctica, snow is the most important water reservoir. Water in vegetation is not important in Antarctica.

Sea Ice

Sea ice cover is a boundary value determined by the boundary forcing. When Sea Surface Temperature drops below $-1.79°C$, sea ice developes. Its thickness is set to 1 m in Antarctica. Sea Ice Fraction as well as Sea Surface Temperature is updated every six hours. The results of a sensitivity study concerning sea ice thickness can be found in B. Here, temperature, MSLP and geopotential at 500 hPa and 300 hPa for sea ice thicknesses of 1 m and 2 m are compared for January and July 2001, showing the importance of a realistic parametrisation of sea ice thickness to the lower value of 1 m in Antarctica. A changing Sea Ice Thickness and the changement of the freezing point with changing salinity are not taken into account.

Clouds - Condensation Scheme

Cloud water q_w is calculated prognostically, whereas liquid water q_l and cloud ice q_i are distinguished diagnostically, based on temperature. The formation of clouds is based on a scheme by Sundqvist (1978), where grid box mean values of temperature, specific humidity and cloud water are calculated depending on their transport rates, as well as condensation and evaporation. In-cloud specific humidity is set to a saturation humidity q_{sat} and the grid point has then a certain cloud fraction.

Boundary Layer

Boundary Layer physics are based on eddy diffusivity. Here turbulent fluxes of cloud water, momentum, heat and specific humidity J_ψ are calculated with the diffusion coefficient K_ψ:

$$J_\psi = -K_\psi \frac{\partial \psi}{\partial z} \tag{3.14}$$

The vertical diffusion is calculated with the following equation:

$$\frac{\partial \psi}{\partial t} = \frac{1}{\rho} \frac{\partial}{\partial z} \left(\rho K_\psi \frac{\partial \psi}{\partial z} \right) \tag{3.15}$$

Turbulence is decreasing with height and set to zero at the top of the boundary layer. It is depending on horizontal wind and a drag coefficient at the surface. The dragging coefficients are calculated individually for heat and moisture according to Monin-Obukhow similarity theory with a von Karman's constant that is set to 0.4. Surface fluxes are calculated with a 1.5 - order closure scheme after Brinkop and Roeckner (1995) where the eddy diffusivity is parameterised after Prandtl-Kolmogorov:

$$K_\psi = c_1 l'_{m,h} \sqrt{E} \times f_{m,h}(Ri) \tag{3.16}$$

where E is calculated from:

$$\frac{\partial E}{\partial t} = -\vec{V} \cdot \vec{\nabla} E - \frac{\partial \overline{\omega' E'}}{\partial z} + \frac{g}{\theta_\nu} \overline{\omega' \theta'_\nu} - c_1^3 \frac{E^{3/2}}{l'_m} - \left(\overline{\omega' u'} \frac{\partial u}{\partial z} + \overline{\omega' \nu'} \frac{\partial \nu}{\partial z} \right) \tag{3.17}$$

Roughness lenght is calculated from sub-grid scale orography, vegetation etc. and over sea depending on sea-ice, resprectively wave-height. The cloud-cover is calculated depending on relative humidity and a threshold relative humidity depending on pressure/height and temperature. After the cloud cover is calculated the physical cloud processes like auto-conversion and accretion are calculated in a set of parametrisations. Cloud water and cloud ice are calculated temperature-dependent. In cloud-free parts evaporation of precipitation is taken into account. Melting of falling snow occurs at temperatures higher then 2°C. There is a parametrisation of gravity wave drag.

All described in this chapter and more detailed information can be found in Christensen et al. (1996).

3.3   Model setup for Antarctica

Grid (vertical and horizontal)

In Figure 3.1, model orography of HIRHAM is plotted. The x- and y-axis show their respective grid points. Here 110×122 grid points with a horizontal resolution of 50×50 km are used, which cover Antarctica up to 60° south, and 25 vertical σ p-coordinate levels up to 10 hPa. A time step of 120 s is employed. In the resolution of 50×50 km the mountain ridges of steeper mountains like the Transantarctic Mountains and the mountains on the Peninsula are smothered, their influence might not be calculated thoroughly. Also effects like katabatic winds cannot be clearly shown in this resolution.
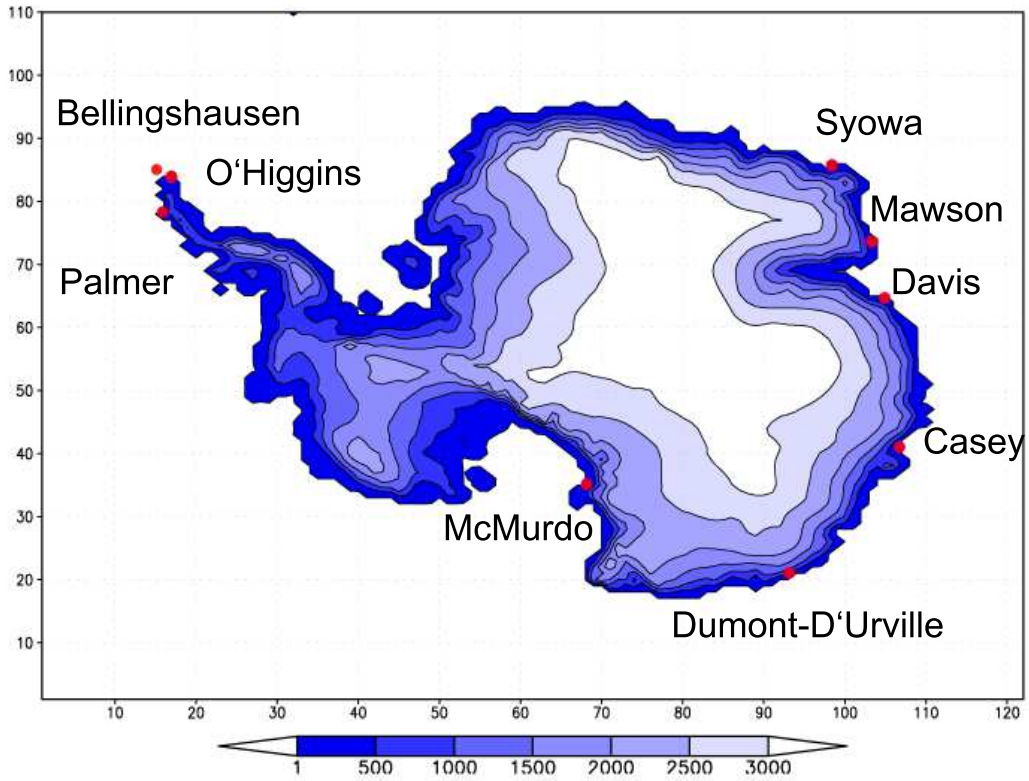
Figure 3.1: Map of HIRHAM-Orography in m and stations.

Lower and boundary forcing

The forcing at the lateral and lower boundaries is provided by ECMWF reanalyses, with a boundary zone of 10 grid points. HIRHAM uses a boundary relaxation scheme after Davies (1976):

$$\hat{u}_k^{\vartheta} = (1 - \alpha_k)u_k^{\vartheta} + \alpha_k \tilde{u}_k^{\vartheta} \tag{3.18}$$

with u as a model field value, and $\tilde{u}$ as value of the corresponding boundary field. $\hat{u}$ is the relaxed value of u, ϑ is the time step and k denotes the grid point relative to the nearest bounday. α_k denotes relaxation weights, a is a constant that depends on the number of relaxation points:

$$\alpha_k = 1 - \tanh(ak) \tag{3.19}$$

With this relaxation scheme, problems with spurious precipitation in the boundary zone occured. For this reason a technique named inflow/outflow formulation is used. Depending on in- or outflow the boundary values at $k = 0$ is calculated according to an outer point / the four nearest neighbouring points inside the model grid Christensen et al. (1996).

The sea-ice thickness is set to 1 m, according to thinner sea-ice in Antarctica compared with the Arctic. HIRHAM4 treats grid points with more than 50% land as land points, there are no lakes in inner Antarctica and every land point is a glacier point. Snow free areas that occur on Antarctica are not resolved. In snow free areas the albedo is lower than over snow, the ground is absorbing the radiation better and thus getting warmer, with a higher exchange of sensible heat between atmosphere and ground and possibly differnt values of latent heat. Following this also the processes in the boundary layer differ. This leads to uncertainties in the calculation of the climate in zones that are snow free in nature. For this study two runs over several years and two sensitivity studies have been conducted:

Run	Boundary	Time Period	Chapter
ERA40 run	ERA40	1 Jan 94 to 31 Dec 99	A, 7, 7.5
ERAint run	ERAinterim	1 Jan 96 to 31 Dec 09	7.5, 8, 9
25Levs	ERA40 25 Lev	Jan 01 and Jul 01	A
46Levs	ERA40 46 Lev	Jan 01 and Jul 01	A
2mSI	ERA40 2m sea ice	Jan 01 and Jul 01	A

Chapter 4

Reanalyses

In this study, the ERA40 reanalysis and the ERAinterim reanalysis are used as boundary forcing for the regional model, ERA40 for the first run from January 1994 to December 1999 and ERAinterim for the integration period of January 1996 to December 2009. Additionally, two global reanalyses, ERA40 and NCEP, are used for the comparison of TWV data for the first integration period from January 1994 to December 1999. Reanalyses assimilate measurements and use forecast techniques to calculate the synoptical situation for a given time period. They assimilate observations from station, ships, buoys for surface data and for higher levels they primarily they use Radiosoundings, since they were the first measuring method that regularly measured the vertical structure of the atmosphere (Uppala et al. (2005), Dee et al. (2011), Kistler et al. (1999)). After 1979 more and more satellite measurements were included to substitute for declining soundings as explained in Uppala et al. (2005).

4.1   NCEP/NCAR Reanalysis

NCEP/NCAR reanalysis (NCEP) with a spatial resolution of 62 waves in horizontal triangular truncation, which equals around 210 km. It has 28 vertical levels up to 300 hPa in humidity variables, the maximum level height differs for other variables. It is providing reanalyses for a period from 1948 to the present for the northern hemisphere, respectively 1957 to the present for both hemispheres, by using 'land surface, ship, rawinsonde, pibal, aircraft, satellite and other data' (c.f. Kistler et al. (1999) - 'pibal' is a short word for 'pilot balloon').
The assimilation scheme remained the same through the whole reanalysis period and is the same as in the operational NCAR weather model. Still, there were changes in observational techniques which lead to perceived climate jumps. In 1957, in the first International Geophysical Year (IGY), the radiosonde network began to establish, with an additional shift in observation times from 03z (6-hourly) to 00z (6-hourly). From 1979 on satellite observations added to radiosondes. NCEP provides meteorological variables that are either directly observed (A), additionally influenced by the model (B) or only determined by the

model (C). Naturally, A variables are most reliable, whereas C variables should be used with caution. Humidity is a (B) variable, which makes a validation with measured data necessary. Mass conservation also cannot be guarantied in a reanalysis model, because especially B and C variables are adapted to measurement, which is not necessarily mass conserving. A detailed description of the NCAR/NCEP reanalysis, as well as the information put here, can be found in Kistler et al. (1999).

For the comparison of the TWV values with measurement, an interpolation by Vey (2007) was used. The vertical interpolation in Vey (2007) employed the equation of Clausius-Clapeyron, to fit the values to station height. For the comparison with HIRHAM and ERA40 data, NCEP was interpolated to the HIRHAM model grid with the CDO operator remapbil (Schulzweida et al. (2009)).

4.2   Reanalyses of the ECMWF

ERA40 is a reanalysis from the ECMWF that has a T159 spatial resolution in a reduced Gaussian grid, which leads to a spacing of around 125 km. ERA40 has 60 hybrid vertical levels up to 0.1 hPa and the lowest level at 10 m over ground. It uses a semi-Lagrangian scheme with two time levels and a finite element scheme vertically. ERA40 is the follow up of ERA15 and covers a period from 1957 to 2003. ERA40, just like NCEP, uses measurements from land stations, ships, radiosondes, satellites and others. In Uppala et al. (2005) it is stated that the accuracy of radiosonde measurement increased over time, but their spatial and temporal coverage declined. This is mostly compensated by other observation types, also the density of wind and temperature measurements via satellite increased. As ERA40 mostly uses the same data sources as NCEP, it has the same jumps in observational quality, like for example the beginning of the satellite era in 1979. It also includes data from ECMWF, NCAR and JMA (Uppala et al. (2005)). For ERA40 different corrections on measuring methods were applied, as radiosonde and satellite corrections, to guarantee values that are as close to nature as possible and in radiosonde measurements temperature instead of height data is assimilated, this leading to ERA40 data being closer to radiosoundings than ERA15 (Uppala et al. (2005)). For data assimilation a 3D-Var method is used with a 6-hourly period centered on the analysis times and surface data is assimilated via an interpolation between surface and the lowest model level derived from background forecasts, described in Uppala et al. (2005). A change in land surface and boundary layer parametrisations led to improvements concerning low level temperature in high latitude land areas in winter time. Especially for Antarctica a new definition of the model orography and the treatment of main permanent shelf ice as land improved surface and low-level temperature calculation. Most improvements of the analysis are due to improvements of the data assimilation (Uppala et al. (2005)). All these, as well as addtional information on ERA40 reanalysis, can be found in Uppala et al. (2005) and Uppala et al. (2004).

ERA-interim was developed when more computer power was available and 4D-Var data assimilation was tested and introduced and it uses a 12-hourly analysis cycle and also com-

bines observations with informations from a forecast model (Dee et al. (2011)). It covers a time period from 1979 onwards and has an enhanced horizontal resolution of T255, which corresponds to a spacing of approximately 79 km, according to Dee et al. (2011). Vertical resolution was kept at 60 levels. It uses similar observations and parameters as ERA40, like temperature, wind or humidity and estimates physical parameters such as precipitation, turbulent fluxes, cloud properties and others (Dee et al. (2011)). Over the years, the number of observations increased. There are shifts in radiosonde measurements that are due to, for example, equipment changes or changes in observation practise, but ERAint showed a good bias handling (Dee et al. (2011)). The main differences to ERA40 are a better formulation of background error constraint, a new humidity analysis that solved problems from ERA40, improved model physics, a more experienced data quality control, improvements in bias handling and an improved usage of radiances. Differences in acquired observations include the usage of altimeter wave-heights, winds and clear-sky radiances, ozone profiles and radio occultation measurements. All information on ERAinterim can be found in Simmons et al. (2007).

In this study, an interpolation of ERA values to the HIRHAM grid was used for the comparison of both data sets. For the comparison of MSLP, TWV and 2m-Temperature, the grid points next to the stations have been taken into account.

Chapter 5

Measurement

5.1 Observation Sites

Fig. 3.1 gives an overview of the HIRHAM4 orography with positions of all used stations. For the study, GPS-measurements from 8 and soundings from 7 Antarctic stations are compared to reanalyses (NCEP and ERA40) and a regional climate model. Find in Table C.1 a list of all stations used in this study, with station position in longitude and latitude, its height and the associated 4 next HIRHAM4 grid points and their height. The study was made with 3 stations on the Antarctic Peninsula and 6 stations around the coast of East Antarctica. Since Palmer and O'Higgins only provide GPS measurements, but no sounding data, these stations are used for the comparison of GPS and sounding from Bellingshausen Station. Bellingshausen provides no GPS measurements but sounding data. Therefore this station is used for the comparison of HIRHAM and sounding. Bellingshausen is 136 km away from O'Higgins and 382 km away from Palmer.
None of the stations is located on shelf-ice, so there should be no significant variance in station-height.

5.2 WMO standard methods

<u>Sounding</u>

Radiosondes are widely used to measure the vertical structure of atmospherical parameters like pressure, temperature or humidity. Wind direction and strength can be retrieved through determination of the position of the radiosonde via GPS. In earlier years other navigation systems where used, such as most commonly the Loran-C navigation, which has an uncertainty in wind speed measurements of about 0.5 to 1.0 m/s (Jaatinen and Kajosaari (2000)). Another system to determine the position of the sonde is radar, for example the very high resolution centrimetric radar, which is described in Barat and Cot (1995) as having an uncertainty of 0.3 m/s in wind speed, but has a decreasing resolution

with height. In the early nineties GPS navigation became more and more common and has a lower uncertainty in wind speed measurement of about 0.15 m/s (Vaisala (2006)). Still, in the first years of the analysis in this thesis the uncertainties of the wind measurement via radiosondes differs from the uncertainties of later measurements, but the reanalyses and HIRHAM use these soundings and are affected by these changes in wind measurement in a similar way. Since sounding is a WMO standard method, it will be used as reference in this study.

Temperature is measured via a capacitive wire. Its total uncertainty in sounding is 0.5°C and also depends on the climbing speed. A thin-film capacitor and a heated twin sensor act as humidity sensor. The absolute error of humidity measurements is around 5% of relative humidity, depending on temperature and humidity and thus on altitude. In Antarctica under extreme cold and dry conditions the uncertainty of humidity measurements is higher. For the pressure measurement a silicon sensor is installed. It has an uncertainty of 1 hPa in the lowest 100 hPa. All information is available in technical sheets from the producers of the commonly used Radiosondes: Vaisala (2006).

For this study sounding data from seven different sites in Antarctica were used: Bellingshausen, Casey, Davis, Dumont-D'Urville, Mawson, McMurdo and Syowa, all stations that have GPS-Data themselves or could be compared to GPS-Data of stations in their vicinity, like Bellingshausen Station which was compared to Palmer and O'Higgins, because the comparison of those two measurement methods is one of the main scopes of this study.

Temperature Measurement

WMO defines air temperature as 'the temperature indicated by a thermometer exposed to the air in a place sheltered from direct solar radiation'. This led to the development of radiation shields. They ought to shield the thermometer from radiation but also from precipitation. Since air temperature is very sensitive to the surrounding atmosphere, objects or vegetation it is recommanded to measure at sites free from obstacles or vegetation and to keep a metadata file of the circumstances of the measurements. Air temperature should be measured at heights of about 1.2 to 2 m above ground level. In Antarctica permanent temperature measurement is mostly conducted at the stations, which are only few.

Pressure Measurement

As mean sea level pressure (MSLP) is an important variable in atmospheric modelling, WMO set some standards in pressure measurement. For synoptical application air pressure is measured in hPa with mostly anaeroid or electronical barometers. Pressure measured at station level is mostly reduced to sea level, if possible.

Wind Measurement

Wind is a three dimensional vector but is mostly measured horizontally, especially in lower level measurements. Large scale flow is genarally superimposed by small scale ran-

dom fluctuations. Wind data is normally averaged over a period of 10 to 60 minutes as wind speed and wind direction, additionally peak gusts are also measured. As stated in Jarraud (2008) it is nearly impossible to find an anemometer location that is representative for a large area. Also the sensors must be kept away from obstacles as far as possible. Wind is measured at 10 m above ground. On sea, especially on ships this is often not possible, so an exposure correction has to be made. Wind speed is measured by e.g. a cup anemometer and wind direction is measured by a wind vane. Combined measurement of both is possible with for example a propeller anemometer. Especially in colder regions like Antarctica, cup anemometers are likely to freeze over, which leads to uncertainties. New systems are e.g. sonic anemometers or remote sensing anemometer systems such as sodar lidar or radar. Sonic systems are easily perturbed.

Precipition Measurement

Precipition is the solid or liquid product of condensation falling from air to ground. Usually it is measured in volumes such as mm = mm/m^2. Snow heights are measured in cm by snow rulers or ultrasonic measurement systems. Rain gauges are often cylinders of a specific surface area that measure the amount of precipitation by a direct volume measurement or by weighing precipitation by counting droplets per tipping buckets. As in wind measurement also in the measurement of precipitation the choice of the specific measurement site is of great importance. The precipitation should not be shielded from the rain gauge but also the use of windshields can be important. Snow measurement is of additional complication because snow should be prevented from being blown out of the gauge but also from beeing blown into the gauge horizontally. In Antarctica there is typically only measurements of snow accumulation instead of direct measurements. Only on the Peninsula precipitation is measured directly.

Humidity Measurement

Definitions of different humidity measures:

- Specific humidity is the ratio between water vapour and moist air mass.

- Total Water Vapour (TWV) is the vertically integrated specific humidity

- Relative humidity is the ratio of observed vapour pressure to saturation pressure at given temperature.

c.f. Jarraud (2008)

Humidity can be measured with different types of hygrometers or psychrometers. Also condensation methods are in use. With humidity measurements it is important to distinguish between water and ice phase. In Antarctica the uncertainties of humidity measurements are higher due to the low temperature and humidity. In this study, the most important humidity measurement method is the measurement of the relative humidity via radiosondes, for which Rowe et al. (2008) showed that in Antarctica the uncertainties in the measurement are around 15% of the relative humidity.

The provided information can be found in Jarraud (2008).

5.3 Total water vapor retrieval via GPS

Ground-based GPS measurements provide water vapor estimates independent of radiosonde data and weather conditions. The GPS signal on its way from the GPS satellite to the receiver is delayed due to the atmospheric constitution, especially by water vapour due to the dipole moment of water molecules and nearly proportional to the quantity of TWV (Businger et al. (1996)). During the GPS data processing this delay (zenith total delay ZTD) is estimated as an additional unknown parameter. Using temperature and pressure measurements on the earth's surface, the ZTD is utilized to derive the TWV content of the atmosphere along the signals path. According to Bevis et al. (1994), the conversion was carried out in two steps. At first, the separation of the zenith hydrostatic delay (ZHD - the signal delay only due to the dry components of the atmosphere) and the zenith wet delay (ZWD - the signal delay due to the humidity) was performed. Subsequently, a conversion factor was introduced to convert the ZWD into the corresponding amount of water vapor. The conversion factor varies as a function of the atmospheric mean temperature and takes additional properties of the atmosphere like refraction constants into account. The application of the temperature and pressure data sets provided by ECMWF and WMO was carried out according to Vey et al. (2009).

5.4 Comparison between Sounding and GPS

The methods of water vapour retrieval via Sounding and via GPS are different. First, the radiosonde and the satellite use different instruments and methods. Then a radiosonde measures the values on a path and the GPS satellites measure integrated values of a certain volume of air. The sonde is drifting a different path then the integrated measuring path of the GPS-satellites.
The last problem was analysed in this study and will be presented in chapter 7.4.

Chapter 6

Analysis Methods

6.1 Statistical Methods

6.1.1 Standard deviation

Standard deviation is calculated with the collection of operators 'Climate Data Operators' CDO Schulzweida et al. (2009) and its command timstd. Standard deviation in CDO is calculated with the following formula:

$$StDev = \sqrt{n^{-1} \sum_{i=1}^{n} (x_i - \overline{x})^2}$$ (6.1)

for a given field over a certain time, where n is the number of values in the field, x_j is a single value and $\overline{x}$ is the mean of the field.

Here standard deviation was calculated for MSLP, temperature and TWV for HIRHAM and its boundary forcing ERA40. For the comparison of differences, the relative standard deviation was calculated, meaning that the standard deviation was devided by its temporal average of the difference:

$$rel.StDev = \frac{\sqrt{n^{-1} \sum_{i=1}^{n} ((x - y)_i - \overline{x - y})^2}}{\overline{x - y}}$$ (6.2)

If the standard deviation is much smaller than the temporal average of a difference between, the value of $rel.StDev$ is much smaller than one. Only for values of $rel.StDev > 0.7$ the difference between x and y can be indicated as significant. Hereafter $rel.StDev$ is referred to as significance. The more common student-t-test was not applied due to the small sample size in the simulations.

6.1.2   Pattern Correlation

Pattern Correlation is a method to compare the same variables in the same region but for different time or of different runs. Here the following formula is used:

$$PattCorr = \frac{\overline{(x_j - \overline{x})(y_j - \overline{y})}}{(x_j - \overline{x})^2(y_j - \overline{y})^2} \tag{6.3}$$

Here, x_j and y_j stand for the single values in the different datasets, overlined variables show the respective mean of all values in one dataset. In this study pattern correlation is used to compare different setups of sensitivity studies.

6.1.3   Root Mean Square Error

Root Mean Square Error (RMSE) is like Pattern Correlation a tool to calculate the correlation between two datasets, in this case depending on time. Here it is used to calculate the correlation between time series of different measuring and modeling methods.

$$rmse = \sqrt{\left(\frac{\sum_{j=1}^{n}(x_{1,j} - x_{2,j})^2}{n}\right)} \tag{6.4}$$

In this equation $x_{1,j}$ and $x_{2,j}$ stand for values of the two datasets that are to be compared, with j denoting one single value and n is the number of values in the datasets.

6.1.4   Timeseries

In this study a monthly mean of TWV was calculated and plotted as time-series for each station. Only months with more than 20 days of measurement were taken into account. To get a closer look at possible uncertainties due to orographic differences, for HIRHAM the 4 grid points next to the station are depicted. For a better clearity in the Figures, only the next ERA40 - interpolated on the HIRHAM grid - grid point is used for the comparison (first in the list). For NCEP, an interpolation made by Vey (2007), like described above, is used.

In comparison of HIRHAM and radiosounding, statistics like a correlation and root mean square error were calculated. These can be found in Table C.2.

The standard deviation of MSLP and TWV for HIRHAM and both reanalyses over the whole integration period from 1994 to 1999 was calculated.

6.1.5   Wind Direction Analysis

The main wind directions at the stations were calculated from the most frequent wind directions in the lowest level of the soundings. Most sounding data was provided 12 hourly,

with some exceptions due to missing data. The main retrieval directions of GPS were analysed for one example day. Since the satellite tracks are highly repetetive, the measuring direction on any other day will not differ much from that of the example day. 27 January 1998 was chosen, because this was the first day with GPS measurements on every station.

6.2 Two dimensional digital Filter

A useful tool for the comparison of a regional climate model with global models and its boundary forcing is a 2-dimensional digital filter developed at Helmholtz-Zentrum Geesthacht. This filter can be applied to any model variable. Feser (2006) found with this tool an added value for medium scale air pressure and near-surface temperature in regional climate models with additional nudging, especially for orography-dependent values like 2m-temperature. Here it is used to analyse patterns of certain scales of pressure, humidity and temperature. With a filter it is possible to analyse planetary scales and synoptical scales seperately from each other, allowing clear statements of processes on each scale. This new approach is used because older approaches like Fourier filters might have problems with linear trends in RCMs, because they might mistake a trend that is cut by the boundary of the model as a wave. Digital filters work under the estimation of the dependence of a value at one point in the grid on its neighbouring points. Additionally linear and polynomial trends can be taken into account by the method of Feser and von Storch (2005) with the help of a pre-filtering tool. The Feser-Method constructs response-funcions for an almost isotropic filter. A response of around one is expected in the wavelength-region, that is to be filtered, around it will be a zero-response. This is working like a running mean with given filter weights. The filter array must be quadratic and symmetrical with respect to zonal and meriodional directions.
There are three possibilities to filter frequencies:

- Lowpass: Only signals with a LOWER frequency than the cut-off-frequency pass the filter.

- Bandpass: Signals with a frequency BETWEEN the lower and the higher cut-off-frequency pass the filter.

- Highpass: Signals with a frequency HIGHER than the cut-off-frequency pass the filter.

A fourier-filter calculates the frequencies from a time series and different boxes cut the frequencies and re-calculate the new filtered time series. A running-mean filter as in the Feser filter-tool works solely in the (2-dimensional - here horizontal) space of the timeseries. A box of a certain width is running over the values and leaves only signals that fit

into it, by multiplying them with one and wider (or smaller) signals with zero.

The Feser-Filter calculates response functions especially for the grid of the regional model. From this set of lowpass, bandpass and highpass filters one can choose the appropriate filter for a study. The response- and their corresponding filter function are sorted by wave numbers. These wave-numbers belong to the special grid of the regional model. The relation between the wave-numbers and the scales is the following:

$$wavenumber = \frac{gpt \times dx}{scales} \tag{6.5}$$

Where gpt is the number of gridpoints in each direction and dx is the horizontal spacing between two grid points, $scales$ is the wavelength. The calculation of the response function is only working for square grids. The smaller of both sides is considered for the calculation, but the filter function still works for any rectangular grid. Also the boundary zone is taken into account.

Here different response functions for bandpasses from 500 km to 1000 km (SYN) and from 200 km to 600 km (MESO) as well as for a lowpass for wavelengths of more than 1000 km (LOW) were calculated with the following wavenumbers:

- LOW: 5

- SYN: 5 x 11

- MESO: 9 x 27

Example of wavenumber-calculation for the LOW-filter:

$$wavenumber = \frac{110 \times 50km}{1000} \tag{6.6}$$

$$wavenumber = 5.5 \tag{6.7}$$

Figure 6.1 show the filter function (left) and the response function (right) of the SYN-Filter:
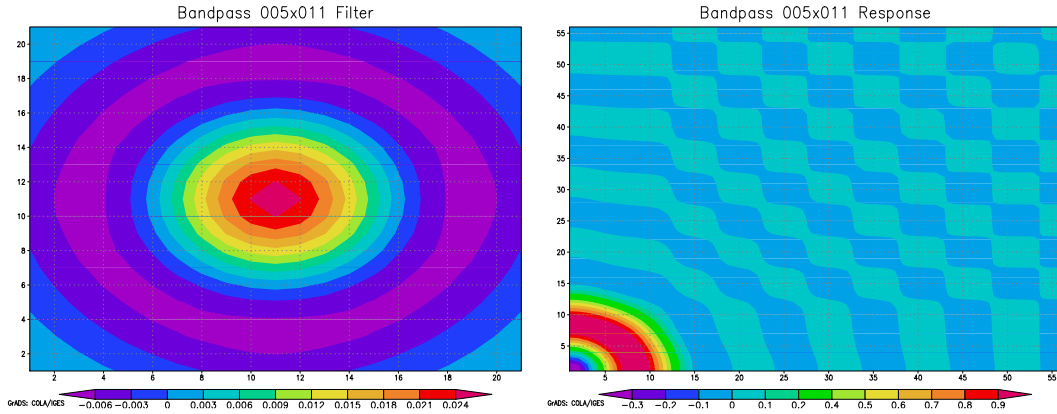
Figure 6.1: Filter function of the SYN-Filter.

These were applied on an ERA40 run from January 1994 to December 1999 and to an ERAinterim run from January 1996 to December 2009. The filters were applied on the surface values MSLP, 2m-temperature and TWV. Furthermore, they were applied to results of geopotential, temperature and relative humidity in the levels 70 hPa, 300 hPa, 500 hPa, 700 hPa and 850 hPa. First the filters were applied on daily averages to seperate structures of the focused-on wavelength. Then averages over the single season of all 6, respectively 14 years or the single seasons of each year were calculated. To show the deviations from the respective spatial means, the mean values were substracted from the filtered data.

6.3 Comparison of Model and Station Data

Since model resolution is coarse compared to the orography around the station site, there are probable differences of station height and grid point height, and also different orographic structures. When hills, valleys and similar landscapes are not represented properly, there might occur problems in the representation of influences the station data, such as katabatic winds, cold pools, etc. The elevation of neighbouring grid points differ from the actual station height (c.f. Table C.1). In the grid area of a station, height differences of more than 1000 m are possible. This explains differences of e.g. TWV and 2m temperature, because humidity and surface temperature are decreasing with height. MSLP values are interpolated from model levels to sea level, a calculation which always has only a limited accuracy, especially in steep orography. The extrapolation is calculated from the lowest level, which is terrain-following to sea level. The sea level pressure is calculated under the assumption of a dry hydrostatic atmosphere with a temperature lapse rate of 6.5K/km, which can be modified for very cold surface temperatures (Unden et al. (2002)). An interpolation from model grid to the position of the stations only blurs differences between station and surrounding grid point, that is itself an interesting object of investigation. For this reason in most parts of this study no interpolation from the model grid to station data was made. Addionally, the land-sea-mask differs from the real coast line. So a grid point that lies next to the station can have different conditions than the station itself, because

it can have a different distance to the coast than the station, or even be a sea point itself. With increasing/decreasing distance to the coast a grid point tends to have lower/higher TWV. The distance between the single grid point is ca. 50 km in this study, so a horizontal variability smaller than this spacing cannot be captured by the simulation. The results will be discussed in chapter 7.

Chapter 7

Validation of HIRHAM data

In this chapter the results from the ERA40 run are compared with reanalyses and measurements. It will be shown that HIRHAM is a reliable tool and reflects measurements correctly. Uncertainties will be explained through differences in orography and station setting.

7.1 Horizontal Structures of Mean Sea Level Pressure, Temperature and Humidity

A first step of the validation of HIRHAM is a comparison with ERA40, which is its boundary forcing reanalysis and NCEP. The differences between all three are shown in plots with absolute values (Figures 7.1, 7.3 and 7.5) and plots that show the differences between HIRHAM and ERA40, respectively HIRHAM and NCEP (7.2, 7.4 and 7.6) and the respective significances. Additionally, an analysis of the single seasons will be shown.

In Fig. 7.1 the average MSLP from the HIRHAM4 simulation run from 1 January 1994 to 31 December 1999 and its ERA40 and NCEP equivalent is shown. Around the Antarctic continent is a low-pressure-ring with a minimum of 981 hPa in the region of Amundsen Sea and Ross Sea. Over the continental plateau is a high (1008 hPa), which covers a broad area. Around the continental coast is a strong pressure gradient. The general MSLP patterns of HIRHAM and the reanalyses fit the patterns described in chapter 8.

Over sea, in the boundary zone, the differences are small, not only between ERA40 and HIRHAM, but also between ERA40 and NCEP (7.2). Both reanalyses have nearly identical values of MSLP over the ocean. The reanalyses show the minimum of the low-pressure-ring more in the Ross Sea, whereas HIRHAM simulation has this minimum more to the West of the Peninsula in the Amundsen Sea. Over land the differences of NCEP and HIRHAM become larger than -27 hPa, which is significant, especially for elevated terrain. This might be due to extrapolation effects, although the same method as in HIRHAM is also used in NCEP. NCEP has a much coarser resolution than ERA40 or HIRHAM, the orography is much more smothered. When NCEP interpolation is covering a greater height than HIRHAM interpolation, the NCEP MSLP values are automaticly higher than HIRHAM

MSLP values. HIRHAM and ERA differences are smaller ($\pm$ 9 hPa) and are not significant.
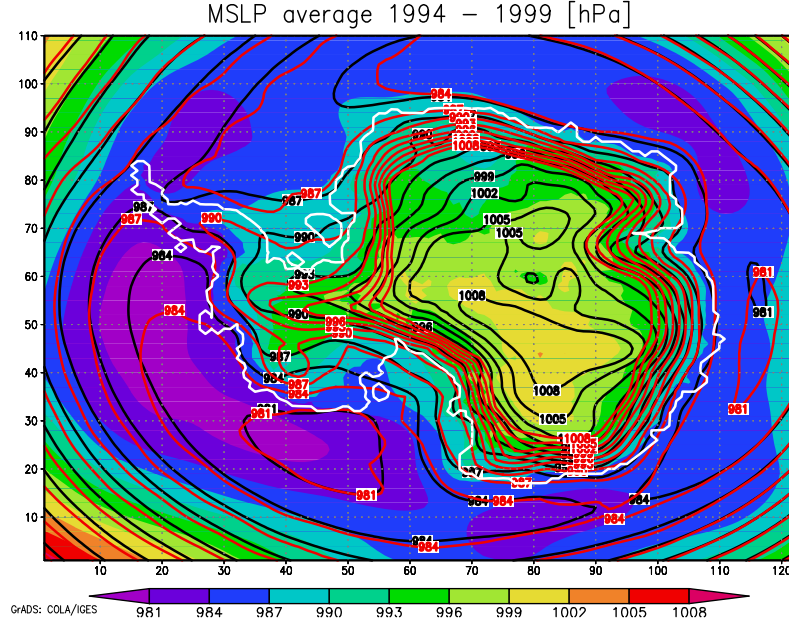
Figure 7.1: MSLP average 1. Jan 1994 - 31. Dec 1999 from HIRHAM (shaded), ERA40 (black contour line) and NCEP (red contour line).
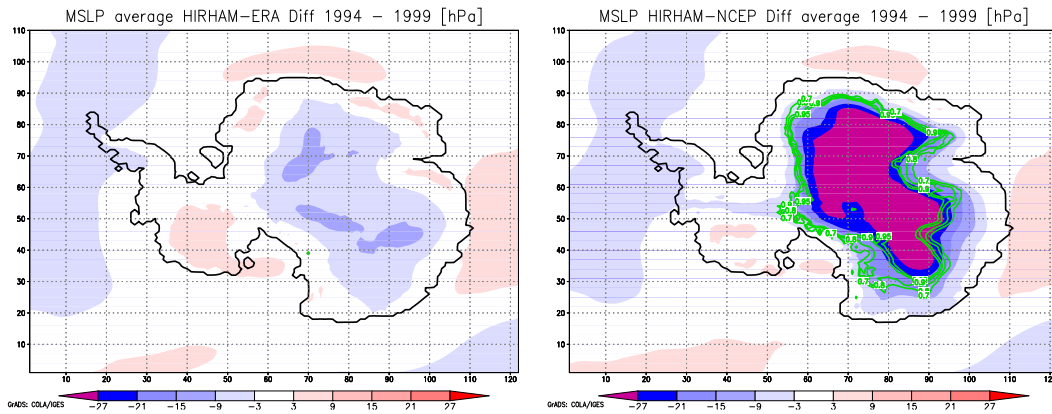
Figure 7.2: Difference of the MSLP average 1. Jan 1994 - 31. Dec 1999 from HIRHAM and ERA (left), respectively HIRHAM and NCEP (right). Green Contour Lines: Significance.

On the chart of mean TWV Fig. 7.3 the average TWV from the HIRHAM4 simulation run from 1 January 1994 to 31 December 1999 and its ERA40 and NCEP equivalents are depicted. The inner region of continental Antarctica is dry for all three of them, with less than 1 g/kg TWV. The dry zone of continental East Antarctica is well displayed. The TWV gradient on the border between land and sea is high. The TWV value is increasing

ca. 3 g/kg around the coast. The shelf-ice-zones in Weddel- and Ross-Sea are also well depicted, as expected, they have a low specific humidity of 3 g/kg to 6 g/kg TWV in the HIRHAM simulation and around 3 g/kg in case of ERA40 and NCEP. One can see an increasing TWV to the North, including higher humidity on the Peninsula.

In Figure 7.4 the differences in the spatial distribution between ERA40 and NCEP are shown. Over the dry continent the absolute differences are reduced, but still resulting in relative differences of 30 % (ERA40) and up to more than 90 % (NCEP). Differences between ERA40 and HIRHAM are small in the boundary zone. Over the continent they are supposedly due to the finer resolution of HIRHAM compared to ERA40 and NCEP. Especially in case of NCEP the same effects occur as for MSLP. When humidity is extrapolated from a greater height, the resulting values are higher than that interpolated from a smaller height.
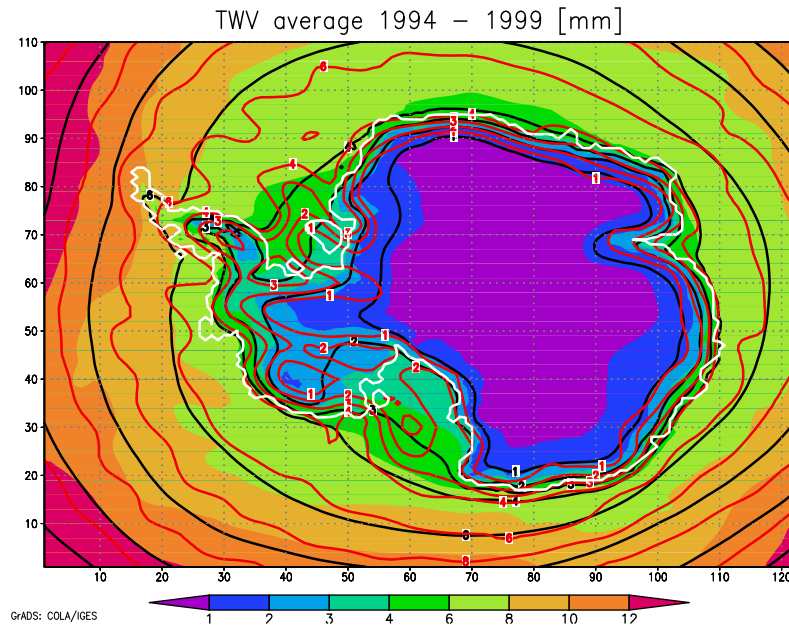
Figure 7.3: TWV average 1. Jan 1994 - 31. Dec 1999 from HIRHAM (shaded), ERA40 (black contour line) and NCEP (red contour line).
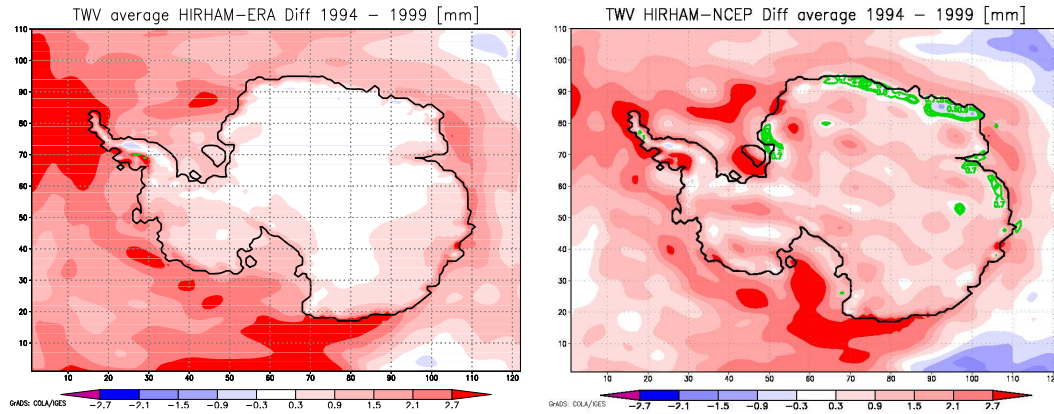
Figure 7.4: Difference of the TWV average 1. Jan 1994 - 31. Dec 1999 from HIRHAM and ERA (left), respectively HIRHAM and NCEP (right). Green Contour Lines: Significance.

Fig. 7.5 shows the average 2m-temperature from the HIRHAM4 simulation run from 1 January 1994 to 31 December 1999 and its ERA40 and NCEP equivalent. The temperature is lowest over the continent ($-40°$C and increases to the North, where it reaches $5°$C. Around the coast is a strong temperature gradient. Over shelf-ice regions the temperature is also very low ($-20°$C to $-25°$C) because of the cooling from the ice compared to the relative warm temperature over the sea.

Although the temperature pattern is similar for HIRHAM and the reanalyses, the differences between ERA40 and HIRHAM are up to 14 K and not significant, whereas the differences between HIRHAM and NCEP are up to 18 K and significant (c.f. 7.6).
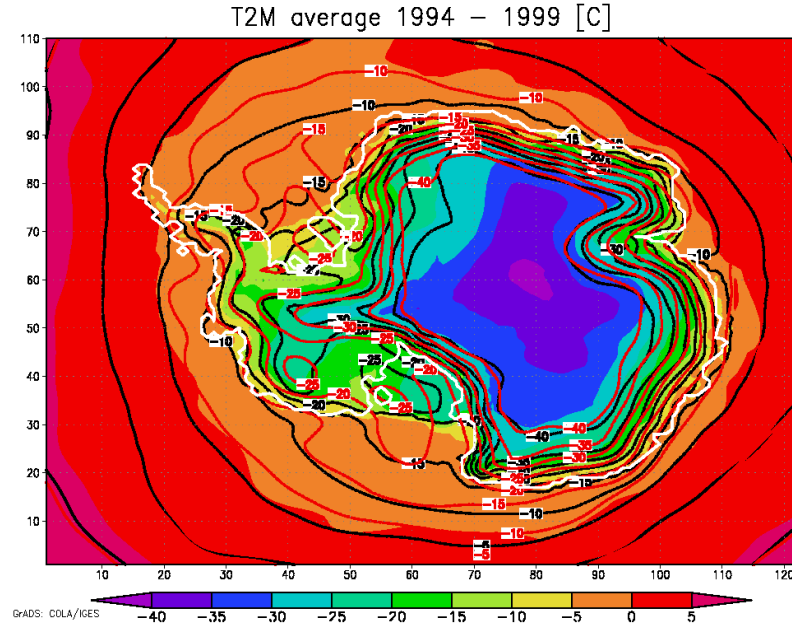
Figure 7.5: 2m Temperature average 1. Jan 1994 - 31. Dec 1999 from HIRHAM (shaded), ERA40 (black contour line) and NCEP (red contour line).
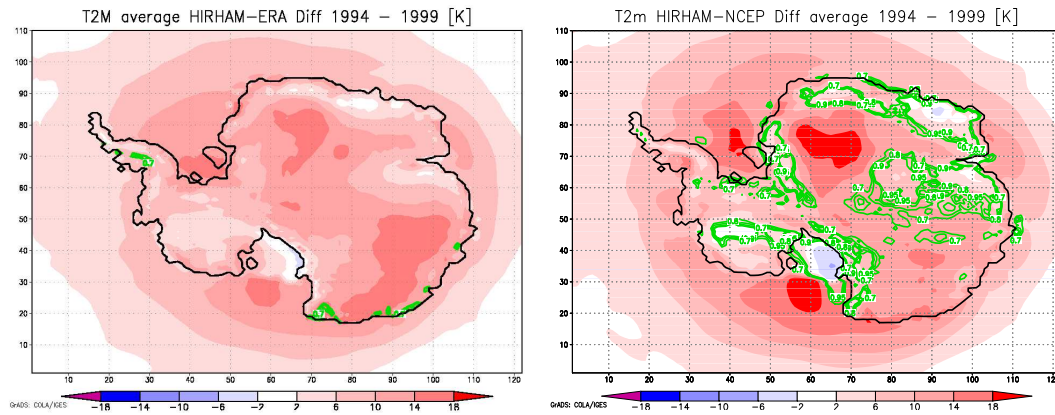
Figure 7.6: Difference of the T2m average 1. Jan 1994 - 31. Dec 1999 from HIRHAM and ERA (left), respectively HIRHAM and NCEP (right). Green Contour Lines: Significance.

The differences between HIRHAM and the two reanalyses can be explained, amongst others, through different orographical setups. This can be seen in the MSLP plots 7.2. Since ERA40 is the boundary reanalysis for this HIRHAM run, the differences have to be smaller than the differences to NCEP, which they are by e.g. 4 K or 18 hPa.
The summer and winter mean differences of the integration period from 1994 to 1999 between HIRHAM and ERA40, respectively HIRHAM and NCEP differ from each other. An overview is shown in the following Table:

Table 7.1: Table of the biases between HIRHAM and ERA, resp. HIRHAM and NCEP for MSLP, T2m and TWV in summer and winter and the whole integration period.

Datasets	MSLP	TWV	T2m
HH-ERA whole period	0.4 hPa	0.3 mm	1.8 K
HH-NCEP whole period	3.0 hPa	0.5 mm	1.1 K
HH-ERA summer	0.8 hPa	0.5 mm	2.8 K
HH-NCEP summer	0.2 hPa	0.7 mm	2.6 K
HH-ERA winter	0.4 hPa	0.2 mm	2.0 K
HH-NCEP winter	4.8 hPa	0.4 mm	0.3 K

The T2m bias is smaller for HIRHAM-NCEP than for HIRHAM-ERA. In the case of TWV the bias of HIRHAM-ERA is smaller than the HIRHAM-NCEP bias. The bias of MSLP can be up to 4.8 hPa for HIRHAM-NCEP in summer, which explains the high overall bias of 3.0 hPa in this case.

TWV in winter is generally smaller than in summer (7.7). For HIRHAM, as well as for ERA40 and NCEP the TWV does not exceed 1 mm in the whole region of the Antarctic Plateau. In summer the region with less than 1 mm TWV is smaller for ERA40 than for HIRHAM and NCEP.
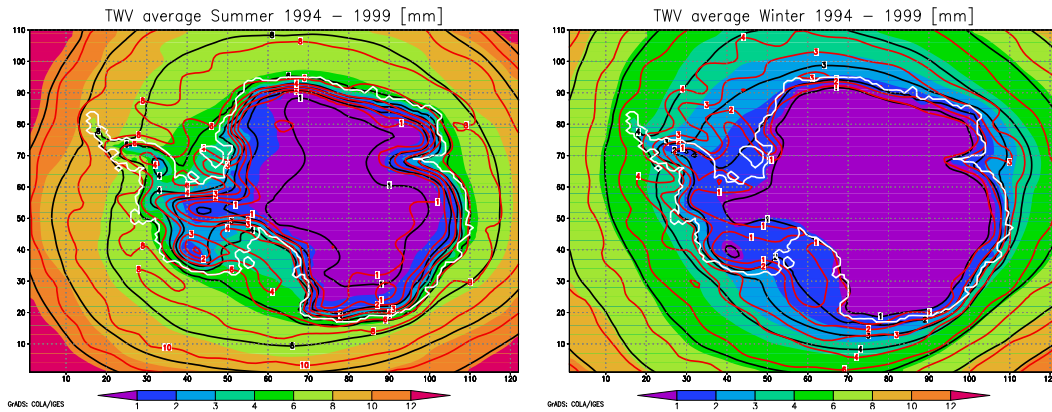
Figure 7.7: TWV average summer (left) and winter (right) 1994 - 1999 from HIRHAM (shaded), ERA40 (black contour line) and NCEP (red contour line).

In winter (7.8 right side) the high over the Antarctic Plateau (region with MSLP > 1008 hPa) covers a wider area in NCEP and ERA40 than in the HIRHAM simulation. The low over the Ross Sea is more intensive in ERA40 (981 hPa) than in NCEP and HIRHAM (984 hPa). In summer (7.8 left side) the maximum of the high in NCEP (1008 hPa) is shifted to the west in comparison with HIRHAM (1002 hPa). The ERA40 high is less intensive and reaches values of only 996 hPa. The low near the West Antarctic coast is

shifted to the Peninsula in comparison with summer. ERA40 and HIRHAM are both in good accordance with each other, both having a minimum of 981 hPa, while NCEP does not fall below 984 hPa and covers a wider area.
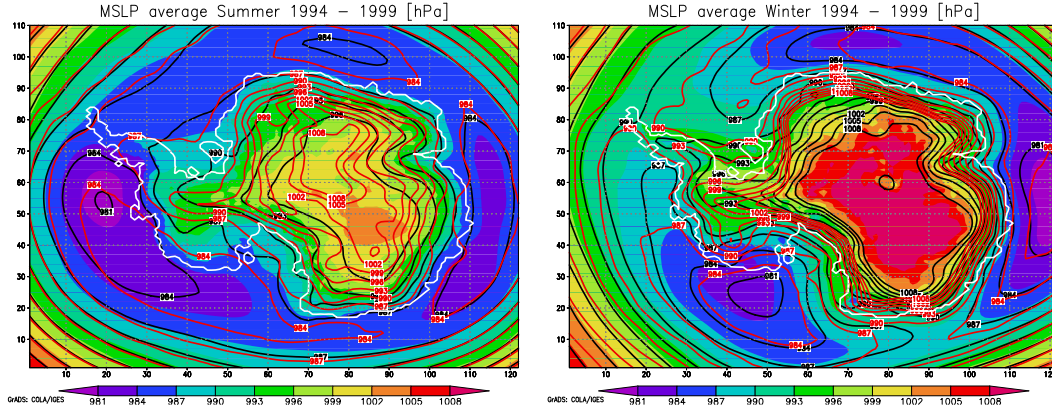
Figure 7.8: MSLP average summer (left) and winter (right) 1994 - 1999 from HIRHAM (shaded), ERA40 (black contour line) and NCEP (red contour line).

In winter (7.9 right side) the region where the temperature falls below $-40°$C spans the same area in all three simulations. In summer (7.9 left side) all three simulations are according well to each other over the ocean. Over the Antarctic Continent, HIRHAM temperatures fall below $-40°$C, whereas ERA40 and NCEP minimum temperatures are around $-30°$C, respectively $-35°$C.
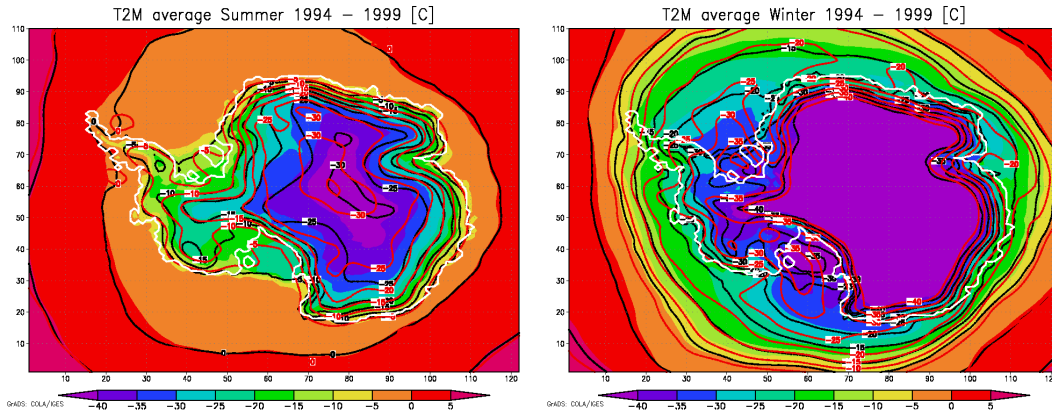
Figure 7.9: T2m average summer (left) and winter (right) 1994 - 1999 from HIRHAM (shaded), ERA40 (black contour line) and NCEP (red contour line).

In summer the absolute values of TWV and 2m-Temperature are higher than in winter, which leads to a higher bias in both cases ERA40-HIRHAM and NCEP-HIRHAM, in winter

the absolute value of MSLP is higher, resulting in a larger bias in case of NCEP compared to HIRHAM. In case of ERA-HIRHAM the MSLP bias is higher in summer than in winter, which has a different origin. During the summer months there is a higher variation in climate and shifts in the positions of low pressure systems as described above, that lead to additional bias in MSLP in case of ERA.

7.2 Vertical Structures of Temperature, Humidity and Wind

For further comparison between HIRHAM, ERA40 and radiosonde measurements, vertical profiles of temperature, specific humidity and wind were interpreted. Most important are here the lowest levels of the atmosphere up to 500 hPa. Differences are most significant there, because of differences in orographic elevation between measurement, reanalysis and model. This comparison concentrates on summer (DJF) and winter (JJA) months of the years 1994 to 1999. In each Figure an average of these months was calculated. As sounding data, every availible radiosounding from each of the stations below was used, usally 00z and 12z soundings. Some data is still missing. Since this can lead to differences between measured and simulated values, only ERA40 and HIRHAM values from times of existing measurments were taken into account.

In the following Figures three charts are depicted, a) temperature in deg C, b) specific humidity in g/kg and c) wind speed in m/s. Each graph represents values from radiosoundings (black line), the next grid point to station from ERA40 (red line) and the 4 next gridpoints to the station from the HIRHAM model (purple lines). Please note, that ERA40 is interpolated to the HIRHAM grid for comparison. Instead of an interpolation of the values from the 4 next grid points or only using the next grid point value as for ERA40, it was important to show the differences between the grid points surrounding the station for HIRHAM on which this study is focused on. Since all stations analysed here are coastal stations, the orography surrounding them is steep and HIRHAM has a different orography than the real Antarctic coast (c.f. C.1).

The following levels were analysed: 1000 hPa, 975 hPa, 950 hPa, 925 hPa, 900 hPa, 875 hPa, 850 hPa, 800 hPa, 750 hPa, 700 hPa. 650 hPa, 600 hPa and 500 hPa for HIRHAM and sounding and 1000 hPa, 925 hPa, 850 hPa, 700 hPa, 600 hPa and 500 hPa for ERA40. The sounding values were taken from the sounding level which was next to the level that was analysed (usually a difference of less than 30 hPa). HIRHAM grid points with a higher ground level then the station height are marked with a green dot, up to their respective model grid point height. Model temperature values are extrapolated down to 1000 hPa according to the barometric formula and can not be compared with measured values.
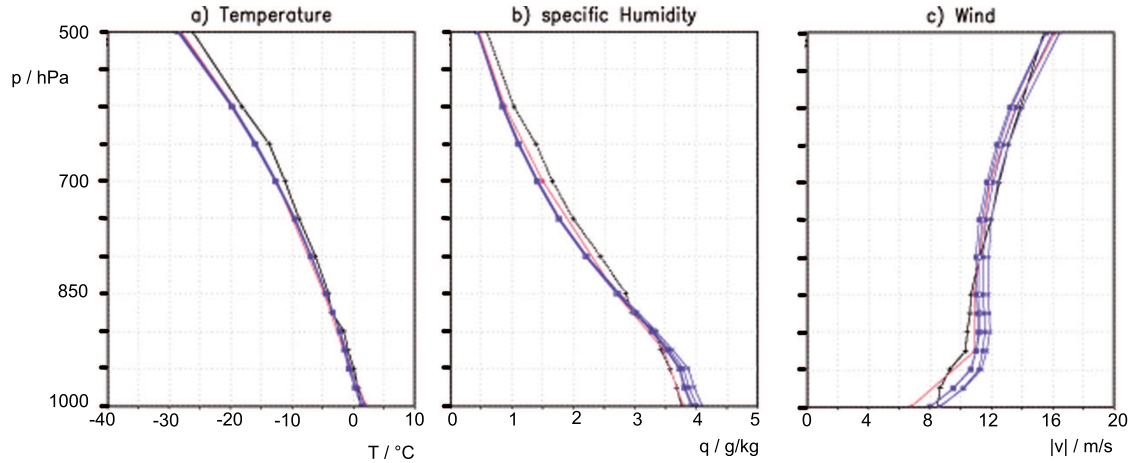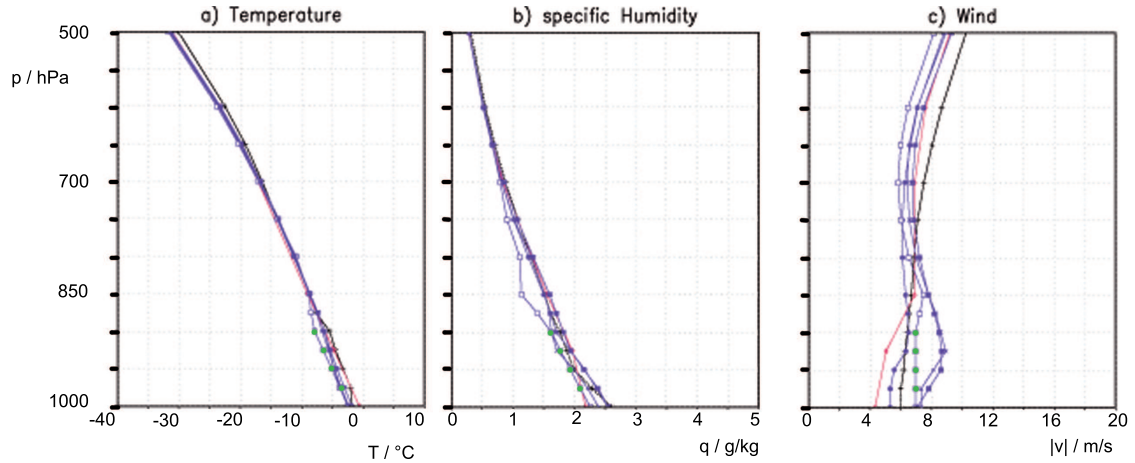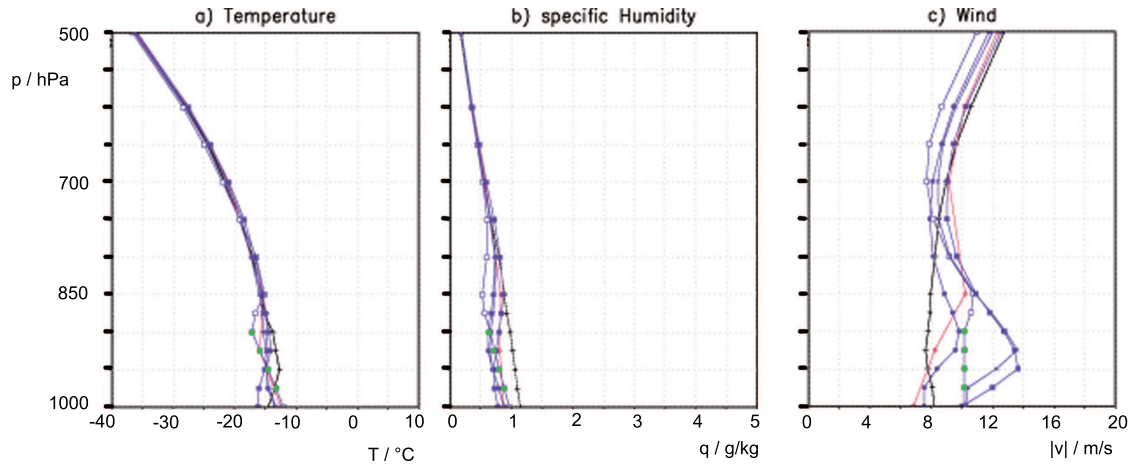
Figure 7.10: Comparison of vertical values of sounding (black), HIRHAM4 (purple) and ERA40 (red) at Bellingshausen Station in summer. Compared were the following variables: a) temperature in deg C, b) specific humidity in g/kg and c) wind speed in m/s.

In Figure 7.10 the summer mean of T, q and wind speed at Bellingshausen is shown. Temperature (a) is decreasing with height in measurement and models. All values show a good accordance with each other, in greater heights especially for ERA40 and HIRHAM, whereas sounding values are higher there (ca. 3 K). The specific humidity is also decreasing with height, with a kink around 950 hPa. ERA40 and sounding show a reasonable accordance in the boundary layer and near the ground (difference around 1 g/kg). The four HIRHAM points are deviating from each other with a maximum difference of 0.4 g/kg. They also show a deviation from ERA40 and sounding of 0.4 hPa, especially near the ground. With increasing height, ERA40 and HIRHAM are more similar to each other and the sounding values are higher than both. The wind speed is increasing with height and has also a kink around 950 hPa. In the boundary layer, HIRHAM has higher values than ERA40 and sounding, with a slight spread between the four grid points. In higher levels, ERA40 and sounding values lie in the spread of the HIRHAM grid points.
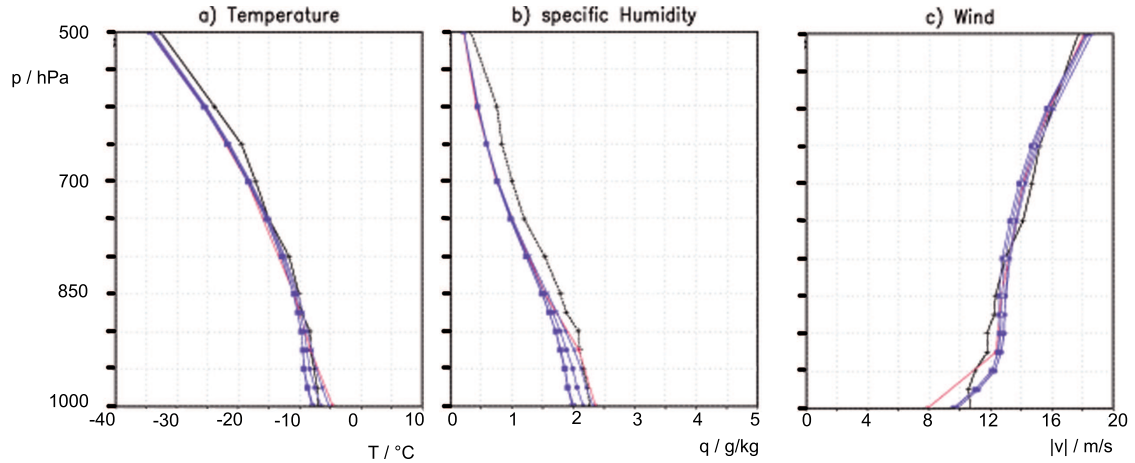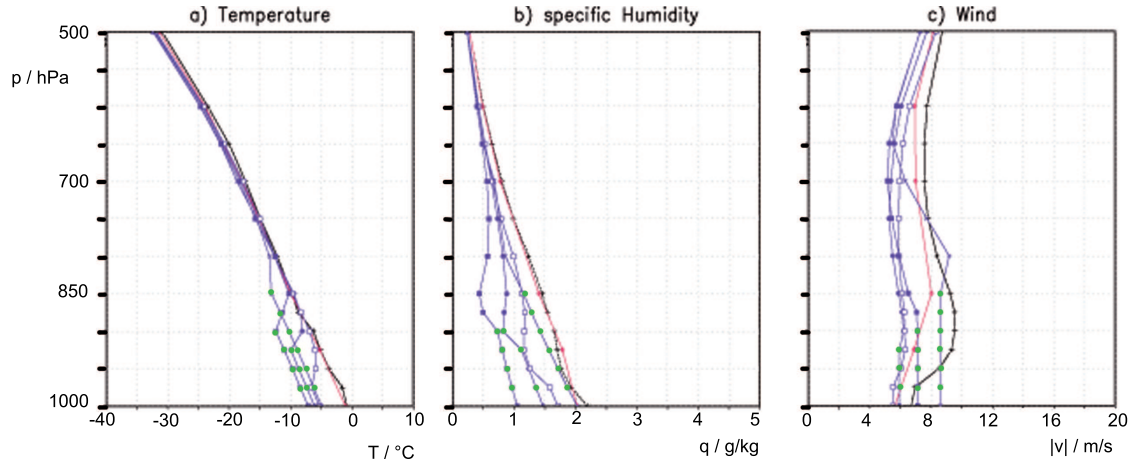
Figure 7.11: Comparison of vertical values of sounding (black), HIRHAM4 (purple) and ERA40 (red) at Bellingshausen Station in winter. Compared were the following variables: a) temperature in deg C, b) specific humidity in g/kg and c) wind speed in m/s.

In Figure 7.11 the winter mean of T, q and wind speed at Bellingshausen is shown. Temperature is below zero near the ground (-5°C to -8°C) and further decreasing with height, reaching -35°C in 500 hPa. Especially for HIRHAM the temperature gradient is increasing around 800 hPa. The accordance of temperature values of HIRHAM and ERA40 is very good in higher levels (difference of less than 1 K), the sounding is slightly warmer. HIRHAM values have again a slight spread in the boundary layer (4 K). Specific humidity has smaller values than in summer (2 g/kg vs. 4 g/kg in summer) near the ground and is decreasing with increasing height, down to less than 0.5 g/kg. The sounding values are higher (0.5 g/kg) then those of HIRHAM or ERA40, with a good accordance with ERA40 in the boundary layer, where HIRHAM values show a spread between the four grid points (0.5 g/kg). Wind speed is increasing with height from ca. 10 m/s to 18 m/s and has a kink between 900 hPa and 950 hPa. HIRHAM values show almost no spread and are in good accordance with ERA40 (less than 2 m/s difference) and sounding especially in higher levels. As there are no height differences between the grid points at Bellingshausen Station, the results of the simulation are very similar.
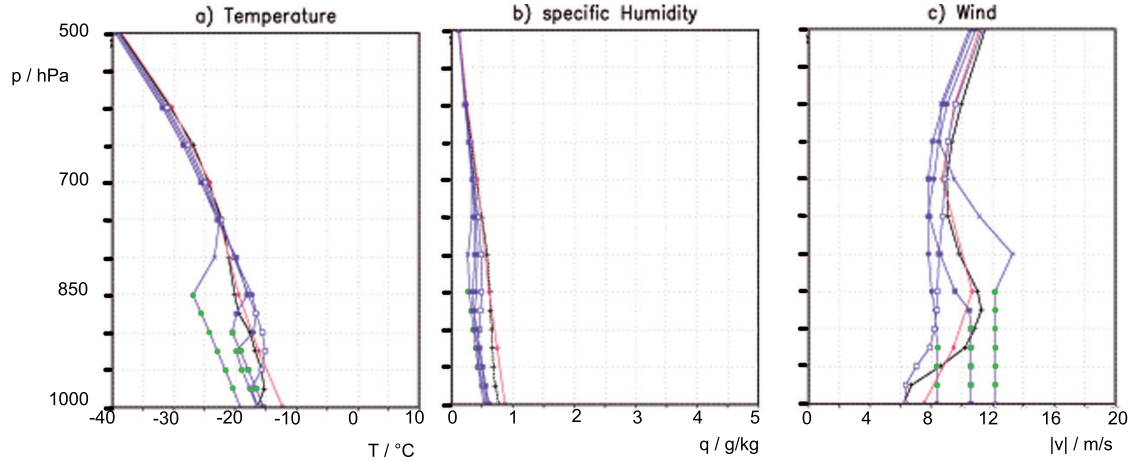
Figure 7.12: Comparison of vertical values of sounding (black), HIRHAM4 (purple) and ERA40 (red) at Casey Station in summer. Compared were the following variables: a) temperature in deg C, b) specific humidity in g/kg and c) wind speed in m/s.

In Figure 7.12 the summer mean of T, q and wind speed at Casey is shown. The temperature has values slightly below zero in low levels and is decreasing with height ($-30°$C in 500 hPa) without kink. The accordance between model, reanalysis and measurement is reasonable (less than 3 K difference), especially in higher levels, where the air is very dry (TWV of 0.5 g/kg). Only in the boundary layer HIRHAM shows a slight spread (2 K). Specific humidity has values beween 2 and 3 g/kg on the ground and is decreasing with height, also without kink. Casey is dryer than Bellingshausen in Summer by ca. 2 g/kg. Bellingshausen is located on the Peninsula, Casey on the East Antarctic Coast (c.f. 3.1). In Figure 7.3 it is shown that the Peninsula region is more humid than the East Antarctic Coast. In lower levels there is a slight spread with the values of the four HIRHAM grid points surrounding ERA40 and sounding (1 g/kg). Wind speed is almost constant with values around 6 m/s and a strong spread between all values. ERA40 has a very low wind speed in the planetary boundary layer ($4\ m/s$). Two of the HIRHAM grid points have a local maximum of 10 m/s around 925 hPa.

Figure 7.13: Comparison of vertical values of sounding (black), HIRHAM4 (purple) and ERA40 (red) at Casey Station in winter. Compared were the following variables: a) temperature in deg C, b) specific humidity in g/kg and c) wind speed in m/s.

In Figure 7.13 the winter mean of T, q and wind speed at Casey is shown. Temperature values are around $-15°$C on the ground and decreasing with height with an increasing temperature gradient reaching $-35°$C in 500 hPa. It has a very good accordance in higher levels and only a slight spread (3 K) in the planetary boundary layer. In winter the temperature is also ca 15 K lower as in Bellingshausen. Humidity is very low, even on the ground there are only values around 1 g/kg. Humidity is decreasing further with height to 0.5 mm. In higher levels the accordance between all values is good, in the planetary boundary layer the sounding values are more humid (0.5 g/kg) than ERA40 and HIRHAM. HIRHAM shows a slight spread in the lower levels (also 0.5 g/kg). The wind speed values are wide spread (6 m/s, especially near the ground. Wind spead is increasing from 700 hPa on, below 700 hPa HIRHAM and ERA40 values have a local maximum of 14 m/s, resp. 10 m/s, even a rather strong one for two HIRHAM grid points, which lie between 950 hPa and 850 hPa. Sounding values have no significant maximum and are slightly increasing with height (from 8 m/s above ground to 12 m/s at 500 hPa). At Casey Station there is a difference between the height of the HIRHAM grid points, ranging from 0 m to 872 m. At the highest grid point the deviation in specific humidity is the strongest, which can be explained with the height difference. This grid point also does not show the wind speed maximum of two of the other grid points, because it is higher than the level of the maximum wind speed which occurs at approximately 950 hPa.

In Figures 7.14 and 7.15 vertical structures of temperature, humidity and wind speed at Davis Station in summer and winter is shown. At Davis the terrain height of the four HIRHAM grid points has large differences from one point to another (c.f. Table C.1). Values below terrain height are only extrapolated with the barometric formula and are not reliable and therefore marked with a green dot.
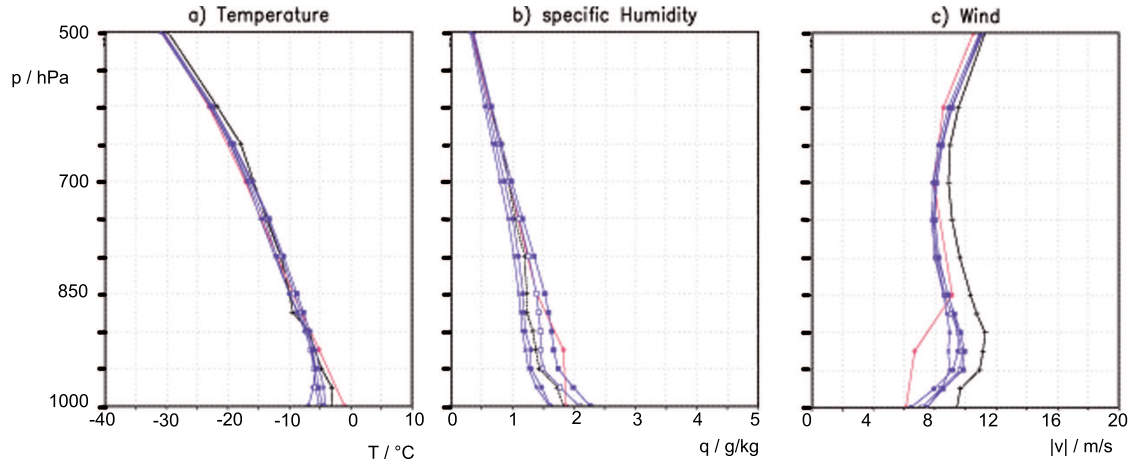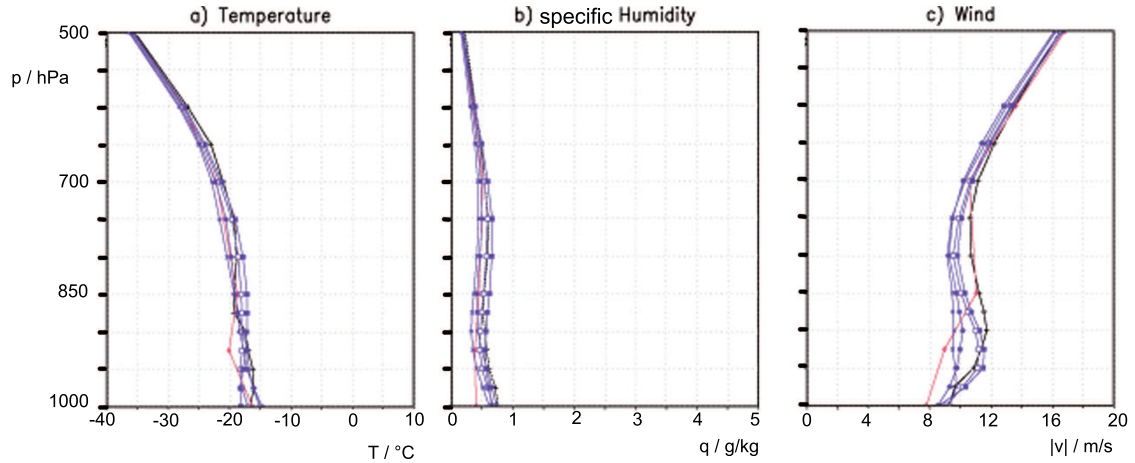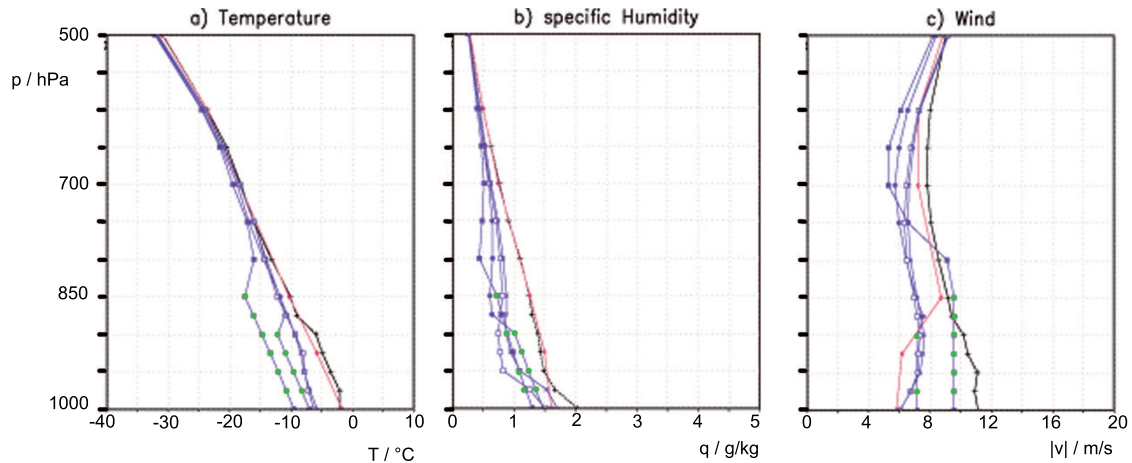
Figure 7.14: Comparison of vertical values of sounding (black), HIRHAM4 (purple) and ERA40 (red) at Davis Station in summer. Compared were the following variables: a) temperature in deg C, b) specific humidity in g/kg and c) wind speed in m/s.

In summer, the temperature is slightly below zero near the ground and further decreasing with increasing height ($-30°C$ in 500hPa). In the temperature graph, there is a good accordance between HIRHAM, ERA40 and sounding, with the sounding only slightly warmer than model and reanalysis (around 2 K difference above the inversion). On the ground, sounding values are matching the ERA values well. HIRHAM values show an inversion of ca. 5 K just above their ground, which means before extrapolation starts (marked with green dots). Specific humidity has values of 2 g/kg and less near the ground and is further decreasing with height. ERA40 and sounding have a good accordance in every level (the same values), whereas the HIRHAM values show a stronger deviation in lower levels (up to 1.5 g/kg). In HIRHAM there is also a humidity minimum which corresponds to the inversion (c.f. a) Temperature). Wind speed has a big spread in every level (ca. 5 m/s) sounding wind speed higher than ERA40 and HIRHAM in almost every level. Wind speed on the ground is almost the same as in 500 hPa (around 8 m/s), with maxima around 900 hPa (sounding), 850 hPa (ERA40) or 800 hPa (one HIRHAM grid point). Since ERA40 only has a coarse resolution, the position of the maximum differs from the corresponding point in sounding.
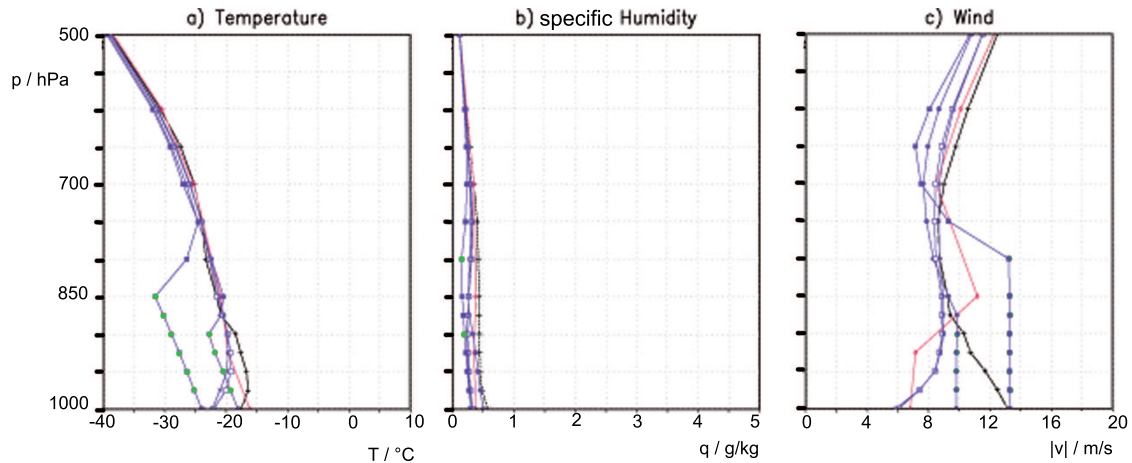
Figure 7.15: Comparison of vertical values of sounding (black), HIRHAM4 (purple) and ERA40 (red) at Davis Station in winter. Compared were the following variables: a) temperature in deg C, b) specific humidity in g/kg and c) wind speed in m/s.

In winter, temperature values have a good accordance especially in higher levels (ca. $-35°$C in 500 hPa for all datasets). In the planetary boundary layer there is a spread of up to 10 K which is due to an inversion starting over ground. Since ground heights differ from sounding and each other for the single HIRHAM point (c.f. C.1, the inverion has different heights. Sounding has only a slight inversion (2 K) and ERA40 has no inversion. Specific humidity is ca. 1 g/kg lower in winter than in summer. All values are below one and decreasing with height. ERA and sounding have a good accordance to each other in every level (less than 0.5 g/kg), but are more humid than HIRHAM in the PBL levels. Above the PBL all three are in good accordance to each other (less than 0.5 g/kg spread). Because of the dryness there is almost no inversion distinguishable. Wind speed has a slight spread of 2 m/s in higher levels, with lower wind speed values for the four HIRHAM grid points. Closer to the ground is a wind speed maximum which is well defined for ERA40 and Sounding (for both ca. 10 m/s). The HIRHAM grid points also show a (weaker) maximum or at least a kink.

In both seasons it can clearly be seen, how the temperature is starting at a minimum value at the lowest level for each grid point and rising temperatures with height in the boundary layer, until in the free atmosphere the temperature is sinking again and the values for each grid point are more similar to each other. The wind plot shows a similar behaviour with a wind speed maximum in the boundary layer. The differences of the grid points in lower levels can be explained through the different starting points of the boundary layer for each grid point.
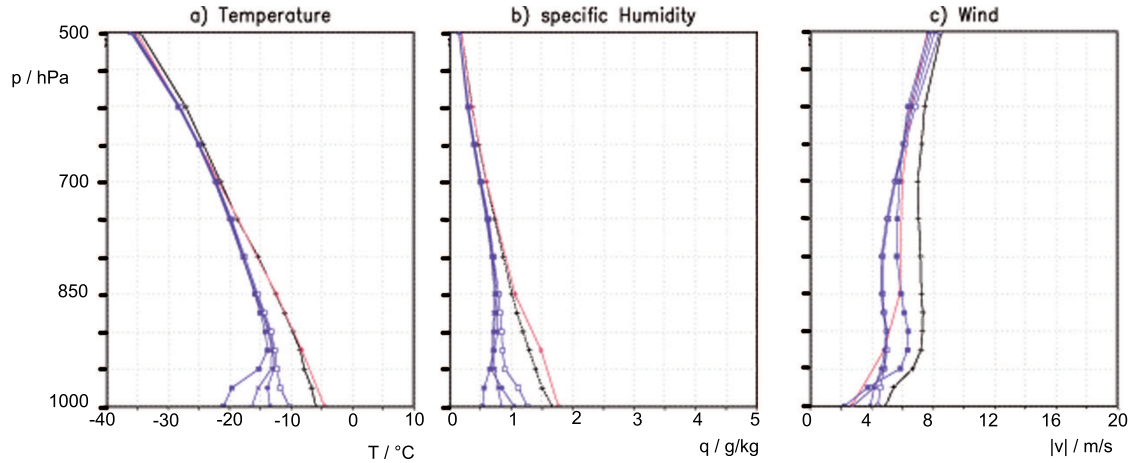
Figure 7.16: Comparison of vertical values of sounding (black), HIRHAM4 (purple) and ERA40 (red) at Dumont-Durville Station in summer. Compared were the following variables: a) temperature in deg C, b) specific humidity in g/kg and c) wind speed in m/s.

Fig. 7.16 shows the summer mean of the variables temperature, specific humidity and wind at Dumont-D'Urville Station. The temperature values range from 0°C to -10°C near the ground and is decreasing with an almost constant gradient. Here HIRHAM values are around 5 K smaller than values of ERA40 or sounding and have a spread of K. They also show a slight inversion or at least constant temperature in the lowest levels. Above these levels the accordance between models and measurement is less than 3 K. Specific humidity has values around 2 g/kg on the ground and is decreasing with height. In the lowest levels there ist a spread of $\pm$ 0.5 g/kg between the four HIRHAM grid points and ERA40 and sounding. There the inversion effect can be seen. With height the accordance between all values is increasing, all datasets have TWV values of 0.5 g/kg in 500 hPa. Wind speed is increasing from 8 m/s over the PBL to 12 m/s in 500 hPa. In the PBL wind speed has a local maximum around 900 hPa to 950 hPa for HIRHAM (10 m/s) and sounding (12 m/s) and at 850 hPa for ERA40 (10 m/s). There is almost no spread between the four HIRHAM grid points, but sounding has a 2 m/s higher and ERA a up to 2 m/s lower windspeed than HIRHAM in the PBL.
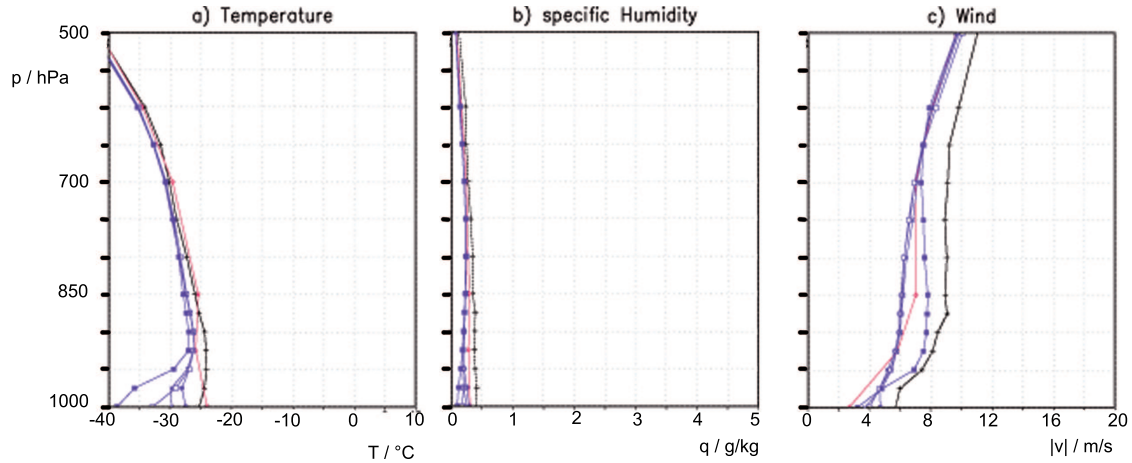
Figure 7.17: Comparison of vertical values of sounding (black), HIRHAM4 (purple) and ERA40 (red) at Dumont-Durville Station in winter. Compared were the following variables: a) temperature in deg C, b) specific humidity in g/kg and c) wind speed in m/s.

Fig. 7.17 shows the winter mean of the variables temperature, specific humidity and wind at Dumont-D'Urville Station. At the ground levels the temperature ranges from $-15°C$ and $-20°C$ and is almost constant in the PBL. ERA40 shows an inversion at 925 hPa. The temperature gradient increases with increasing height over the PBL. In all levels the accordance between reanalysis, model and measurement lies in a range of 3 K. Specific humidity is very low with values around 0.5 g/kg. HIRHAM values have a small local minimum of 0.5 g/kg in the PBL. At Dumont-D'Urville Station in winter the wind speed is higher than 8 m/s, and reaches values of 16 m/s) in the free atmosphere over the PBL. In the PBL the wind speed has values of around 10 m/s and a local maximum of 12 m/s between 850 hPa and 950 hPa. The values of this maximum show a spread of 4 m/s. Over the PBL the accordance is good. Since all grid points are approximately at station height, the accordance between model and measurements is good.
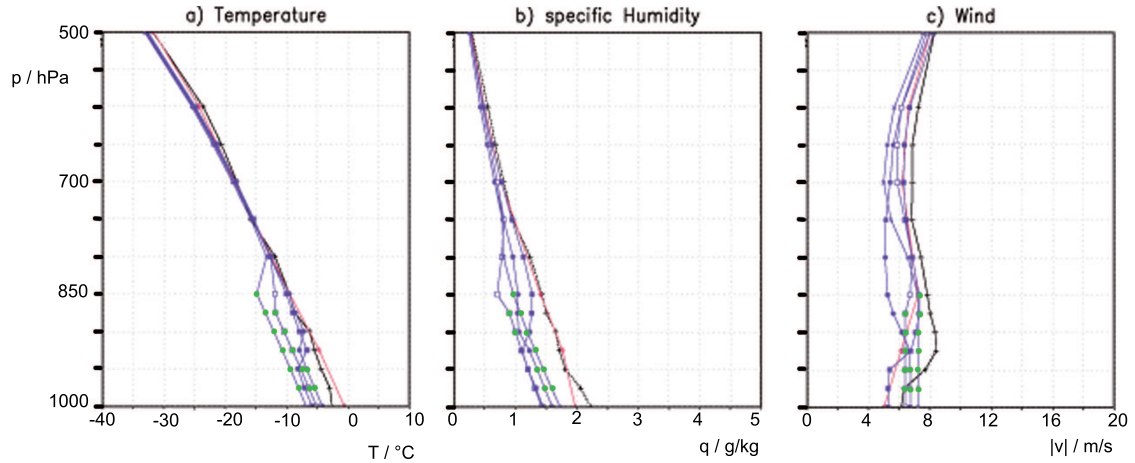
Figure 7.18: Comparison of vertical values of sounding (black), HIRHAM4 (purple) and ERA40 (red) at Mawson Station in summer. Compared were the following variables: a) temperature in deg C, b) specific humidity in g/kg and c) wind speed in m/s.

Figure 7.18 shows the 1994 to 1999 summer mean of the variables temperature, specific humidity and wind speed. At Mawson two of the four HIRHAM grid point have a high elevation, only two of them lie on sea level, further referred to as HIRHAM ground points (see C.1). As for Davis Station one must consider the necessary extrapolation. The temperature is decreasing almost linearly from values of around 0°C on the ground in cases of ERA40 and sounding. The both HIRHAM points that reach ground level are starting from less than −5°C on the ground. The higher HIRHAM points have an inversion over their starting point. From 750 hPa on the accordance between HIRHAM, ERA40 and sounding is good (spread of less than 3 K). Specific humidity has values of around 1.5 g/kg on the ground. Sounding and both HIRHAM ground points have a humid layer (TWV gradient of more than 0.5 g/kg between ground and 950 hPa) just above the ground, which ERA does not have. Above this humid layer ERA40 does not differ from the sounding. HIRHAM is almost everywhere up to 1 g/kg dryer than the other two, only at 500 hPa the accordance is well. Wind speed is almost constant in the PBL but has a big spread of 6 m/s there. In the PBL the wind speed has in almost every case a local maximum of 8 to 12 m/s. The local maxima of the HIRHAM grid points are rather weak, and HIRHAM has an up to 6 m/s lower wind speed than sounding. ERA with its coarse resolution has this maximum (9 m/s) at 850 hPa. The highest HIRHAM grid point has a wind speed of 10 m/s at its ground level. This grid point presumably lies in a katabatic wind zone.
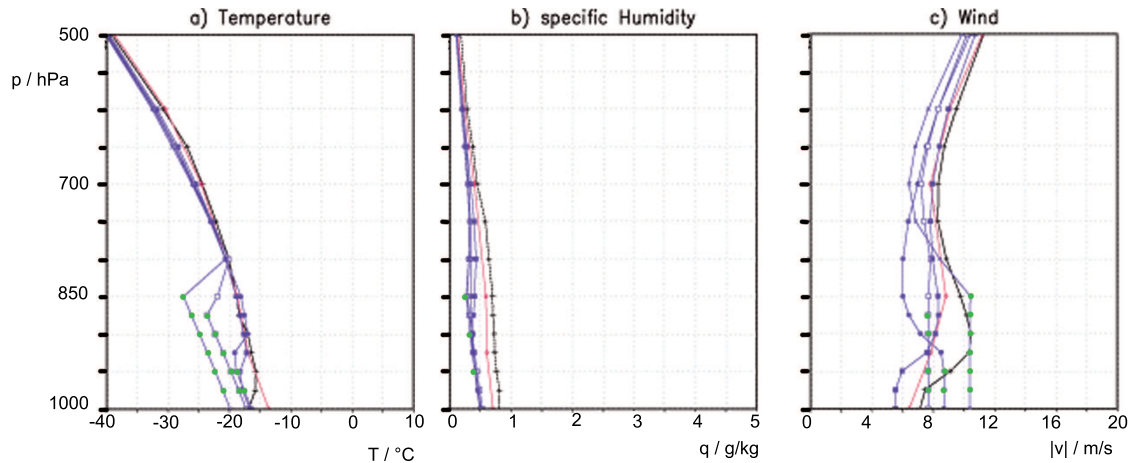
Figure 7.19: Comparison of vertical values of sounding (black), HIRHAM4 (purple) and ERA40 (red) at Mawson Station in winter. Compared were the following variables: a) temperature in deg C, b) specific humidity in g/kg and c) wind speed in m/s.

Figure 7.19 shows the 1994 to 1999 winter mean of the variables temperature, specific humidity and wind speed at Mawson Station. Temperature is only around $-20°C$ on the ground with an inversion in the sounding data (less than 5 K) and both HIRHAM ground points (5 K). The other two HIRHAM points also show an inversion, but this is even stronger (up to 10 K) and colder ($-32°C$, resp. $-23°C$) since they lie on a higher level. ERA40 data shows no inversion. Above the inversions all data sets have a spread of less than 3 K. Specific humidity is very small with only 0.5 g/kg on the ground and a difference of less than 0.5 g/kg between all data sets. Wind speed has a large spread of up to 8 m/s almost everywhere. As in summer, over the PBL the wind speed is increasing for all data sets. A significant difference of 8 m/s occurs between sounding and both HIRHAM ground points. The HIRHAM points have a minimum of 6 m/s above ground and increasing wind speed, whereas sounding wind speed is 13 m/s above ground, decreasing with height. ERA40 has a wind speed profile structure which is more similar to that of HIRHAM, 7 m/s above ground, and a local maximum of 11 m/s in 850 hPa.

The reasons for the differences between the grid points are the same as at Davis Station. The elevated grid points are each having their respective boundary layer, with temperature inversion and wind speed maxima, only that the ground level for the elevated grid points is higher than the station height.

Figure 7.20: Comparison of vertical values of sounding (black), HIRHAM4 (purple) and ERA40 (red) at McMurdo Station in summer. Compared were the following variables: a) temperature in deg C, b) specific humidity in g/kg and c) wind speed in m/s.

In Fig 7.20 the vertical plots of McMurdo station in summer are shown. The temperature is around $-5°$C for ERA40 and sounding. HIRHAM temperature is for all four grid points lower ($-21°$C to $-10°$C) and they have a strong inversion of up to 10 K, above HIRHAM ground height. Three of the four HIRHAM grid points are sea points that are not covered with sea ice in summer (c.f. 8.6 and 8.7 for a plot of the seasonal sea ice extent), which leads to a temperature difference of up to 10 K between HIRHAM grid points. Additionally the land point is treated as glacier point with ice characteristics. Up to 925 hPa there is a spread between the HIRHAM values. ERA40 and sounding are everywhere in good accordance, HIRHAM values are similar to the two other data sets only from 700 hPa on. The same happens for specific humidity, ERA40 and sounding are in good accordance and HIRHAM shows strong deviations below 700 hPa. HIRHAM is dryer than ERA40 and sounding which have ground level values of around 1.5 g/kg. HIRHAM values have a spread of almost 1.0 g/kg which reaches up to 925 hPa. A comparison of wind speed is complicated because of the different HIRHAM ground level heights. Above 700 hPa, the wind speed shows a similar behaviour for all data sets, with differences of 4 m/s.

Figure 7.21: Comparison of vertical values of sounding (black), HIRHAM4 (purple) and ERA40 (red) at McMurdo Station in winter. Compared were the following variables: a) temperature in deg C, b) specific humidity in g/kg and c) wind speed in m/s.

In Fig 7.21 the vertical plots of McMurdo station in winter are shown. The temperatures are around $-25°C$ near the ground for ERA40 and sounding. HIRHAM has a huge spread of 10 K. Every HIRHAM grid point is at least 10 K colder than ERA40 and sounding which are in good accordance to each other (less than 3 K difference). Sounding and HIRHAM show inversions, in case of sounding it is weak (less than 4 K), in the HIRHAM grid points the inversion is stronger (up to 15 K for the land point). Specific humidity is always smaller than 0.5 g/kg. The wind speed has values of around 5 m/s and is increasing with a strong gradient up to 900 hPa, where the gradient becomes smaller. Sounding has in every level the highest wind speed (6 to 10 m/s) and deviates from HIRHAM and ERA by up to 5 m/s. Three of the four HIRHAM points are in good accordance with each other and ERA40. The temperature differences at McMurdo station can be explained through the different land-sea-fractions. Land points are always treated as glacier and over ice the temperatures are lower than over open sea for example, which can occur for the other grid points. So since the temperature is an average over the whole winter season, the sea points experiences also ice free phases with higher ground temperature, whereas this does not occur for the land point, which keeps its cold temperature the whole time.

Figure 7.22: Comparison of vertical values of sounding (black), HIRHAM4 (purple) and ERA40 (red) at Syowa Station in summer. Compared were the following variables: a) temperature in deg C, b) specific humidity in g/kg and c) wind speed in m/s.

Figure 7.22 shows the summer mean of the variables temperature, specific humidity and wind speed at Syowa station. At this station all four HIRHAM grid points have a significant elevation over sea level and are higher than the station itself (Table C.1). So it is hard to compare HIRHAM grid point to ERA40 and sounding on lower levels. Near the ground, ERA40 and Sounding have temperatures of around $-5°C$ to $0°C$, with ERA40 values extrapolated to 1000 hPa. From these values, temperature is decreasing linearly with increasing height. HIRHAM grid points each have an inversion of ca. 5 K from their ground level on. Over this inversion the accordance between the different data sets is good (less than 3 K difference). Specific humidity starts from values of around 2 g/kg on the ground levels in ERA40 and sounding data sets. ERA40 and sounding are more humid than HIRHAM by 1 g/kg, especially in the PBL. Over the ground sounding has a humid layer, whereas HIRHAM grid points start from their ground level with lower humidity which is increasing upt to 0.5 g/kg for a few layers until it reaches a local maximum. Wind speed has values of around 6 m/s to 8 m/s in every level. The spread between data sets and between the single HIRHAM grid points is up to 4 m/s. In every level, that is not extrapolated, sounding has the highest wind speed.

Figure 7.23: Comparison of vertical values of sounding (black), HIRHAM4 (purple) and ERA40 (red) at Syowa Station in winter. Compared were the following variables: a) temperature in deg C, b) specific humidity in g/kg and c) wind speed in m/s.

Figure 7.23 shows the winter mean of the variables temperature, specific humidity and wind speed at Syowa station. Temperature is starting fom ca. $-15°C$ at ground level (ERA40 and sounding) and, after a small inversion, sinking with a slightly increasing gradient. Sounding and HIRHAM grid points have an inversion over their respective ground level, which is with 10 K strong for the highest HIRHAM grid points. ERA shows no inversion, due to the extrapolation of the values to groud height. Over the inversions, where temperature is sinking again, the accordance between the different data sets is good (less than 3 K spread). Specific humidity is very small with values between 0.3 g/kg and 0.8 g/kg. Sounding is the most humid data set and HIRHAM the dryest. The accordance between the datasets is not well especially in the PBL, they are spreading up to 0.6 g/kg with absolute values of less than 1 g/kg. Wind speed has a spread of 6 m/s between the datasets and the single grid points. It has a minimum of 5 m/s at the beginning of the PBL, around 700 hPa. The lowest two HIRHAM grid points, as well as sounding and ERA40 have a lower wind speed on the ground levels, which is increasing to a local maximum (ca. 8 m/s) that lies in the PBL.

Also at Syowa Station, as at Davis and Mawson, the difference in grid point height leads to different values of the grid points at the same pressure level, because each grid point has its own boundary layer with the typical behaviour. Only in the free atmoshere the values are more similar to each other, when the influence of the ground is lower. Massom et al. (1998) analysed polynyas in East Antarctica and found among others a polynya near Syowa Station. Due to the higher humidity over open water, the results from the sounding show a higher humidity than HIRHAM simulation where smaller polynyas can not be resolved. The Syowa Polynya they analysed had a mean area of 2500 km^2 which is grid area size and unlikely to be clearly resolved.

As a summary of this comparison it can be stated that, in higher levels HIRHAM has mostly a good accordance to ERA40, because in these levels the influence of different

ground setups is less important. ERA40 values are similar to the sounding, also near the ground, where differences between ERA40 and HIRHAM occur in several cases even without extrapolation of data to 1000 hPa. In these cases HIRHAM ground values differ from ERA40 boundary values, because of the different ground setups. ERA40 values, on the other hand, are depending on measurements, also soundings. The spread of HIRHAM values from the different grid points near the ground is mostly due to different ground height. In many cases HIRHAM grid points are higher than station height as can be seen in Table C.1, which leads to dryer air parcels, lower temperature and wind that is more influenced by katabatic winds, that tend to be especially strong at the steep coastal orography. Other grid points lie over sea ice and are influenced trough evaporation and melting processes. This can for example lead to higher temperatures over sea ice points during melting periods. These differences are less important in greater heights. As seen for example in Figure 7.23, the comparably coarse structure of ERA40 cannot depict possible inversions as clearly as a RCM like HIRHAM can. A more accurate interpretation of how sea-ice-grid-points differ from land stations regarding TWV can be found in the next section.

In comparison with measurements, different results of the models, especially in lower layers, occur because of a coarse model resolution. Larger polynyas cover an area of several 1000 km^2 (c.f. Massom et al. (1998)), which is about the size of the HIRHAM grid area of 50×50km and bigger. Still, especially smaller polynyas might not be resolved accourately or at all in the model. Around the coast of Antarctica, often due to a katabatic wind regime, latent heat polynyas are the most important polynya types, with a latent heat transport of several 100 W/m^2 and water vapour transport from the open sea areas (c.f. Massom et al. (1998)).

7.3 Local comparison of total water vapor - time series

Figures 7.24 to 7.27 show the results of the comparison in TWV time series and a time series of the bias between sounding and all others. The plots show monthly averaged TWV for each station from January 1994 to December 1999. The upper half plots show absolute values of TWV from the 4 next HIRHAM grid points, GPS, NCEP, ERA40 and Sounding. The lower half depicts the difference between Sounding and HIRHAM, GPS, NCEP and ERA40. The sounding is considered as reference and any biases are related to this reference.
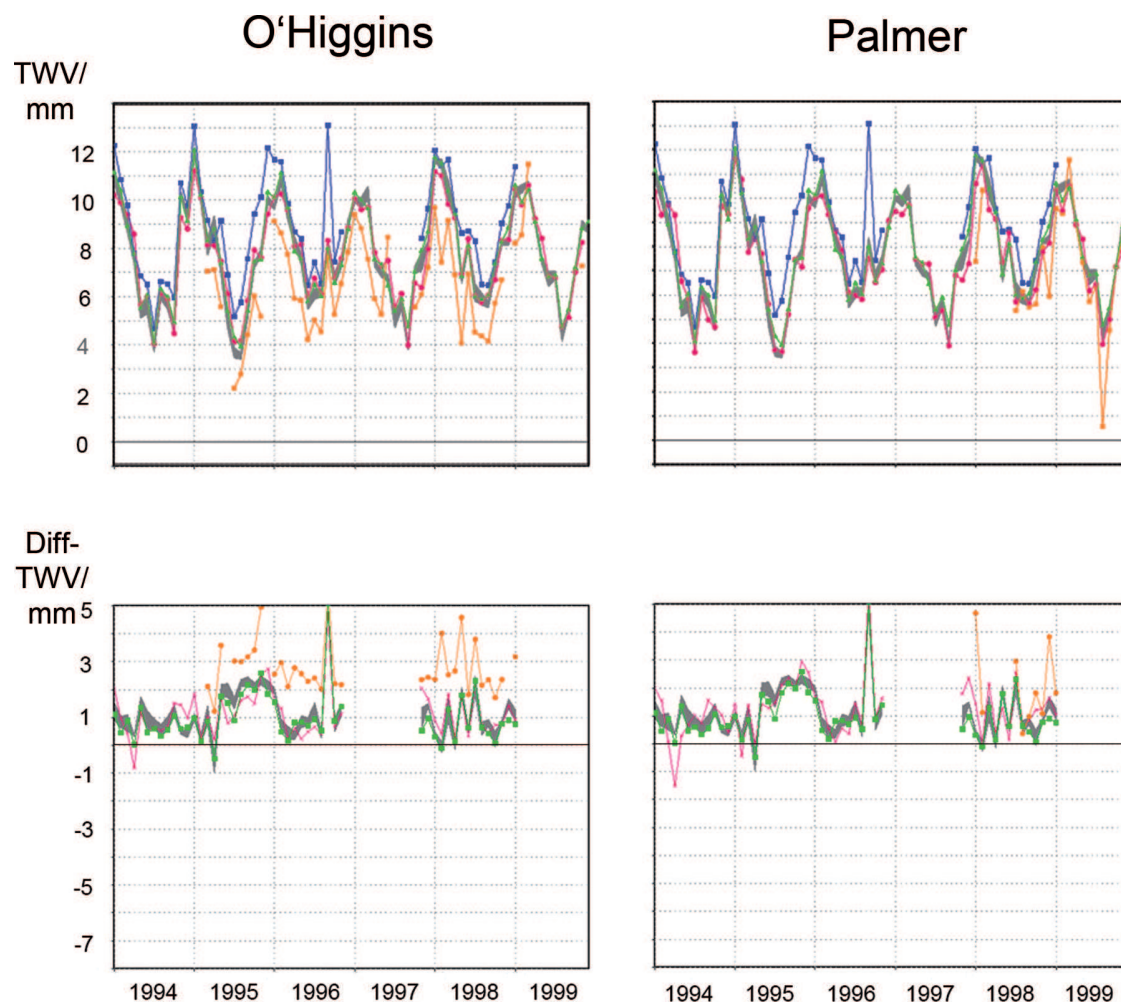
Figure 7.24: Time series of TWV (upper) and TWV-bias (lower) at O'Higgins and Palmer. TWV: Grey: HIRHAM (4 next gridpoints), orange: GPS, red: NCEP, blue: Sounding, green: ERA40. TWV-bias: Grey: Sounding-HIRHAM (4 next gridpoints), orange: Sounding-GPS, red: Sounding-NCEP, green: Sounding-ERA40.
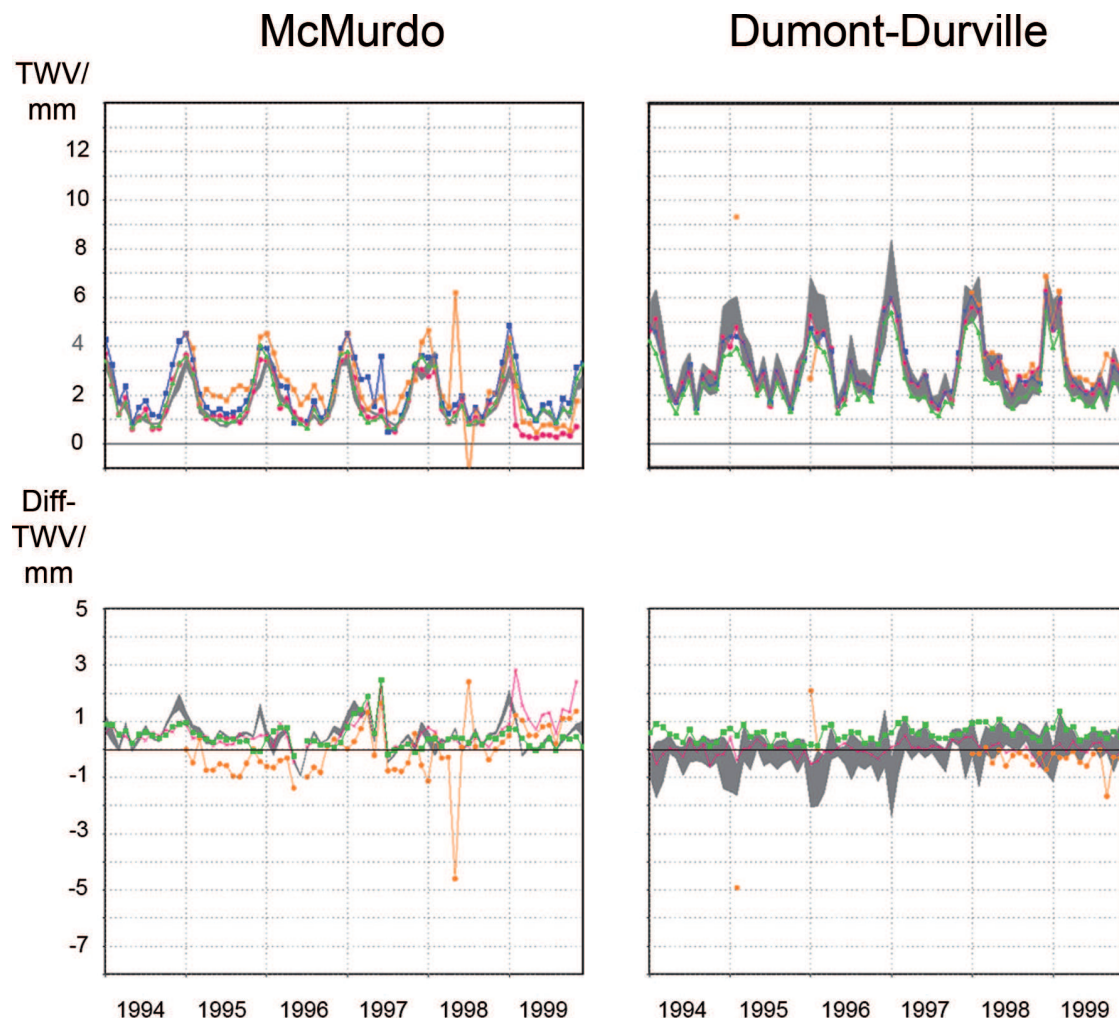
Figure 7.25: Time series of TWV (upper) and TWV-bias (lower) at Dumont-D'Urville and McMurdo. TWV: Grey: HIRHAM (4 next gridpoints), orange: GPS, red: NCEP, blue: Sounding, green: ERA40. TWV-bias: Grey: Sounding-HIRHAM (4 next gridpoints), orange: Sounding-GPS, red: Sounding-NCEP, green: Sounding-ERA40.
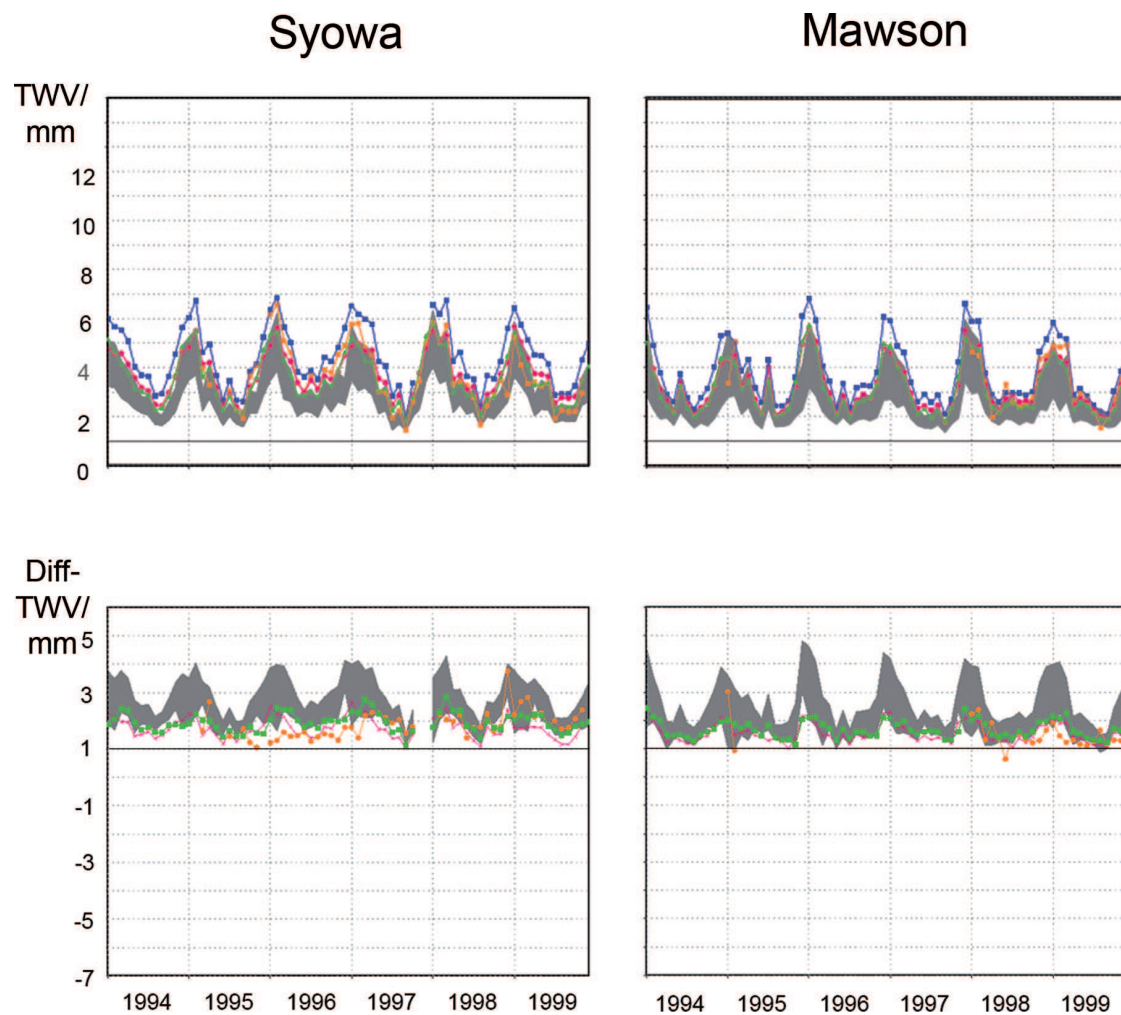
Figure 7.26: Time series of TWV (upper) and TWV-bias (lower) at Mawson and Syowa. TWV: Grey: HIRHAM (4 next gridpoints), orange: GPS, red: NCEP, blue: Sounding, green: ERA40. TWV-bias: Grey: Sounding-HIRHAM (4 next gridpoints), orange: Sounding-GPS, red: Sounding-NCEP, green: Sounding-ERA40.
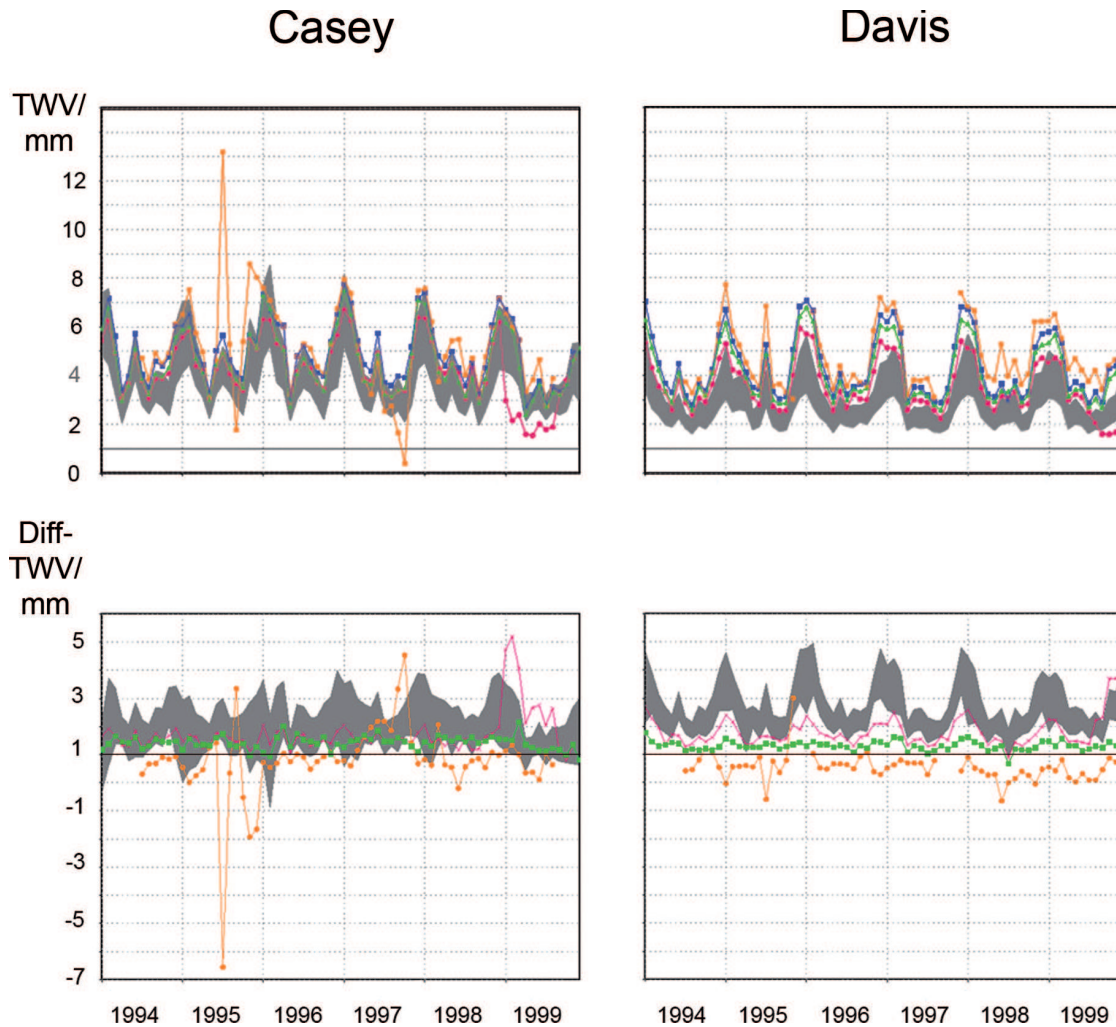
Figure 7.27: Time series of TWV (upper) and TWV-bias (lower) at Casey and Davis. TWV: Grey: HIRHAM (4 next gridpoints), orange: GPS, red: NCEP, blue: Sounding, green: ERA40. TWV-bias: Grey: Sounding-HIRHAM (4 next gridpoints), orange: Sounding-GPS, red: Sounding-NCEP, green: Sounding-ERA40.

Palmer and O'Higgins show the same data except for the GPS measurements, with sounding data and model results from Bellingshausen station. This leads to differences between TWV from sounding and TWV from GPS. On both stations a dry bias is found which is the result of the distance of Bellingshausen and Palmer (2 mm), respectively O'Higgins (3 mm). Since Bellingshausen Station is farthest North, its TWV values are higher than those of the other two stations in the comparison, which are located more to the South and are thus drier. On the Peninsula, the soundings show the highest TWV values, compared to the other stations. One reason for this behaviour could be that the influence of the sea is bigger than assumed in the models. The HIRHAM results are almost identical to each other for the four grid points and are almost the same as the ERA40-values, which was expected, as these grid points lie near the boundary zone of HIRHAM.

The difference between HIRHAM and NCEP is less than 1 mm. In this flat orography, the differences between global and regional models should not be significant, so the results show a good performance of HIRHAM compared to the reanalyses. The analysis of the standard deviation 8.1 gives further explaination for this behaviour.

TWV at McMurdo also has only a small variance between the four HIRHAM grid points. Only the third grid point is above sea level and a complete land point. As it has a height of only 31 m, the difference to real station height of 24 m is only 7 m. HIRHAM and the reanalyses have a difference of less than 4 mm. Only NCEP shows too small TWV values during 1999. Like at the Peninsula, the sounding data has higher humidity than the models, but contrary to the Peninsula stations, here the GPS still shows a higher humidity than the sounding most of the time. Due to the northern wind direction at McMurdo most sondes drift to the dryer south, especially in winter, whereas GPS measure from the north through humid air (c.f. 7.4). Chenoli et al. (2013) found strong wind events at McMurdo station at wind directions of 135° to 180° and 45° to 90°, but with a high variability in occurence.

The biggest spread of TWV across the HIRHAM grid points can be found at the East Antarctic coastal stations (Syowa, Mawson, Davis and Casey). All of the four stations have a wide spread of grid point height around the station of more than 1000 m height-difference. At Casey the grid point with the least difference to the sounding has a bias of less than 1 mm. Casey has a station height of 42 m, and the third grid point has a height of 0 m, whereas the second lowest grid point (grid point number 4) has a height of 217 m. Both Syowa and Davis have lowest grid points that are higher than their original station height, 208 m lowest grid point height compared to 13 m station height at Davis and 328 m lowest grid point height compared to 29 m station height at Syowa. At points with a higher model orography less TWV is simulated. The situation at Mawson seems to be more complicated, as it has two grid points at 0 m, but still shows a pronounced bias of 3 mm in summer months. TWV at Syowa, Mawson and Casey is in good agreement between HIRHAM and ERA40 values, the green line in the upper panel lies mostly in the shaded areas of the plots. For the summer months at Casey station, HIRHAM4 seems to resolve the higher TWV values even better than ERA40.

Dumont-D'Urville also has almost the same TWV values at all four grid points. Its four grid points all have the same height of 0 m, so there can be no TWV differences between the HIRHAM points due to different grid point height. It is the only station, where HIRHAM calculates higher TWV values than sounding or ERA40. It is also the only station with a grid point height below station height for all four grid points. Lower grid points tend to have higher TWV values than higher grid point, or, in this case, the station. The better display of orographical features of HIRHAM in comparison with ERA40, leads to a more accurate display of TWV.

In Table C.2, the root mean square error (RMSE), the relative RMSE and the temporal correlation between sounding data and HIRHAM for each grid point at the Antarctic stations is shown. It can be seen that Dumont-D'Urville, McMurdo and certain grid points of Casey, Davis, Mawson and Syowa only have a small RMSE of around 0.4 mm. All other values are around 1.1 mm or less. The higher RMSE at Bellingshausen still leads

to a small relative RMSE, due to the higher values of TWV on the Peninsula. For the East Antarctica stations, the RMSE should be lower than at Bellingshausen, higher values indicate uncertainties. The correlation is high for all stations except Syowa, with values of around 0.9 mm and higher, even for grid points that have a bias. This indicates the good representation of temporal variability on seasonal and interannual scale in HIRHAM.

7.4   Comparison of Measurement Methods

Sounding and GPS retrieval are two technically different methods to measure TWV. TWV from sounding is calculated from the vertical integration of specific humidity (q). Therefore it is also known under the other name QVI (q vertically integrated). GPS satellites retrieve TWV via the measurement of a signal delay (c.f. 5.3. The different methods will result in differences of the measured TWV values. In this chapter possible reasons for these differences will be analysed.

In Figure 7.28, a comparison between the main wind directions in summer and winter, retrieved from sounding and an example GPS satellite track for each East-Antarctica station is shown. The different retrieval directions deduced from these Figures will show one explaination for different results of TWV measurements of both methods. Since the satellite tracks are highly repetitive, the shown example of each station is representative for all measurements, provided by Christoph Knöfel (TU Dresden). GPS and Sounding provide significantly different methods of water-vapor-retrieval. Not only the usage of different instruments, but also the different volumes that are measured, have to be taken into account. Radiosondes use direct measurements of relative humidity, from which TWV is calculeted after the measurement. GPS measures TWV via signal delay. TWV retrieval via GPS uses signals of at least three satellites and is thus measurering a volume instead of a path as the radiosondes. Furthermore, no GPS-satellite has an elevation of more than 60° south, which leads to a horizontal component in the measured volume. Radiosoundings also show a horizontal component in their measurements, but for different reasons. As the radiosondes drift horizontally with the wind, they also do not measure exactly vertical over the station. Both measuring directions can be significantly different from each other.
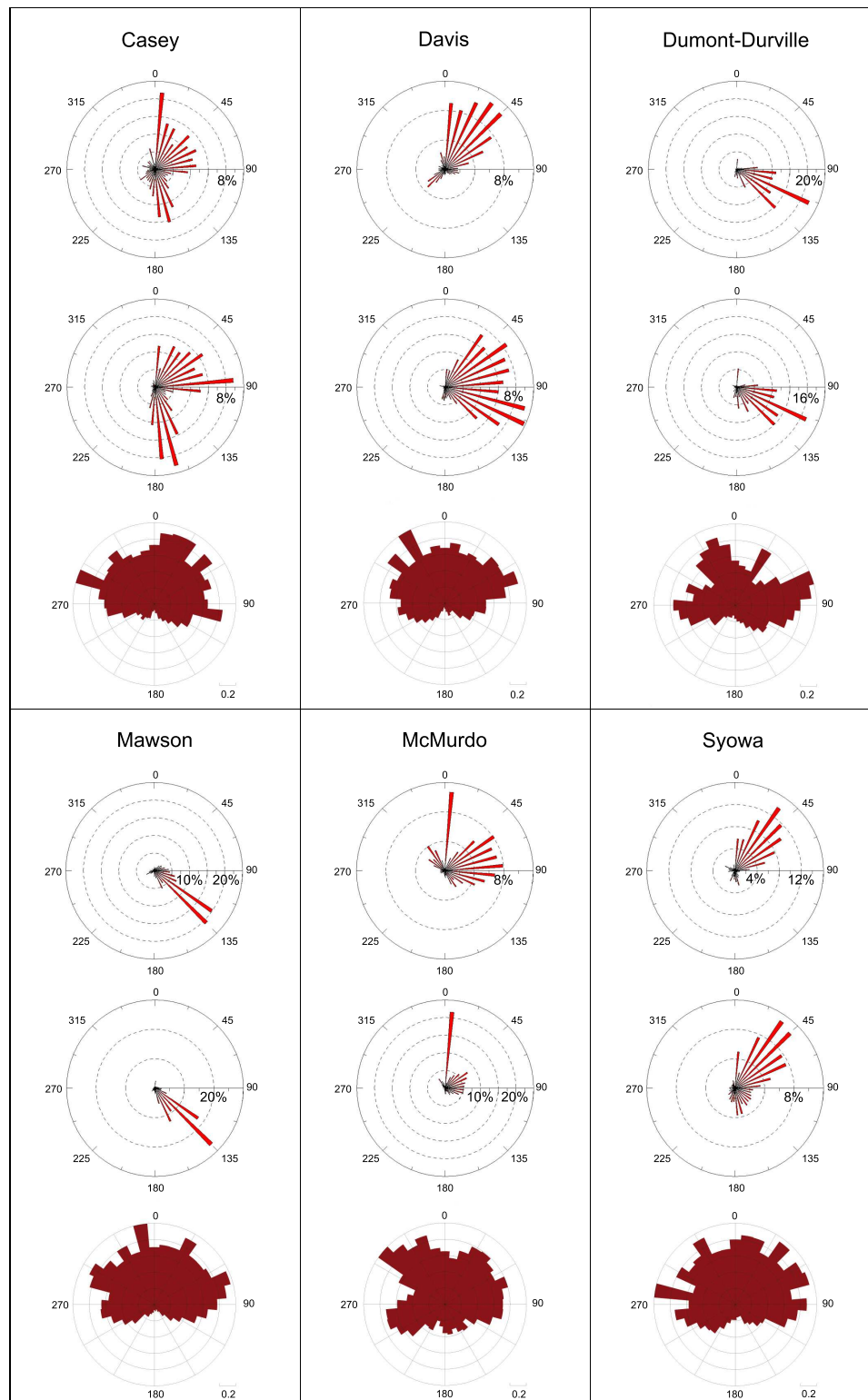
Figure 7.28: Comparison of main wind directions in summer (upper) and winter (middle) from the lowest sounding level (1994 to 1999) and elevation and azimut of satellite tracks (lower) for one example day (27 January 1998) for selected East Antarctica stations. Note the different scales.

The stations are listed in alphabethical order from Casey (a) to Syowa (f). The upper plot of each panel depicts the main wind direction from the lowest sounding level in summer (DJF), the middle plot shows the main wind direction in winter (JJA) and the lower plot is a graphic of the measuring direction of the GPS-satellites from one example day. The main wind direction for summer and winter is calculated via bins from the wind directions at the lowest levels of the sounding, even though the wind direction can be changing with height. Each of the 12 hourly measurements from summer respectively winter from 1994 to 1999 is ordered by 10° bins, starting from 0° to 10° and so on. The plot shows the amount of counted wind directions in each bin as percentage of all derived directions. As GPS satellite-tracks are highly redundant, it is enough to show one example day. The 27 January 1998 is chosen, because it is the first day with measurements at each station. A detailed description can be found in 6.1.5. In the Figure, the elevation and the azimut of each satellite while it is measuring is shown. The main measuring direction of the GPS-Satellites covers a region from Northwest over North to Northeast.

The main wind directions in summer and winter are similar for each station. This is due to the steep orography at the Antarctic coast, katabatic winds tend to blow mainly from one direction. Compared to the satellite tracks, the radiosondes often drift to another direction than the measuring direction of the satellites. If one takes Syowa as an example, the main wind direction at the lowest level of the sounding is around 40° to 50°, in summer as in winter. Most of the radiosondes will thus drift to the Southwest, which means a drift along the coast. As GPS has only a small dry bias compared to the radiosounding (c.f. 7.3, it could be assumed that the sondes are still measuring humid air from the sea. The dry bias could be a result of technical differences of both methods.

At McMurdo, the main wind direction is 10°. Another two maxima can be found around 320° and 80°. This could be explained through two hills that lie north of the station and let the wind flow between them (first maximum at 10°) or around them (second maxima eastern and western of the hills). McMurdo is a good example for the results of the different measuring directions of sounding and GPS. Most sondes tend to drift to the South due to the northern wind direction, which means a drift to continental and drier regions. Most GPS measurements are made from a northern direction, the sea, which is more humid then the continent. Accordingly, the TWV time series of McMurdo in Fig. 7.24 and 7.25 shows a humid bias of GPS compared to the sounding.

Another humid GPS bias can be seen at Casey Station. It has got two main wind directions, one around 45° with a more northern direction in summer and a more eastern direction in winter, which lead to a radiosonde drift to the Southwest. The other main wind direction is 170°, with less influence in summer. In both seasons, the wind blows from the Northeast most of the time, shifting the radiosondes over the continent which leads to a higher humidity in GPS measurements, just like McMurdo.

Davis also shows a similar pattern. The main wind direction lies around 30° in summer and between 40° and 120° in winter. Most radiosondes thus drift to the Southwest, over the continent and measure different air masses than GPS. Davis has like Casey and McMurdo a humid bias.

Mawson has a main wind direction of 135° for both summer and winter. This means, most

radiosondes drift to the northwest which lies in the mean measuring region of GPS. One would assume that this results in only a small bias between GPS and sounding and by taking a look at Figure one can see that the bias is indeed not too big.

This is also the case for Dumont-D'Urville. It has almost no bias between Sounding and GPS. Figure 7.28 shows, that the main wind direction for Dumont-D'Urville lies around 120°. The radiosondes should drift to Westnorthwest and measure humid sea air, just like the GPS satellites.
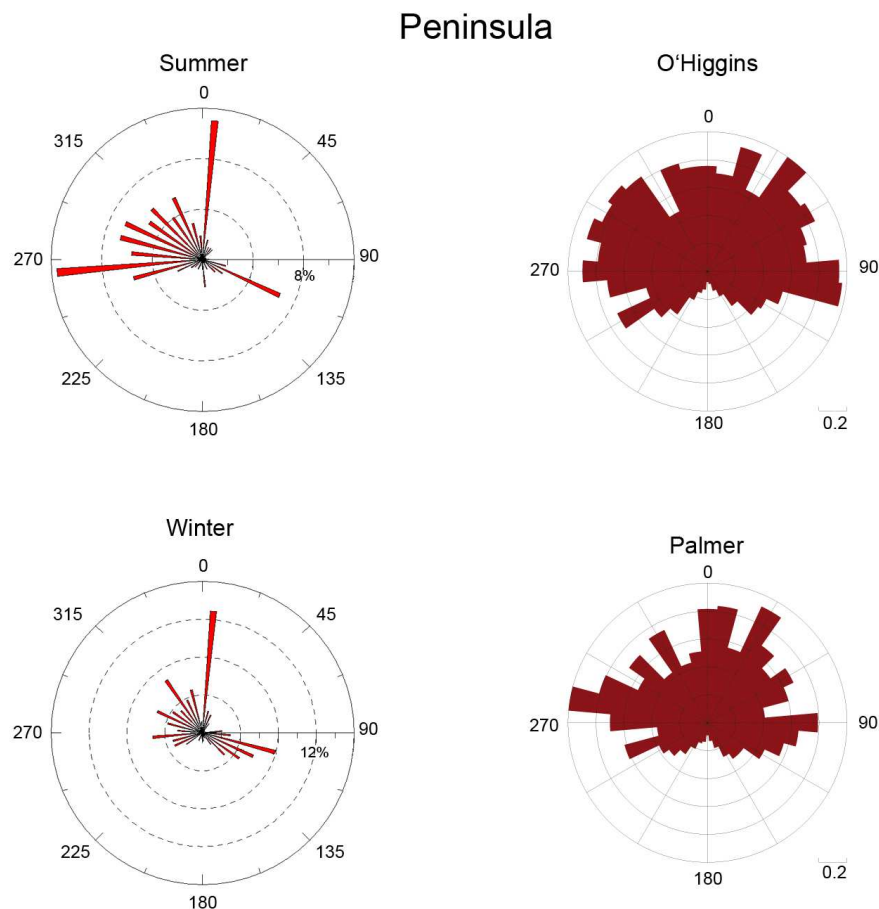
Figure 7.29: Comparison of main wind direction in summer (upper left) and winter (lower left) from the lowest sounding level (1994 to 1999) at Bellingshausen with elevation and azimut of an example satellite track of one day (26 January 1998) of O'Higgins (upper right) and Palmer (lower right).

In Figure 7.29 the main wind directions at Bellingshausen in summer (upper left) and winter (lower left) as well as the measuring directions of the GPS satellites at O'Higgins

(upper right) and Palmer (lower right) are depicted. The TWV values on the Peninsula are in general higher than at the continental stations (see Figures 7.24 and 7.25), because of the sea climate. The main wind direction should not have a big influence, because the air over King-George-Island should be as humid as the surrounding sea air. Considering the main wind directions at Bellingshausen, it can be seen that one main wind direction is north (in summer and winter) with two other maxima in summer at 260° and 120°. The GPS measuring direction is again north for both stations. Both stations (Palmer and O'Higgins) have a dry bias of around 3 mm which is more than the bias of the model and the reanalyses. As stated before the measurement of different air masses can not be the reason for this. Since Palmer and O'Higgins lie south of Bellingshausen, they should have a lower specific humidity than Bellingshausen station.

As an additional comparison, here the wind directions of the respective seasons and stations from the ERA40 run of HIRHAM (1994 to 1999) and the ERA40 reanalysis are shown: (Figures 7.30 to 7.43):
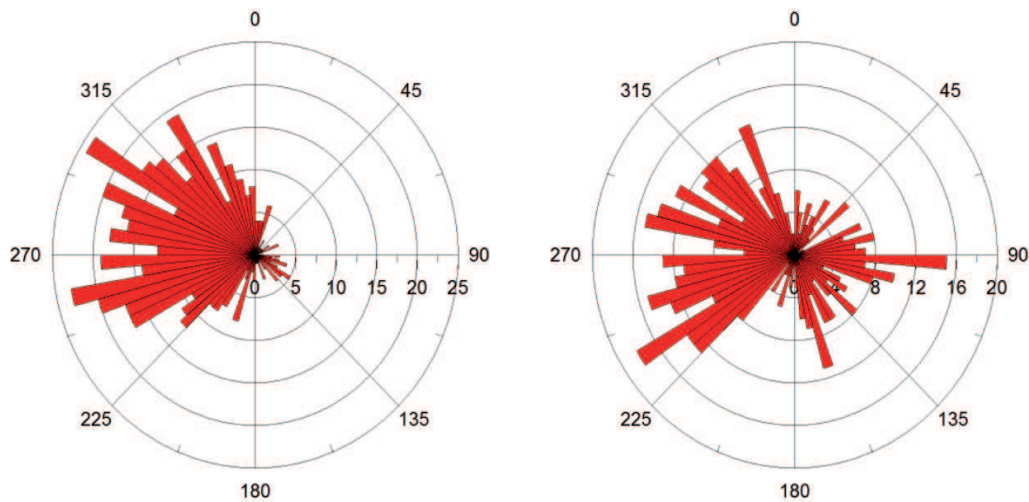
Figure 7.30: Main wind direction in summer (left) and winter (right) 1994 to 1999 at Bellingshausen. HIRHAM, ERA40 run.
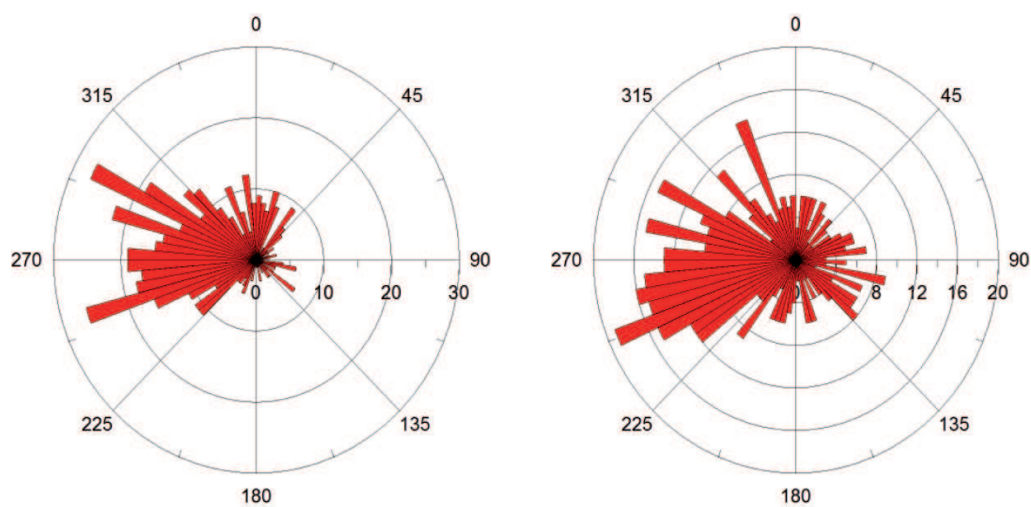
Figure 7.31: Main wind direction in summer (left) and winter (right) 1994 to 1999 at Bellingshausen. ERA40.
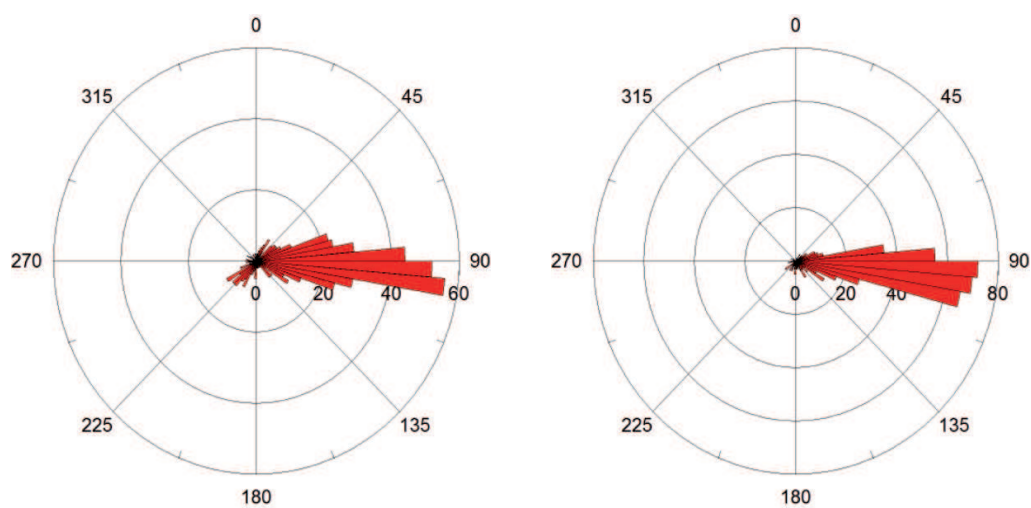
Figure 7.32: Main wind direction in summer (left) and winter (right) 1994 to 1999 at Casey. HIRHAM, ERA40 run.
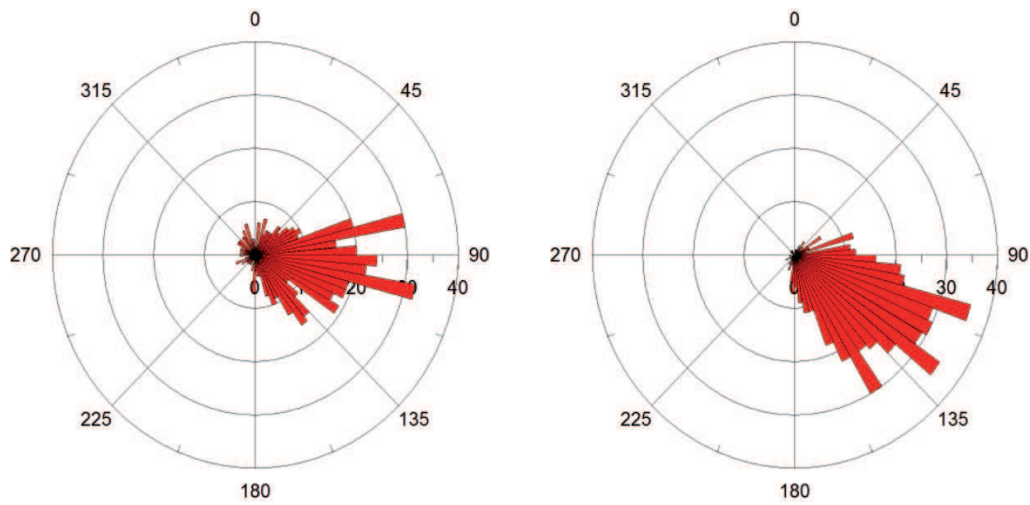
Figure 7.33: Main wind direction in summer (left) and winter (right) 1994 to 1999 at Casey. ERA40.
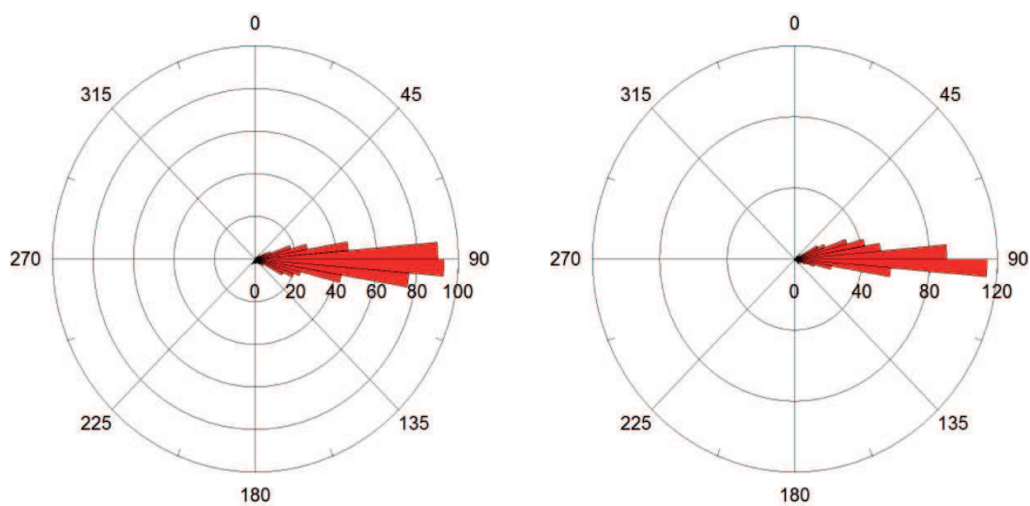
Figure 7.34: Main wind direction in summer (left) and winter (right) 1994 to 1999 at Davis. HIRHAM, ERA40 run.
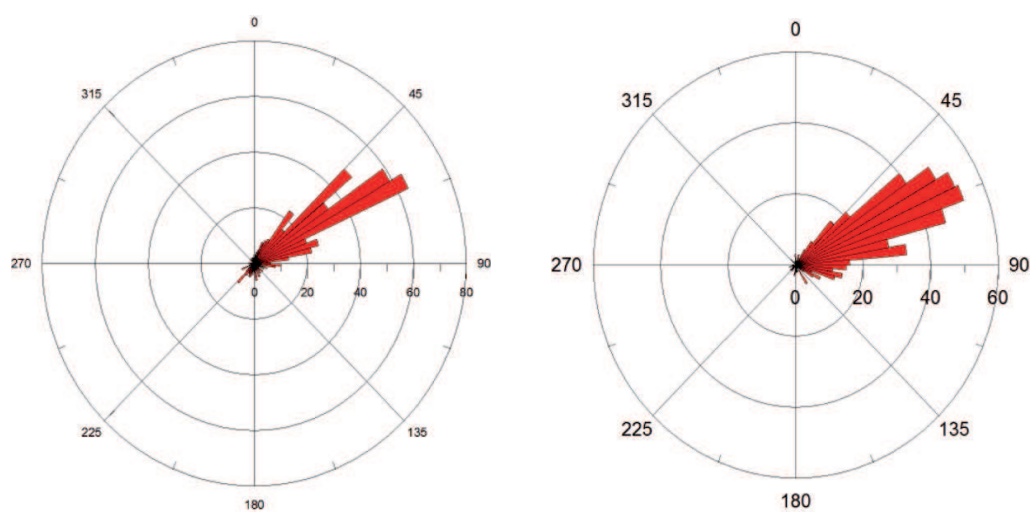
Figure 7.35: Main wind direction in summer (left) and winter (right) 1994 to 1999 at Davis. ERA40.
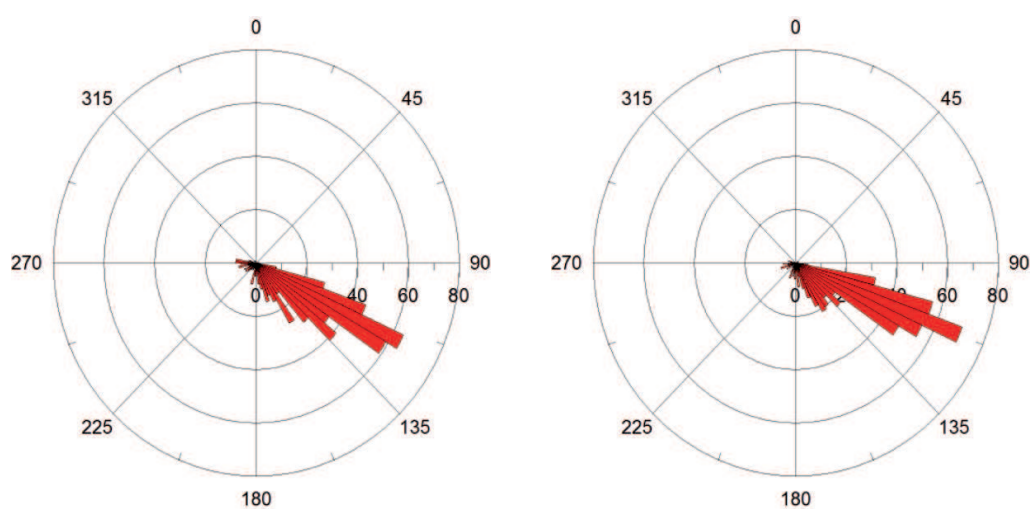
Figure 7.36: Main wind direction in summer (left) and winter (right) 1994 to 1999 at Dumont-D'urville. HIRHAM, ERA40 run.
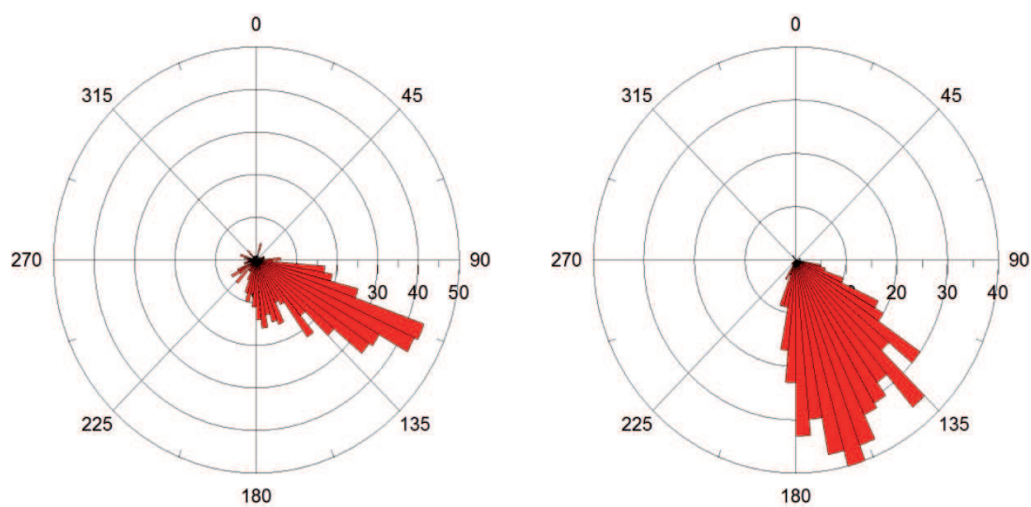
Figure 7.37: Main wind direction in summer (left) and winter (right) 1994 to 1999 at Dumont-D'Urville. ERA40.
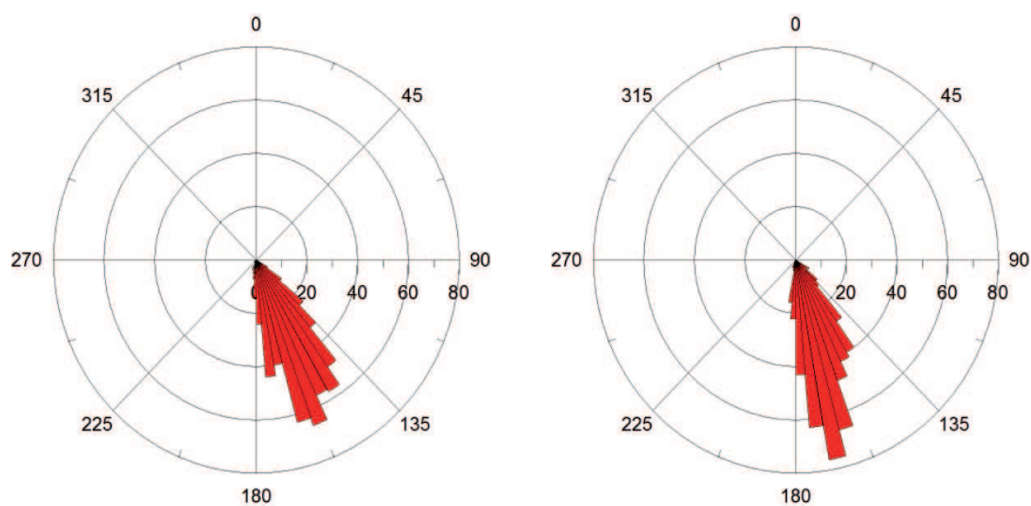
Figure 7.38: Main wind direction in summer (left) and winter (right) 1994 to 1999 at Mawson. HIRHAM, ERA40 run.
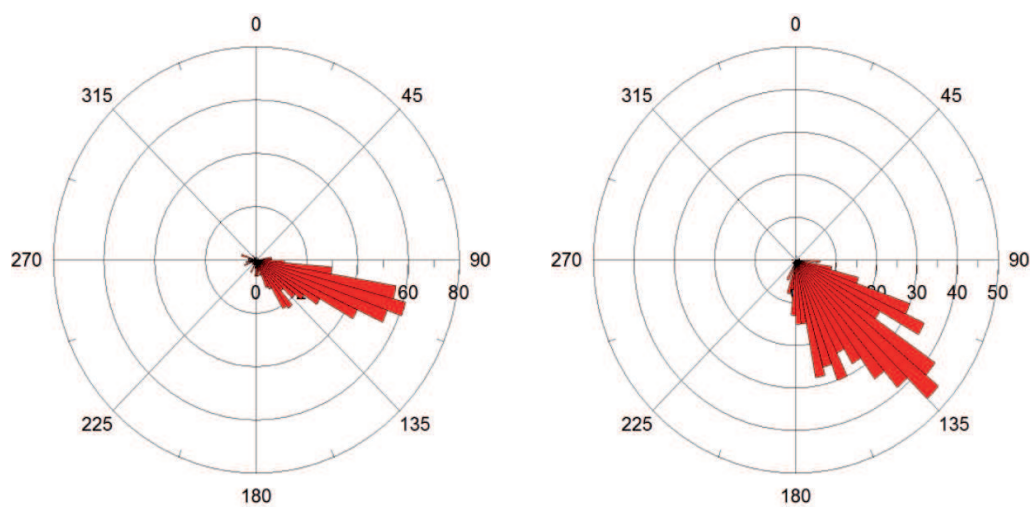
Figure 7.39: Main wind direction in summer (left) and winter (right) 1994 to 1999 at Mawson. ERA40.
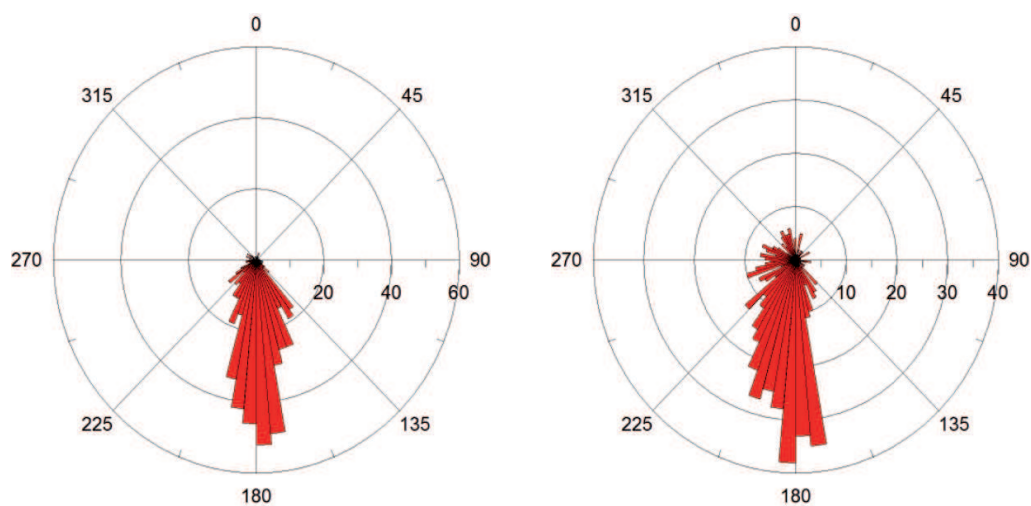
Figure 7.40: Main wind direction in summer (left) and winter (right) 1994 to 1999 at McMurdo. HIRHAM, ERA40 run.
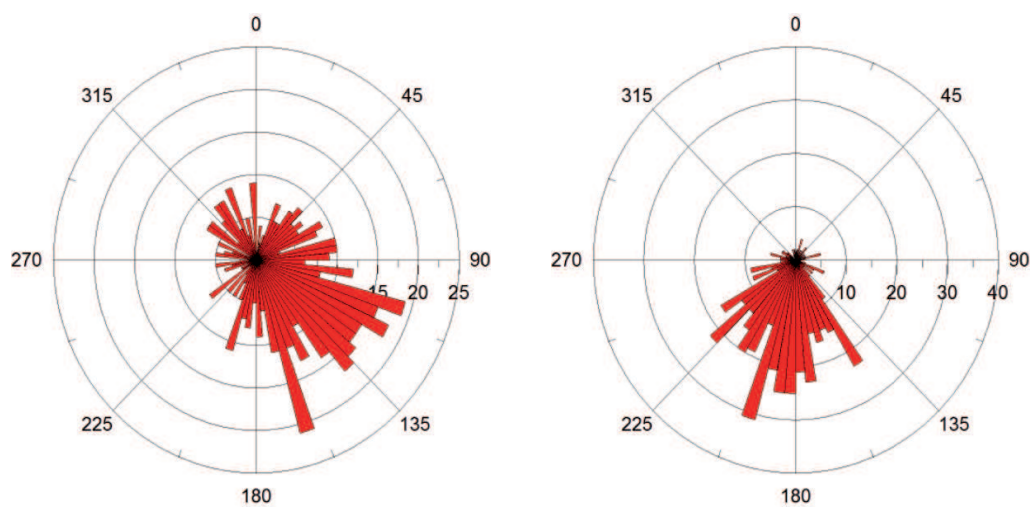
Figure 7.41: Main wind direction in summer (left) and winter (right) 1994 to 1999 at McMurdo. ERA40.
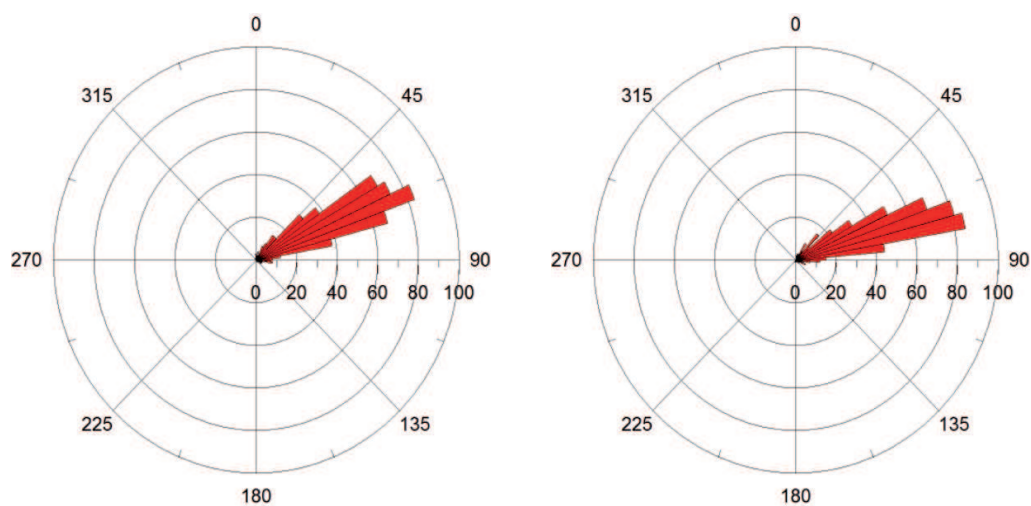
Figure 7.42: Main wind direction in summer (left) and winter (right) 1994 to 1999 at Syowa. HIRHAM, ERA40 run.
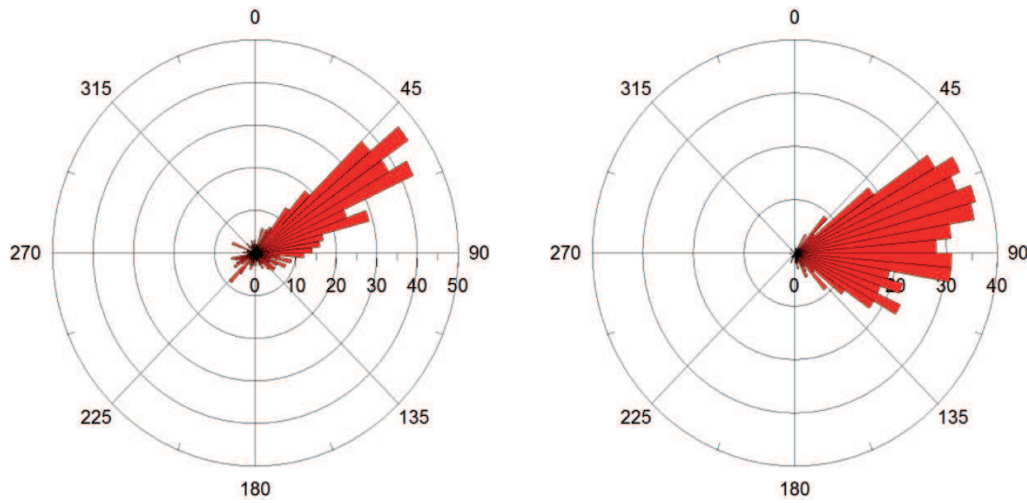
Figure 7.43: Main wind direction in summer (left) and winter (right) 1994 to 1999 at Syowa. ERA40.

In most cases there is a good accordance between ERA40 and HIRHAM. On some stations, like Casey, McMurdo or Syowa, the wind direction of ERA40 is not as concentrated on one direction as the HIRHAM wind direction. At the stations Davis, Dumont-D'Urville and Mawson ERA40 and HIRHAM wind directions slightly deviate from each other, in a northern direction (Davis), southern (Dumont-D'Urville) or eastern (Mawson) direction. Especially in case of McMurdo Station the wind directions of both models differ from the sounding wind directions, which can be explained through the different representation of the orography. ERA has a coarser grid resolution than HIRHAM. Especially in the steep coastal region, differences in orography lead to differences in wind direction. Note also that in the wind measurement via sounding changed to GPS retrieval. Since radiosondes determine the boudary conditions for the reanalyses and also for HIRHAM, the influence of the lower uncertainties with GPS measurement should be similar for sounding, reanalysis and model. Also all wind direction plots shown here are averaged over several years.

7.5 Comparison of the ERA40 run and the ERAinterim run

To evaluate the ERAinterim run (ERAint-setup) a comparison with the ERA40 run (ERA40-setup) has been conducted. Since ERA40-setup has an integration period from January 1994 to December 1999 and ERAint-setup was integrated from January 1996 to December 2009, the comparison period spans over the overlapping years 1996 to 1999. If the differences between both setups are not significant, the validation of the ERA40-setup is also valid for the ERAint-setup. Differences in MSLP, TWV and 2m-temperature are shown below. These variables have been chosen for the comparison because they are analysed

more accurate in this study. The differences were calculated for the 4-year-mean of the years from 1996 to 1999 from both runs. The ERAint-setup mean was substracted from the ERA40-setup mean.

In Figure 7.44 the difference of the 4-year-mean of ERA40-setup and ERAint-setup MSLP is shown. The differences are not significant and almost everywhere smaller than one. In the ERA40 run the depression north of Amundsen Sea is weaker than in the ERAinterim run, as well as the high over the East Antarctic Plateau. In the ERAinterim run the amplitude in the spatial pattern of pressure is ca. $\pm$ 1 hPa bigger than in the ERA40 run.
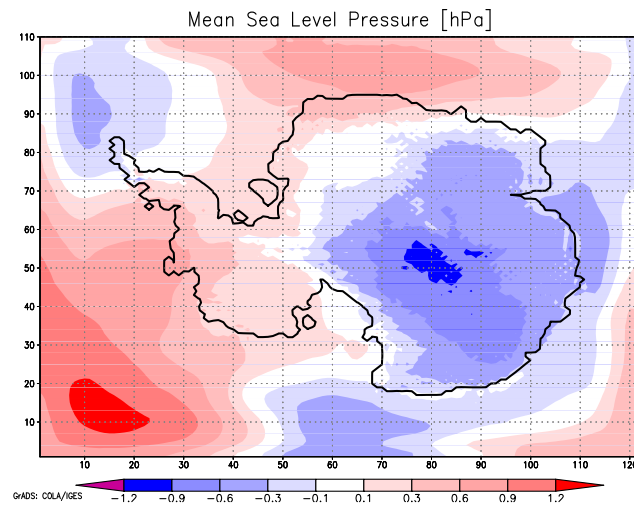
Figure 7.44: Difference of the ERA40 run minus the ERAinterim run. Temporal mean of MSLP over the years 1996 to 1999 (shaded). Significance (green contour line).

Figure 7.45 shows the difference between the ERA40-run and the ERAinterim-run in TWV. The difference in TWV is only small in the whole region and does not exceed 0.6 mm. The biggest difference can be found in the boundary zone of the HIRHAM area.
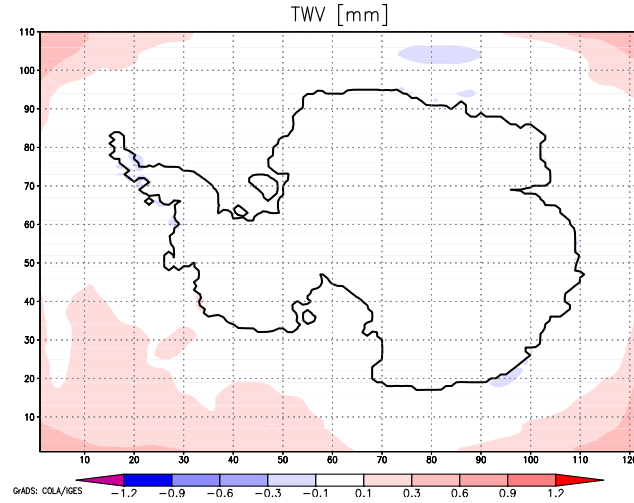
Figure 7.45: Difference of the ERA40 run minus the ERAinterim run. Temporal mean of TWV over the years 1996 to 1999 (shaded). Significance (green contour line).

The difference between the 4-year-mean of 2m-temperature from the ERA40-run and the ERAinterim-run is depicted in Figure 7.46. Except of the coastal zone the difference does not exceed 0.9 K throughout the whole integration region, and is not significant. On the coast the differences are higher in amplitude, positive or negative, but only along a small band. At the boundary of the integration region the ERA40 run has a slightly higher temperature than the ERAinterim run.
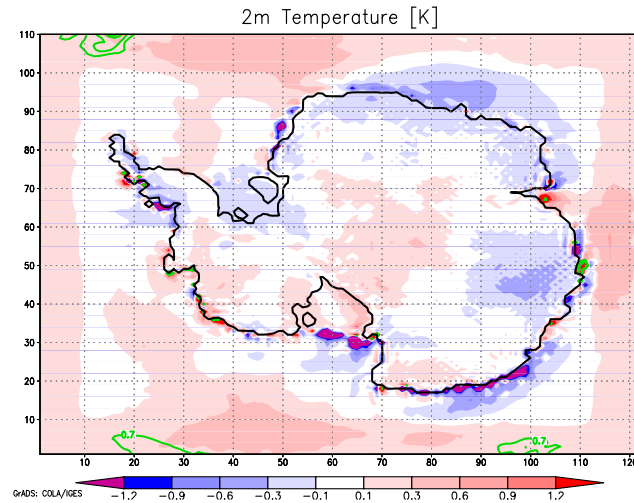
Figure 7.46: Difference of the ERA40 run minus the ERAinterim run. Temporal mean of 2m temperature over the years 1996 to 1999 (shaded). Significance (green contour line).

There are differences between the run with ERA40 boundaries and the run with ERAinterim boundaries, but they are not significant. So both setups are comparable with each other and the measurements. Especially in the HIRHAM boundary-zone these differences result from the different values of the reanalyses. Ground variables as MSLP and 2m-temperature are also influenced by the boundary reanalysis and thus show differences in the inner region of the model. Since ERAinterim has a finer resolution than ERA40, and a finer orography, the 2m-temperature differs around the continental edge, even after calculation processes in the regional model. Still, both setups are applied to the same orography, so that orographical structures cannot be seen directly in the differences. MSLP is calculated for a certain height throughout the whole model region and is not that sensitive to orographic differences.

Chapter 8

Analysis of Synoptic Structures

In this chapter structures of synoptical phenomena are analysed to distinguish them by their frequency and dimension. Two statistical tools are used here: The calculation of the standard deviation and a digital filter for regional models by Feser and von Storch (2005). Additionally the mean baroclinity of the ERA-interim run, as well as its summer and winter mean was calculated with a method based on Hoskins and Valdes (1990)

The standard deviation has high values in zones with a strong variation of a variable, and show regions where values of synoptical data are changing frequently.

A filter helps identifying processes of a certain dimension and are commonly used to distinguish e.g. large scale, synoptical scale and mesoscale phenomena. As the regional climate model used here has a grid size of 50 km it should be ideal to focus on mesoscale phenomena.

This analysis is focused on MSLP, TWV and 2m-temperature. These variables are strongly linked to synoptical systems and thus to each other. A detailed analysis of these values alows to draw conlusions refering to the behaviour of cyclones.

8.1   Standard Deviation

A standard deviation shows the variation of a value, here over time at a certain location. Zones of small variation have low standard deviation values. In zones where a value is changing frequently over time and with a high amplitude, such as zones with frequent cyclone passing, will give a strong standard deviation signal. In this study, standard deviation was calculated for each season of the years 1994 to 1999 for HIRHAM, its boundary forcing ERA40 and another reanalysis (NCEP). The studied variables are MSLP and T2m. Their standard deviation was calculated from the daily mean data of the single seasons: spring (SON), summer (DJF), autumn (MAM) and winter (JJA) 1994 to 1999, and averaged afterwards.

Fig. 8.1 shows the TWV standard deviation of HIRHAM, ERA40 and NCEP in the years 1994 to 1999. The patterns look similar to the ones in 7.3 and show a low standard deviation in zones with low absolute values of TWV.
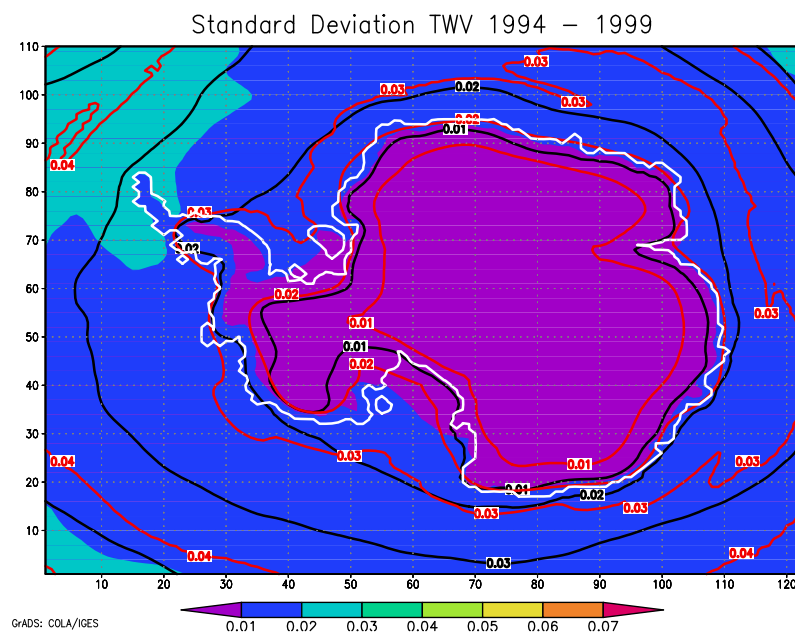
Figure 8.1: Standard deviation of TWV from HIRHAM (shaded), ERA40 (black contour lines) an NCEP (red contour lines). 1994 - 1999

In Figure 8.2 the similarity between HIRHAM and ERA40 in TWV can be seen. There is a difference of 0.01 mm between NCEP and HIRHAM, respectively ERA40, especially in winter. The differences in the other three seasons are smaller.
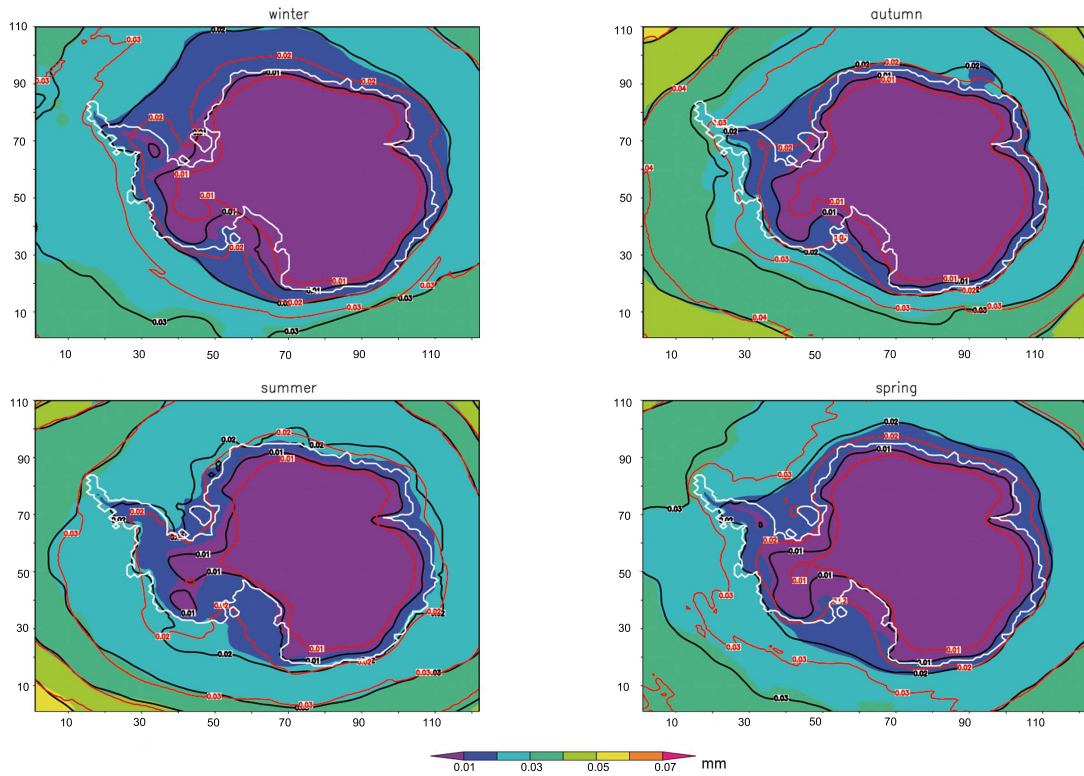
Figure 8.2: Standard deviation of TWV from HIRHAM (shaded), ERA40 (black contour lines) an NCEP (red contour lines). Summer (upper left), winter (lower left), autumn (upper right), spring (lower rights). 1994 - 1999

The standard deviation of TWV is small in inner Antarctica and growing to the North. Since the amount of TWV in Antarctica is small, the absolute variation is decreasing to the south. Apart from continental structures, hardly any pattern can be seen. The standard deviation of TWV is low in Antarctica for all four seasons (Fig.8.2). Still, there are differences between summer and winter. In winter the zone of a standard deviation of less than 0.02 mm reaches further north than in summer. First, the sea ice extension in winter is bigger than in summer, and the humidity variability over ice is lower than over the open sea, due to evaporation or the lack of it. A second reason of the lower standard deviation of TWV in winter is the lower humitity in general in winter months. Cold air can hold less specific humidity, so the specific humidity decreases during the cold season, which also lowers the standard deviation.

There are no significant differences between the standard deviations of HIRHAM and those of ERA40 and NCEP.

Figure 8.3 shows the MSLP standard deviation of HIRHAM, ERA40 and NCEP from 1994 to 1999. The patterns of HIRHAM and ERA40 look similar, but ERA40 has up to 5 hPa higher values than HIRHAM. NCEP MSLP standard deviation is higher than 18 hPa over East Antarctica.
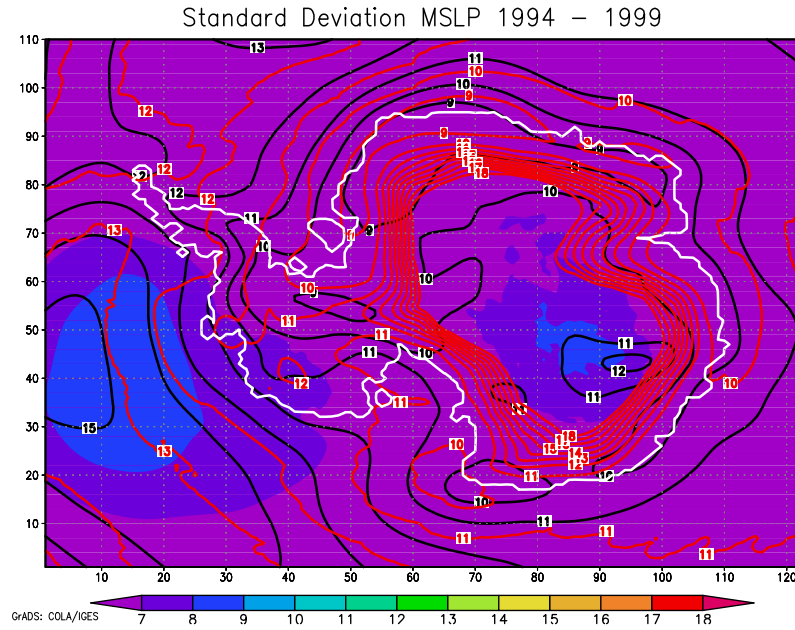
Figure 8.3: Standard deviation of MSLP from HIRHAM (shaded), ERA40 (black contour lines) an NCEP (red contour lines). 1994 - 1999

The plot 8.4 of MSLP standard deviation also shows a good agreement between HIRHAM and ERA40. Their maxima have the same values (17 hPa in Amundsen Sea and 15 hPa over the Antarctic Plateau) and cover the same regions. NCEP shows a different pattern, especially in the inner part of the continent with a maximum of 20 hPa, but also in Amundsen sea, with a maximum of only 15 hPa, that is also shifted to the west. Here again, the strongest differences occur in winter.
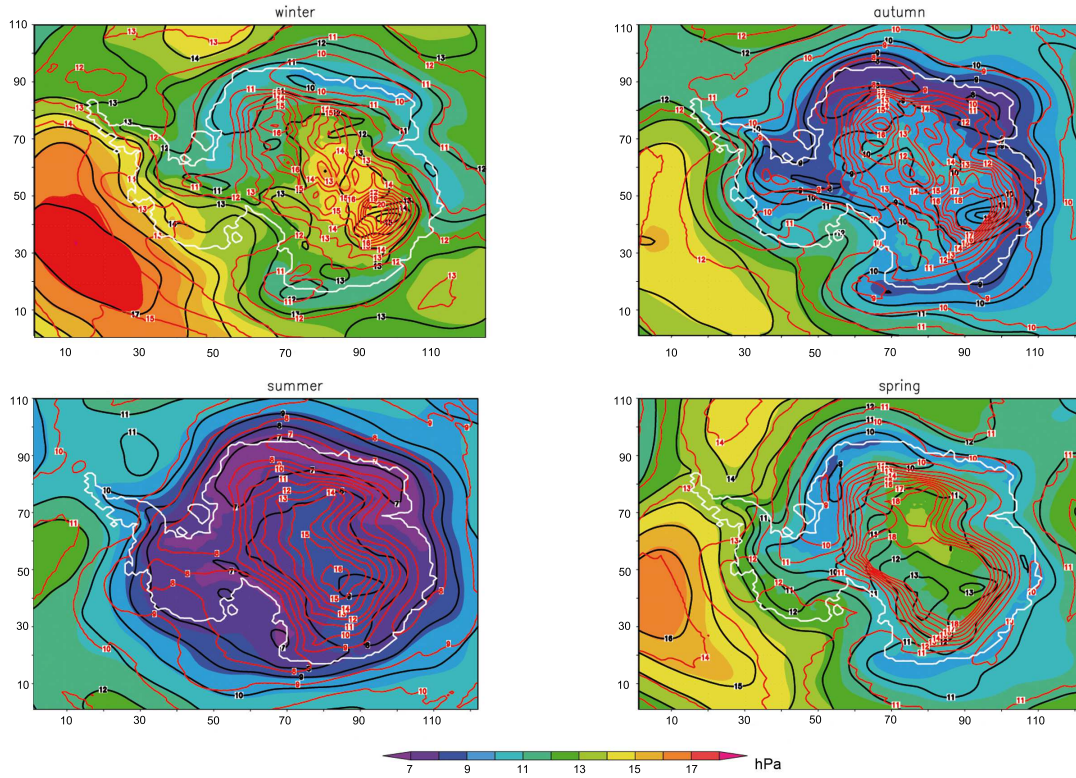
Figure 8.4: Standard deviation of MSLP from HIRHAM (shaded), ERA40 (black contour lines) an NCEP (red contour lines). Summer (upper left), winter (lower left), autumn (upper right), spring (lower rights)

Since it is assumed that TWV biases between HIRHAM and measurements partly have their origin in uncertainties of modelled cyclones, it is necessary to take a closer look at the cyclone tracks. A simple tool for a first approach is to calculate the standard deviation of MSLP. If the standard deviation is large it means that the MSLP values in the respective region are changing much in the respective time period, which is from one day to another in this case, since the standard deviation was calculated based on daily means. The usual time scale of a cyclone is 2 to 6 days, so their development and decay is covered with this approach. The standard deviation maxima can be interpreted as the formation of cyclones or their repeated passing. In Fig. 8.4, the standard deviation of MSLP for each season over the integration time of HIRHAM, ERA40 and NCEP is shown. Strong standard deviations of HIRHAM MSLP can be seen on the coast of West Antarctica - Amundsen Sea in winter. Maximum values reach up to 18 hPa. Also in autumn and spring the highest standard deviation can be found in this zone, but with less pronounced maximum of 15 hPa (autumn) and 16 hPa (spring). Another but weaker maximum of MSLP standard deviation of 14 hPa can be found north, respectively northeast of the Weddel Sea. The maxima in the sea around Antarctica can be interpreted as cyclone breeding zones or zones with frequent cyclone passing (cyclone tracks). Additionally, a maximum of the standard deviation is

found on the continental East Antarctica in winter, which shows the formation of a high during winter (ca. 1010 hPa), as the temperature falls and the air is descending and thus forming a high. Between the cyclone activity north of Antarctica and the formation of the high on the continental plateau, the temporal variation in MSLP is low, which explaines the low standard deviation of MSLP at the continental coast. Hoskins and Hodges (2005) found, that in summer, the maximum of the cyclone activity in the southern hemisphere is shifted northwards compared to the cyclone activity in winter. So the activity in the HIRHAM grid area is smaller in summer than in winter.

By comparing the HIRHAM MSLP standard deviations with those of ERA40, it becomes obvious that the spatial patterns are similar (pattern correlation coefficient of 0.9). Small differences, in the order of 2 hPa, are due to the finer resolution of HIRHAM. Over the continental plateau, ERA40 and NCEP MSLP standard deviations are different from those of HIRHAM, especially in regions with steep orography. A reason for this behaviour is the difference in model orography between HIRHAM, ERA40 and NCEP.

Marshall and King (1998) showed cyclone track density in the southern hemisphere for certain winters (1974, 1976, 1978, 1980, 1983, 1987 and 1989). The highest density in their study can be found around 60°S, a zone not completely covered by the HIRHAM integration area. Thus, the MSLP standard deviation maxima zone in this study is splitted and reaching the boundary zone. The cyclones are mostly in the boundary zone of the model and thus held by the ERA40 boundary values with less chances to develop independently in the HIRHAM model grid. Except for Mawson and McMurdo, the differences in station and grid point heights as well as the effects of land and sea point can explain the bias between model and sounding. But in Mawson as well as in McMurdo all four HIRHAM grid points have a dry bias compared to sounding data, regardless of grid point height or whether the grid points are land or sea points. Another explaination is lower humidity in synoptical less active regions.

8.2 Signals on different wave-lengths

In this chapter digital filters of different wave lenghts are compared, to show signals of MSLP, T2m and TWV in different scales.

A standard deviation shows zones of strong variation. This means a value that is changing much in time or another dimension, on which its standard deviation is calculated, shows strongest variation. So standard deviation depicts active zones, but can not distiguish the size of the processes which lead to this activity.

With filteres of different wavelengths processed data highlights patterns of a certain size, for example Rossby-waves, synoptical-size cyclones or mesoscale lows, depending on the filter type and the chosen wavelength. The filter seperates the wavelengths and allows analyses of only the regarded scales. It is possible to distinguish effects of the seperate scales without disturbance from higher or lower wavelengths.

In a first experiment three filter types were applied, a lowpass (LOW) with ca. 1000 km as boundary-wavelength, and two bandpasses: SYN, which filtered between 500 km and 1000

km and MESO with a pass between 200 km and 600 km (c.f. 6.2). All plots depict the 1994 to 1999 mean deviation from the temporal and spatial mean (1994 to 1999, HIRHAM grid region). After filtering daily averages, an average over the years 1994 to 1999 (ERA40 run), respectively 1996 to 2009 (ERAinterim run), was calculated.
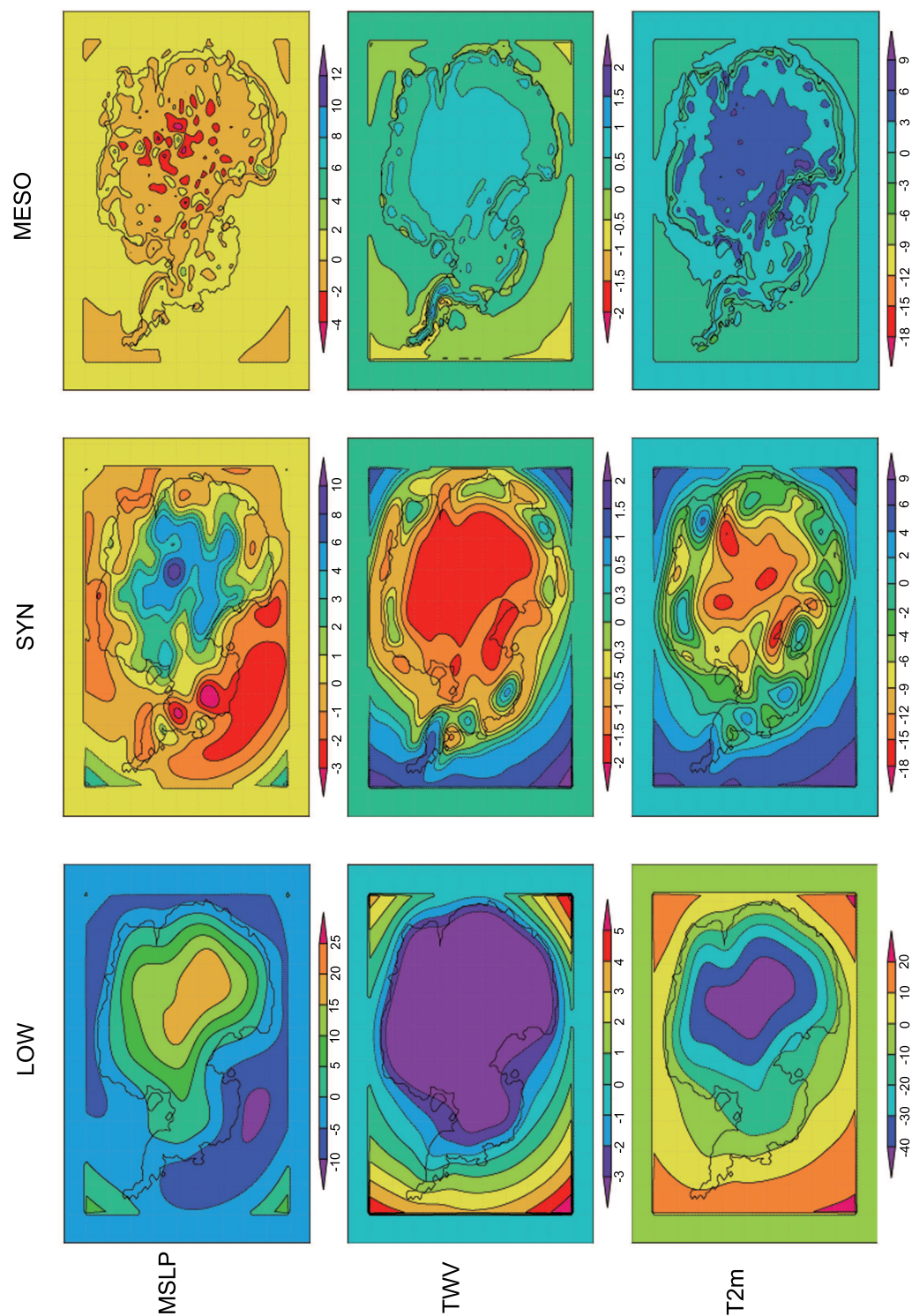
Figure 8.5: (Please note that the Figure is turned by 90°). From left to right: Lowpass 005x009 (LOW), Bandpass 005x011 (SYN), Bandpass 009x027 (MESO). Top to bottom: MSLP, TWV, 2m-Temperature. ERA40 run 1994 to 1999

In Figure 8.5 the different scales can be easily distinguished. Both, LOW and SYN MSLP show similar patterns as in the standard deviation analysis. Additionally to the significant depression pattern in Ross-Sea and Amundsen-Sea, there are some wave-train like pattern around the coast in SYN. In MESO neither one nor the other can be seen, only some small scale patterns over the continent. This is consistent for both the other variables, specific humidity and 2m-temperature. The comparison of the three filter types represents cyclone activity best. The patterns shown in SYN, reflect the active zones that where found in the standard deviation analysis, described in 8.1 and will thus be analysed further.

8.3 Seasonal Mean

After the comparison of different analysis methods (c.f. 8.2) synoptical patterns will be analysed seperately for each season and both runs. The season means are calculated from the daily mean data of the single seasons, like in 8.1, but especially in the scale of 500 to 1000 km. The ERA40 run from 1994 to 1999 will be decribed in 8.3.1 and the ERAint run from 1996 to 2009 will be described in 8.3.2.

8.3.1 ERA40 run - 1994 to 1999

For the Analysis of the season mean of the years 1994 to 1999 the filter SYN was used. It shows phenomena of roughly synoptical size. The variables that were analysed are MSLP, TWV and T2m. Additionally shown in the plots is the season mean of sea ice extension of the years 1994 to 1999 from the boundary force ERA40.

In Figures 8.6 and 8.7 the seasonal mean of filtered MSLP of the years 1994 to 1999 is shown. One can see a depression in Ross-Sea that is streching to Amundsen-Sea, also in summer, when the standard deviation 8.4 is small (less than 13 hPa). So there is a low pressure zone in Ross and Amundsen Sea, but the variation in this zone is small. The same applies for coastal regions. An area with a high MSLP standard deviation indicates pressure changes and thus zones of development and decay of cyclones. The maxima in 8.4 show cyclone breeding zones and the minima in 8.6 and 8.7 show areas with a low pressure in the temporal mean. Over the East-Antarctic plateau is a high pressure area. Both phenomena can also be distinguished in the Standard-Deviation plots. Additionally there are wave trains like structures, which are very prominent in West Antarctica and the Peninsula. They still occur less strong at the coast of East Antarctica.
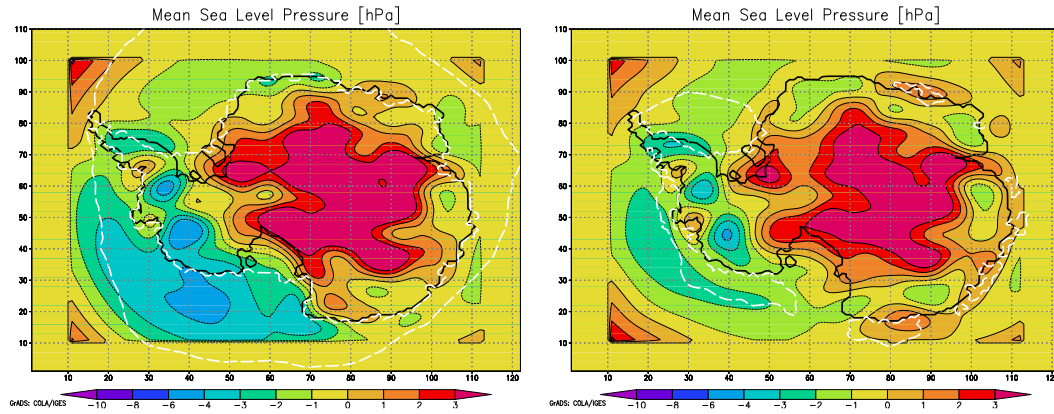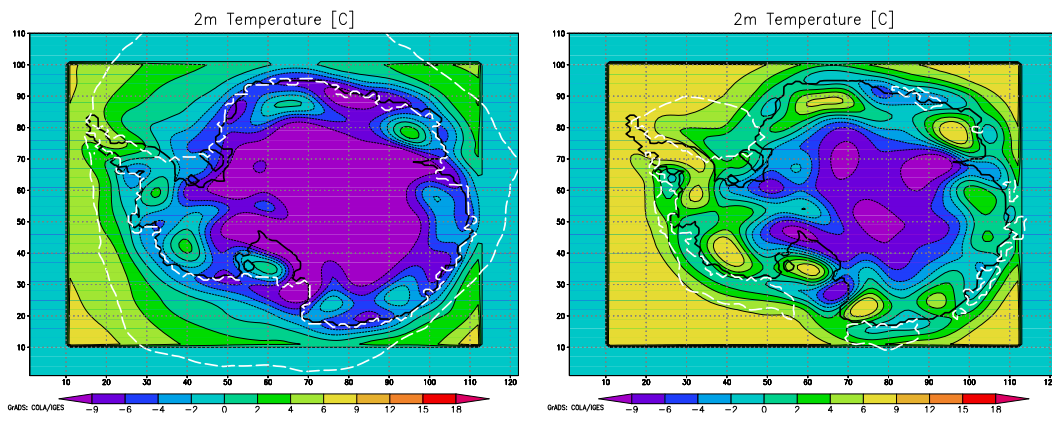
Figure 8.6: Filtered seasonal mean of MSLP of the years 1994 to 1999 (ERA40 run) in spring (left) and summer (right). White dashed line: Mean Seasonal Sea Ice. Used filter: SYN
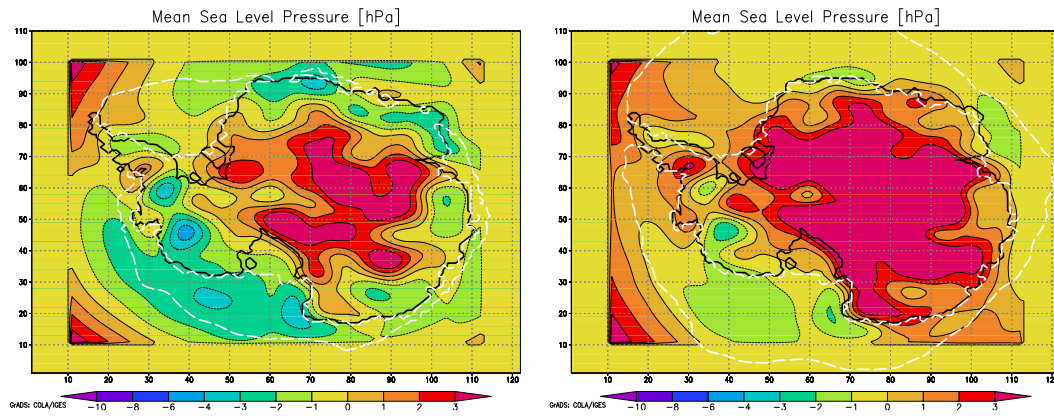
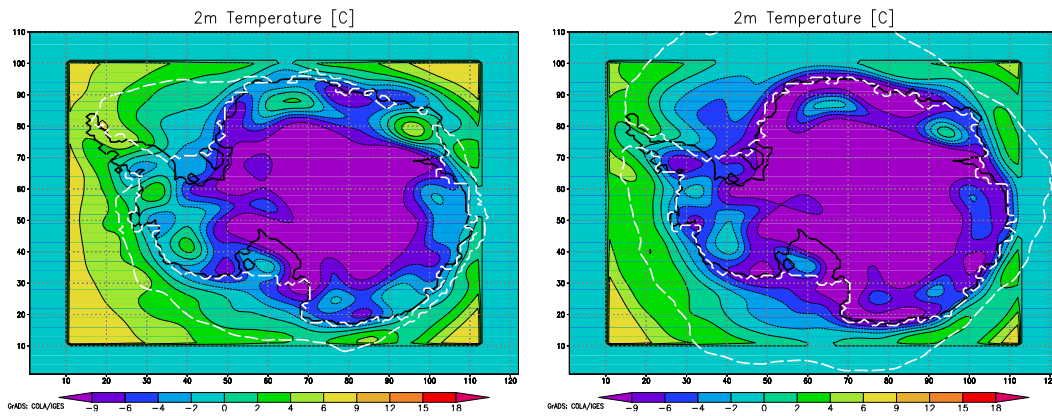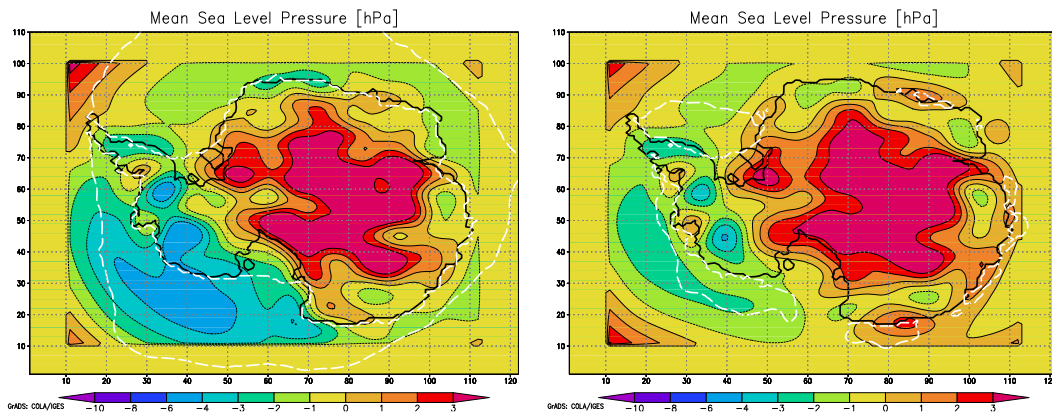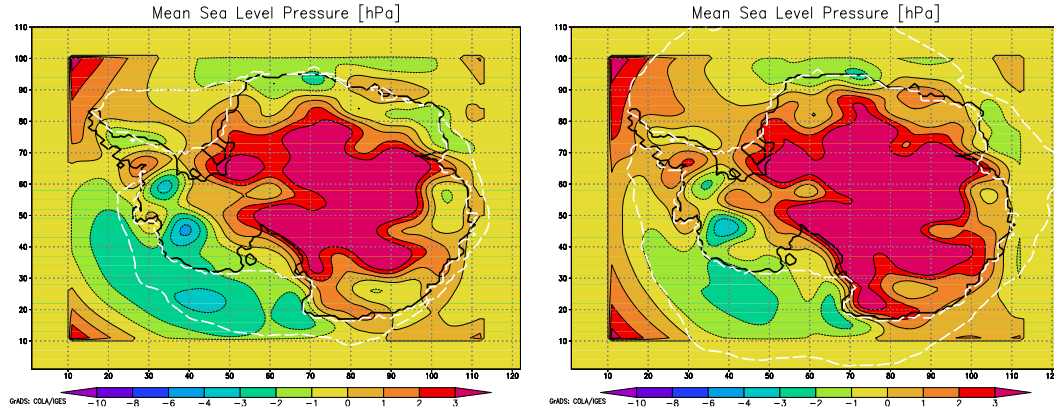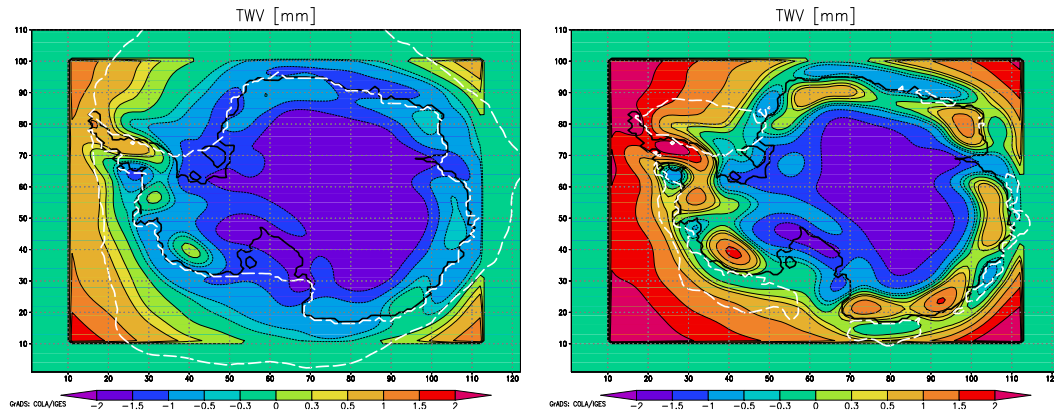Figure 8.7: Filtered seasonal mean of MSLP of the years 1994 to 1999 (ERA40 run) in autumn (left) and winter (right). White dashed line: Mean Seasonal Sea Ice. Used filter: SYN

The Ross/Amundsen-Sea depression and the high over the plateau are strongest in spring and autumn. In contrast to Figure 8.4, where the standard deviation of MSLP was strongest in winter, the lows themselfs have their maximum intensitiy in spring and autumn. In winter only the variation of MSLP is strong. The location of the depression is changing. It can be found more to the East in summer and more to the West in winter. The wave-trains are fixed over the seasons, which leads to the assumption that they are orographically induced. Their strength changes with the driving lows (the Ross/Amundsen-Sea depression and the partial ring around East-Antarctica). They have their maximum strenght in spring, like the driving depressions. The wave pattern with the strongest maximum can always be found next to the location of the strongest maximum of the depression.

In Figures 8.8 and 8.9 the season mean of filtered TWV of the years 1994 to 1999 is shown.

The East-Antarctic plateau is dry compared to the six year spatial mean (a difference of -2 mm), all other regions are more humid (+2 mm to the north). The most humid season is summer. Around Antarctica, to the North, the specific humidity is increasing. The wave train, that was in 8.6 and 8.7, also occurs here, with higher humidity in areas with lower pressure. The minima and maxima are fixed to a certain location, only changing in amplitude. It is most prominent in summer. There is a dry tongue stretching from the continental plateau down Prydz-Bay. The zones over shelf ice, especially Ronne-Filchner- and Ross-shelf-ice are also dry (2 mm deviation from the temporal and spatial mean).
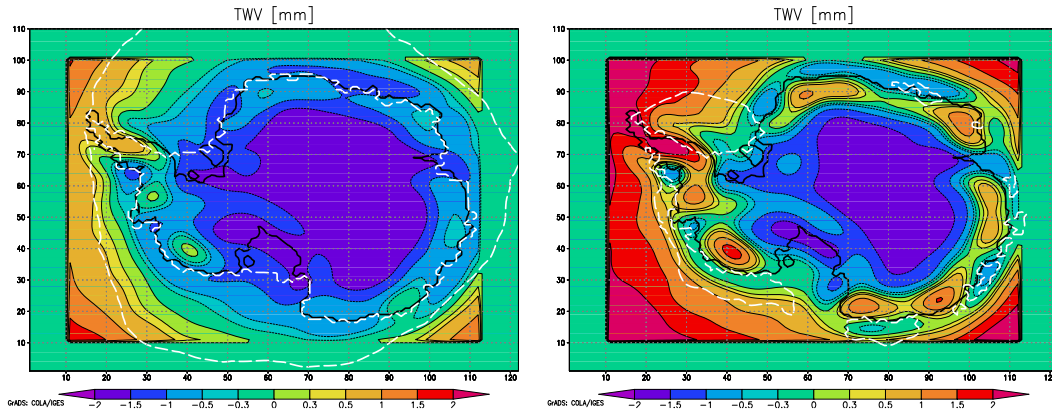
Figure 8.8: Filtered seasonal mean of TWV of the years 1994 to 1999 (ERA40 run) in spring (left) and summer (right). White dashed line: Mean Seasonal Sea Ice. Used filter: SYN
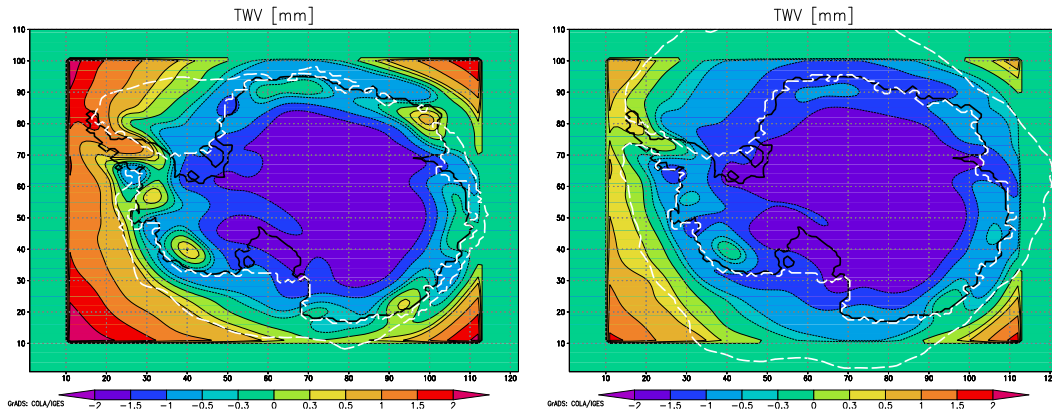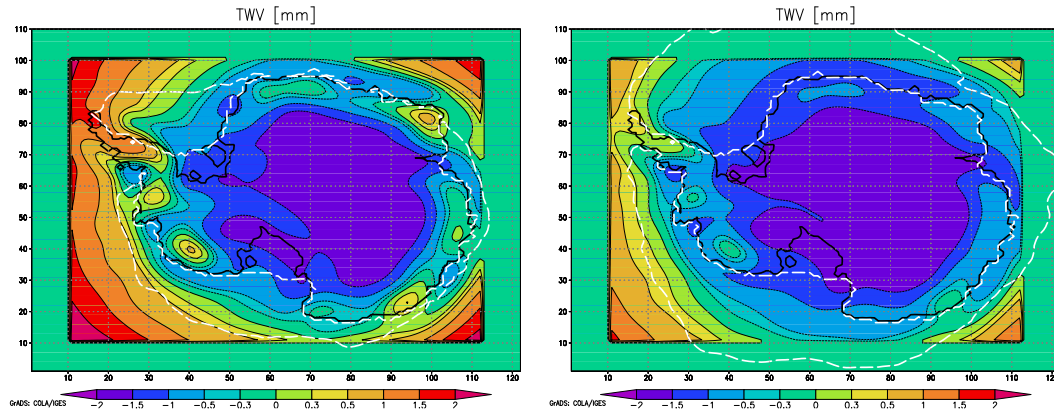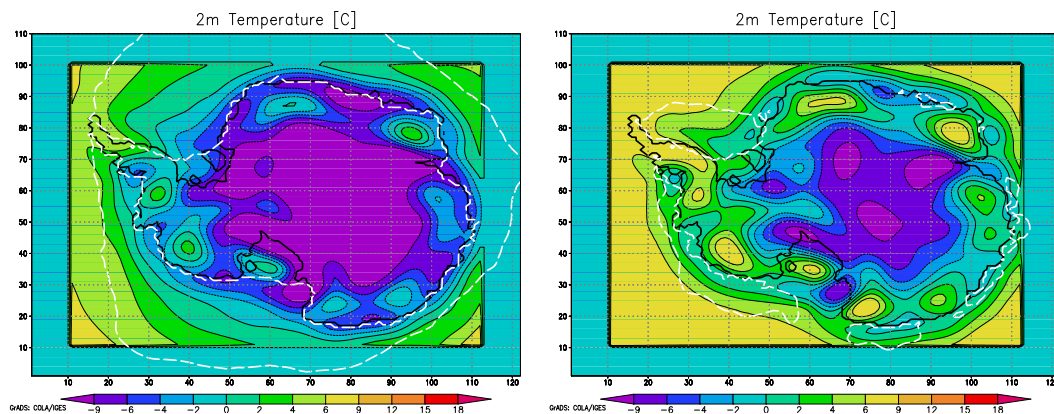

Figure 8.9: Filtered seasonal mean of TWV of the years 1994 to 1999 (ERA40 run) in autumn (left) and winter (right). White dashed line: Mean Seasonal Sea Ice. Used filter: SYN

The patterns of the filtered data look similar to the patterns of the 7.3 in case of TWV. So also in the scale from 500 to 1000 km, the Antarctic Plateau is always the dryest zone

in Antarctica. It has a high elevation and a continental climate. Differences in comparison with 7.5 occur mainly on the continental edge.

In Figure 8.10 and 8.11 the season mean of filtered 2m-Temperature of the years 1994 to 1999 (ERA40 run) is shown. The patterns look similar to 7.5. Around the coast is a high temperature gradient, as well as a similar wave-train pattern as in the other two Figures 8.6 and 8.7 and 8.8 and 8.9. There is no temperature signal in Ross- and Amundsen-Sea, like in MSLP, presumably because synoptical induced temperature patterns are superimposed by the strong northward temperature gradient. The wave train like patterns over West Antarctica and the Peninsula are the same as in 8.6 and 8.7 and 8.8 and 8.9.

Figure 8.10: Filtered seasonal mean of 2m-Temperature of the years 1994 to 1999 (ERA40 run) in spring (left) and summer (right). White dashed line: Mean Seasonal Sea Ice. Used filter: SYN
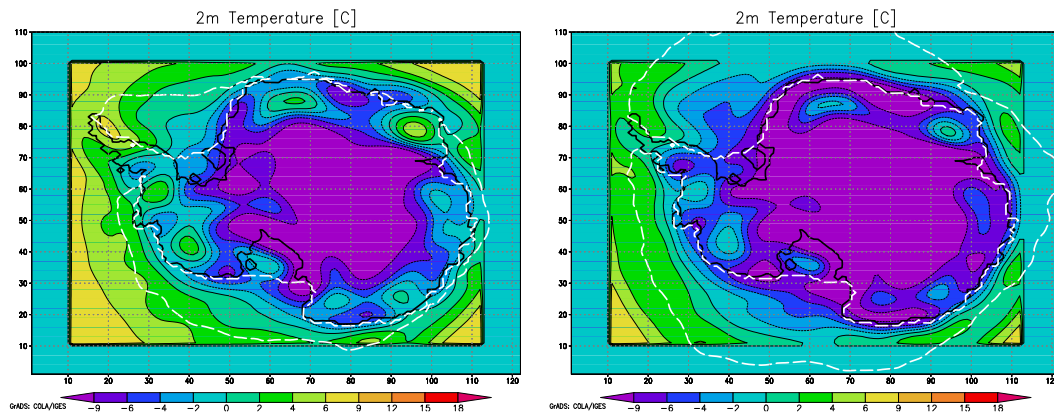

Figure 8.11: Filtered seasonal mean of 2m-Temperature of the years 1994 to 1999 (ERA40 run) in autumn (left) and winter (right). White dashed line: Mean Seasonal Sea Ice. Used filter: SYN

Summer is the warmest season with a deviation from the temporal and spatial mean

of -12 K to more than +9 K, winter the coldest, with a difference of more than -18 K over the Antarctic Plateau. The 2m-temperature shows a strong orographic pattern, including a cold tongue in the Prydz-Bay. 2m-temperature is related to the orographical structure, but seemingly not to synoptical phenomena.

In all three Figures typical wave patterns can be found. They are bound to orographical structures around the coast of Antarctica, fixed to one location and only changing in amplitude or strength. They do not have their origin in synoptical phenomena, but are due to extrapolation to sea level (MSLP) and terrain height (T2m and TWV). The same uncertainties occured in 7.2.

MSLP depicts the depression regions as expected. Also T2m and TWV show the expected pattern, like warming and more humitity to the North.

8.3.2 ERAinterim run - 1996 to 2009

As for the ERA40 run, also for the ERAinterim run from 1996 to 2009 the filter tool SYN was used to compare synoptical patterns (scale 500 Km to 1000 Km) in both periods. The analysed variables are MSLP, TWV and T2m as season mean in the integration period. Here the absolute values of the filtered data will be shown, the differences between the ERA40 run and the ERAint run will be analysed in detail in 8.3.3.

The first Figure is 8.12 and 8.13 and shows the MSLP deviation from the spatial and temporal mean from 1996 to 2009 in the HIRHAM grid region. The pattern looks generally similar tor 8.6 and 8.7.

Figure 8.12: Filtered seasonal mean of MSLP of the years 1996 to 2009 (ERAint run) in spring (left) and summer (right). White dashed line: Mean Seasonal Sea Ice. Used filter: SYN

Figure 8.13: Filtered seasonal mean of MSLP of the years 1996 to 2009 (ERAint run) in autumn (left) and winter (right). White dashed line: Mean Seasonal Sea Ice. Used filter: SYN

Again, in spring the depression system in Ross and Amundsen Sea is strongest and of largest extent compared to the other seasons. In the transitional seasons the amplitudes of the lows are most intensive. In winter the sea ice extent stabilises the atmospherical conditions, which also applies for 8.3.1.

Figure 8.15 and 8.15 shows the seasonal means of TWV filtered with the SYN filter. As in Fig. 8.8 and 8.9, over the continent there is a dry zone that has its largest extent in winter and its smallest extent in summer. To the North, the air becomes more humid, especially north of the sea ice edge.

Figure 8.14: Filtered seasonal mean of TWV of the years 1996 to 2009 (ERAint run) in spring (left) and summer (right). White dashed line: Mean Seasonal Sea Ice. Used filter: SYN

Figure 8.15: Filtered seasonal mean of TWV of the years 1996 to 2009 (ERAint run) in autumn (left) and winter (right). White dashed line: Mean Seasonal Sea Ice. Used filter: SYN

In summer the air is more humid in general because it is warmer and can thus hold more humidity. In winter the general humidity is less, especially over the continent and sea ice. In the transitional seasons it shows that humidity is bound to the sea ice edge. Over open sea the air is more humid than over ice, which adds in northern regions to the effect of higher temperature.
In Figure 8.16 and 8.17 the SYN filtered 2m-temperature from 1996 to 2009 is depicted. Again the Figure shows the deviation from the spatial and temporal deviation in this region and integration period. The patterns in this Figure look similar to the patterns in 8.10 and 8.11.

Figure 8.16: Filtered seasonal mean of 2m-Temperature of the years 1996 to 2009 (ERAint run) in spring (left) and summer (right). White dashed line: Mean Seasonal Sea Ice. Used filter: SYN

Figure 8.17: Filtered seasonal mean of 2m-Temperature of the years 1996 to 2009 (ERAint run) in autumn (left) and winter (right). White dashed line: Mean Seasonal Sea Ice. Used filter: SYN

In the plots with absolute values of MSLP, T2m and TWV the differences between 8.3.1 and 8.3.2 can hardly be distinguished. The differences between both runs will be analysed in 8.3.3.

8.3.3 Difference between both periods

To compare the synoptical patterns from both runs, the difference of the years 1994 to 1999 (ERA40 run), respectively 1996 to 2009 (ERAint run), was calculated for different variables, after they have been filtered. In the following Figures the differences of the all year means are plotted seasonally for the variables MSLP, TWV and T2m. Both runs are comparable with each other as verified in 7.5. Here changes between the two time periods are shown.

In Figure 8.18 the difference of the filtered 1994 to 1999, resp. 1996 to 2009 mean of MSLP is shown. The differences in spring and summer are only small, with slightly lower MSLP values of ERA40 in spring and slightly higher MSLP values of ERA40 in summer over different continental regions. In winter the ERA40 MSLP is smaller than the ERAinterim MSLP, especially over West Antarctica. In autumn ERA40 has higher pressure over the continent. The deviations between both runs are higher than in the other seasons.

The difference between both runs in the different years is due to synoptical changes over these years, since the comparability of both runs was proven in 7.5. The signal of the wave trains over West Antarctica and the Peninsula vanished in the plots of the differences between both runs. This shows that they are not driven orographically but rather have their origin in extrapolation processes.
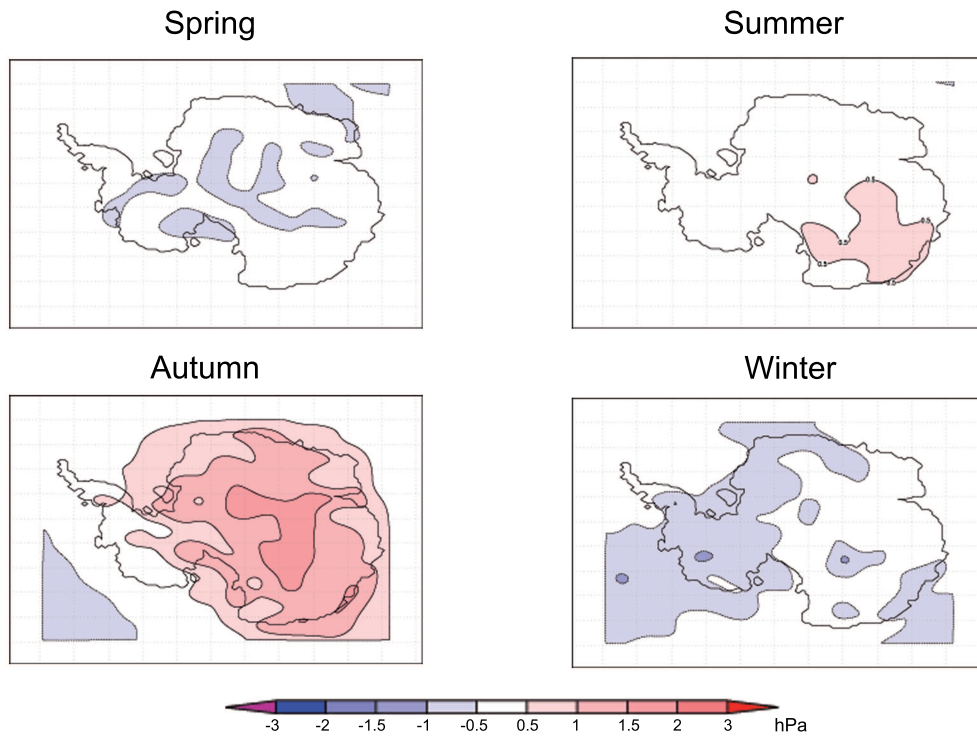
Figure 8.18: Seasonal MSLP difference of ERA40 run from 1994 to 1999 minus ERAint run from 1996 to 2009. Used filter: SYN

The difference of the 2m-temperature of both runs is shown in Figure 8.19. There are wave-like deviations around the coast which can be due to interpolation processes and different orographies of the boundary datasets. Apart from that, the differences in summer are around zero. In spring and autumn the temperatures of the ERAinterim-run are lower than in the ERA40 run. In winter the temperatures in the ERAint run are higher than in the ERA40 run.
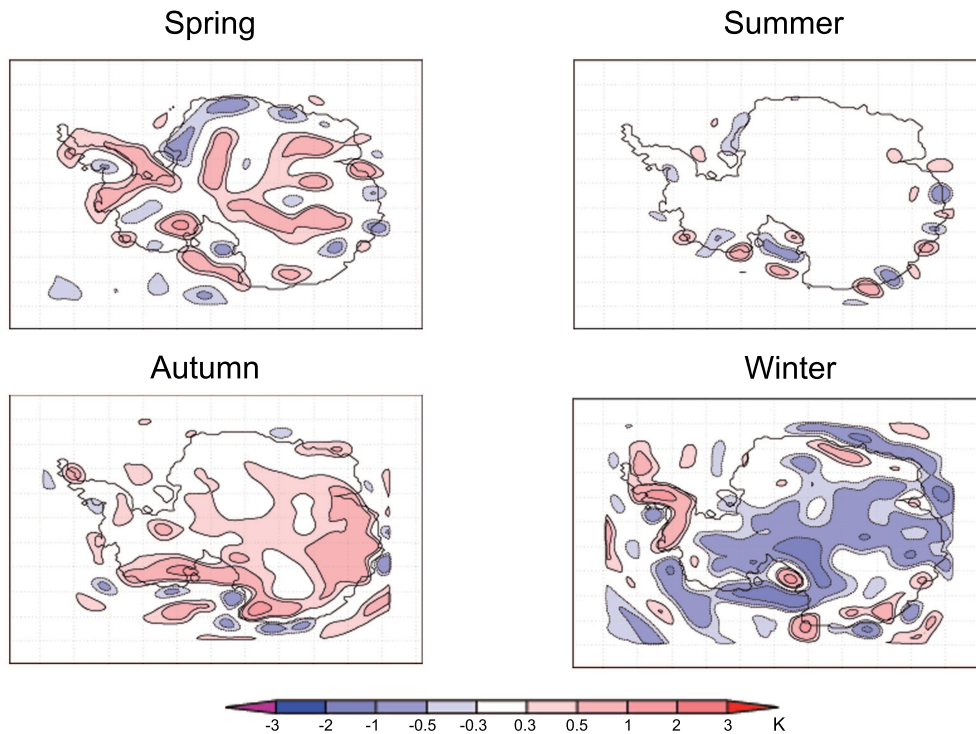
Figure 8.19: Seasonal T2m difference of ERA40 run from 1994 to 1999 minus ERAint run from 1996 to 2009. Used filter: SYN

In Figure 8.20 the TWV-difference of both model runs is plotted. Over the continent, the deviation of the model integrations is around zero. Over open sea, the differences show small, almost wave-like structures. In spring these differences are only small. In summer the differences are up to ± 0.3 mm with a higher rate of smaller TWV-values in the ERA40-run. In autumn and winter the patterns cover wider areas, with different zone of positive, respectively negative differences.
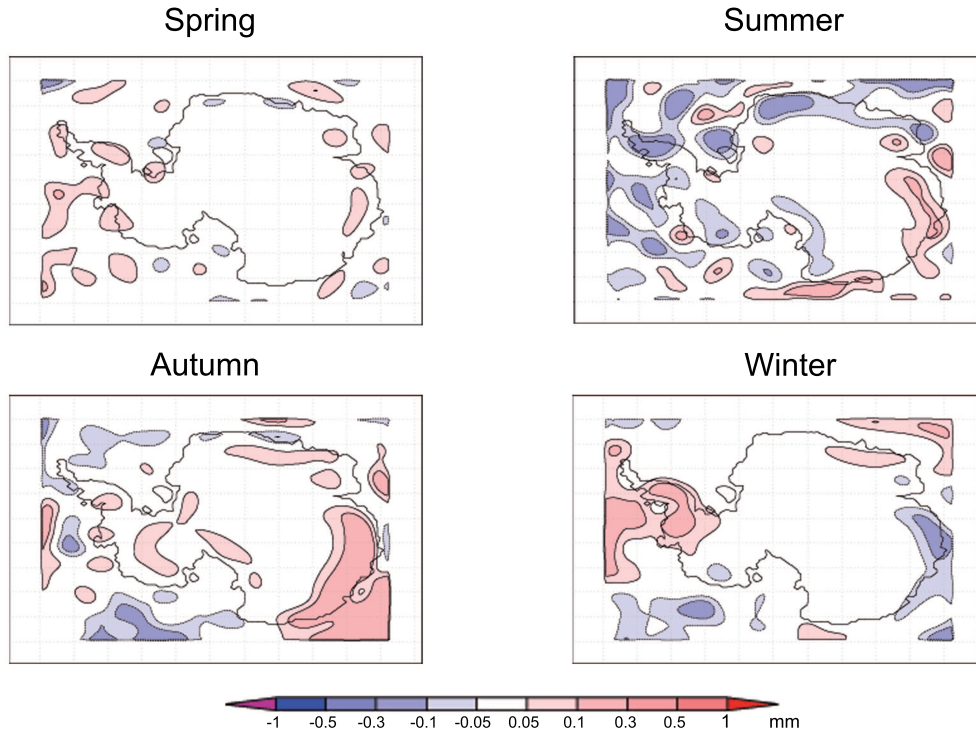
Figure 8.20: Seasonal TWV difference of ERA40 run from 1994 to 1999 minus ERAint run from 1996 to 2009. Used filter: SYN

The differences between the two time period are only small. The vanished wave train like signal in comparison to 8.3.1 and 8.3.2 shows that these signals were due to extrapolation and not to synoptical processes.

8.4   Structures on different Levels

To have a closer look on the synoptic structures over Antarctica, especially the wave structures over Western Antarctica and the Peninsula, variables on different levels were analysed.
The filter SYN was applied on geopotential at 300 hPa, 500 hPa, 700 hPa and 850 hPa. Again, the to be filtered data were substracted from the 6-year spatial mean. After the filtering process seasonal averages were calculaded and will be described below. The Figures of the single seasons are sorted by level.
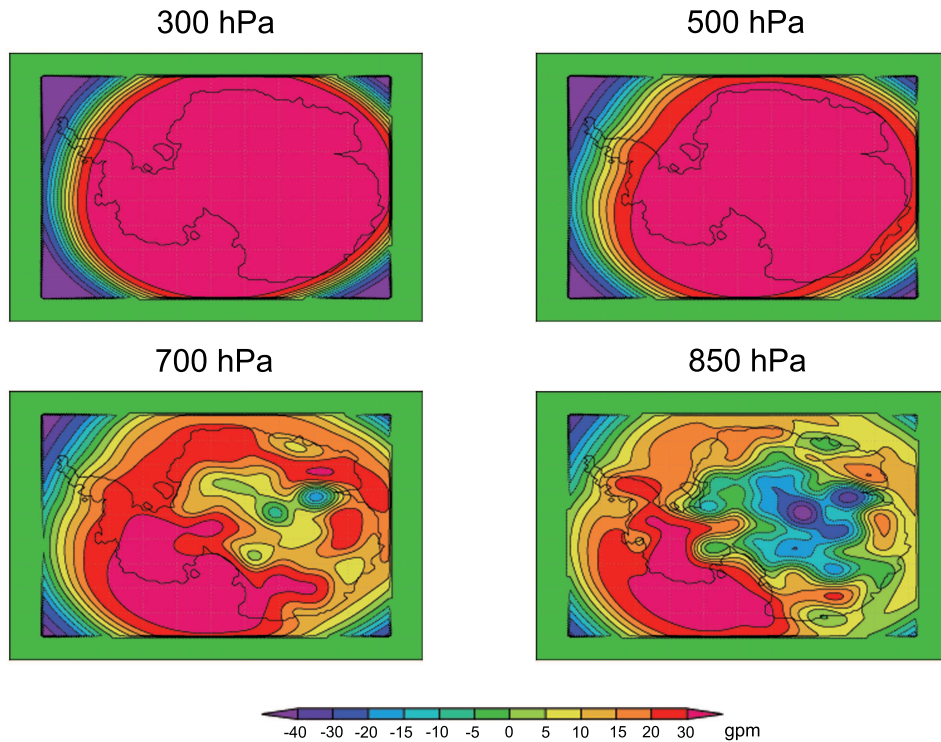
Figure 8.21: Spring Geopotential on the levels 300 hPa (upper left), 500 hPa (upper right), 700 hPa (lower left) and 850 hPa (lower right). 1994 to 1999 (ERA40 run). Used filter: SYN

In spring the polar low covers a big region in the upper levels. The amplitude is strong. On 700 hPa the cycone ring is clearly depicted. At the 850 hPa level the cyclone and high pattern are well pronounced and have structures similar to the ones in the ground level Figures.
In spring the Polar Low is still strong, since warming process has just begun. For the same reason the cyclone ring around Antarctica is almost as strong as in winter.
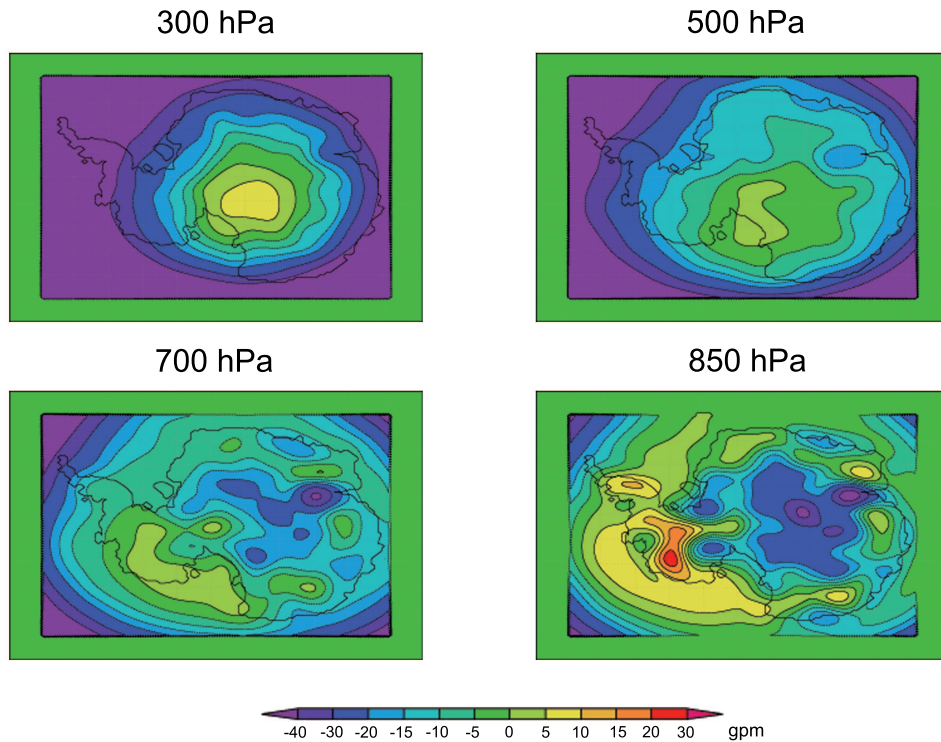
Figure 8.22: Summer Geopotential on the levels 300 hPa (upper left), 500 hPa (upper right), 700 hPa (lower left) and 850 hPa (lower right). 1994 to 1999 (ERA40 run). Used filter: SYN

In Summer the amplitude of geopotential deviations is smaller than in all other seasons, but the structures are similar. Most deviations are positive, since the polar low, which is the most prominent pattern in the higher levels of Antarctica is strongest in winter months and weaker in summer months. The polar low has a weak negativ deviation in 300 hPa. In 850 hPa the cyclonic structures that can also be found in the ground level Figures are observable.

The structures in this season are weaker than in all other seasons. In summer the MSLP is generally higher than in all other seasons. The low pressure zone is less intensive and so the values of geopotential are more similar to the spatial mean of the whole integration period.
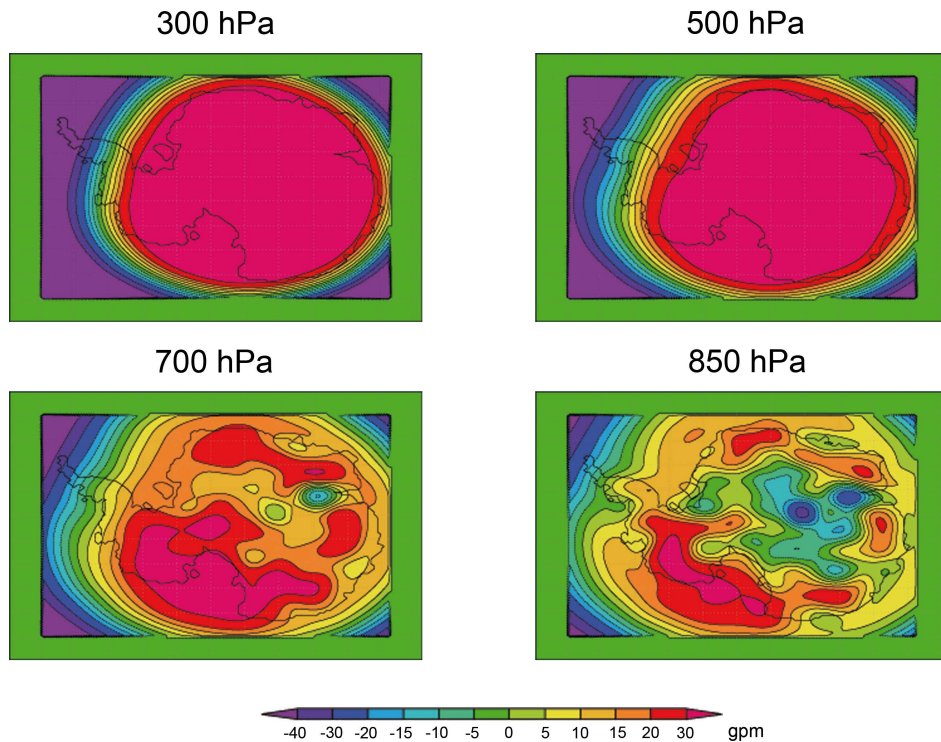
Figure 8.23: Autumn Geopotential on the levels 300 hPa (upper left), 500 hPa (upper right), 700 hPa (lower left) and 850 hPa (lower right). 1994 to 1999 (ERA40 run). Used filter: SYN

In autumn the Polar Low is weaker than in winter or spring. Likewise the cyclone ring and the high over the Antarctic Plateau are weaker than in winter and spring, but their structures are similar to both seasons that are following.

The Polar Low, as well as the lower level structures are still developing in autumn. With the beginning of the polar night, that reaches its maximum at the beginning of winter, the cyclones grow stronger but migrate more to the North.
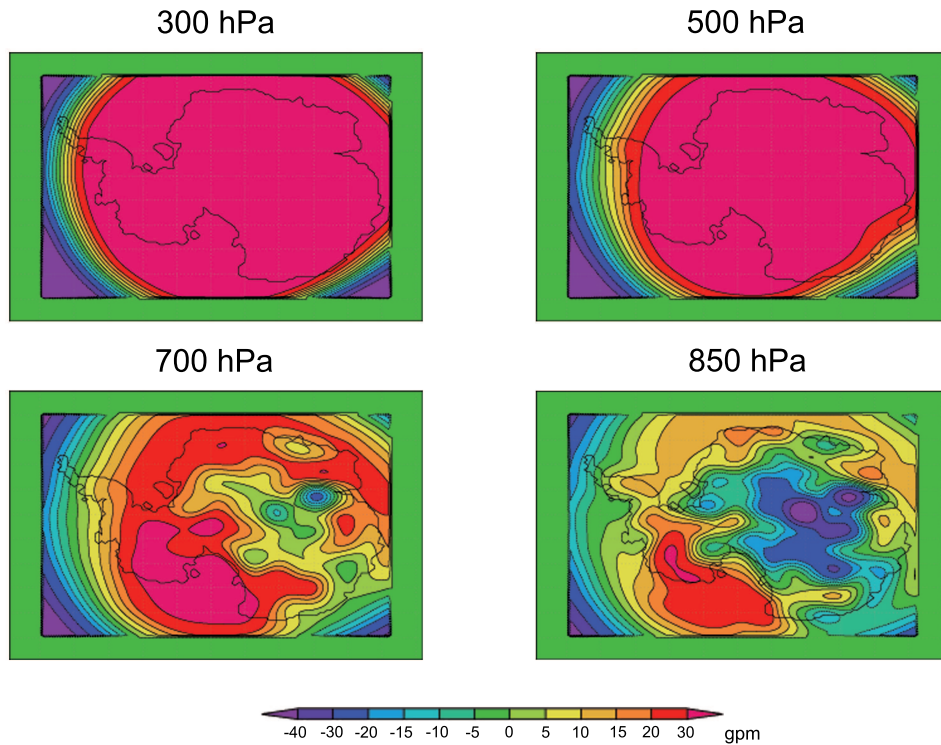
Figure 8.24: Winter Geopotential on the levels 300 hPa (upper left), 500 hPa (upper right), 700 hPa (lower left) and 850 hPa (lower right). 1994 to 1999 (ERA40 run). Used filter: SYN

In winter the Polar Low is strongest, even stronger than in spring. On 700 hPa the clear structure of the cyclone ring and the high at the entrance of Prydz-Bay can be seen. The high over the Antarctic Plateau at 850 hPa is clearly pronounced.

Due to the reduced radiation in the polar night, the Polar Low is strongest in winter. This leads to a strong pressure gradient at its edge which forces the developement of cyclones. These cyclones, that can be seen in levels of the middle troposphere are also strongest in winter and occur in a ring around Antarctica. Especially in winter, this ring is shifted more to the North. In combination with the long wave radiation and thus cooling over the Antarctic Plateau, a high over the Antarctic continent is developing.

The wave train like structures can be identified below 700 hPa, which is an evidence that they have their origin in model orography. When the wave patterns are coupled to the orography, they are not necessarily synoptical effects, but can still be influenced through synoptical phenomena. They are certainly no gravity wave drags or similar phenomena, because they would not be seen in mean plots over monthly or longer time periods. In heights from 500 hPa and above the Polar Low can be seen clearly. Wave patterns in lower levels can also be due to interpolation effects since the orographic features reach through these levels. The nearer a level is to the ground, the more it looks similar to the ground

level Figures. It is important to notice, that especially the 850 hPa level already reaches ground on the Antarctic Plateau. Geopotential values are extrapolated to 850 hPa, which lies beneath the ground.

8.5   Baroclinity

As an additional tool to analyse Synoptic Structures, the baroclinity of the ERA-interim run was calculated based on a method by Hoskins and Valdes (1990):

$$\sigma = 0.31 * \frac{f}{N} \times \left| \frac{\partial(u, v)}{\partial z} \right| \tag{8.1}$$

with the Brunt-Vaisala-Frequency:

$$N = \sqrt{\frac{g}{\theta} \frac{\partial \theta}{\partial z}} \tag{8.2}$$

the potential temperature:

$$\theta = T \left(\frac{p_0}{p} \right)^{\kappa} \tag{8.3}$$

the Coriolis-Parameter:

$$f = 2\Omega \sin \varphi \tag{8.4}$$

The baroclinity was calculated from temporal mean values over the whole integration period of the ERA-interim run and its summer (DJF) and winter (JJA) mean respectively in 500hPa and 850hPa height.
In Figure 8.25 the mean baroclinity over the time period fom January 1996 to December 2009 at 500hPa is shown. Over the continent, the baroclinity is generally lower than over the sea. The orographically structured terrain shows distinctive patterns that are due to a certain wind shear in mountainous areas. Over the ocean and especially further north the baroclinity values are increasing, which is due to decreasing stability northwards. Figures showing only wind shear and Brunt-Vaisala-Frequency can be found in the appendix.
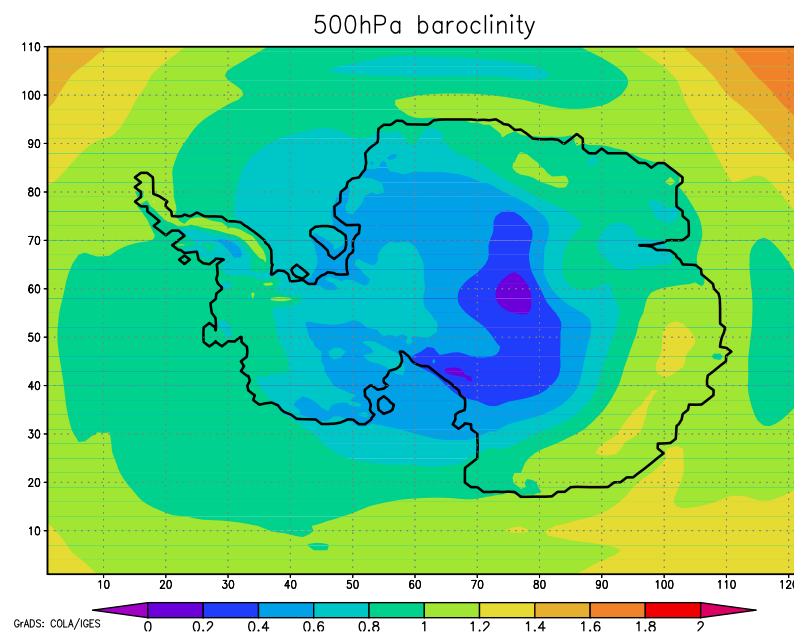
Figure 8.25: Mean Baroclinity of the ERA-interim run (Jan. 1996 to Dec. 2009) at 500 hPa.

The baroclinity at 850 hPa, shown in Figure 8.26, is strongly influenced by orographic structures, mostly due to wind shear in steep areas. It is generally lower than the baroclinity on 500hPa. Therefore for further analysis, concerning differences between summer and winter, only 500 hPa baroclinity will be considered.
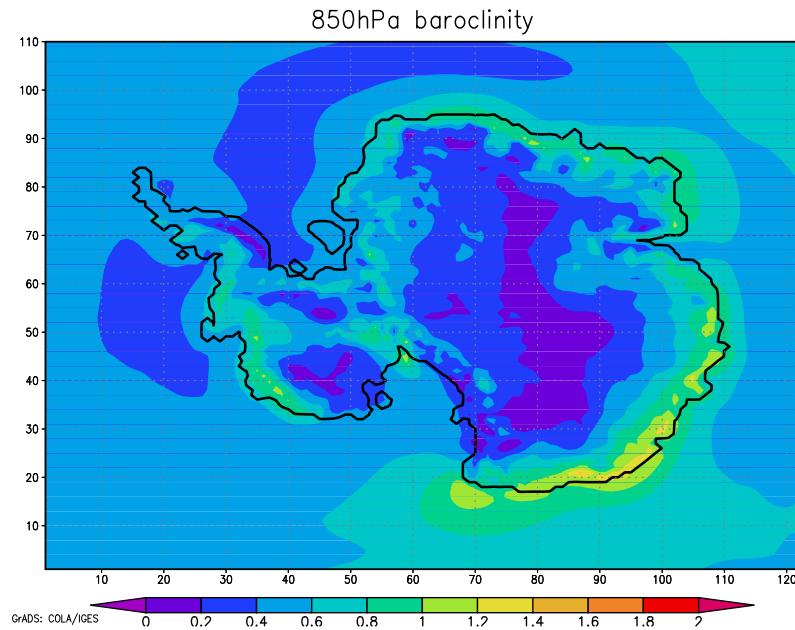
Figure 8.26: Mean Baroclinity of the ERA-interim run (Jan. 1996 to Dec. 2009) at 850 hPa.

Figures 8.27 and 8.28 show the mean 500 hPa baroclinity in summer, respectively winter months from 1996 to 2009. In winter the baroclinity values are lower than in summer, showing a seemingly concentric pattern around Antarctica. In summer there are three maxima around the continent and a minimum over the continent. By comparing those two Figures to 8.12 and 8.13, one can see similarities between filtered MSLP and baroclinity. The baroclinity maxima occur in regions, where filtered MSLP also has higher values. But in baroclinity there is a clearer wave-like-pattern.
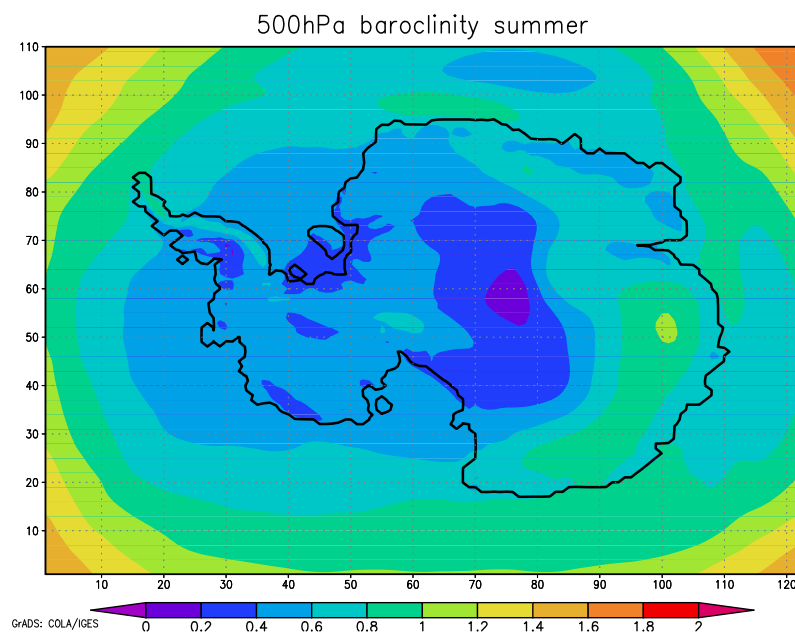
Figure 8.27: Mean Baroclinity of the ERA-interim run (summer DJF 1996 to 2009) at 500 hPa.
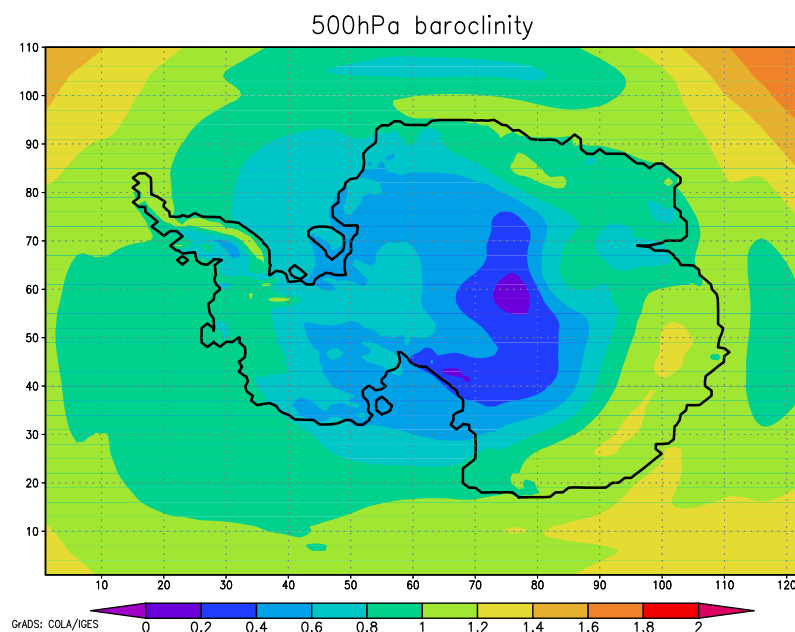
Figure 8.28: Mean Baroclinity of the ERA-interim run (winter JJA 1996 to 2009) at 500 hPa.

The baroclinity patterns support the results of the analysis with the filter tool, concerning the positions of synoptical systems.

Chapter 9

Analysis of AAO-phases

AAO is the Antarctic Oscillation as described in 2.1. In this chapter typical AAO patterns in positive and negative phases will be analysed, seperately for winter and summer months. Of the years 1996 to 2009, modelled in the ERAint run, three summers with positive AAO phases and three summers with negative AAO phases as well as three winters with positive, respectively negative AAO phases are chosen for this study. The AAO-phases of these years were calculated with ERA-interim-data at 700 hPa geopotential height, and from $-20°$ to the Southpole.
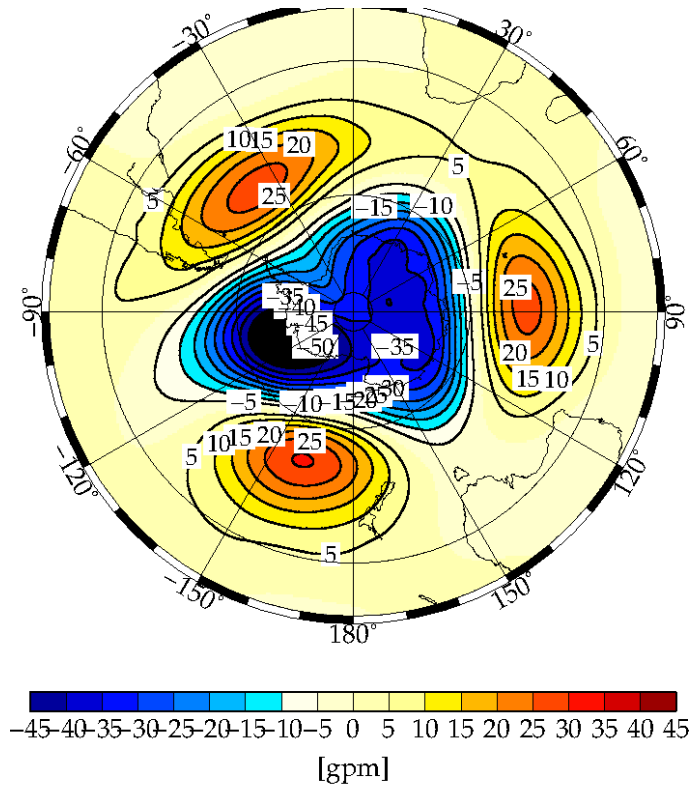
Figure 9.1: First EOF of Antarctica in the years 1996 to 2010 at 700hPa.

The years chosen for this study are the following:

- Summer AAO positve: 2000, 2002, 2008

- Summer AAO negative: 2001, 2004, 2006

- Winter AAO positve: 1998, 2004, 2008

- Winter AAO negative: 2002, 2007, 2009

Summer months are December of the previous year and January and February of the actual year. Winter months are June, July and August.
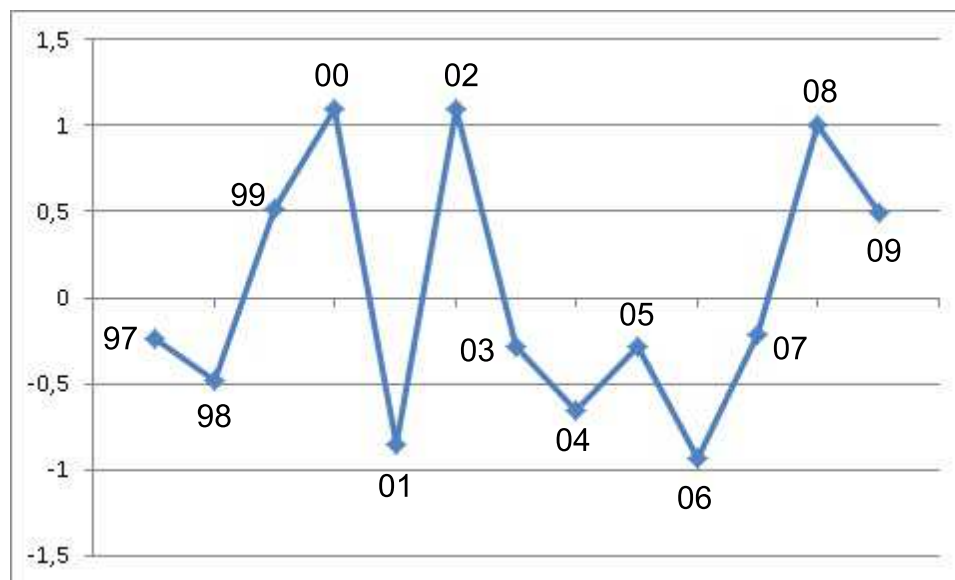
Figure 9.2: AAO phases of summer seasons of the years 1997 to 2009.
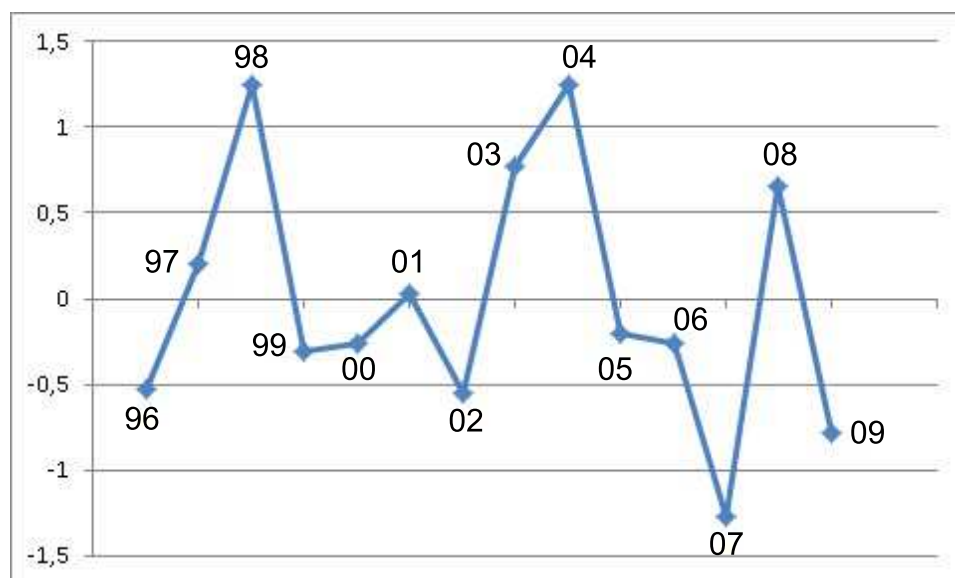
Figure 9.3: AAO phases of winter seasons of the years 1996 to 2009.

9.1 AAO-Phases on Synoptical Scales

MSLP, TWV and T2m datasets of these seasons were filtered using the SYN filter tool to show the impact of the different AAO-phases on synoptic scales. The SYN-filtered data shows the deviation from the 15-year temporal and model-area spatial mean of the model run. Low pressure deviation, for example, has a negative deviation from the average,

meaning the mean values were substracted from the filtered data. Respectively dryer air in the filtered data has negative values as well as lower temperature.

For the Figure 9.4 a seasonal mean of the positive phases and respectively the negative phases for each variable was calculated. From these mean values a difference was calculated, substracting the mean of the seasons with positive phases from the mean of the seasons with negative phases.

In summer, the seasons of AAO+ have a -5 hPa stronger low over Amundsen- and Ross-Sea, but also over West-Antarctica. The pressure is lower in AAO+ years than in AAO-years for almost the whole integration area. The low over Amundsen-Sea is in AAO+ winters -4 hPa stronger than in AAO- winters, there is also a stronger low over Prydz-Bay in East-Antarctica. On a synoptical scale of 500 km to 1000 km the AAO phases have their strongest impact in West-Antarctica and the corresponding seas. Glushak (2007) finds similar MSLP patterns in her study of different AAO phases from 1958 to 1998.

As in positive years the humidity over the Peninsula and the region north and east of it is 0.5 mm higher than in negative years, in summer as well as in winter, the humidity seems to be coupled with the low pressure system in Amundsen and Ross Sea. The coastal region of East Antarctica, especially western of Ross Sea is 0.5 mm dryer in positive years than in negative years. This region lies upstream of the Ross/Amundsen-Low, whereas the Peninsula lies downstream of this low. This leads to a humidity transport via the Ross/Amundsen-Low from Dumont-D'Urville-Sea to Bellingshausen Sea. van den Broeke and van Lipzig (2004) found a similar behaviour of humidity in their study of a 1980 to 1994 RACMO/ANT1 simulation.

Also the temperature is higher in positive years (up to 4 K in winter) over the Peninsula, whereas it is lower in those years over East-Antarctica. These results correspond to the study of Kwok and Comiso (2002a). They studied the dependence of surface temperature, retrieved from AVHRR Radiometer, from the AAO phase. This could correspond to a heat transport from east to west via the Ross/Amundsen-Low. In winter this pattern is stronger than in summer. In summer, the temperature gradient around the coast is weaker than in winter. So in winter, heat transport has in general a stronger effect than in summer.

As a comparison between filtered and unfiltered data, in Figure 9.5 the same variables as in Fig. 9.4 is shown, but for unfiltered data. The differences between the AAO phases is stronger for the unfiltered data (e.g. 7 hPa for MSLP). The patterns of both look similar, although in 9.5 small scale phenomena can be distinguished, which are not due to synoptical activities.
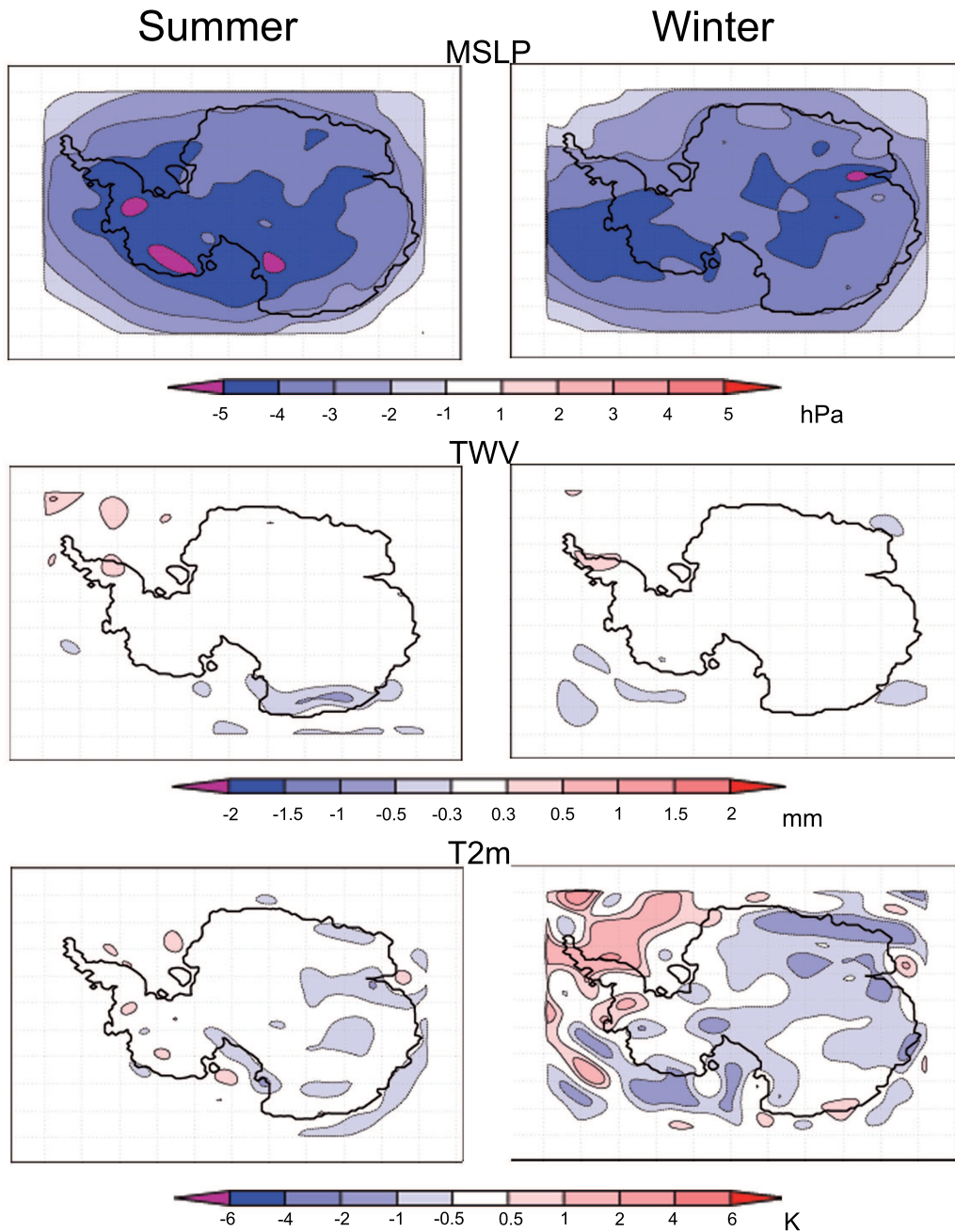
Figure 9.4: Difference of the mean of the filtered values from the positive AAO years (Summer: 2000, 2002, 2008 and Winter: 1999, 2001, 2006) minus the mean of the filtered values from the negative AAO years (Summer: 2001, 2004, 2006 and Winter: 1997, 2004, 2009). Difference of MSLP summer (upper left), difference of TWV summer (middle left) and difference of T2m summer (lower left) and the difference of MSLP winter (upper right), difference of TWV winter (middle right) and difference of T2m winter (lower right). Used filter: SYN.
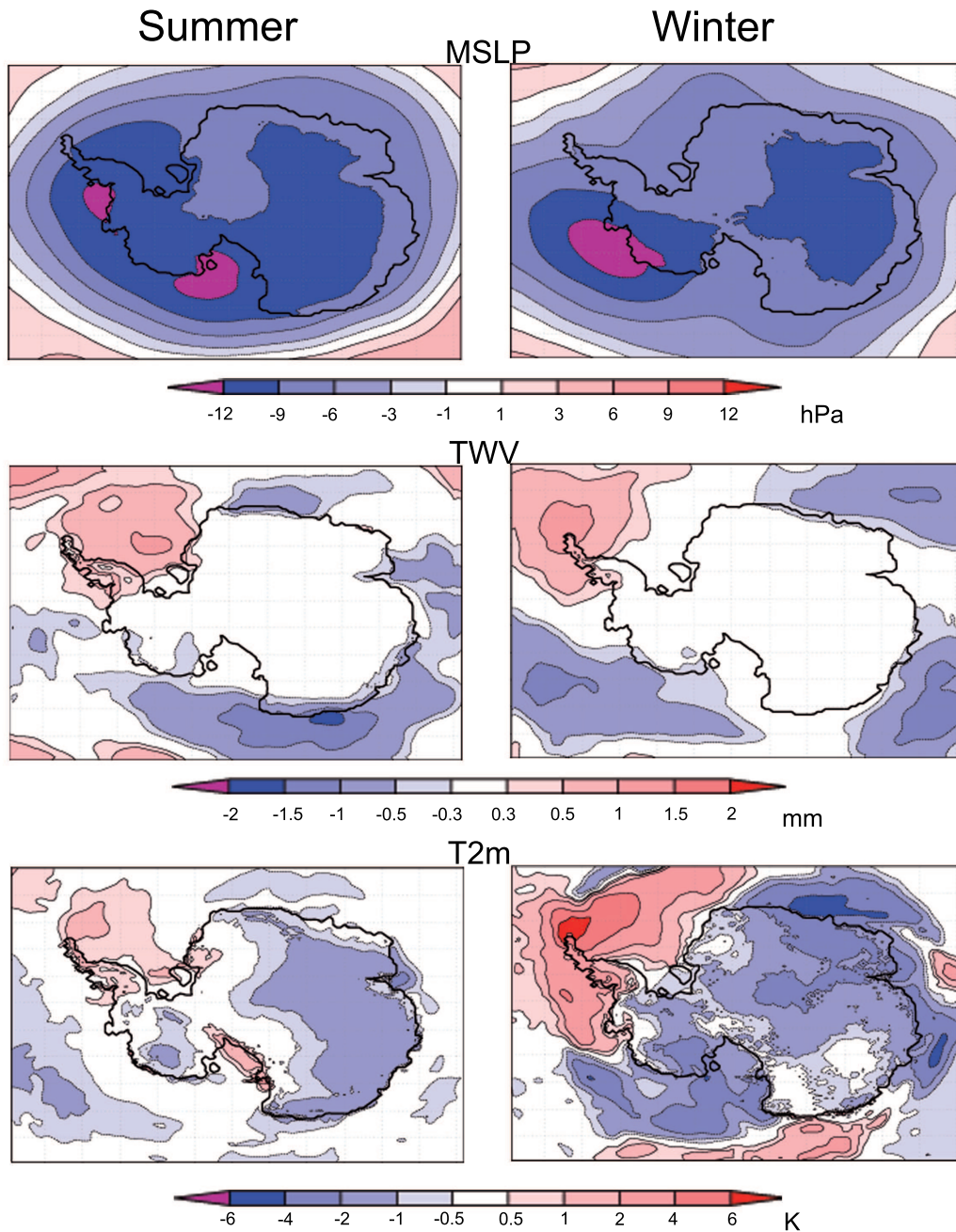
Figure 9.5: Difference of the mean of the filtered values from the positive AAO years (Summer: 2000, 2002, 2008 and Winter: 1999, 2001, 2006) minus the mean of the filtered values from the negative AAO years (Summer: 2001, 2004, 2006 and Winter: 1997, 2004, 2009). Difference of MSLP summer (upper left), difference of TWV summer (middle left) and difference of T2m summer (lower left) and the difference of MSLP winter (upper right), difference of TWV winter (middle right) and difference of T2m winter (lower right).

The differences between AAO+ and AAO- phases ist strongest for MSLP, so this variable will be analysed further. In the following Figures the three positive and negative phases of each season of MSLP are shown in a panel, sorted by season.

In the Figures 9.6 to 9.8 the MSLP of the positive and negative AAO seasons for each of the chosen years is shown. The Figures are sorted in couples, for better clarity. The comparison is made for all six chosen seasons. In the positive summers MSLP around Antarctica is generally lower than in negative years, but with different strengths. The differences between the single AAO-positive phases is less pronounced in summer than in winter. All three AAO-positive summer seasons (2000, 2002 and 2008) show a strong low in Ross/Amundsen-Sea, only the strenght of the high over East Antarctica is varying.

In the winter season, which is shown in Figures 9.9 to 9.11, one can also see differences in the MSLP pattern in the positive and negative years. Also, as in the summer season, generally speaking, the MSLP is lower in the positive years, than in the negative years. In the year 2002 (upper left), the Ross/Amundsen-Low is exceptionally weak, but instead of this low, the low pressure zone around East Antarctica is stronger than in the other two negative winters. The positive winter of 1998 (upper right) has a very strong Ross/Amundsen-Low. In the year 2004 (middle right) the Ross/Amundsen-Low is weaker, but the lows from Dronning-Maud-Land to Prydz-Bay are pretty strong, making the connection between these two low pressure systems seem like a see-saw.
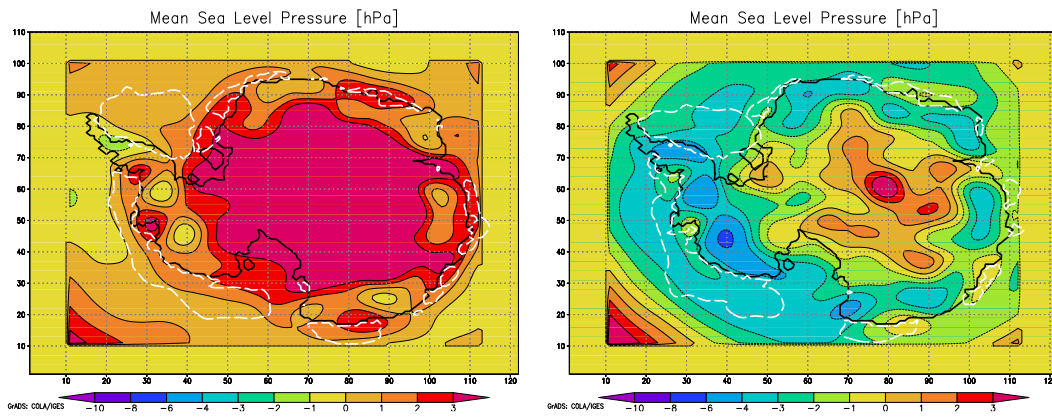
Figure 9.6: Filtered MSLP of the AAO-negative summer 2001 (left) and the AAO-positive summer 2000 (right). Used filter: SYN. Difference from the spatial and temporal average over the whole period.
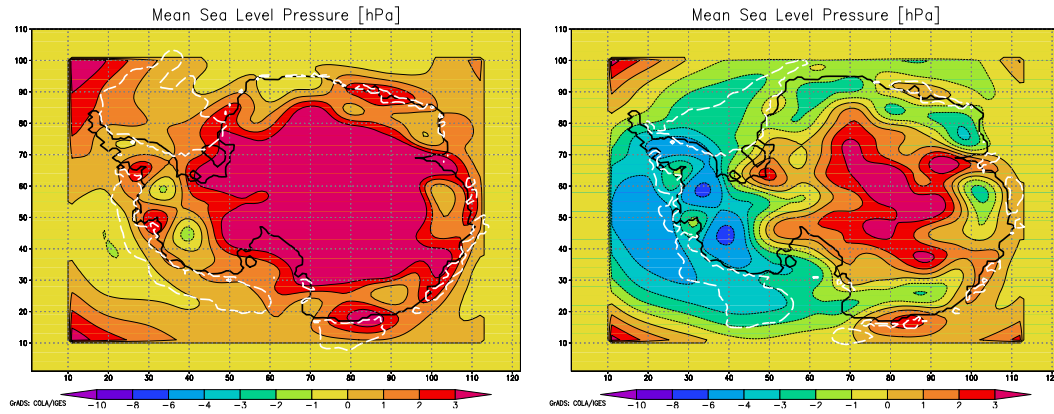
Figure 9.7: Filtered MSLP of the AAO-negative summer 2004 (left) and the AAO-positive summer 2002 (right). Used filter: SYN. Difference from the spatial and temporal average over the whole period.
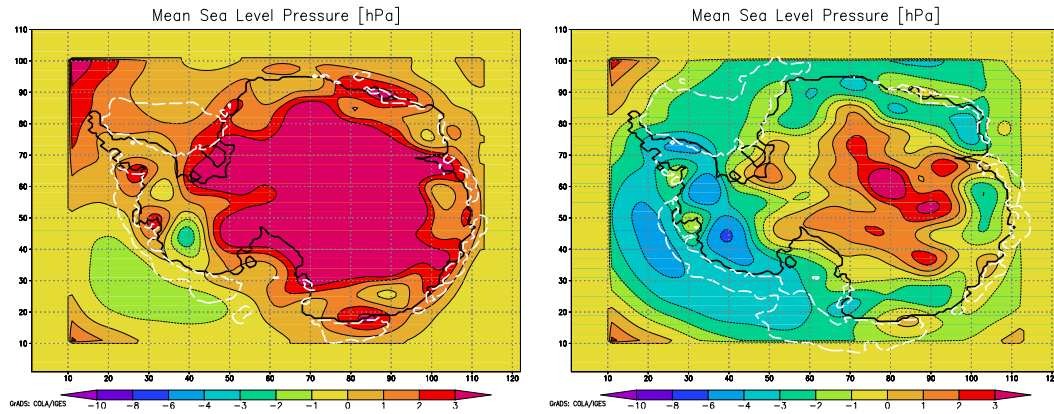
Figure 9.8: Filtered MSLP of the AAO-negative summer 2006 (left) and the AAO-positive summer 2008 (right). Used filter: SYN. Difference from the spatial and temporal average over the whole period.
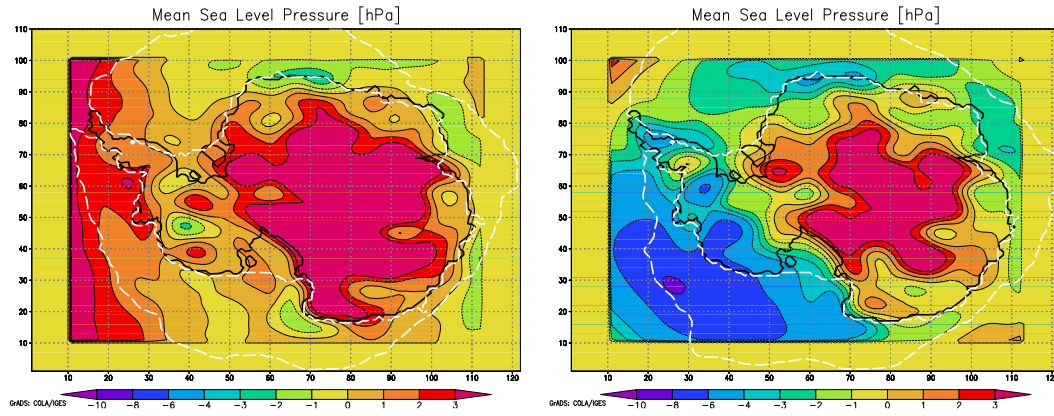
Figure 9.9: Filtered MSLP of the AAO-negative winter 2002 (left) and the AAO-positive winter 1998 (right). Used filter: SYN. Difference from the spatial and temporal average over the whole period.
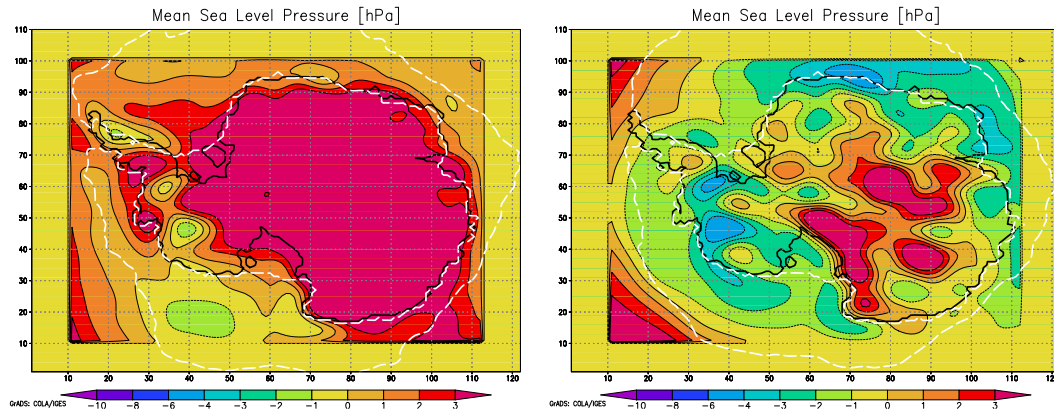
Figure 9.10: Filtered MSLP of the AAO-negative winter 2007 (left) and the AAO-positive winter 2004 (right). Used filter: SYN. Difference from the spatial and temporal average over the whole period.
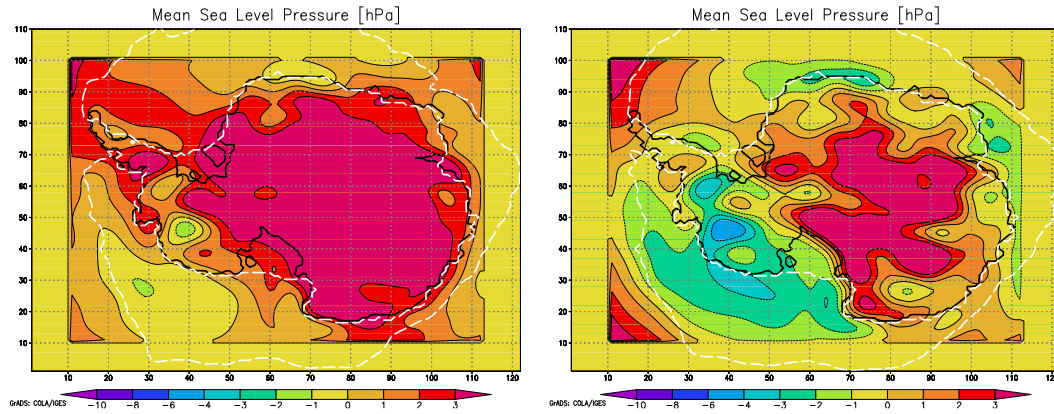
Figure 9.11: Filtered MSLP of the AAO-negative winter 2009 (left) and the AAO-positive winter 2008 (right). Used filter: SYN. Difference from the spatial and temporal average over the whole period.

9.2 P-E in different AAO-Phases

Another important field of study are the precipitation budgets in the different AAO-Phases. The precipitation minus evaporation (P-E) budgets were calculated as a mean value of the three positive and negative summers, respectively winters. Precipitation consists of large-scale and convective precipitation, although the latter does not play a significant role in Antarctica. The P-E values shown here are a seasonal means of daily P-E budget. The daily data is more accurate since both seasons, summer and winter have a different number of days.

The mean of the absolute P-E values are shown for the positive and negative summers (9.12). On the right side the difference between both phases is shown as the difference of the mean of the positive years minus the mean of the negative years (c.f. 9.13). The precipitation budget has almost everywhere positive values, in positive as well as in negative years. Over the continent the budget is around zero, it is balanced. Over West-Antarctica and around the coast, P-E is positive, which means that the snow intake exceeds the loss, and the glaciers should be growing, when outflow is not taken into account. In the positive years, the P-E mean has even higher values over the Peninsula than in negative years.
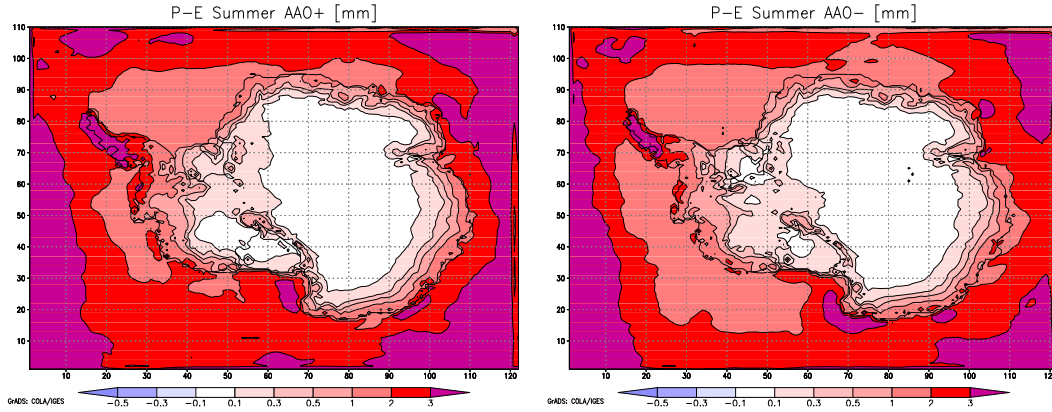
Figure 9.12: P-E mean of the AAO-positive (left) and AAO-negative (right) summers.
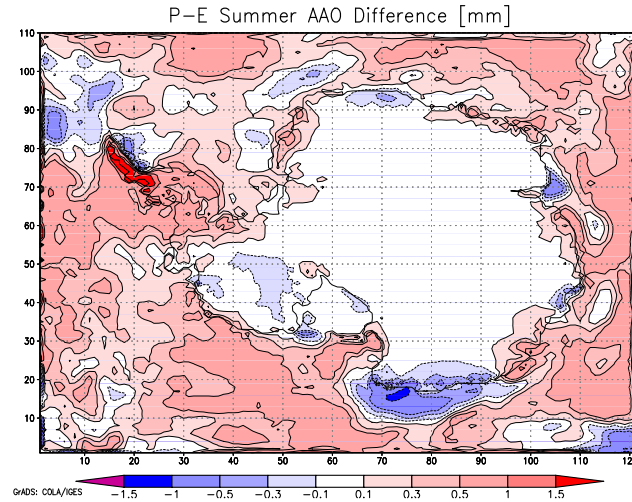
Figure 9.13: P-E difference of positive minus negative summers.

Figure 9.14 (left side) shows the absolute P-E values of the positive, Figure 9.14 (right side) depicts of the negative winters. The difference between the AAO-positive and AAO-negative years is shown in Fig. 9.15. Also here, the budget is mostly positive, except for the central continent and the shelf-ice-zones. In winter, as in summer, the positive years also have a higher P-E-bugdet than the negative years over the Peninsula. In positive years the precipitation input on the Peninsula is obviously higher than in negative years, which is linking the AAO-Phases to the P-E budget.
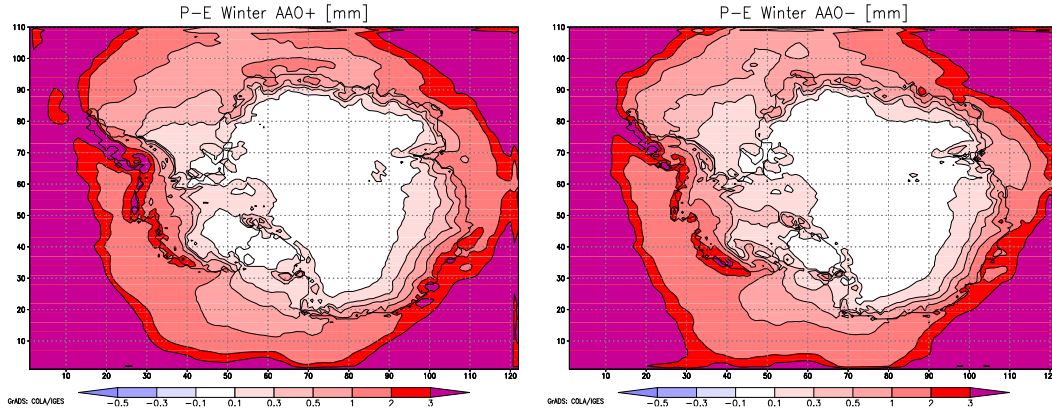
Figure 9.14: P-E mean of the AAO-positive (left) and AAO-negative (right) winters.
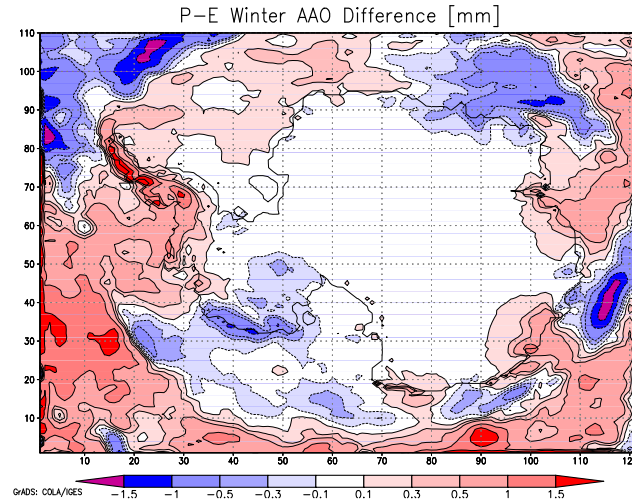
Figure 9.15: P-E difference of positive minus negative winters.

As could be seen in the Figures above, the mean precipitation minus evaporation budget is higher in the AAO-positive phases. This has a direct effect on the Peninsula and some other coastal regions, leading to glacier growth, if the outflow rate stay constant over the changing phases. In inner Antarctica a direct effect could not be shown by HIRHAM calculations. But due to an effect that is not part of the parametrisation of the model, horizontal snowdrift, higher precipitation income will also lead to glacier growth in the inner regions of East Antarctica.

Chapter 10

Summary

Antarctica is a very sensitive region concerning climate change. Melting glaciers and decaying shelf-ice, such as Larsen-B, are a hint for certain modifications in the climate of this continent. But not only is the changing climate influencing Antarctica, it also works vice versa. Changes in Antarctica influence the climate in the whole world. The glaciers of Antarctica are a huge white shield with a high albedo, a decay would lead to an even faster rise of 2m-temperature than recently measured. Changes in humidity also have a big influence on whether the ice-sheet is decaying or growing.

Humidity is one important point this study focuses on, the other is pressure patterns, both on decadal time scales. To understand humidity it is important to know the mean pressure patterns. Humidity transport is bound to synoptical pressure systems, cyclones are contributing a good part to precipitation especially in the coastal zones. Since atmospheric measurements are rare in Antarctica, model results can help closing gaps of knowledge. After a validation of the model against measurements from stations, the model results are proven to be reliable and model output helps to understand the estimated behaviour of the antarctic atmosphere.

Measurements were provided from GPS satellite retrieval and radiosounding data. These measurements have been compared to the regional climate model HIRHAM and the re-analyses ERA and NCEP. Radiosondes provide data of the most important meteorological variables, pressure, wind, temperature and humidity, GPS retrieval only offers total water vapour (TWV) data, which equals vertically integrated specific humidity. Both methods are profoundly different, technically and in the air volume they measure. For this reason measuring directions of both methods have been compared to each other. As radiosondes mostly tend to drift to the south, GPS satellites do not have an elevation of more than $60°$ south, so both methods are measuring different air volumes, which also shows in the data. By comparing GPS-derived data with data from Radiosondes, certain differences can be explained through the different observing regions of Sounding and GPS. If the sonde tends to drift over the continent, a dry bias in the comparison can be seen, because GPS signals are always covering the northern region of the station, which is located over the sea for coastal stations. Still, GPS retrieval is a good addional method for humidity measurement. A finer net of measuring sites could improve the uncertainties of the measurement, espe-

cially in case of the GPS-measurement, pressure measurements should be provided close to the GPS-station. The measuring equipment should be kept under frequent maintenance, to prevent freezing or snow on the cover.

HIRHAM is a regional climate model consisting of model dynamics from HIRLAM and model physics from ECHAM. Here it is integrated over Antarctica with 122×110 grid points and 25 levels. Its grid point spacing is 50 km. Sea ice thickness is set to 1m, which is thinner than in the Arctic-Setup and determined by the boundary forcing. Boundary layer physics, cloud-condensation-scheme, hydrology and soil temperature are parametrised. It is run with boundary conditions from ERA40 (1994 to 1999) and ERAinterim (1996 to 2009). Both setups differ slightly from each other, but not significantly. So both time periods are comparable with each other, if no other analysis tool is applied to one or the other. All results have been analysed with different statistical analyses, such as standard deviation, pattern correlation and a spatial filter, developed at the HZ Geesthacht (Feser and von Storch (2005)).

HIRHAM data has been compared to the reanalyses ERA40 and NCEP for the mean of the values of MSLP, 2m-Temperature and TWV over the period from 1 January 1994 to 31 December 1999. Over sea there are only small differences for all three variables, but over land the values differed more, even significantly for the comparison of HIRHAM and NCEP. Most differences can be explained through the coarser resolution und thus different representation of the orography of the reanalyses. Since ERA40 is the boundary reanalysis for HIRHAM, the differences between both are smaller and not sgnificant.

Also HIRHAM results have been validated against the measurements and the reanalyses at the station sites. TWV data has been compared with time series concering monthly means over a period from 1994 to 1999. For this comparison instead of an interpolation to station position, the four surrounding HIRHAM grid points have been taken into account. It shows that the steep antarctic orography leads to differences between measurements and model. Although the stations have heights of about sea level, some of the surrounding grid points can be more than 1000 m high. Since humidity is sinking profoundly with height, most HIRHAM grid points tend to be dryer than the measurements provided by the station. A finer model resolution can help to solve this problem, but it should be kept in mind, that in steep orographies even distances of 25 km can lead to profound heigh differences. Still, HIRHAM provides a good performance considering TWV simulation on decadal time scales, if problems with the direct station to grid point comparison are taken into account.

The same applies for the comparison between HIRHAM and ERA40 data and radiosounding via vertical plots. For a more detailed validation of HIRHAM, here also wind and temperature have been compared as well as specific humidity on different heights. Again, the differences in station and grid point height have to be taken into account. In lower levels height differences between station and model grid point lead to different temperature and humidity, but the higher the levels get, the more similar to each other are the data from model and measurement. This proofs that the RCM HIRHAM is a useful tool in analysing atmospheric structures.

Not only as an explaination for different TWV values derived from sounding and GPS, the

main wind directions at the stations sites have been compared with the main measuring
direction of the GPS signal paths. The main wind direction of the soundings have been put
into bins of 10° over the period from 1 January 1994 to 31 December 1999. The satellite
tracks are plotted for one example day (26 January 1998), as they are highly repetitive.
GPS satellites mostly measure air masses north of the stations from over the ocean, but
radiosondes drift with wind and sometimes mainly drift along the coast or over the land,
thus measuring a different and drier air mass. Additionally the main wind directions of the
HIRHAM-ERA40-run and ERA40 itself have been compared in the same manner. Mostly
they are in good accordance to each other. In some cases the direction differs slighty or
the wind directions in ERA is not as constant as in HIRHAM. Those differences are most
likely due to the coarser resolution in ERA40 and the resulting different representation of
the orography. The results show that HIRHAM displays the directional constancy of the
antarctic wind regime well, which is one of the characteristics of katabatic winds.

When comparing the RCM with measurements, differences can occur due to changes in
measurement methods and due to resolution and parametrisation of the model. An im-
portant measuring method in this thesis is the measurement of wind, temperature and
total water vapour with radiosondes. During the early nineties, around the time period
of the HIRHAM-ERA40-run, the positioning technique of radiosondes has changed from
LORAN-C (Omega) or radar to positioning via GPS. Since radiosondes provide boundary
conditions for the reanalyses and the RCM, changes apply for radiosondes and models in
a similar way. In HIRHAM, ice free zones on the continent are not resolved, the whole
continent is covered with glacier. Polynyas are on average about the size of a grid area,
or even bigger, but small polynyas can not be resolved in the model. Differences in the
represantation of ice free zones on the continent and over sea lead to differences in latent
heat and humidity.

After the validation of the model, its data has been analysed concerning synoptical pat-
terns. A simple, but useful tool to do so is the pattern analysis via standard deviation.
The standard deviation has been analysed from daily means, typical synoptical patterns
last 2 to 6 days, so their frequency is covered well enough by this method. Here it could be
shown, that in the HIRHAM grid area the most active region is the Ross- and Amundsen-
Sea region. The MSLP standard deviation shows that the main cylone tracks are north of
the East Antarctic Coast stations. This is one reason for the humidity being lower in this
region. Additionally, it can be supposed that cyclone tracks are fixed to boundary forcing
values, because most cyclones develop in an area that lies near or in the boundary zone or
even north of it, so that they are not performed in the regional climate simulation. Antarc-
tica is a continent with low humidity and a strong humidity gradient around the coast.
This is because of the different humidities over land and over sea, but also because of the
steep orography in Antarctica. Peninsula stations naturally have a higher humidity than
East Antarctic coastal stations. This behaviour explains the results found in analysing
the TWV timeseries.

For a finer analysis of pressure patterns, a filter tool developed at the HZ Geesthacht has
been used. Typical zones of high and low pressure, sorted by wave lengths could be iden-
tified. Over the Antarctic Continent there is a high pressure zone, over the seas around

it, especially in latitudes of ca. 60° mostly low pressure structures can be found. The patterns, with active zones from Ross Sea, stretching to Amundsen Sea and the Peninsula, do also occur, if the signals are spatially filtered in wavelength ranges of 500 to 1000 km, showing that these zones are synoptically active. In higher levels there is a significant polar low, right over the continent and opposed to the high pressure area over the continent. Spring is the synoptically most active season, in the ERA40 run as well as in the ERAint run. This is also the season with the least differences between both runs. In autumn the high over the plateau is stronger in the ERA40 run and in winter the lows over West Antarctica and Amundsen sea is more intensive than in the ERAint run. The intensity of the synoptical patterns in the single seasons is also changing from year to year. The most intensive pattern in the spring season occur in the years 1998, 1999, 2001, 2005, 2007 and 2008. The two different time periods are not comparable in this analysis, as the shown values are deviations from the respective period mean (1994 to 1999 and 1996 to 2009).

To find AAO-positive and AAO-negative seasons for an analysis of the synoptical behaviour in different AAO-phases, the first EOF of the Antarctic region has been calculated with ERA-interim data of the years 1996 to 2009. AAO-positive summers could be found in the years 2000, 2002 and 2008, AAO negative summers in the years 2001, 2004 and 2006. AAO-positive winters were 1998, 2004 and 2008, AAO-negative winters 2002, 2007 and 2009. Patterns of MSLP, T2m and TWV were analysed mainly based on filtered data. In AAO-positive phases the pressure is lower than in AAO-negative phases, especially in the region around West Antarctica. This effect is coupled to a higher humidity in this region on AAO-positive seasons. The T2m patterns are more complicated with an increased temperature in the Peninsula region and a decreased temperature over East Antarctica in AAO-positive winters. The strenght and the position of the lows varies from year to year with possible shifts of the minimum from Ross/Amundsen-Sea to Dronning-Maud-Land. Based on the before found positive and negative AAO-phases, also the P-E-budget in the different seasons has been analysed. It was shown, that for a seasonal mean of daily P-E-budgets, the precipitation is stronger in AAO-positive phases. which is also consistent with the higher humidity and stronger lows in these seasons. The results of the analysis of the AAO-Phases on synoptical scales are according well to the results in the studies of van den Broeke and van Lipzig (2004) and Kwok and Comiso (2002a).

The data of the RCM is a valuable addition to measurements in the only sparcely covered Antarctica. The application of the regional climate model HIRHAM on the Antarctic shows a synoptical active region most pronounced in Ross/Amundsen-Sea. It is clearly shown, than in AAO-positive phases the cyclones are more active than in AAO-negative phases. In the future HIRHAM should be adapted more for the special conditions in Antarctica, especially concerning the planetary boundary layer and the strong temperature inversion. A finer model could also give a better representation of katabatic winds and polynyas. With those ameliorations it would be possible to calculate the changes in Antarctica more detailed and to understand the connections between the global climate and Antarctica better.

Appendix A

Sensitivity Studies

A.1   Sensitivy studies concerning vertical resolution

To ascertain a good display of the atmospheric boundary layer (ABL), a sensitivity study was conducted, with 25 and 46 vertical levels. 46 level HIRHAM (46Levs) needs a smaller timestep (60 s) than 25 level HIRHAM (25Levs) (120 s) because of numeric instabilities. Despite the finer vertical resolution and the smaller timestep the setup was the same for both model runs. To compare both model setups only two months were simulated for each: January 2001 and July 2001. The ratio of the monthly mean of a difference and its standard deviation shows the significance of a difference between two setups. If this ratio is lower than 0.7, it can be considered as not significant.

In Figures A.1 and A.2 the MSLP differences between 46Levs and 25Levs are plotted. In both, summer and winter, the differences between 46Levs and 25Levs is smaller than $|1.2|$ hPa in almost the whole model area, with a slightly better accordance in summer. The pattern correlation between both sensitivity runs is 0.99 for every variable (c.f. Table C.3). The biggest differences can be found on the Plateau and winter in Amundsen Sea near the West-Antarctic coast.
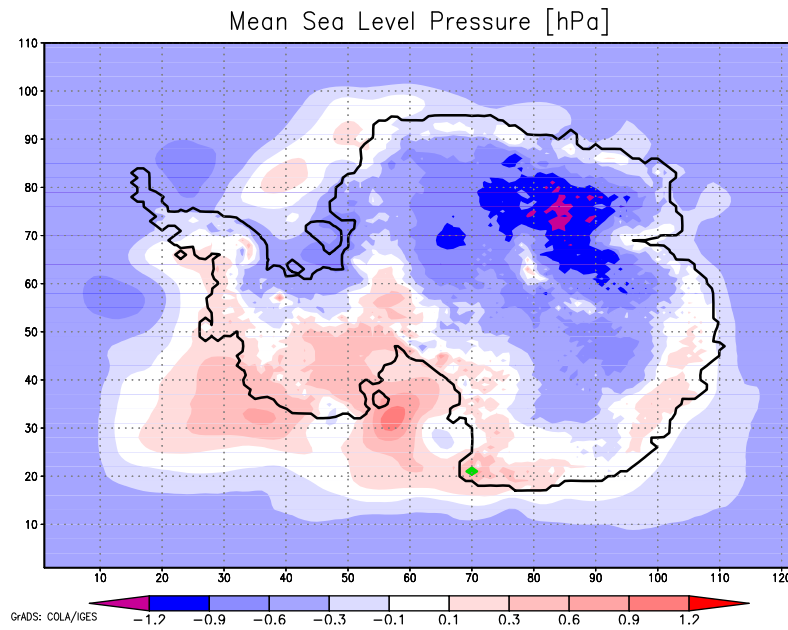
Figure A.1: MSLP difference between 46lev and 25lev in January 2001. Green: Significance.
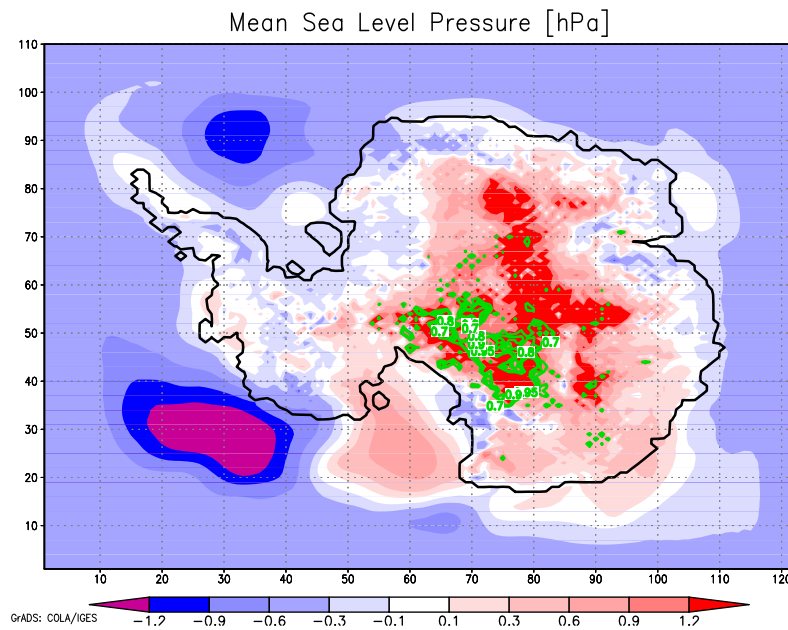
Figure A.2: MSLP difference between 46lev and 25lev in July 2001. Green: Significance.

Figures A.3 and A.4 show the differences in T2m between 46Levs and 25Levs. In summer 46Levs is colder then 25Levs, in almost the whole model-region. Nevertheless the

difference never exceeds 1.2 K. In winter 46Levs is around 0.6 K warmer than 25Levs in certain regions like East Antarctica or the sea. The differences exceed a value of 1.2 K, especially in the Ross Sea and in mountainous areas.
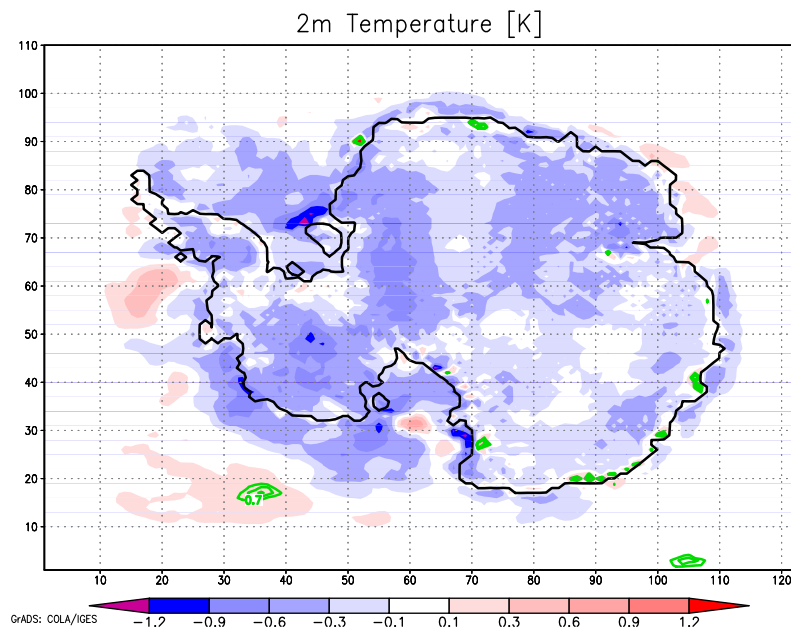
Figure A.3: T2m difference between 46lev and 25lev in January 2001. Green: Significance.
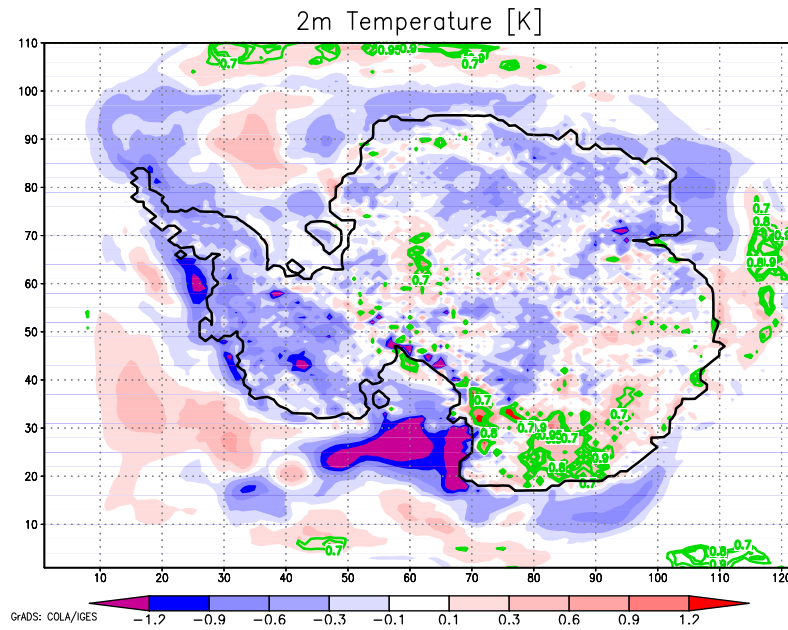
Figure A.4: T2m difference between 46lev and 25lev in July 2001. Green: Significance.

The differences in TWV are shown in Figures A.5 and A.6. Generally, the differences between both runs are smaller than 1.0 g/kg, in winter they are even smaller than 0.3 g/kg. 46Levs is dryer than 25Levs, which is consistent with the T2m-difference.
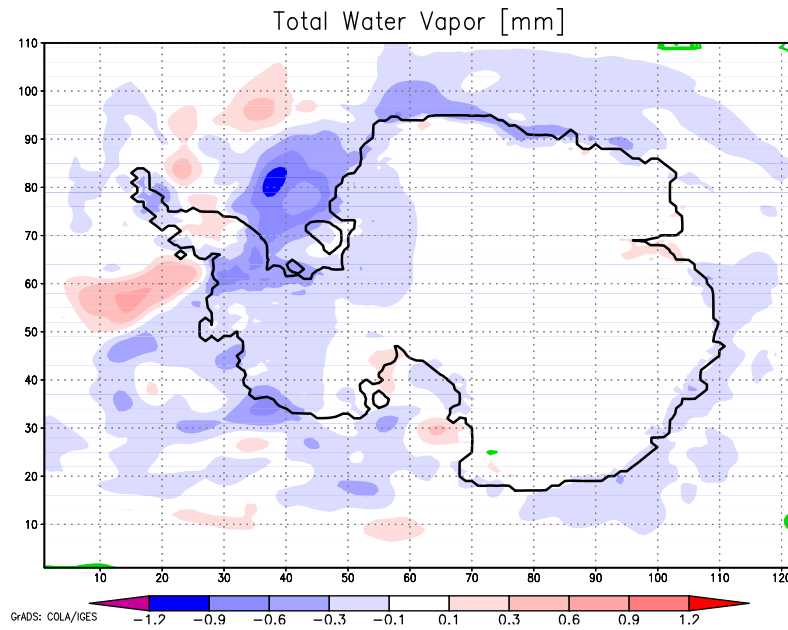
Figure A.5: TWV difference between 46lev and 25lev in January 2001. Green contour lines: Significance.
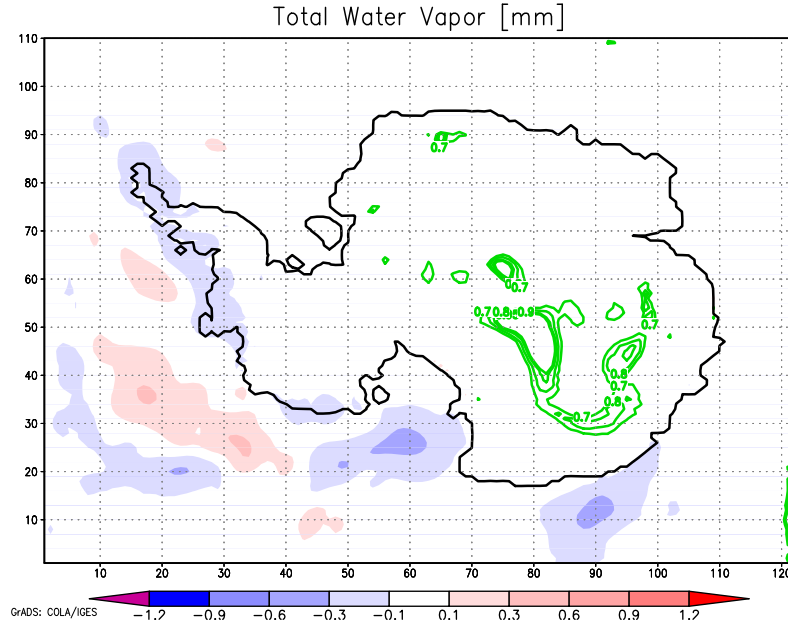
Figure A.6: TWV difference between 46lev and 25lev in July 2001. Green contour lines: Significance.

In Figures A.8 to A.11 vertical cross sections over the HIRHAM integration region are
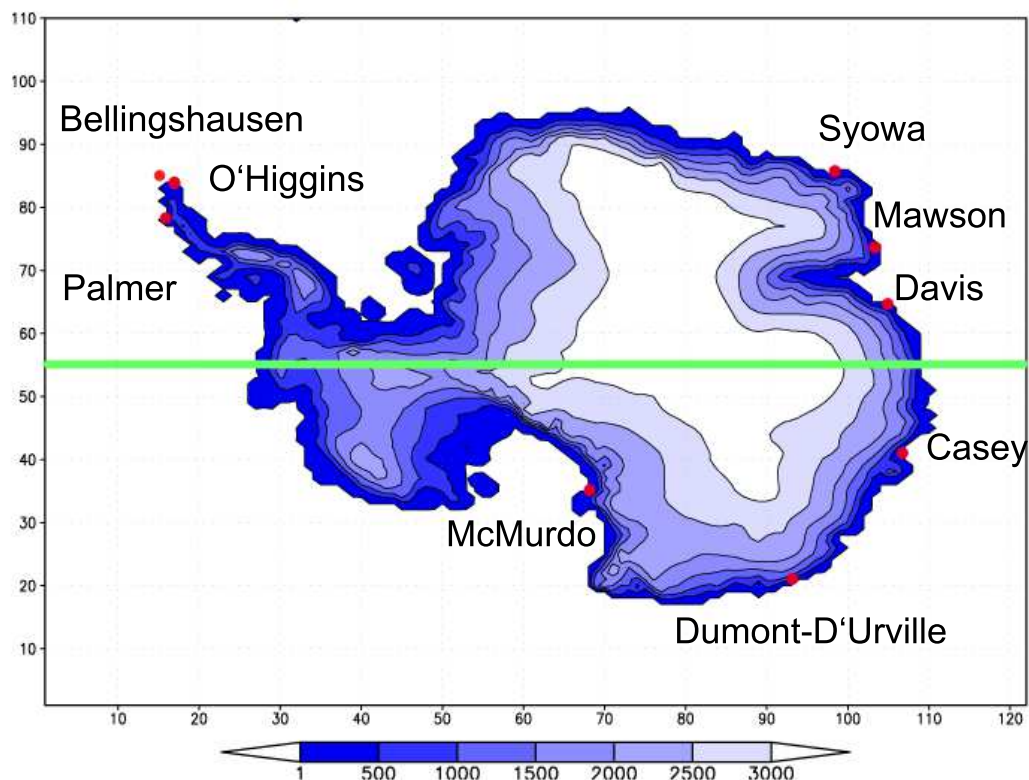
Figure A.7: Map of HIRHAM-Orografie and stations with line of the cross section.

shown. The cross section is cut along the 55th latitudinal grid point and thus running over West Antarctica the South Pole and East Antarctica:

Figures A.8 and A.9 show the temperature differences of 46Levs minus 25Levs in the cross section. Especially in summer, 46Levs is up to 1 K colder than 25Levs. In winter the temperature differences between both setups is with values of up to 0.6 K in levels over 600 hPa smaller than in summer. Addionally, in summer there are zone in which 46Levs is warmer than 25Levs, which means a weakening of the temperature gradient between higher and lower latitudes in 46Levs.
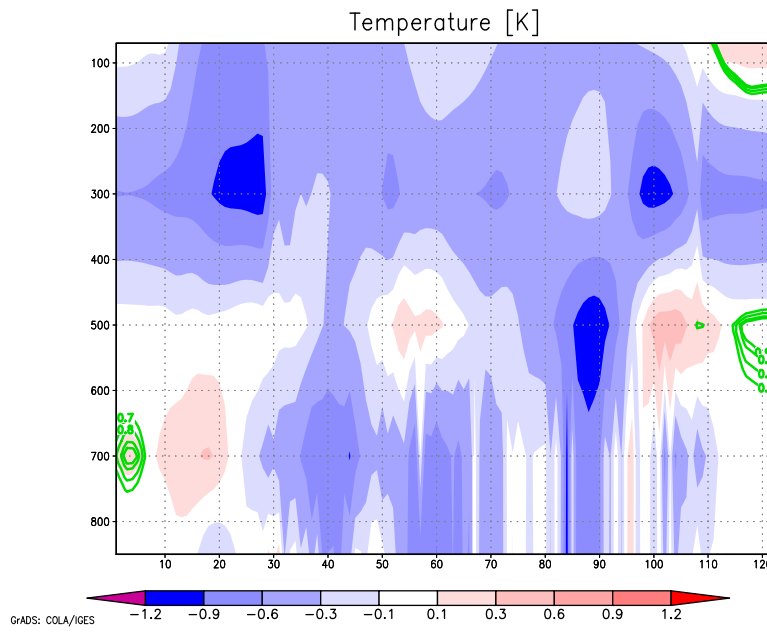
Figure A.8: Temperature difference between 46lev and 25lev in January 2001. Green contour lines: Significance.
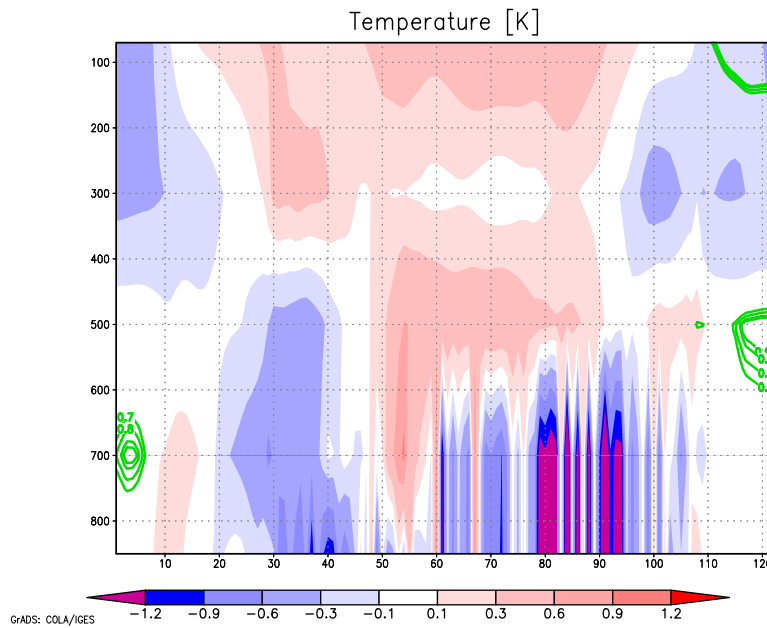
Figure A.9: Temperature difference between 46lev and 25lev in July 2001. Green contour lines: Significance.

The differences in wind velocity are shown in Figures A.10 and A.11. In the 46Levs

setup the wind velocity in the cross section is higher than the 25Levs wind velocity, for both seasons. Especially in the levels of 500 hPa and higher.
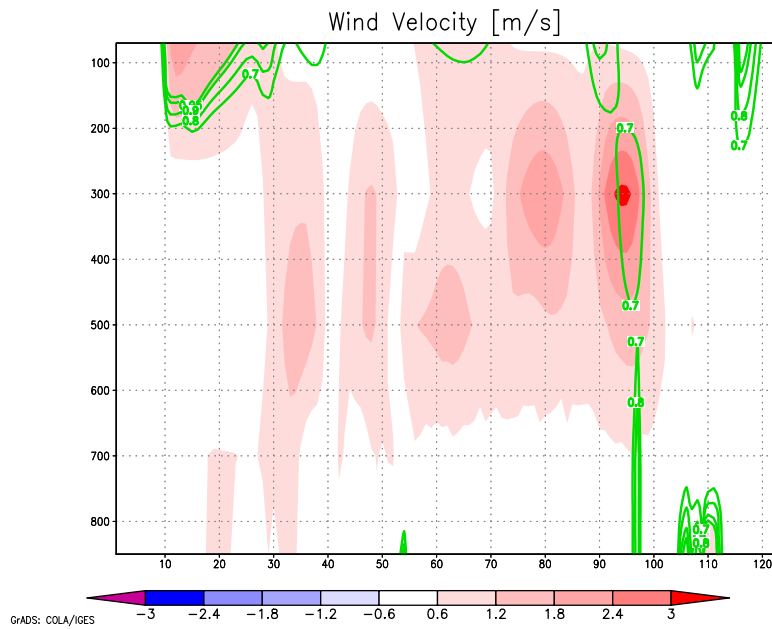
Figure A.10: Wind velocity difference between 46lev and 25lev in January 2001. Green contour lines: Significance.
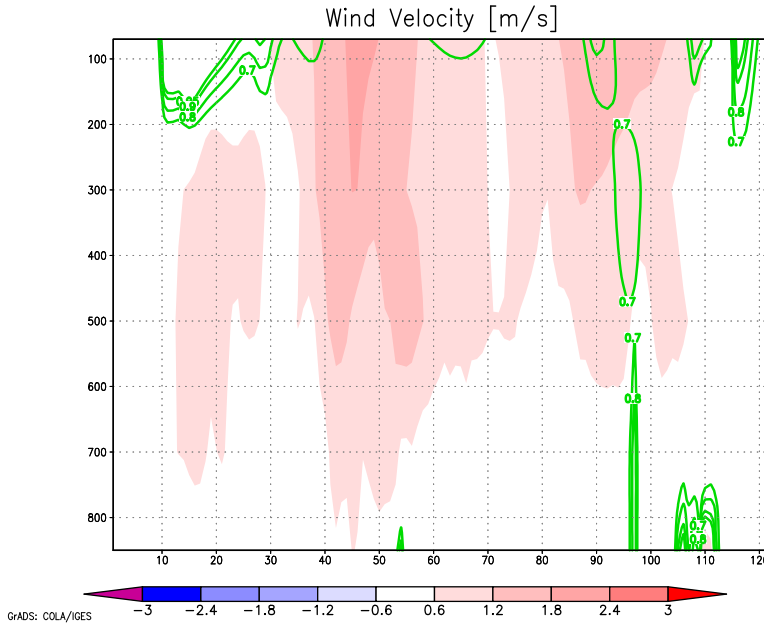
Wind Velocity [m/s]

Figure A.11: Wind velocity difference between 46lev and 25lev in July 2001. Green contour lines: Significance.

In this thesis the majority of the studied variables are ground level variables like MSLP, 2m-temperature and TWV. The differences between both model setups is not significant for these three variables in most parts of the model area. Roeckner et al. (2006) showed differences due to changes in the vertical resolution for the general circulation model ECHAM5. They found the biggest differences occuring in higher levels, up from 300hPa and only small differences in lower levels, e.g. temperature differences of less than 1 K near the ground. These results are in accordance with the results presented in this study.

A.2   Sensitivity studies concerning sea ice

HIRHAM parametrisation in this study does not provide a variable sea ice thickness. The usual HIRHAM setup for the Arctic has a sea ice thickness of 2 m. In Antarctica sea ice usally is thinner, because the open sea around Antarctica is more to the north and less poleward, plus most Antarctic sea ice is one year ice. Also Budd (1991) showed an average sea ice thickness of approximately 1 m, except for regions near the shelf ice. Contrary to that earlier HIRHAM simulations (e.g. Glushak (2007)) used the same sea ice setup as in the Arctic, which led to a sea ice thickness of 2 m. Here, the sea ice thickness in the Antarctica setup of HIRHAM is set to 1 m. Different sea ice thickeness will lead to different results as shown in Figures A.12 to A.17. This section shall provide a comparison between the old and the new setup.
In a sensitivity study two model runs with different setups were conducted, both over a summer month (January) and a winter month (July) in 2001. In the first setup sea ice

thickness was set to 2 m as in Arctica (2mSI), the second setup was the usual Antarctic
setup with 1 m sea ice thickness (1mSI). For the Figures A.12 to A.25 a monthly mean of
MSLP and 2m-temperature of the months January and July 2001 was calculaded for both
setups and afterwards substracted from each other (2mSI minus 1mSI).

In January, almost the whole region of the Antarctic continent 2mSI has a lower tem-
perature than 1mSI (c.f Fig. A.12). This is possible because thicker sea ice isolates the
comparably warm sea better. The connection between the better isolating 2 m sea ice and
the worse isolating 1 m sea ice and their effect on pressure an wind will also be shown in
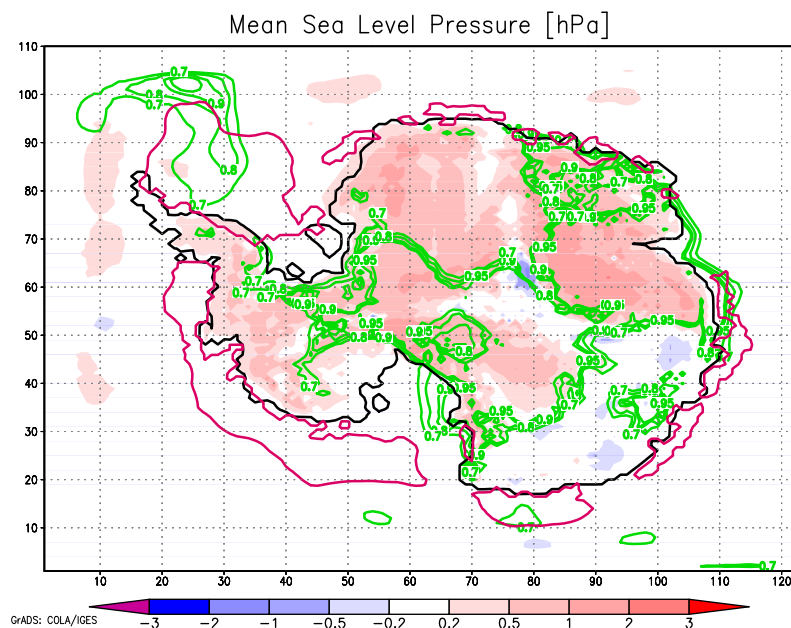this section.
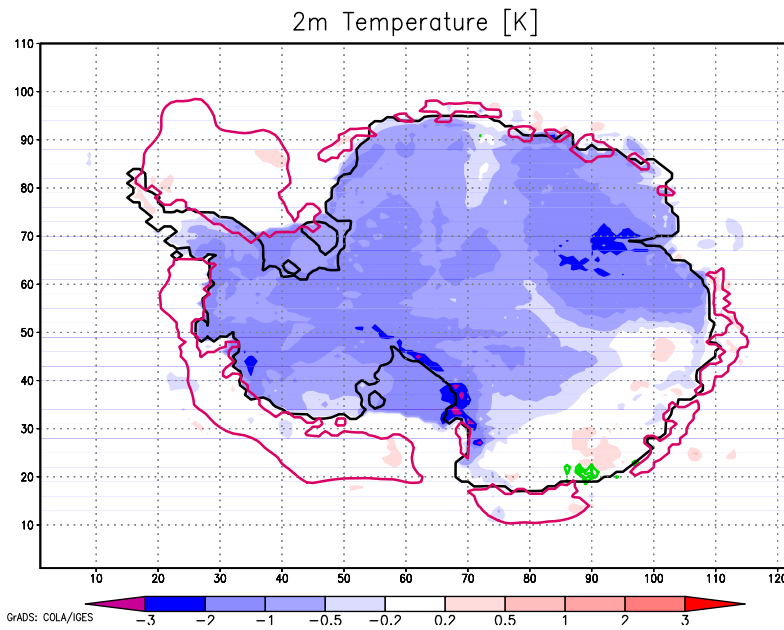
Figure A.12: 2m temperature difference between 2mSI and 1mSI as HIRHAM setup.
Monthly average January 2001. Violet contour lines: sea ice extent. Green contour lines:
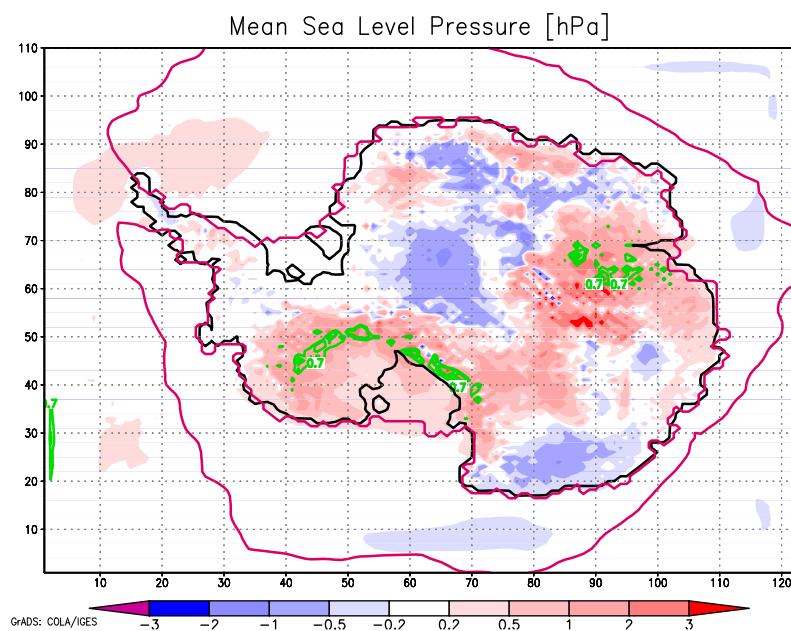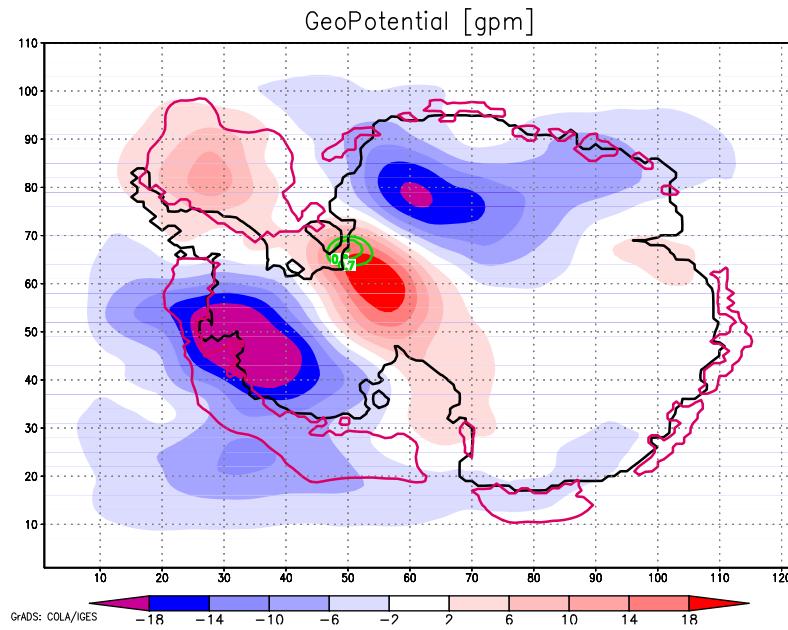significance.

In winter the isolating process has a more complicated influence (A.13). 2mSI is cooler
in the sea around Antarctica and in certain regions on the continent as for example Prydz
Bay or West Antarctica. In East Antarctica are regions with a significant positive tem-
perature difference of up to 2 K. The cooling effect of the thicker sea ice stabilises the
atmosphere and adds the developement of high pressure systems, c.f. A.16. Here the lower
temperature over the continent in the 2mSI setup confers with higher pressure. In Fig.
A.17 the regions with a positive temperature difference also confer with regions of negative
temperature deviation.
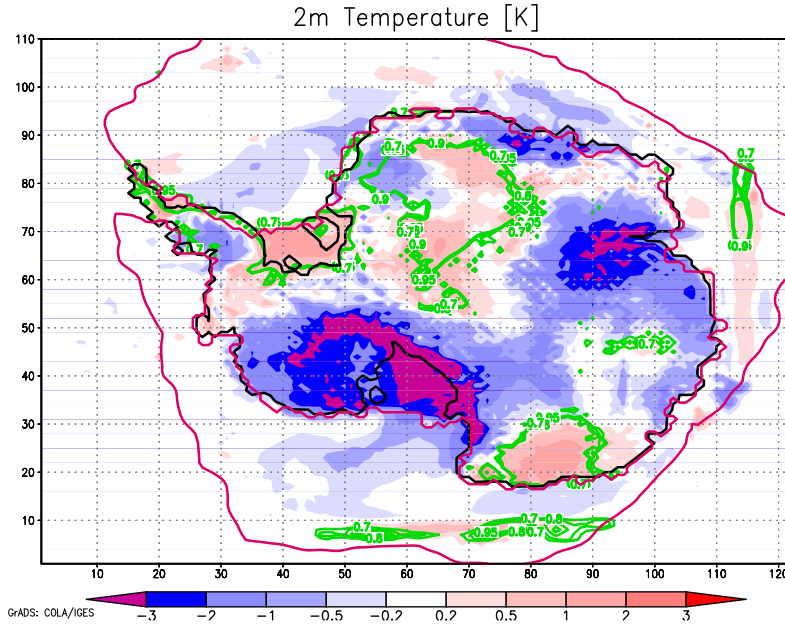
Figure A.13: 2m temperature between 2mSI and 1mSI as HIRHAM setup. Monthly average July 2001. Violet contour lines: sea ice extent. Green contour lines: significance.

Figures A.14 and A.15 show the differences of the temperature gradient between surface and 2m height. In both months the differences of the temperature gradients is not significant. In January (A.14) there are differences of up to 0.5 K, with a higher gradient of 2mSI over West Antarctica and a lower gradient of 2mSI over East Antarctica. In July 2mSI has a up to 1 K higher gradient than 1mSI over almost the whole sea ice extent. A reason for this is the better insulation of thicker sea ice. Over the continent the temperature gradient is smaller for 2mSI than for 1mSI.
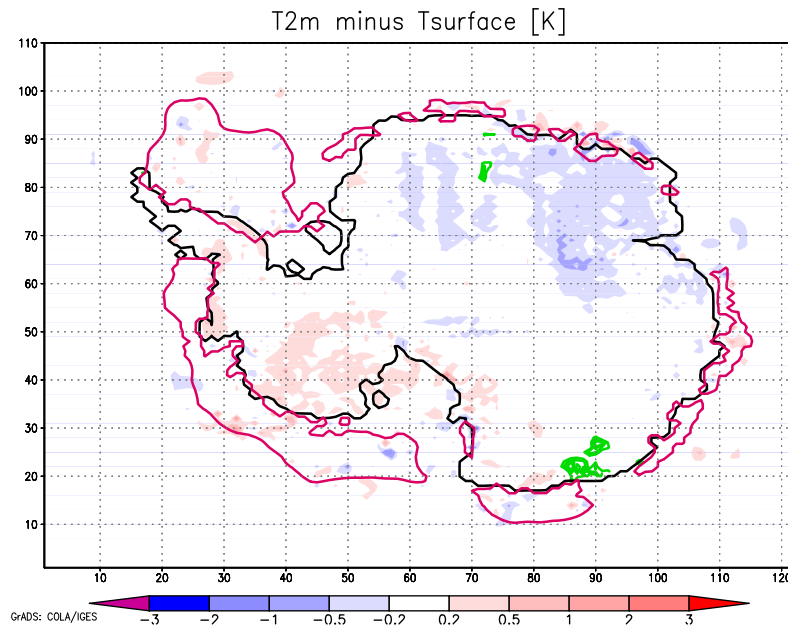
Figure A.14: T2m minus Tsurface difference between 2mSI and 1mSI as HIRHAM setup. Monthly average January 2001. Violet contour lines: sea ice extent. Green contour lines: significance.
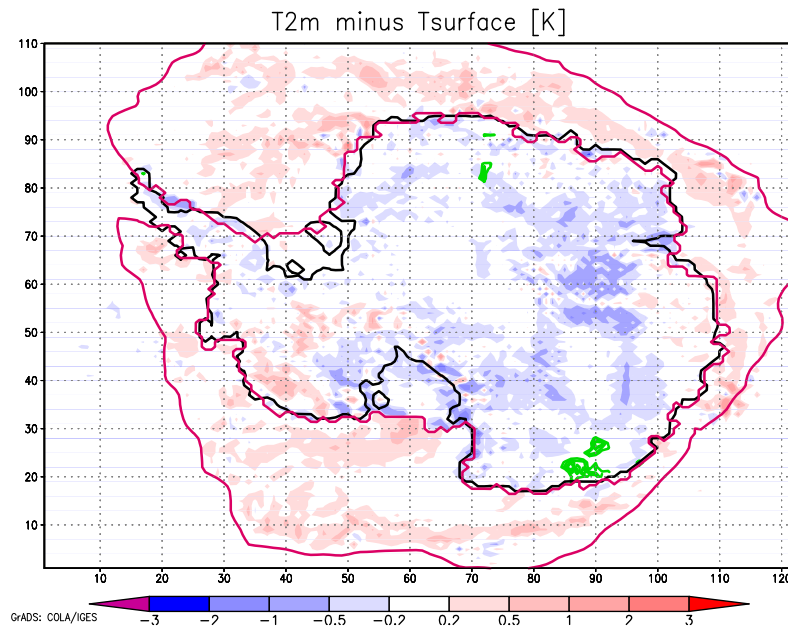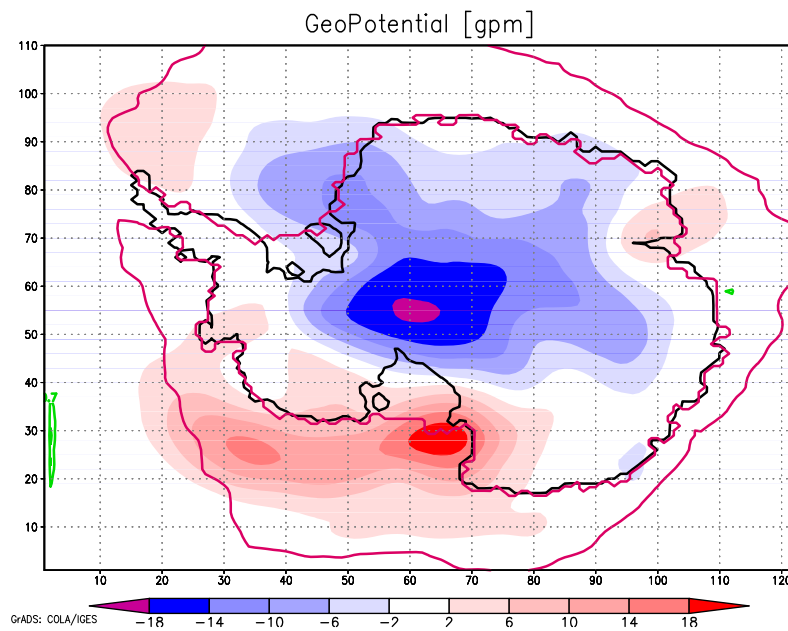

Figure A.15: T2m minus Tsurface difference between 2mSI and 1mSI as HIRHAM setup. Monthly average July 2001. Violet contour lines: sea ice extent. Green contour lines: significance.

By comparing the temperature plots with the MSLP plots, cooler regions in 2mSI confer with regions of higher pressure in 2mSI, since pressure and temperature are connected. In January the pattern of temperature difference, respectively pressure difference looks different than in July. The greater sea ice extent leads to higher temperatures over the continent in the 2mSI setup.

Figure A.16: MSLP difference between 2mSI and 1mSI as HIRHAM setup. Monthly average January 2001. Violet contour lines: sea ice extent. Green contour lines: significance.

Figure A.17: MSLP difference between 2mSI and 1mSI as HIRHAM setup. Monthly average July 2001. Violet contour lines: sea ice extent. Green contour lines: significance.

In Figures A.18 to A.21 the difference of the geopotential height between the two setups is shown. The difference has values of up to ± 18 gpm, but does not exceed ± 10 gpm in the greater part of the integration area. In January there is a band of higher geopotential values for 2mSI over continental Antarctica in 500 hPa as well as in 300 hPa. In July a similar pattern can be found in both levels, but with a shift of the positive band to Ross and Amundsen Sea.

Figure A.18: Geopotential difference at 500 hPa between 2mSI and 1mSI as HIRHAM setup. Monthly average January 2001. Violet contour lines: sea ice extent. Green contour lines: significance.
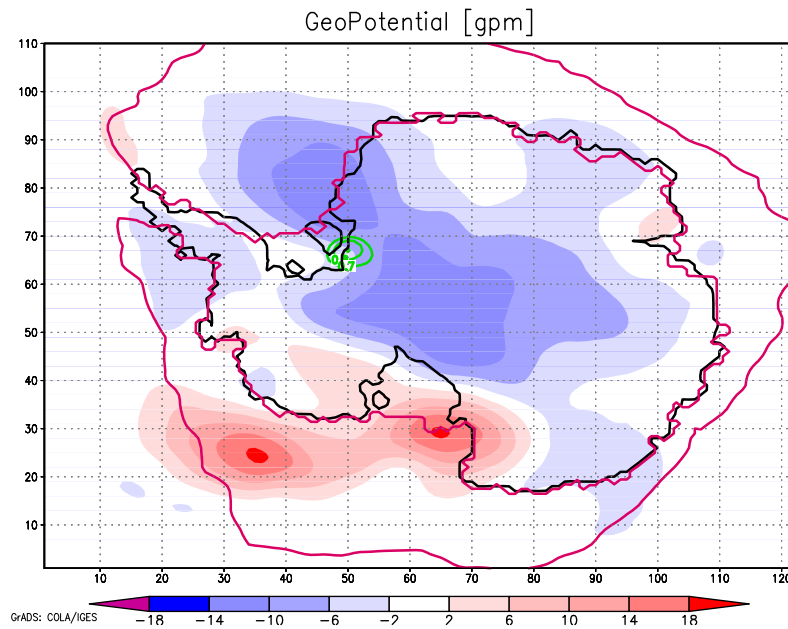
Figure A.19: Geopotential difference at 500 hPa between 2mSI and 1mSI as HIRHAM setup. Monthly average July 2001. Violet contour lines: sea ice extent. Green contour lines: significance.
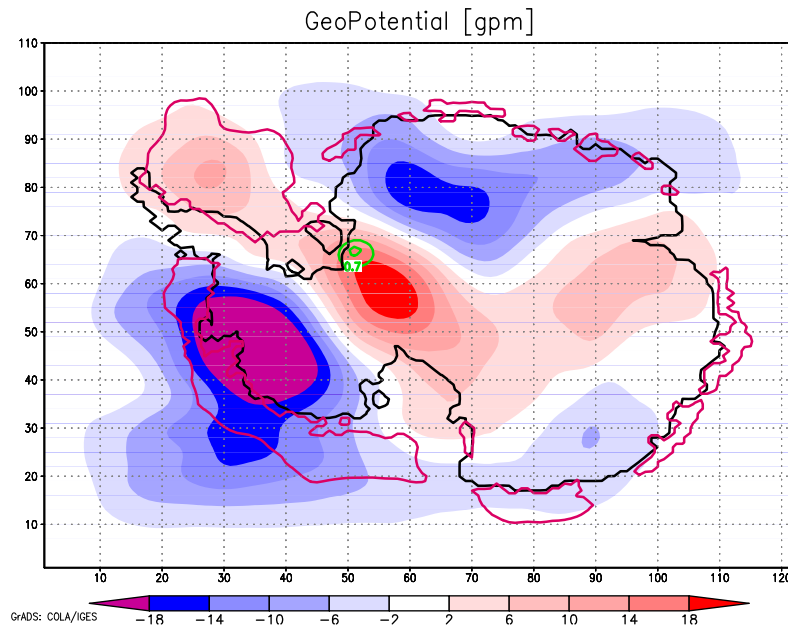
Figure A.20: Geopotential difference at 300 hPa between 2mSI and 1mSI as HIRHAM setup. Monthly average January 2001. Violet contour lines: sea ice extent. Green contour lines: significance.

Figure A.21: Geopotential difference at 300 hPa between 2mSI and 1mSI as HIRHAM setup. Monthly average July 2001. Violet contour lines: sea ice extent. Green contour lines: significance.

Figures A.22 and A.23 show the cross sections of the temperature differences between 2mSI and 1mSI in January and July 2001. In January there is a positive temperature difference of ca. 0.6 K over East Antarctica and a negative difference of up to -0.9 K over West Antarctica. In 300 hPa height the difference becomes positive and reaches values of up to 0.6 K, which is also significant.
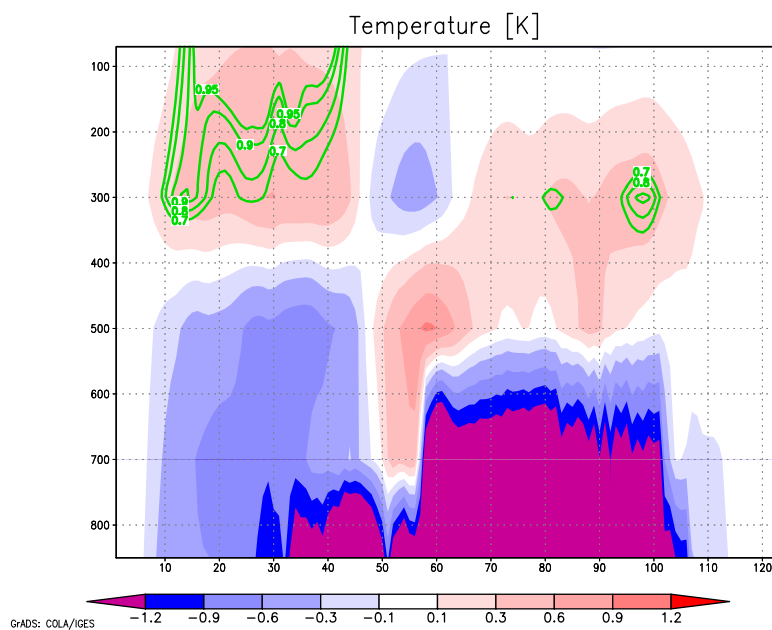
Figure A.22: Temperature difference between 2mSI and 1mSI as HIRHAM setup in January 2001. Green contour lines: Significance.
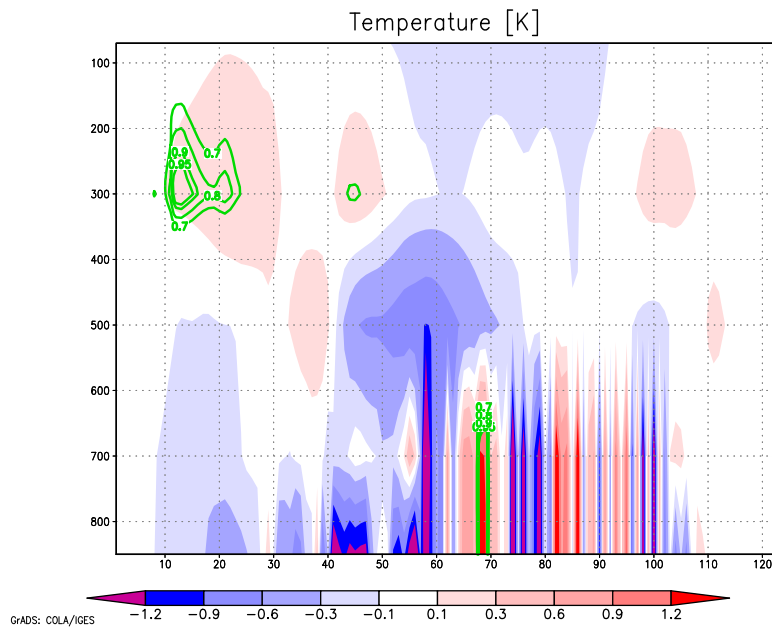
Figure A.23: Temperature difference between 2mSI and 1mSI as HIRHAM setup in July 2001. Green contour lines: Significance.

In Figures A.24 and A.25 the wind velocity difference between 2mSI and 1mSI is plotted. 2mSI has a higher wind speed than 1mSI in the shown region. In January the value of the difference reaches up to 3 m/s between 300 hPa and 500 hPa. In January the difference is slightly smaller with values of up to 1.2 m/s. These values are significant.
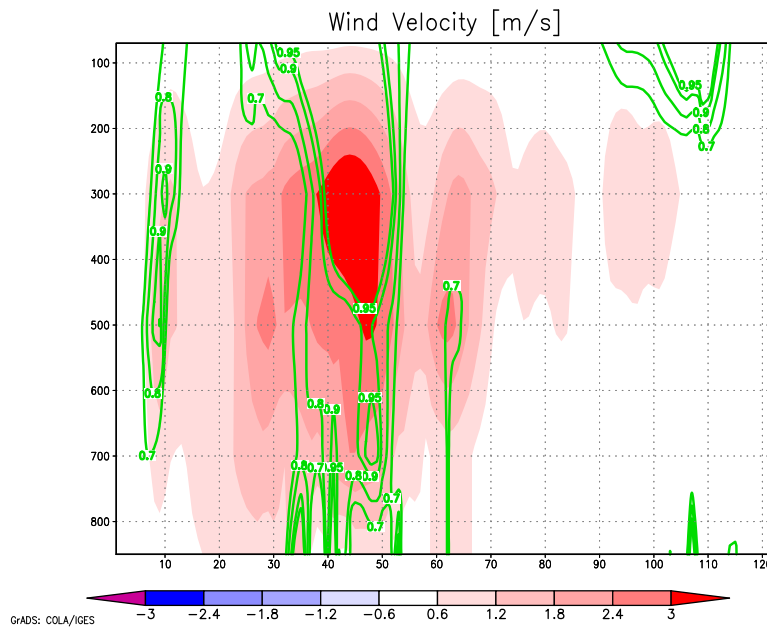
Figure A.24: Wind velocity difference between 2mSI and 1mSI as HIRHAM setup in January 2001. Green contour lines: Significance.
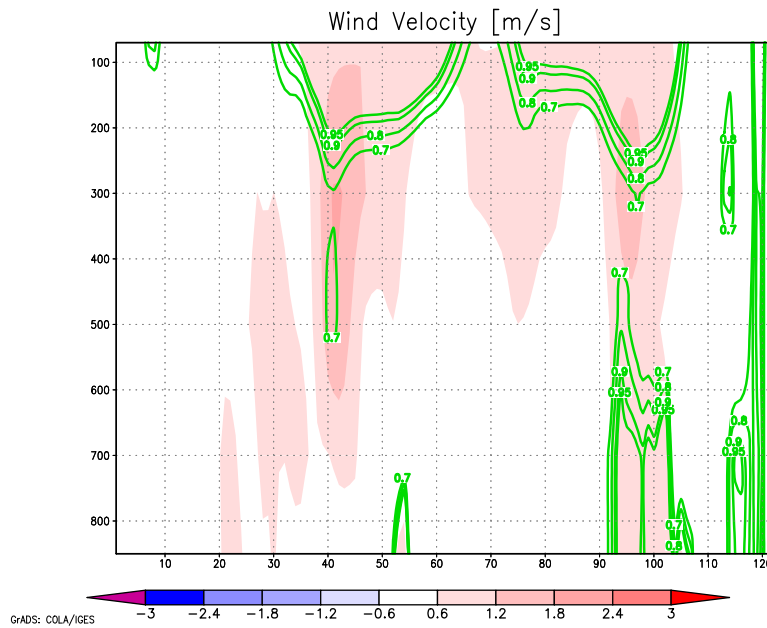
Figure A.25: Wind velocity difference between 2mSI and 1mSI as HIRHAM setup in July 2001. Green contour lines: Significance.

In January the behaviour of pressure and temperature differences is as expected. The

thicker sea ice insulates the sea, leading to a stabilisation of the atmosphere over the continent and thus a higher pressure, which results in a lower temperature. In July there are zones over the continent in which the pressure in the 2mSI setup is lower than in the 1mSI setup with a corresponding higher temperature. In the cross section A.23 and the geopotential plots A.21 and A.19 a lower 2mSI pressure over the continent can be seen. This is the polar low, which is stronger in the 2mSI setup, and reaches down to 500 hPa, that is ground pressure in East Antarctica. Thus, the ground temperature fits to the lower pressure and is higher in 2mSI than in 1mSI.

Appendix B

Single Year Seasonal Means

In this section the annual change of MSLP in the scale from 500 to 1000 km will be analysed from the data of the ERA40 run and the ERAint run. There are differences in pattern and strength of MSLP between the single years of the integration period.

The filtered data of the following Figures show a MSLP deviation from the average of the years 1994 to 1999, resp. 1996 to 2009. The temporal average over the integration period (6 years or 14 years) was substracted from the daily averages which were filtered afterwards with the SYN-filter. For each year a seasonal mean was calculaded. The Figures are ordered by season and by year. Due to the different temporal means both runs, the results of the single years are not directly comparable with each other.

B.1 ERA40 run - 1994 to 1999

In Fig. B.1 and B.2 and B.3 the MSLP of each spring of the years 1994 to 1999 can be seen. The strongest cyclones occur in the years 1998 and 1999. Less strong cyclones occur in both the years 1995 and 1996. The weakest cyclones occur in 1994.

The high with the strongest maximum over the Antarctic Plateau occurs in 1996. The high that covers the smallest area occurs in the year 1999, which is one of the years with the strongest low.
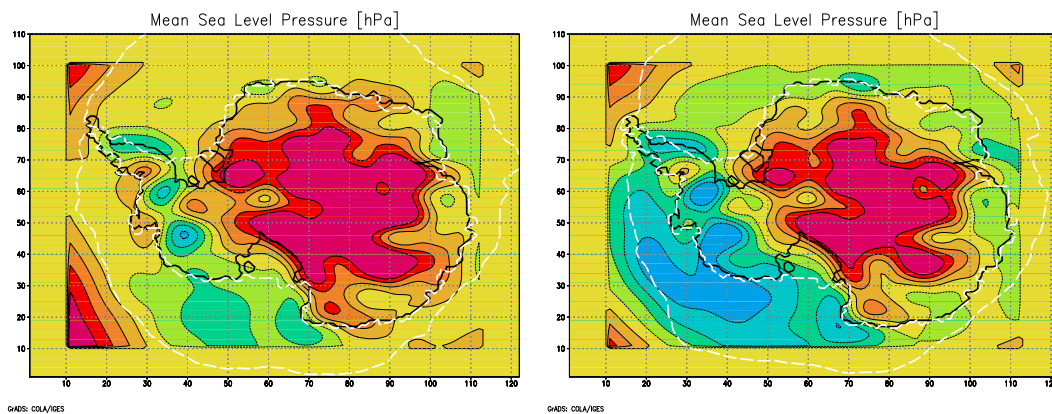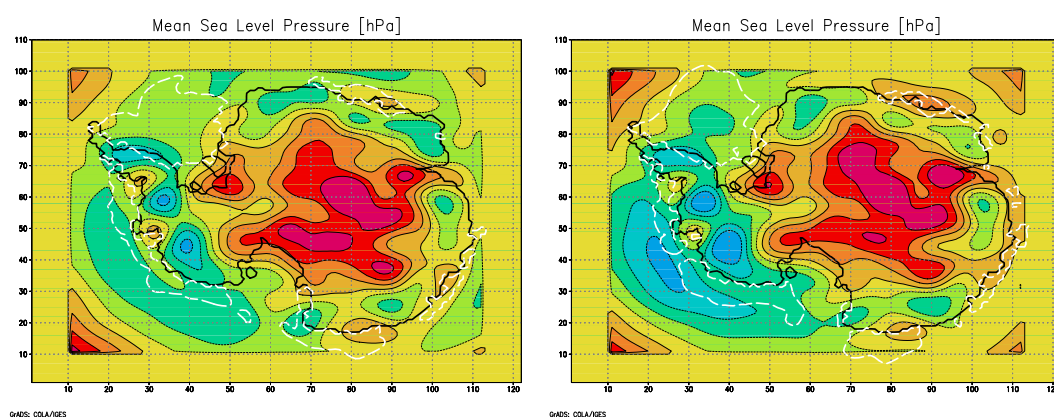
Figure B.1: Spring Mean of MSLP of 1994 and 1995 (ERA40 run). White dashed line: Mean Seasonal Sea Ice. Used filter: SYN
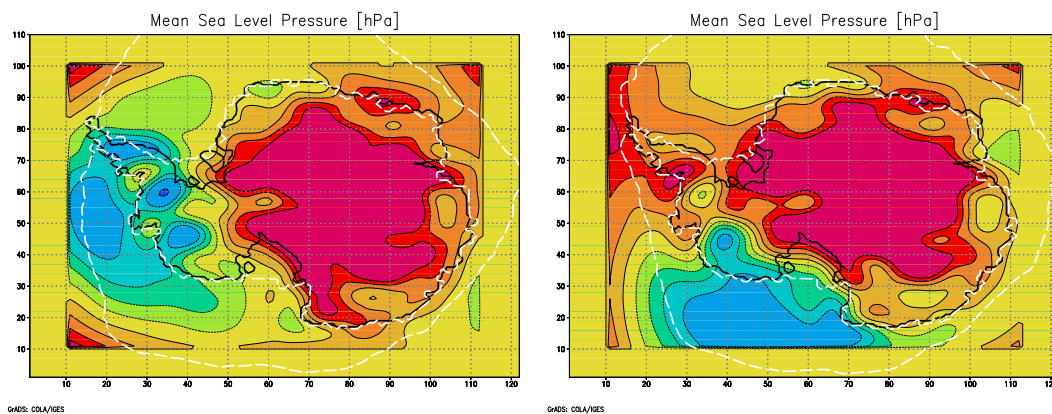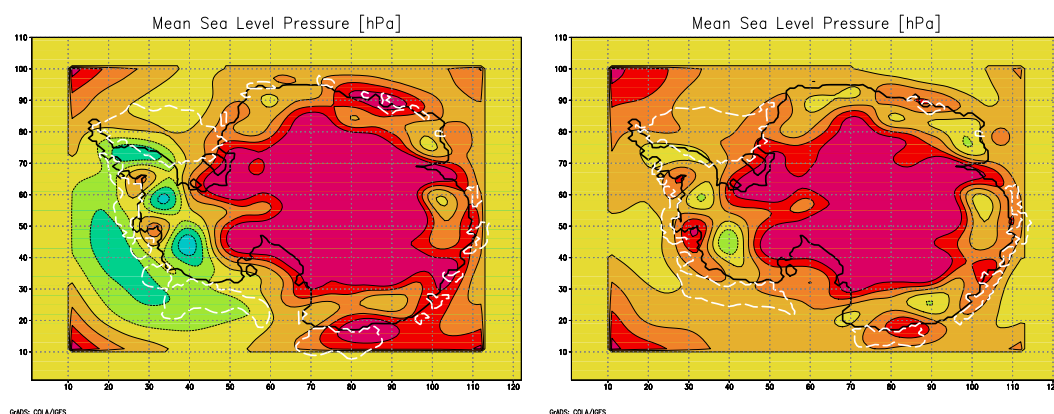

Figure B.2: Spring Mean of MSLP of 1996 and 1997 (ERA40 run). White dashed line: Mean Seasonal Sea Ice. Used filter: SYN
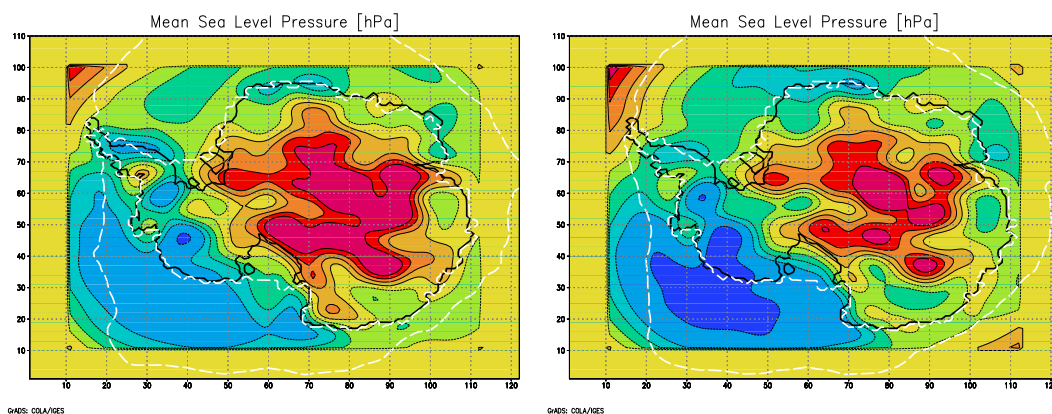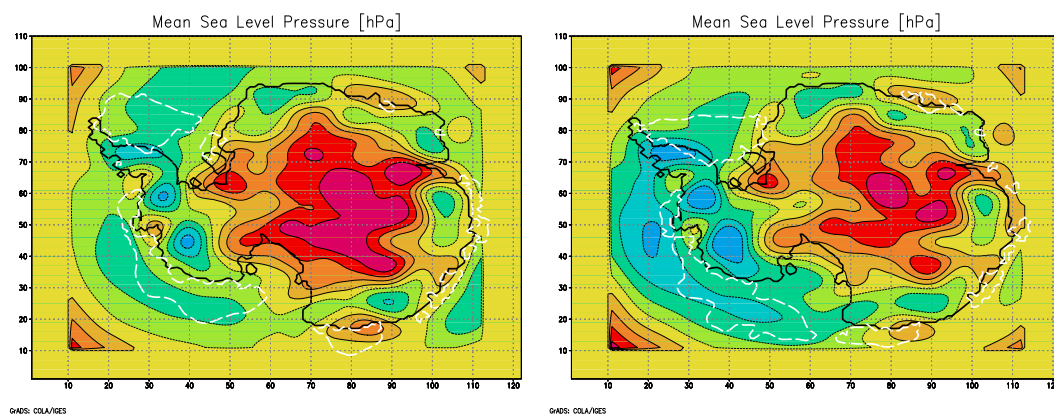

Figure B.3: Spring Mean of MSLP of 1998 and 1999 (ERA40 run). White dashed line: Mean Seasonal Sea Ice. Used filter: SYN

The less intense patterns in 1994 and 1996 show a high that covers a wider area than in the other years. In years with stronger maxima and minima the cyclones penetrate more southern areas. This shows that cyclones need a certain strength to intrude in continental areas.

In Fig. B.4 and B.5 and B.6 the MSLP of each summer of the years 1994 to 1999 can be seen. The strongest cyclones occur in the years 1995 and 1999, the weakest cyclones occur in the year 1996 and 1997. 1996 is also the year with the strongest high, which covers the widest area in comparison with MSLP pattern of all other years. The other weak cyclone year, 1997, also covers a wide area.
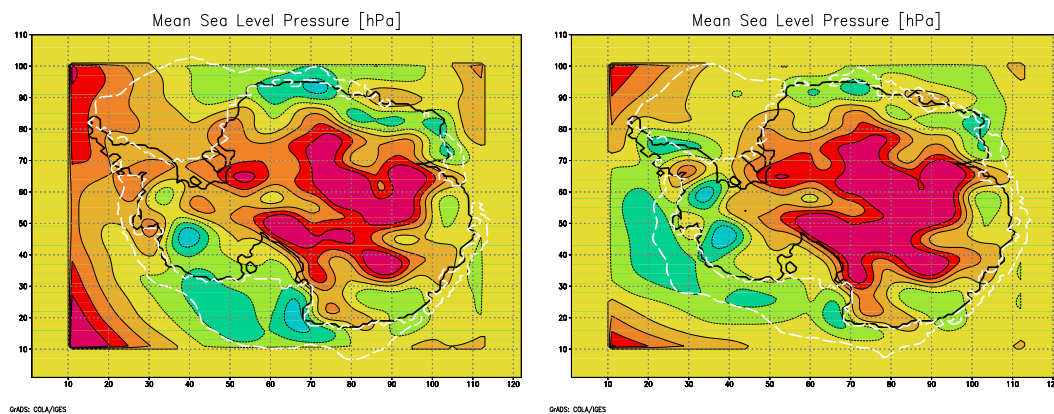

Figure B.4: Summer Mean of MSLP of 1994 and 1995 (ERA40 run). White dashed line: Mean Seasonal Sea Ice. Used filter: SYN
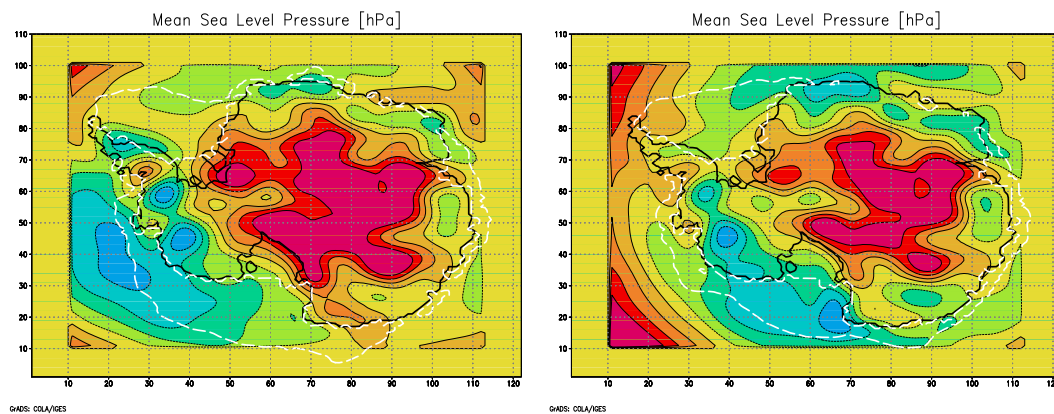

Figure B.5: Summer Mean of MSLP of 1996 and 1997 (ERA40 run). White dashed line: Mean Seasonal Sea Ice. Used filter: SYN
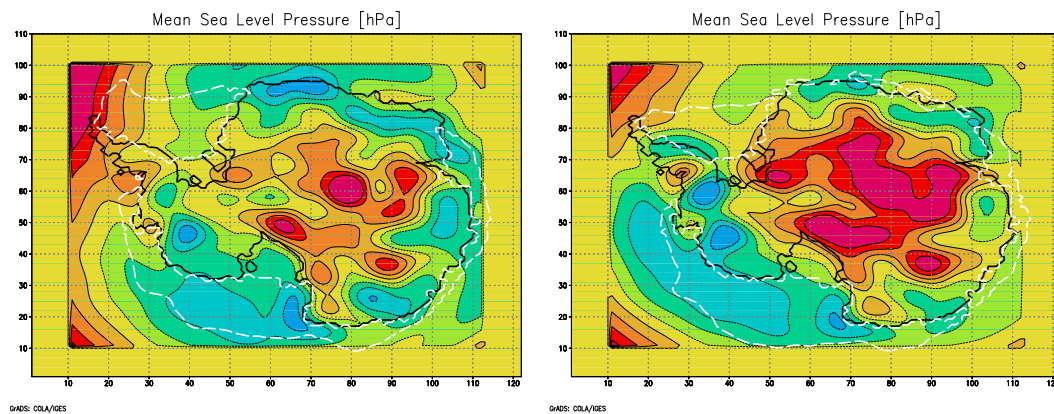
Figure B.6: Summer Mean of MSLP of 1998 and 1999 (ERA40 run). White dashed line: Mean Seasonal Sea Ice. Used filter: SYN

The less intense pattern in 1997 shows a less intense but wider high than in the other years. A strong high over the Antarctic Plateau leads to cyclones that occur more to the North.

In Fig. B.7 and B.8 and B.9 the MSLP of each autumn of the years 1994 to 1999 can be seen. The most intense cyclones occur in the years 1996 and 1999. In these years and in 1995 the cyclones have their maximum north of Amundsen Sea. The the other years the maximum of the depressions is north of Ross Sea. The most intense highs occur in 1996 and in 1995 and 1997, which are slightly less intense. The weakest high which also covers the smallest area occurs in 1998.
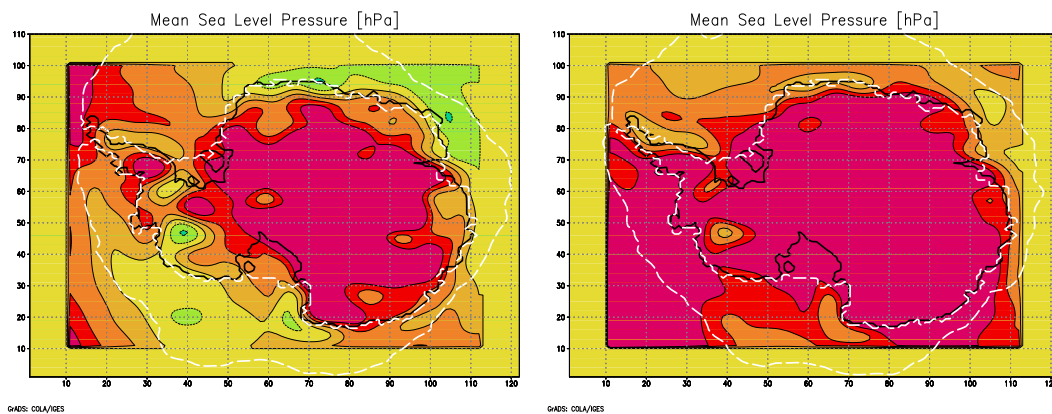

Figure B.7: Autumn Mean of MSLP of 1994 and 1995 (ERA40 run). White dashed line: Mean Seasonal Sea Ice. Used filter: SYN
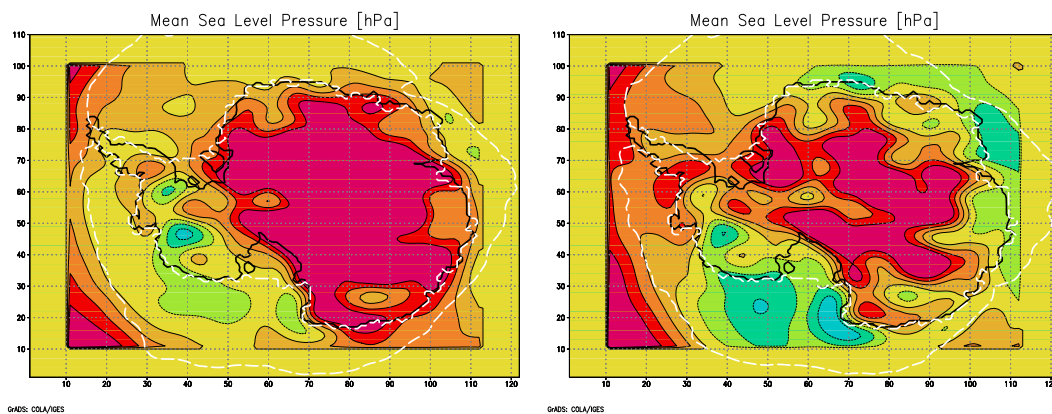
Figure B.8: Autumn Mean of MSLP of 1996 and 1997 (ERA40 run). White dashed line: Mean Seasonal Sea Ice. Used filter: SYN

Figure B.9: Autumn Mean of MSLP of 1998 and 1999 (ERA40 run). White dashed line: Mean Seasonal Sea Ice. Used filter: SYN

All years show the typical pattern. In 1994 and 1995 the depression is not as intense as in the other years.
In Fig. B.10 and B.11 and B.12 the MSLP of each winter of the years 1994 to 1999 is depicted. 1998 is the year with the strongest cyclonal maximum and the smallest high with the weakest maximum. In 1995 occurs a high which is strong and covers a wide area. In Ross Sea is a strong pressure gradient which is prominent in 1997 and 1998.

Figure B.10: Winter Mean of MSLP of 1994 and 1995 (ERA40 run). White dashed line: Mean Seasonal Sea Ice. Used filter: SYN

Figure B.11: Winter Mean of MSLP of 1996 and 1997 (ERA40 run). White dashed line: Mean Seasonal Sea Ice. Used filter: SYN
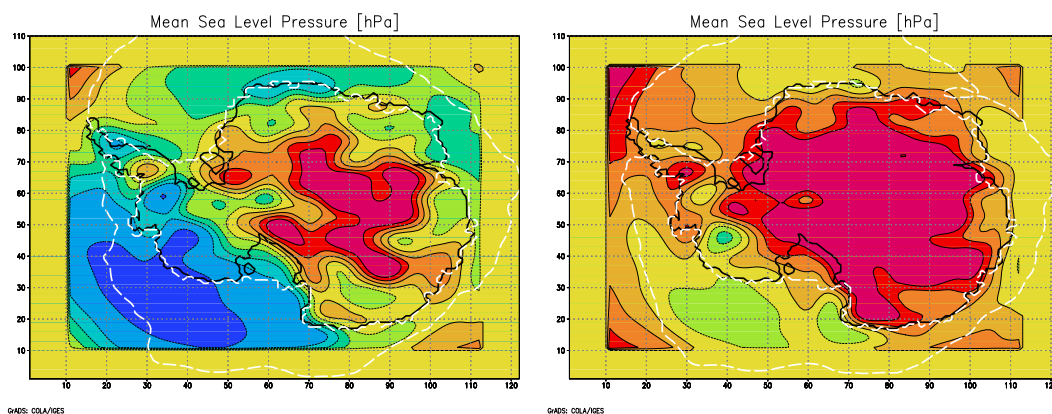

Figure B.12: Winter Mean of MSLP of 1998 and 1999 (ERA40 run). White dashed line: Mean Seasonal Sea Ice. Used filter: SYN

In 1998 wide areas have a less MSLP then the 6-year-spatial mean, 1995 has a higher MSLP than that. The other years show typical and expected pattern.

To analyse the correlation of the seasons in a single year, the pattern correlation of every the MSLP of every single season with the MSLP of the other seasons in the respective year was calculated. Here, two seasons are considered as correlated, when they have a correlation coefficient of 0.85 or higher. This applies for the following seasons:

Table B.1: Table of the MSLP pattern correlation of the seasons in the years 1994 to 1999 (ERA40 run).

Year	Seasons	Correlation
1994	spring-summer	0.86
	spring-autum	0.85
	spring-winter	0.89
1995	spring-summer	0.91
	spring-autumn	0.92
	summer-autumn	0.86
1996	spring-summer	0.92
	spring-autumn	0.90
	spring-winter	0.88
	summer-autumn	0.86
	summer-winter	0.91
1997	autumn-winter	0.87
1998	spring-summer	0.86
	spring-winter	0.96
1999	spring-summer	0.87
	spring-autumn	0.89
	summer-autumn	0.88

Spring is the month that has the most correlations to other seasons of the same year (12). Winter only has 5 correlations to other seasons of the same year. The year with the most internal correlation is 1996 with 5 pairs of correlated seasons.

B.2 ERAinterim run - 1996 to 2009

The following Figures (B.13 to B.40) show the seasonal mean of MSLP for the single years of the ERAint run (1996-2009).

The first season shown is spring (B.13 to B.19). The years with the strongest cyclones (-8 hPa or more deviation from the MSLP mean) are 2001, 2005, 2007 and 2008. The years

with the weakest cyclones (a deviation of less than -4 hPa) are 1998, 2000 and 2006. In the year 2004 the cyclone activity is shifted from Ross/Amundsen-Sea to the Peninsula / Weddel Sea.
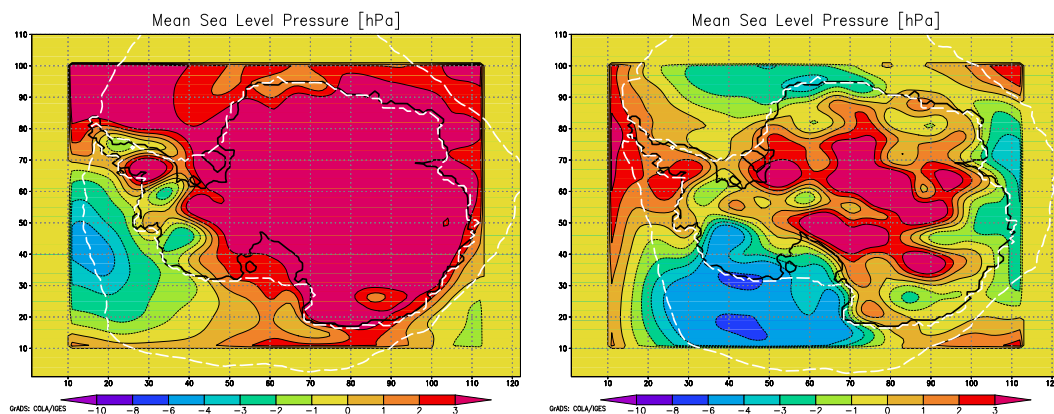

Figure B.13: Spring Mean of MSLP of 1996 and 1997 (ERAint run). White dashed line: Mean Seasonal Sea Ice. Used filter: SYN
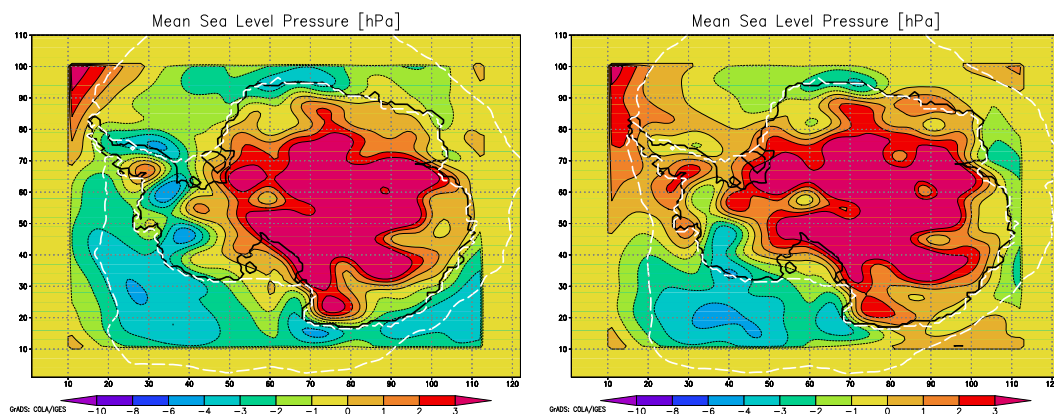

Figure B.14: Spring Mean of MSLP of 1998 and 1999 (ERAint run). White dashed line: Mean Seasonal Sea Ice. Used filter: SYN
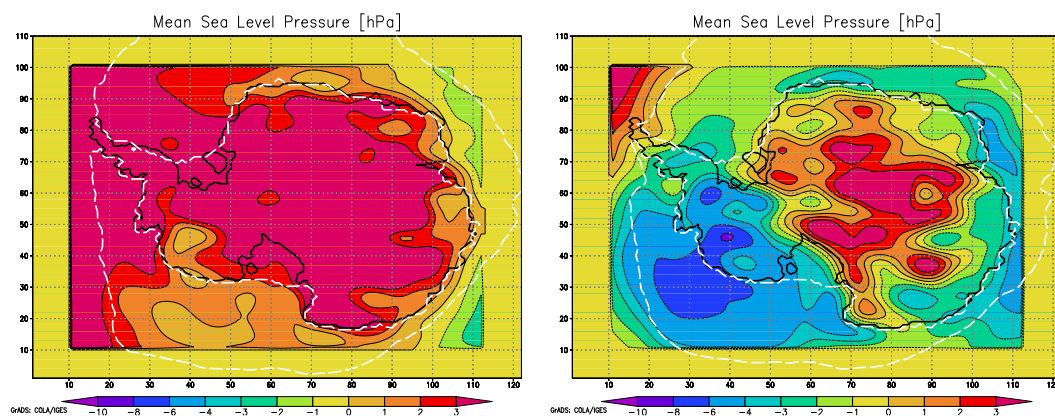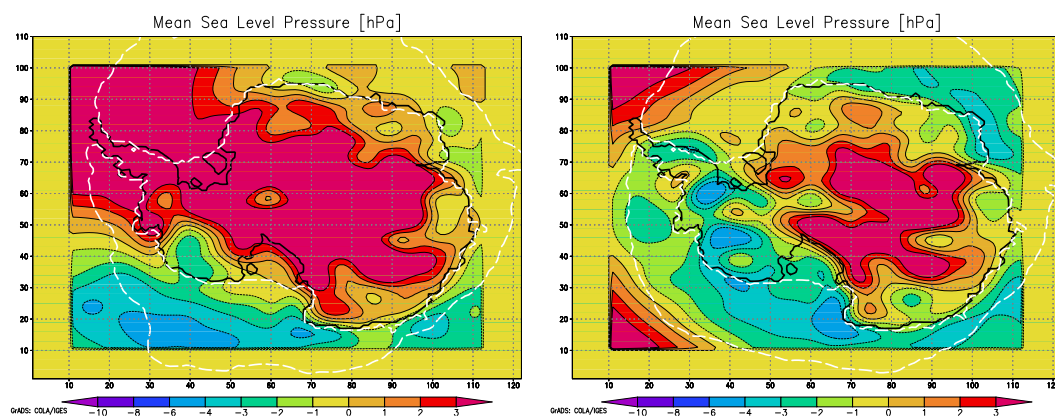
Figure B.15: Spring Mean of MSLP of 2000 and 2001 (ERAint run). White dashed line: Mean Seasonal Sea Ice. Used filter: SYN

Figure B.16: Spring Mean of MSLP of 2002 and 2003 (ERAint run). White dashed line: Mean Seasonal Sea Ice. Used filter: SYN
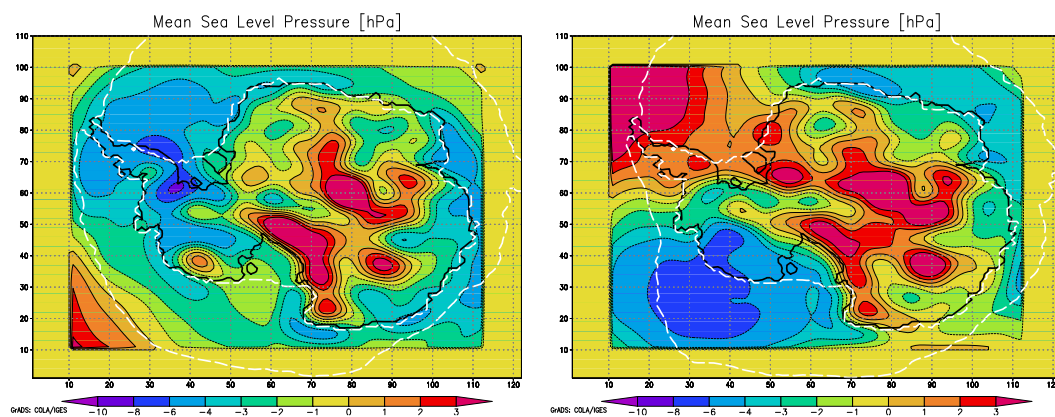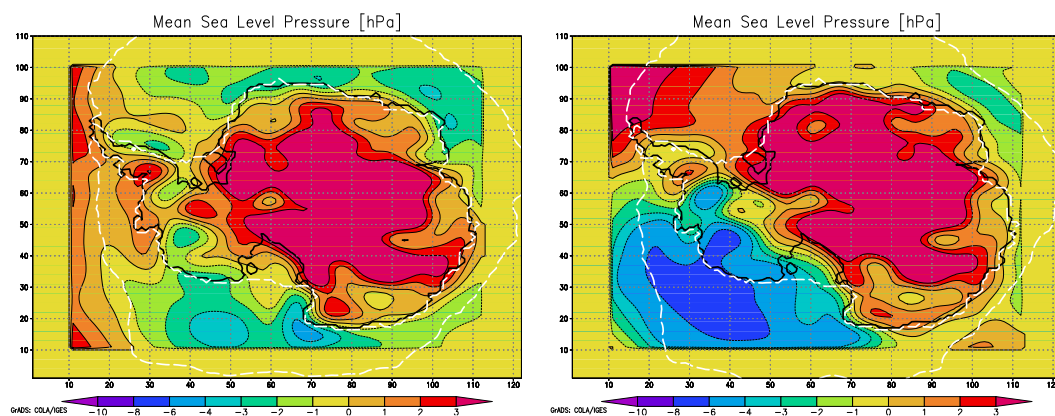

Figure B.17: Spring Mean of MSLP of 2004 and 2005 (ERAint run). White dashed line: Mean Seasonal Sea Ice. Used filter: SYN

Figure B.18: Spring Mean of MSLP of 2006 and 2007 (ERAint run). White dashed line: Mean Seasonal Sea Ice. Used filter: SYN
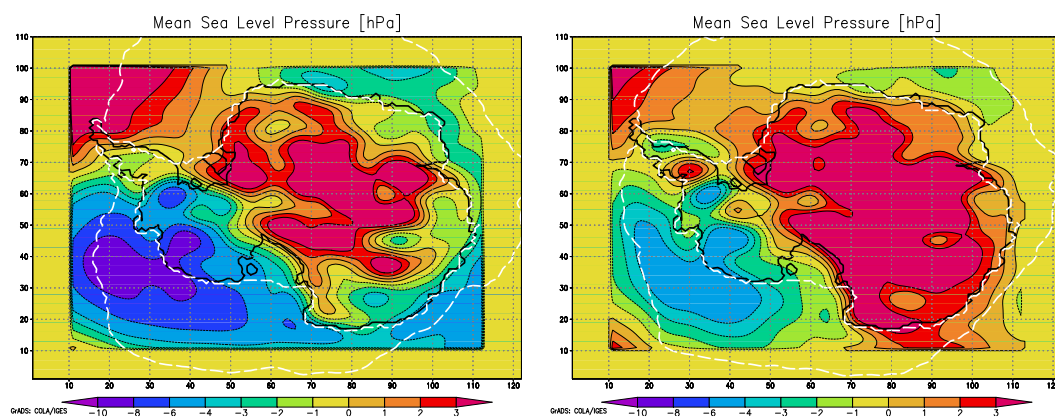

Figure B.19: Spring Mean of MSLP of 2008 and 2009 (ERAint run). White dashed line: Mean Seasonal Sea Ice. Used filter: SYN

Figures B.20 to B.26 show MSLP in the summers of the years 1996 to 2009 in the ERAint run. Here the cyclones are less intense than in spring, the deviation from the mean is hardy exceeding -6 hPa. The most intensive cyclones of the summer season occur in the years 1999, 2000, 2008 and 2009. The weakest cyclones with a deviation of less than -3 hPa appears in the years 1998, 2003 and 2006.
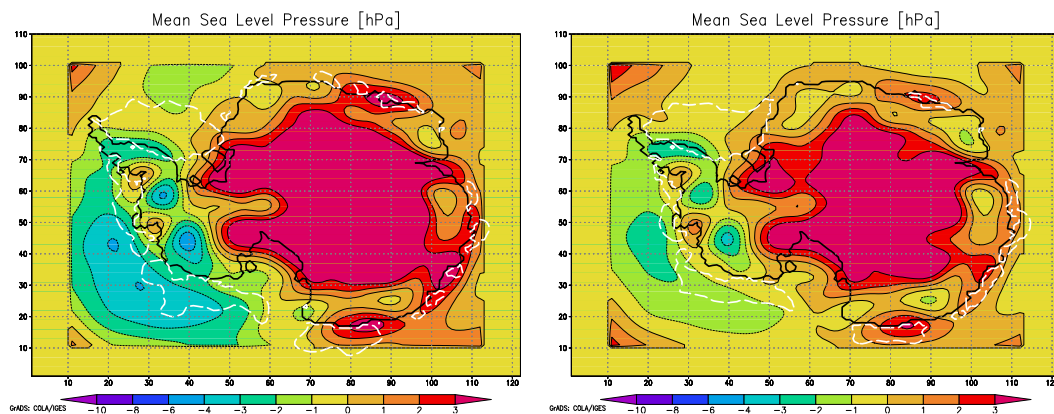
Figure B.20: Summer Mean of MSLP of 1996 and 1997 (ERAint run). White dashed line: Mean Seasonal Sea Ice. Used filter: SYN
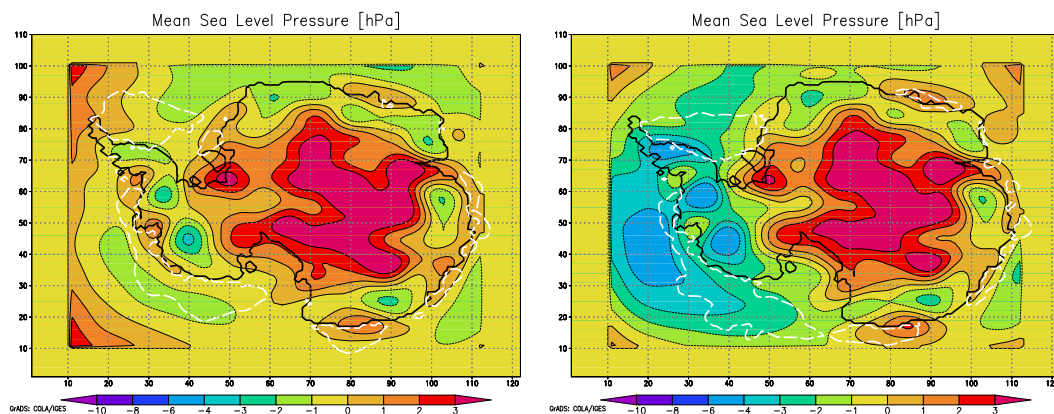

Figure B.21: Summer Mean of MSLP of 1998 and 1999 (ERAint run). White dashed line: Mean Seasonal Sea Ice. Used filter: SYN
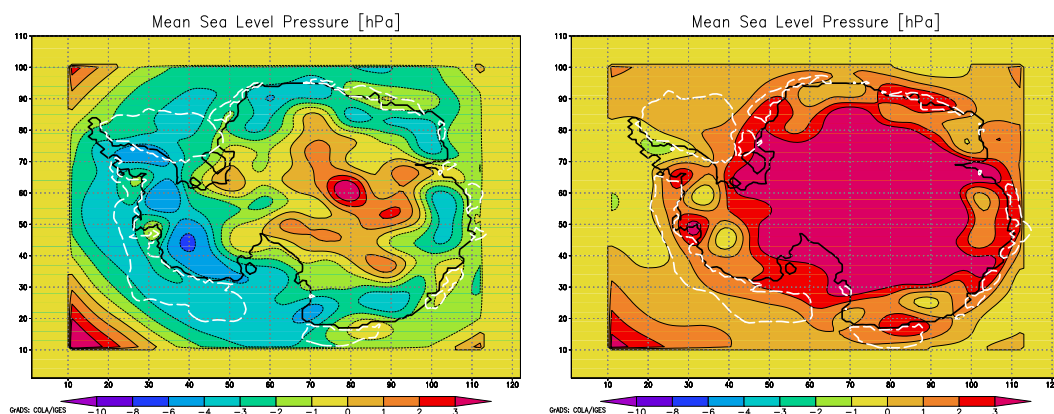

Figure B.22: Summer Mean of MSLP of 2000 and 2001 (ERAint run). White dashed line: Mean Seasonal Sea Ice. Used filter: SYN

Figure B.23: Summer Mean of MSLP of 2003 and 2004 (ERAint run). White dashed line: Mean Seasonal Sea Ice. Used filter: SYN

Figure B.24: Summer Mean of MSLP of 2005 and 2006 (ERAint run). White dashed line: Mean Seasonal Sea Ice. Used filter: SYN

Figure B.25: Summer Mean of MSLP of 2006 and 2007 (ERAint run). White dashed line: Mean Seasonal Sea Ice. Used filter: SYN

Figure B.26: Summer Mean of MSLP of 2008 and 2009 (ERAint run). White dashed line: Mean Seasonal Sea Ice. Used filter: SYN
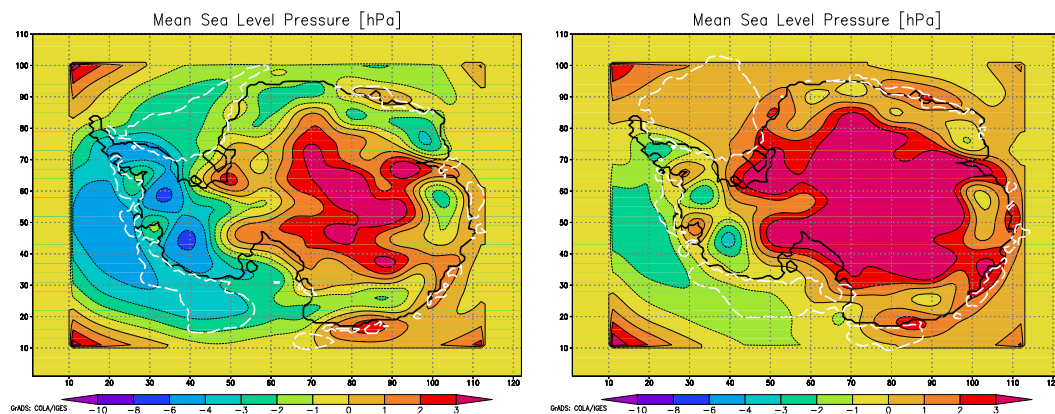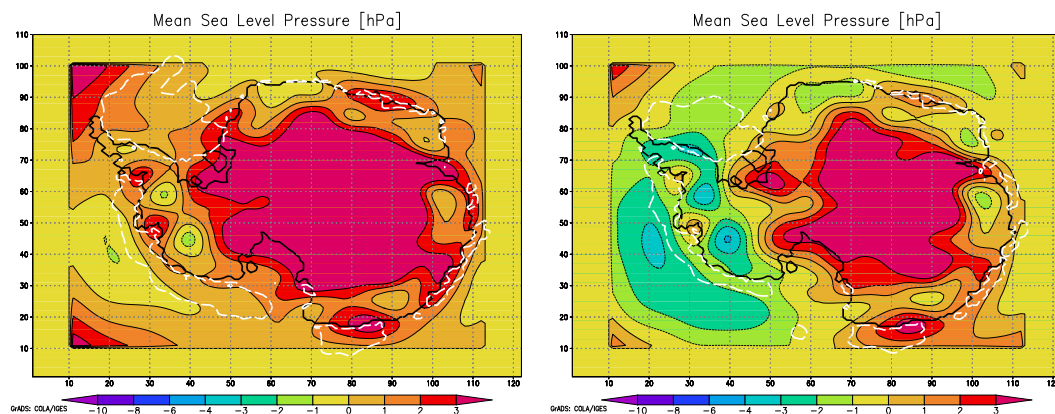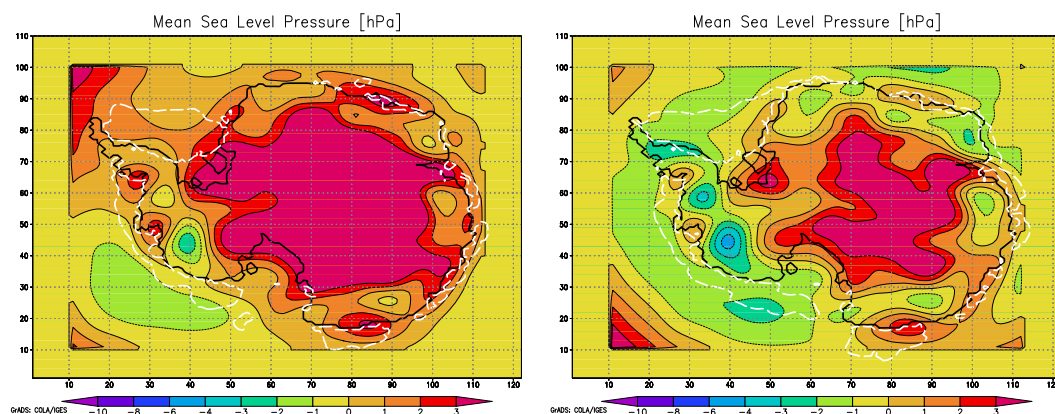
In Fig. B.27 to B.33 the autumn MSLP in the years 1996 to 2009 (ERAint run) is shown. The cyclones in autumn have similar intensities as in summer with the strongest deviations, that occur in the years 1996, 1999. 2003 and 2006, hardly exceeding values of more than -6 hPa. The year with the weakest cyclones is 2002.

Figure B.27: Autumn Mean of MSLP of 1996 and 1997 (ERAint run). White dashed line: Mean Seasonal Sea Ice. Used filter: SYN

Figure B.28: Autumn Mean of MSLP of 1998 and 1999 (ERAint run). White dashed line: Mean Seasonal Sea Ice. Used filter: SYN

Figure B.29: Autumn Mean of MSLP of 2000 and 2001 (ERAint run). White dashed line: Mean Seasonal Sea Ice. Used filter: SYN
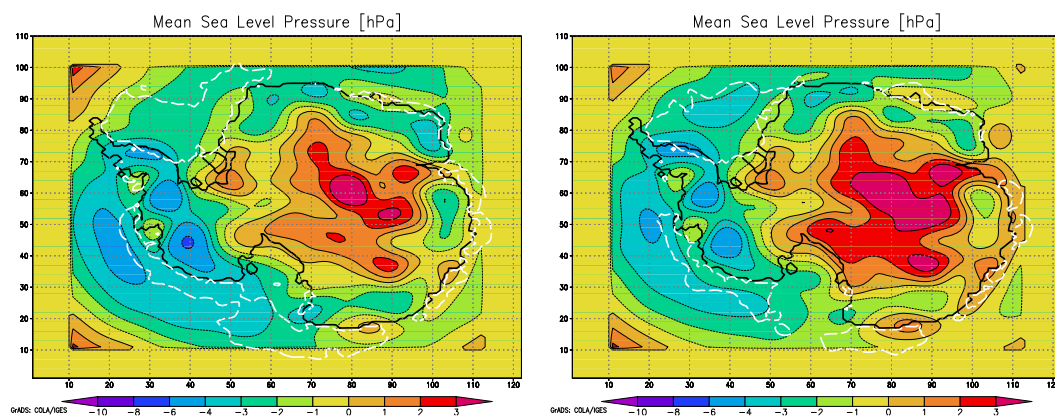

Figure B.30: Autumn Mean of MSLP of 2002 and 2003 (ERAint run). White dashed line: Mean Seasonal Sea Ice. Used filter: SYN

Figure B.31: Autumn Mean of MSLP of 2004 and 2005 (ERAint run). White dashed line: Mean Seasonal Sea Ice. Used filter: SYN
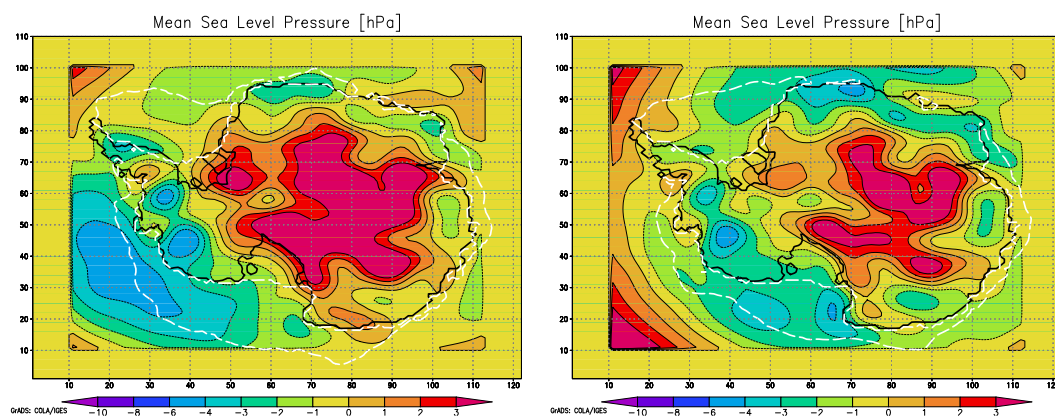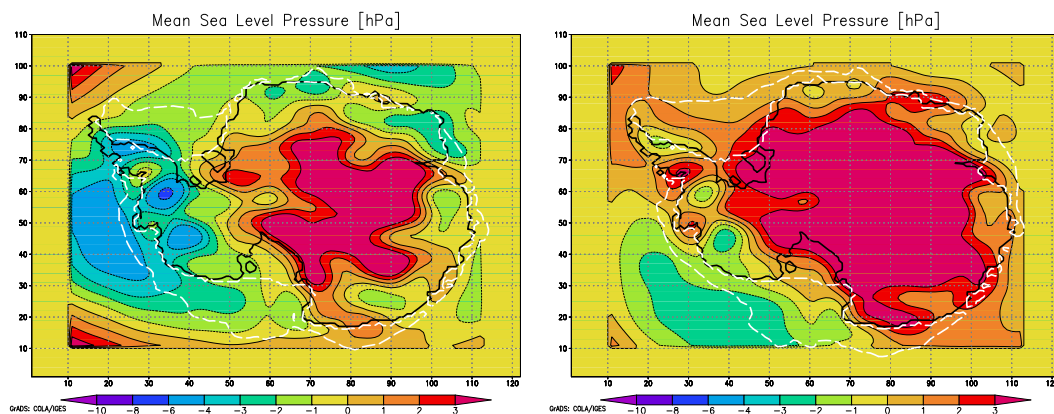

Figure B.32: Autumn Mean of MSLP of 2006 and 2007 (ERAint run). White dashed line: Mean Seasonal Sea Ice. Used filter: SYN
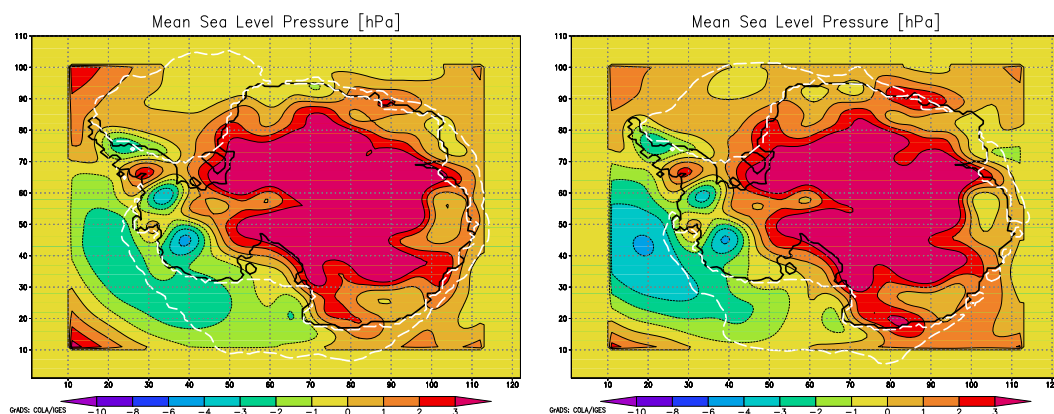
Figure B.33: Autumn Mean of MSLP of 2008 and 2009 (ERAint run). White dashed line: Mean Seasonal Sea Ice. Used filter: SYN

The MSLP in winter 1996 to 2009 is shown in B.34 to B.40. In winter the stongest cyclones occur in the years 1998 (as in the ERA40 run), 2003 and 2006. Except of the year 1998, where the deviation from the spatial mean MSLP is -10 hPa, the winter cyclones are weak compared to spring cyclones. The weakest cyclones occur in the years 2002, 2007 and 2009.
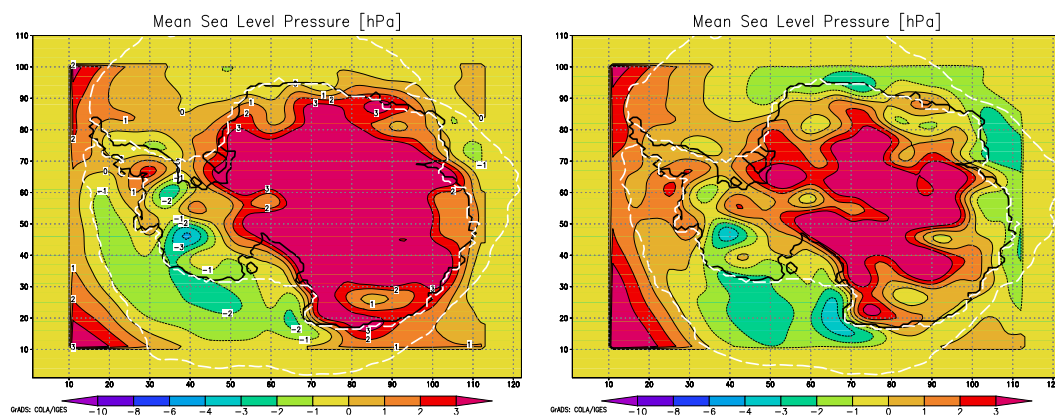
Figure B.34: Winter Mean of MSLP of 1996 and 1997 (ERAint run). White dashed line: Mean Seasonal Sea Ice. Used filter: SYN
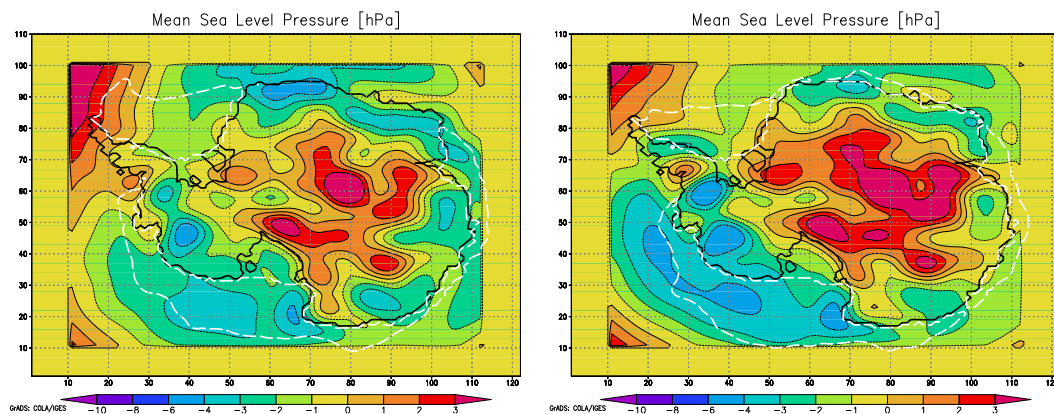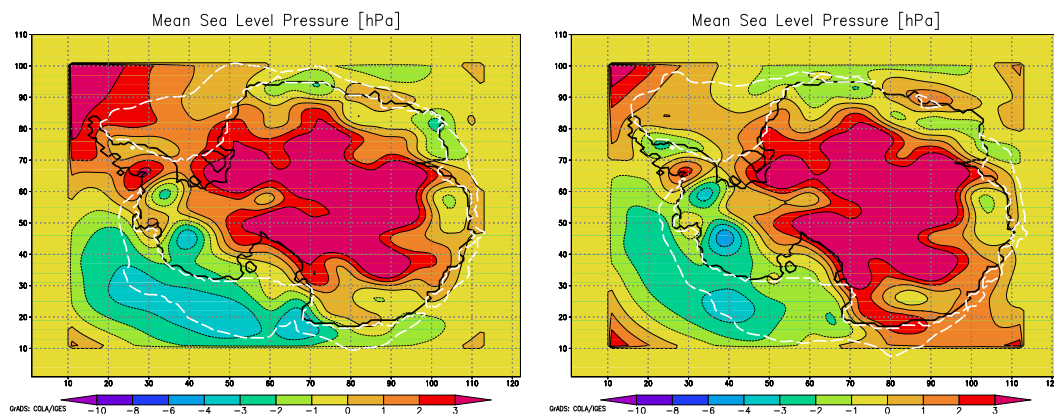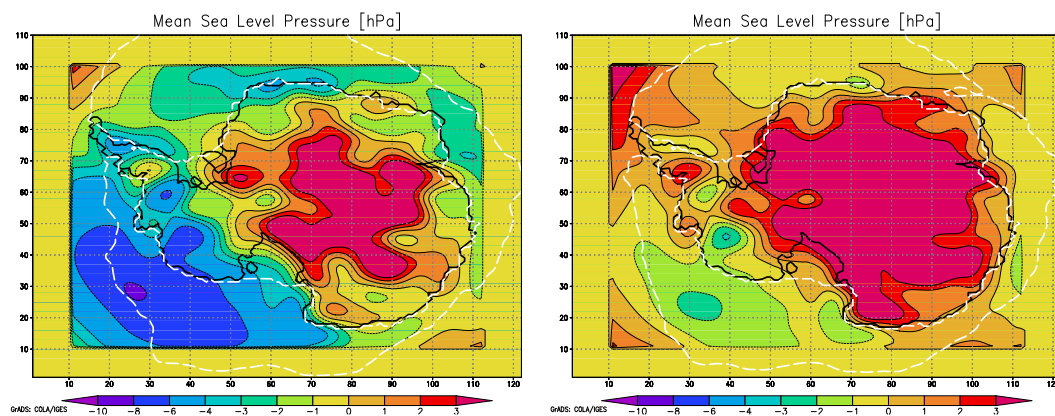

Figure B.35: Winter Mean of MSLP of 1998 and 1999 (ERAint run). White dashed line: Mean Seasonal Sea Ice. Used filter: SYN
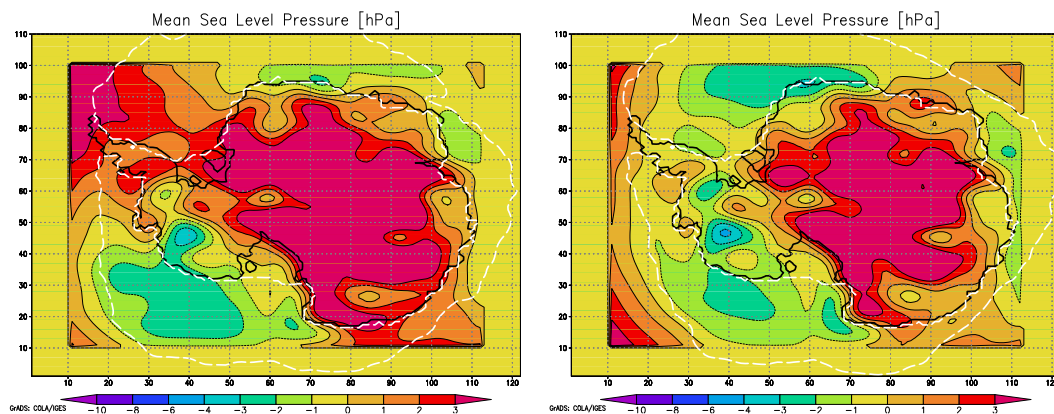
Figure B.36: Winter Mean of MSLP of 2000 and 2001 (ERAint run). White dashed line: Mean Seasonal Sea Ice. Used filter: SYN
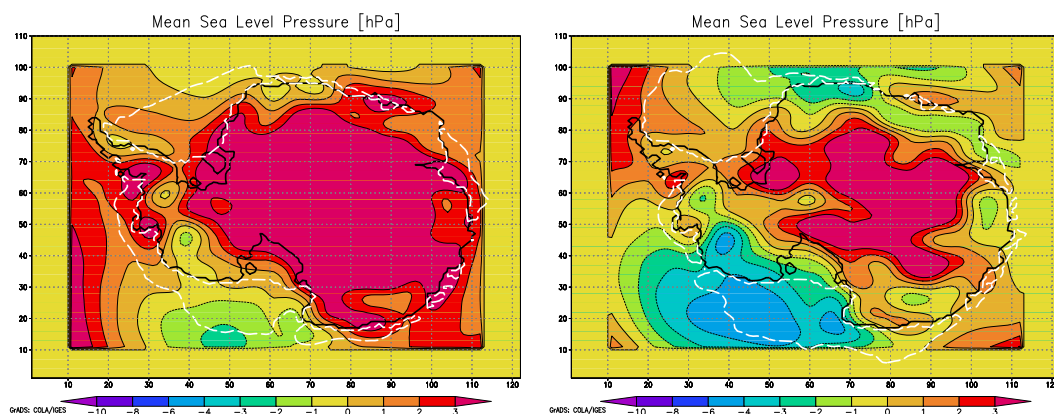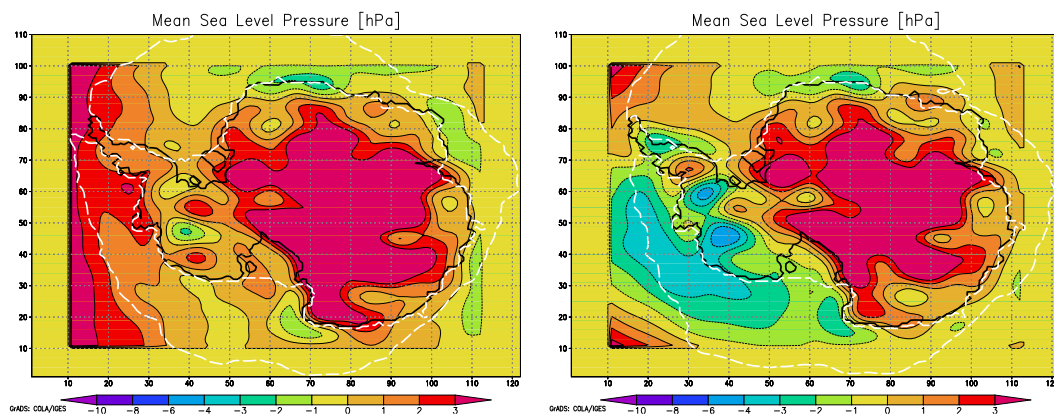

Figure B.37: Winter Mean of MSLP of 2002 and 2003 (ERAint run). White dashed line: Mean Seasonal Sea Ice. Used filter: SYN
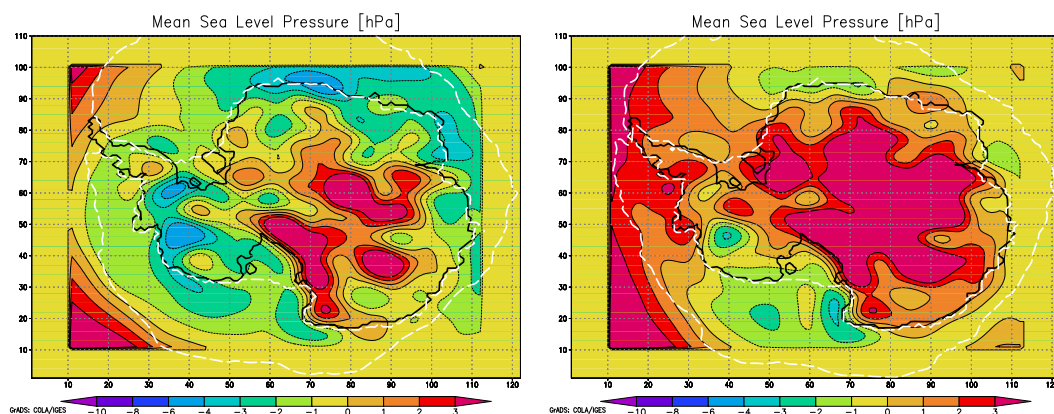
Figure B.38: Winter Mean of MSLP of 2004 and 2005 (ERAint run). White dashed line: Mean Seasonal Sea Ice. Used filter: SYN
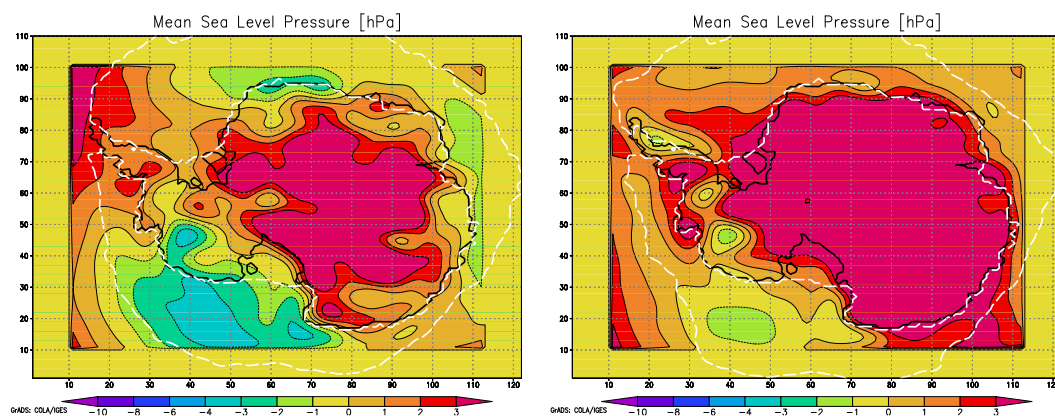
Figure B.39: Winter Mean of MSLP of 2006 and 2007 (ERAint run). White dashed line: Mean Seasonal Sea Ice. Used filter: SYN
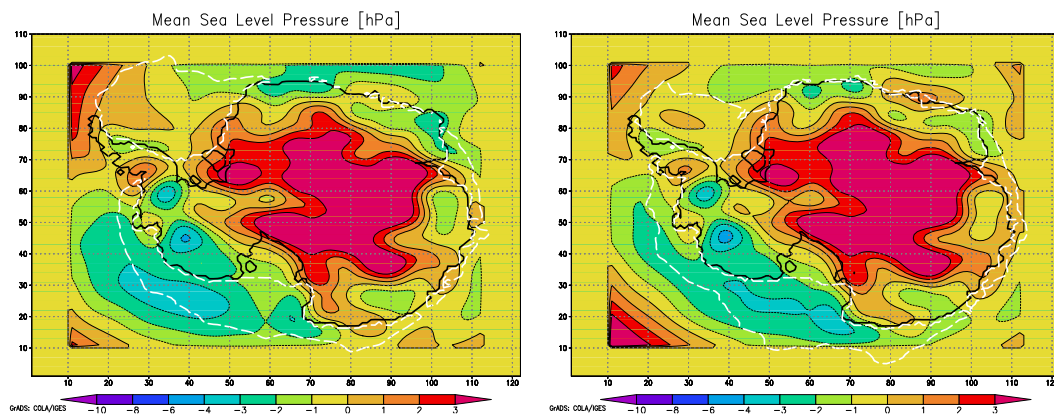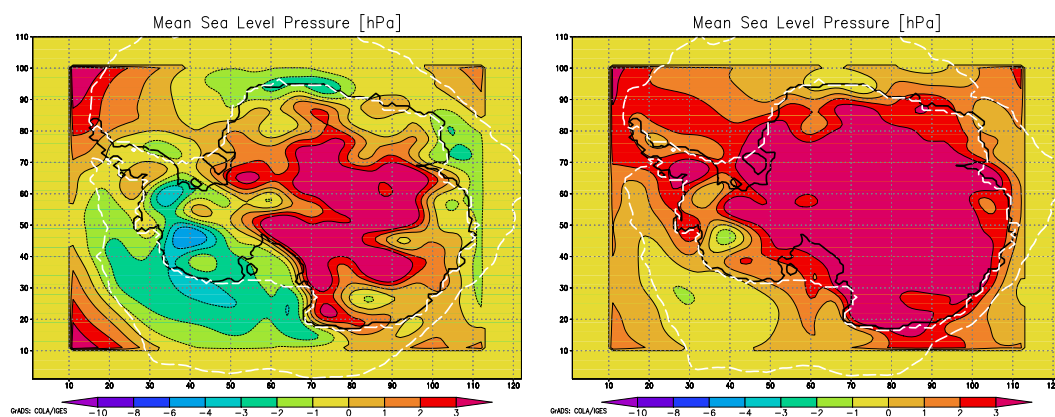

Figure B.40: Winter Mean of MSLP of 2008 and 2009 (ERAint run). White dashed line: Mean Seasonal Sea Ice. Used filter: SYN

Table B.2: Table of the MSLP pattern correlation of the seasons in the years 1996 to 2009 (ERAint run).

Year	Seasons	Correlation
1996	spring-summer	0.87
	spring-winter	0.87
	summer-autumn	0.91
	summer-winter	0.90
	autumn-winter	0.85
1997	autumn-winter	0.87
1998	spring-winter	0.85
1999	spring-winter	0.94
2000	autumn-winter	0.92
2001	autumn-winter	0.90
2002	autumn-winter	0.86
2003	summer-winter	0.91
	autumn-winter	0.85
2005	summer-autumn	0.85
2006	spring-winter	0.91
	summer-winter	0.86
2007	summer-autumn	0.86
	autumn-winter	0.95
2008	autumn-winter	0.88
2009	spring-autumn	0.94
	spring-winter	0.86

The pattern correlations in the ERAint run are not the same as in the ERA40 run for the three overlapping years. Still, 1996 is the year with the most correlations (5). The season with the most correlations to the other seasons of the same year is winter (16 correlations).

Appendix C

Tables

Table C.1: Table of all Stations and the used HIRHAM4 grid points. Positions in longitude and latitude, respectively grid point number and corresponding height. First line of each station shows the station name, its geographical coordinates and height. The following four lines depict HIRHAM related information.

Station	x-Coordinate	y-Coordinate	height	Land Sea Fraction
Bellingshausen	−58.93	−62.20	*16* m	
Grid point 1	13	83	0 m	0.07
Grid point 2	14	83	0 m	0.09
Grid point 3	14	82	0 m	0.12
Grid point 4	12	83	0 m	0.00

Station	x-Coordinate	y-Coordinate	height	Land Sea Fraction
Casey	110.52	−66.27	*42* m	
Grid point 1	107	39	250 m	0.62
Grid point 2	106	39	872 m	1.00
Grid point 3	108	38	0 m	0.00
Grid point 4	107	38	217 m	0.61

Station	x-Coordinate	y-Coordinate	height	Land Sea Fraction
Davis	77.95	−68.58	*13* m	
Grid point 1	104	64	569 m	0.98
Grid point 2	105	64	208 m	0.53
Grid point 3	103	64	873 m	1.00
Grid point 4	103	63	1397 m	1.00

Station	x-Coordinate	y-Coordinate	height	Land Sea Fraction
Dumont-Durville	140.00	−66.66	*43* m	
Grid point 1	93	20	0 m	0.00
Grid point 2	93	19	0 m	0.00
Grid point 3	94	19	0 m	0.00
Grid point 4	92	20	0 m	0.37

Station	x-Coordinate	y-Coordinate	height	Land Sea Fraction
Mawson	62.86	−67.59	*16* m	
Grid point 1	102	75	782 m	1.00
Grid point 2	103	75	0 m	0.31
Grid point 3	101	75	1399 m	1.00
Grid point 4	103	76	0 m	0.07

Station	x-Coordinate	y-Coordinate	height	Land Sea Fraction
McMurdo	166.66	−77.84	*24* m	
Grid point 1	68	31	0 m	0.15
Grid point 2	68	30	0 m	0.00
Grid point 3	67	33	31 m	1.00
Grid point 4	68	32	0 m	0.41

Station	x-Coordinate	y-Coordinate	height	Land Sea Fraction
Syowa	39.58	−69.00	*29* m	
Grid point 1	89	87	540 m	0.87
Grid point 2	90	87	1095 m	1.00
Grid point 3	90	88	328 m	0.56
Grid point 4	89	86	1253 m	1.00

Station	x-Coordinate	y-Coordinate	height	Land Sea Fraction
O'Higgins	−57.53	−63.19	*13* m	
Palmer	−64.05	−64.77	*31* m	

Table C.2: Table of the root mean square error and the correlation with Souding for TWV at all stations for all used HIRHAM4 grid points. ERA40 run 1994 to 1999.

Bellingshausen	RMSE	relative RMSE	Correlation
Grid point 1	0.70 mm	0.09	0.92
Grid point 2	0.77 mm	0.1	0.92
Grid point 3	0.77 mm	0.1	0.92
Grid point 4	0.63 mm	0.8	0.92

Casey	RMSE	relative RMSE	Correlation
Grid point 1	0.45 mm	0.14	0.94
Grid point 2	0.93 mm	0.42	0.93
Grid point 3	0.24 mm	0.06	0.95
Grid point 4	0.42 mm	0.13	0.94

Davis	RMSE	relative RMSE	Correlation
Grid point 1	0.83 mm	0.43	0.95
Grid point 2	0.54 mm	0.22	0.96
Grid point 3	1.06 mm	0.72	0.91
Grid point 4	1.12 mm	0.85	0.97

Dumont-Durville	RMSE	relative RMSE	Correlation
Grid point 1	0.23 mm	0.06	0.94
Grid point 2	0.28 mm	0.08	0.95
Grid point 3	0.40 mm	0.11	0.95
Grid point 4	0.30 mm	0.11	0.95

Mawson	RMSE	relative RMSE	Correlation
Grid point 1	0.70 mm	0.45	0.96
Grid point 2	0.40 mm	0.19	0.96
Grid point 3	0.97 mm	0.92	0.94
Grid point 4	0.32 mm	0.12	0.96

McMurdo	RMSE	relative RMSE	Correlation
Grid point 1	0.39 mm	0.23	0.88
Grid point 2	0.35 mm	0.2	0.89
Grid point 3	0.41 mm	0.25	0.89
Grid point 4	0.41 mm	0.25	0.88

Syowa	RMSE	relative RMSE	Correlation
Grid point 1	0.76 mm	0.37	0.81
Grid point 2	0.99 mm	0.61	0.81
Grid point 3	0.49 mm	0.19	0.83
Grid point 4	1.07 mm	0.78	0.80

Table C.3: Table of the pattern correlation of the test runs with different vertical resolution - 25Levs and 46Levs.

Month	January 2001
mlsp	0.99
t2m	0.99
qvi	0.99

Month	July 2001
mlsp	0.99
t2m	0.99
qvi	0.99

Table C.4: Table of the A and B parameters for 25Levs and 46Levs.

ps=   101300

A (25Levs) =	00000.000000	02000.000000	04000.000000	06046.110595
	08267.927560	10609.513232	12851.100169	14698.498086
	15861.125180	16116.236610	15356.924115	13621.460403
	11101.561987	08127.144155	05125.141747	02549.969411
	00783.195031	00000.000000	00000.000000	00000.000000
	00000.000000	00000.000000	00000.000000	00000.000000
	00000.000000	00000.000000		
B (25Levs) =	0.0000000000	0.0000000000	0.0000000000	0.0003389933
	0.0033571866	0.0130700434	0.0340771467	0.0706498323
	0.1259166826	0.2011954093	0.2955196487	0.4054091989
	0.5249322235	0.6461079479	0.7596983769	0.8564375573
	0.9287469142	0.9432648000	0.9580097000	0.9729851852
	0.9793752000	0.9858072000	0.9922814815	0.9948476000
	0.9974205000	1.0000000000		

| A (46Levs) = | 00000.000000 | 01356.474609 | | |
	01680.640259	02082.273926	02579.888672	03196.421631
	03960.291504	04906.708496	06018.019531	07306.631348
	08765.053711	10376.126953	12077.446289	13775.325195
	15379.805664	16819.474609	18045.183594	19027.695313
	19755.109375	20222.205078	20429.863281	20384.480469
	20097.402344	19584.330078	18864.750000	17961.357422
	16899.468750	15706.447266	14411.124023	13043.218750
	11632.758789	10209.500977	08802.356445	07438.803223
	06144.314941	04941.778320	03850.913330	02887.696533
	02063.779785	01385.912598	00855.361755	00467.333588
	00210.393890	00065.889244	00007.367743	00000.000000
	00000.000000			
B (46Levs) =	0.00000000	0.00000000		
	0.00000000	0.00000000	0.00000000	0.00000000
	0.00000000	0.00000000	0.00000000	0.00000000
	0.00007582	0.00046139	0.00181516	0.00508112
	0.01114291	0.02067788	0.03412116	0.05169041
	0.07353383	0.09967469	0.13002251	0.16438432
	0.20247594	0.24393314	0.28832296	0.33515489
	0.38389215	0.43396294	0.48477158	0.53570992
	0.58616841	0.63554746	0.68326861	0.72878581
	0.77159661	0.81125343	0.84737492	0.87965691
	0.90788388	0.93194032	0.95182151	0.96764523
	0.97966272	0.98827010	0.99401945	0.99763012
	1.00000000			

Appendix D

Additional Figures
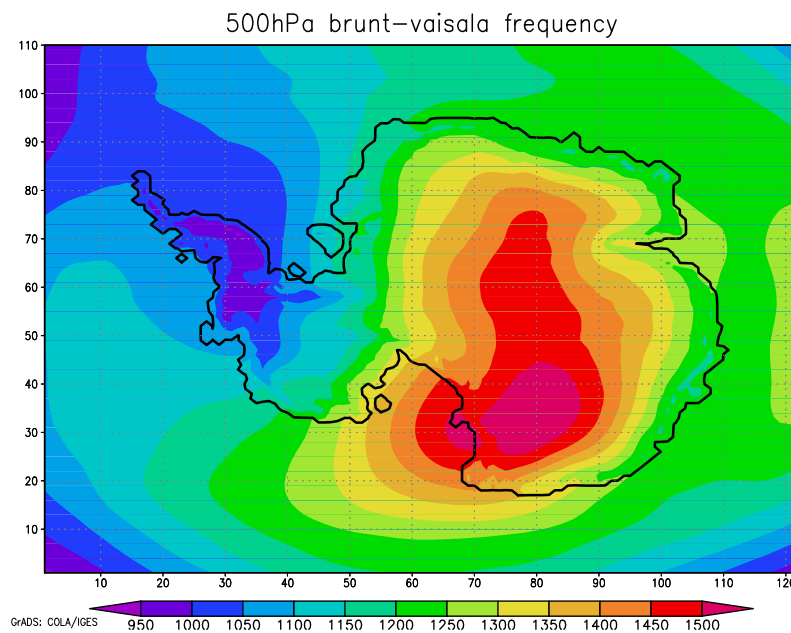
Figure D.1: Mean Brunt-Vaisala-Frequency of the ERA-interim run (Jan. 1996 to Dec. 2009) at 500 hPa.

Figure D.2: Mean Brunt-Vaisala-Frequency of the ERA-interim run (Jan. 1996 to Dec. 2009) at 850 hPa.

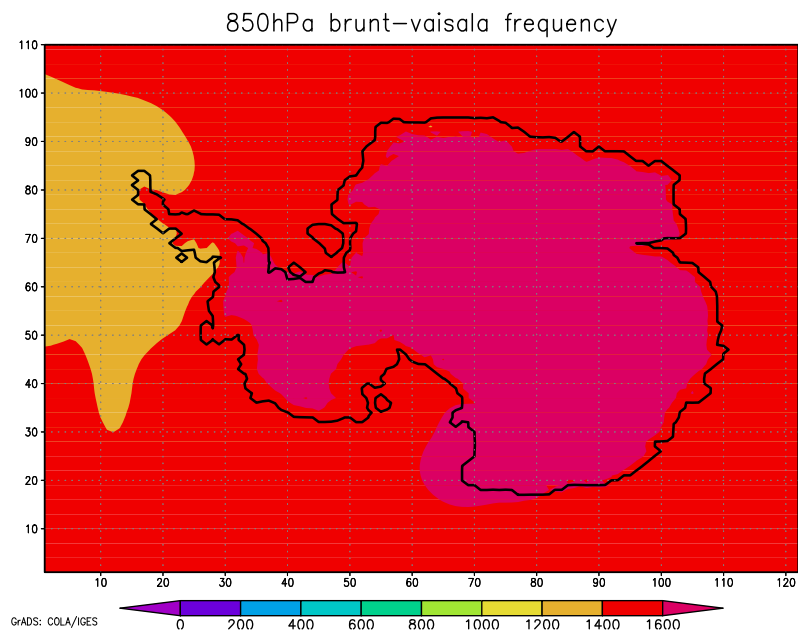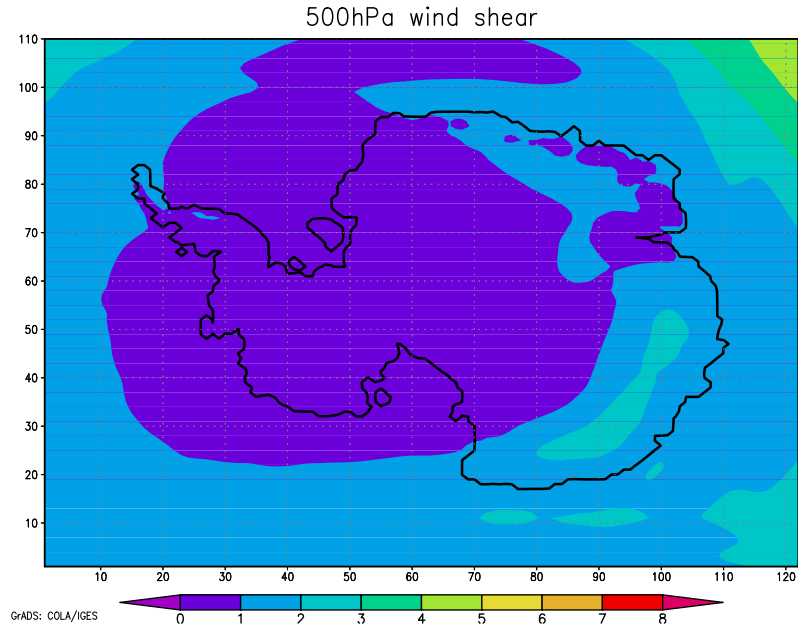Figure D.3: Mean wind shear of the ERA-interim run (Jan. 1996 to Dec. 2009) at 500 hPa.
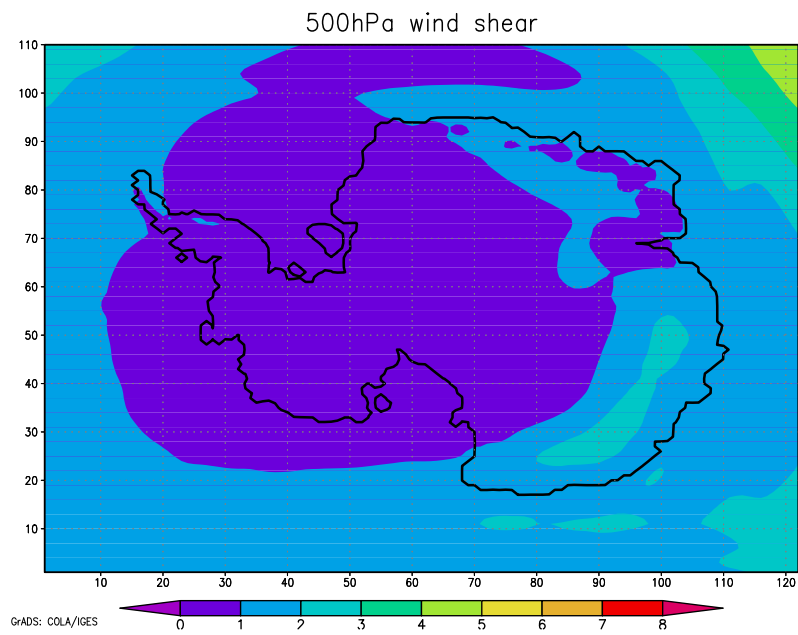
Figure D.4: Mean wind shear of the ERA-interim run (Jan. 1996 to Dec. 2009) at 850 hPa.

Figure D.5: Filtered TWV of the AAO-negative summers 2001 (upper left), 2004 (middle left) and 2006 (lower left) and the AAO-positive summers 1999 (upper right), 2000 (middle right) and 2008 (lower right). Used filter: SYN
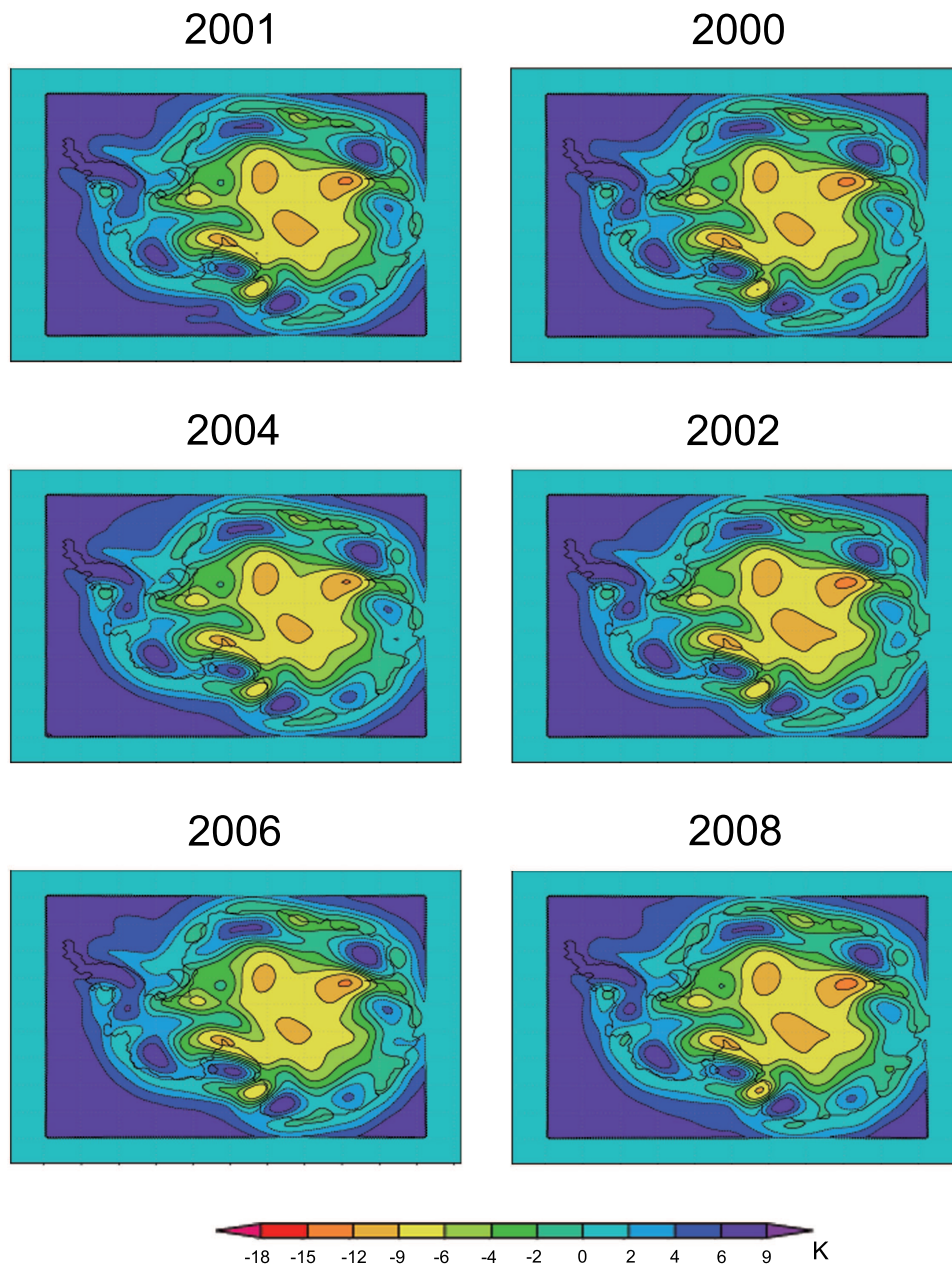
Figure D.6: Filtered T2m of the AAO-negative summers 2001 (upper left), 2004 (middle left) and 2006 (lower left) and the AAO-positive summers 1999 (upper right), 2000 (middle right) and 2008 (lower right). Used filter: SYN
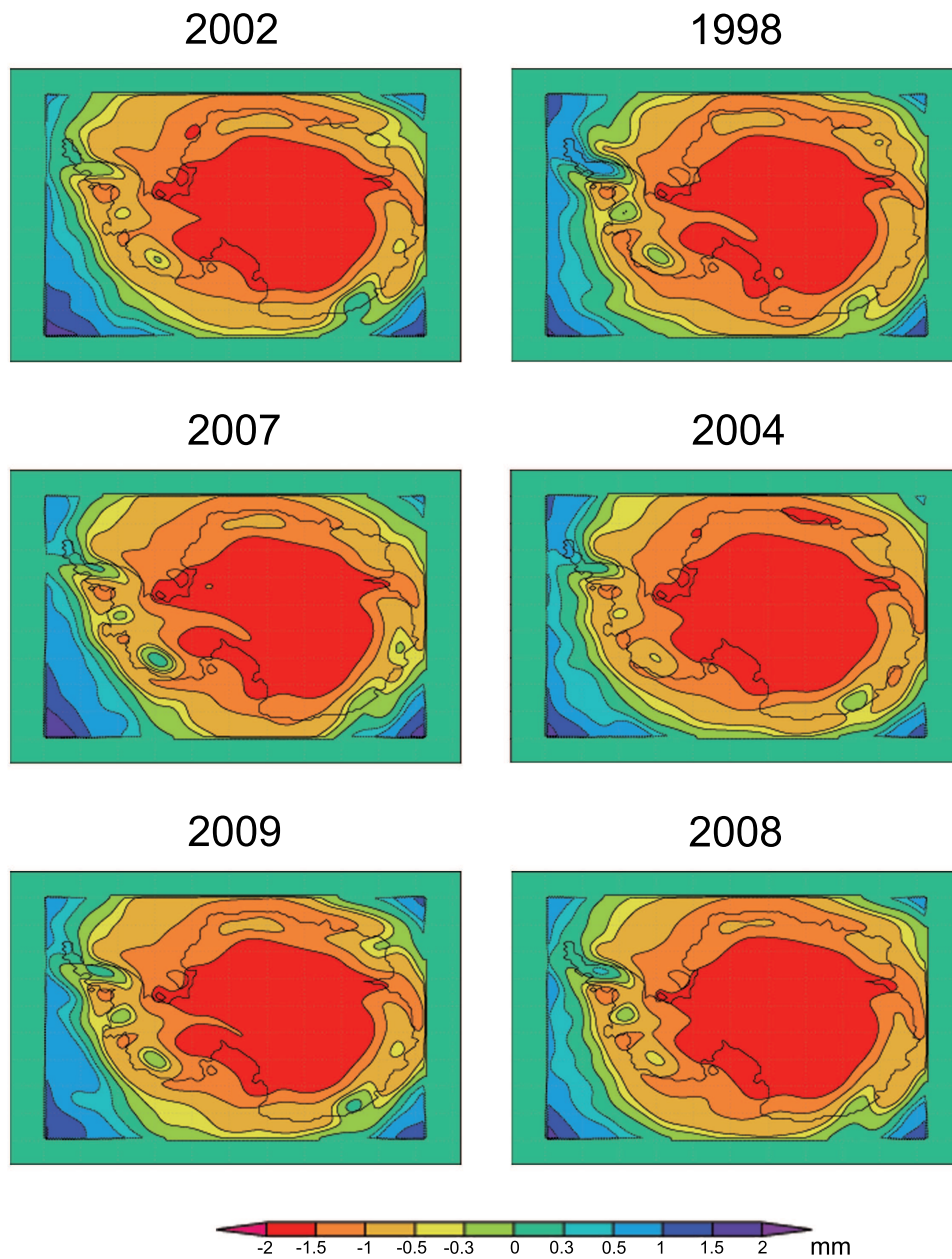
Figure D.7: Filtered TWV of the AAO-negative winters 1997 (upper left), 2004 (middle left) and 2009 (lower left) and the AAO-positive winters 1999 (upper right), 2001 (middle right) and 2006 (lower right). Used filter: SYN

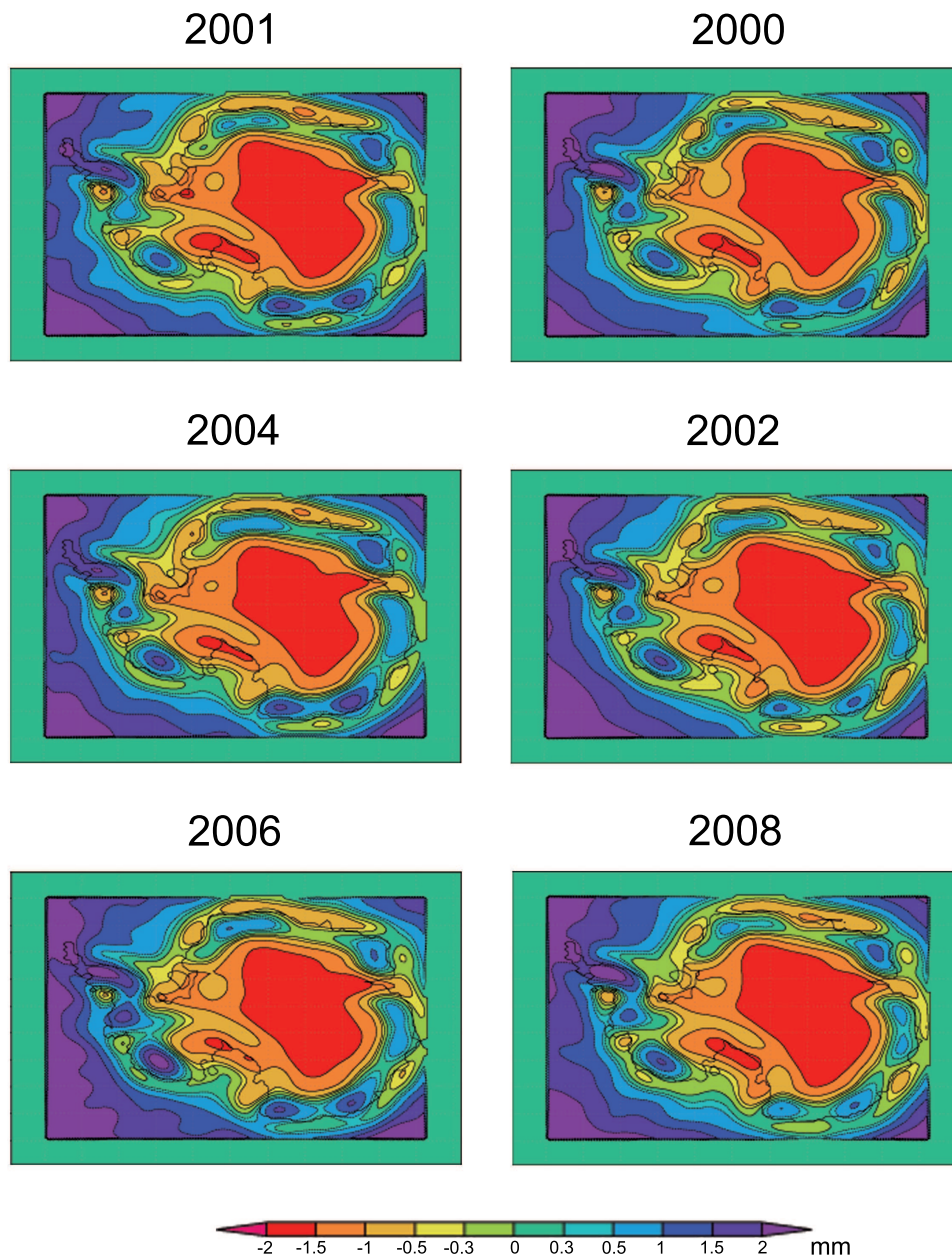Figure D.8: Filtered T2m of the AAO-negative winters 1997 (upper left), 2004 (middle left) and 2009 (lower left) and the AAO-positive winters 1999 (upper right), 2001 (middle right) and 2006 (lower right). Used filter: SYN
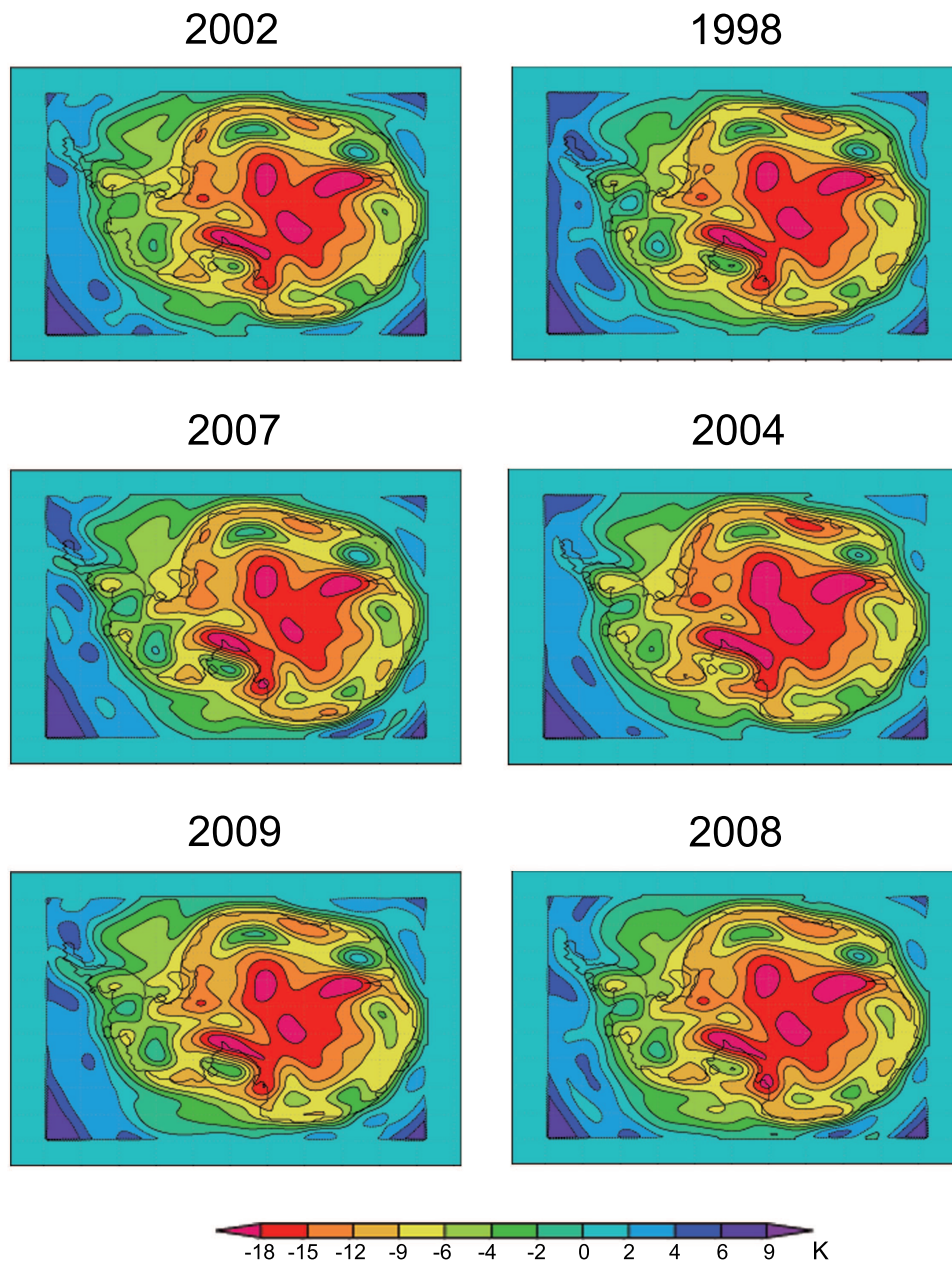
Appendix E

Symbols

AAO	Antarctic Oscillation
AMS	Automatic Weather Station
AVHRR	ECHAM is an atmospheric general circulation model
C_i	Specific Heat
CDO	Climate Data Operators
CPC	Climate Prediction Center
e	Eulers Number
ECHAM	ECHAM is an atmospheric general circulation model
ENSO	El Nino - Southern Oscillation
EOF	Empirical Orthogonal Function
ERA	Global Atmospheric Reanalysis by ECMWF
η	Vertical Coordinate
f	Coriolis Parameter
GCM	Global Climate Model
HIRHAM	Regional Climate Model
HIRLAM	Regional Weather Model
K_x	Diffussion Processes
κ	Heat Capacity Ratio
λ	Horizontal Coordinate
LOW	Lowpass Filter (1000km)
m	Mixing Ratio
MESO	Mesoscale Filter (200km to 600km)
MSLP	Mean Sea Level Pressure
N	Brunt-Vaisala-Frequency
∇	Nabla
NCAR	National Center for Atmospheric Research
NCEP	National Centers for Environmental Prediction
p	Pressure
P_x	Physical Processes
PatCorr	Pattern Correlation
PBL	Planetary Boundary Layer
P-E	Precipitation minus Evaporation

ϕ	Geopotential
q	Humidity
q_i	Cloud Ice
q_l	Cloud Water
q_{sat}	Saturation Humidity
q_w	Liquid Water
QVI	Vertically Integrated Humidity
RCM	Regional Climate Model
rel.StDev	Relative Standard Deviation
ρ	Density
rmse	Root Mean Square Error
S_ψ	Semi-Implicit Correction
SOI	Southern Oscillation Index
SST	Sea Surface Temperature
StDev	Standard Deviation
SYN	Synoptical Scale Filter (500km to 1000km)
t	Time
T	Temperature
T2m	2m-Temperature
θ	Horizontal Coordinate
Θ	Potential Temperature
TWV	Total Water Vapour
$\vec{v}$	Wind Vector
WMO	World Meteorological Organisation

Appendix F

Literature

Bibliography

Andreas, E. L., W. B. Tucker III and S. F. Ackley (1984): Atmospheric Boundary-Layer Modification, Drag Coefficient, and Surface Heat Flux in the Antarctic Marginal Ice Zone. Journal of Geophysical Research **89**: 649–661.

Barat, J. and C. Cot (1995): Accuracy Analysis of Rubsonde-GPS Wind Sounding System. Journal of Applied Meteorology **34**: 1123–1132.

Bevis, M., S. Businger, S. Chiswell, T. A. Herring, R. A. Anthes, C. Rocken and R. H. Ware (1994): GPS Meteorology: Mapping zenith wet delays onto precipitable water. Journal of Applied Meteorology **33(3)**: 379–386.

Bintanja, R. (2001): Snowdirft Sublimation in a Katabatic Wind Region of the Antarctic Ice Sheet. Journal of Applied Meteorology **40**: 1952–1966.

Brandt, R. E., S. G. Warren, A. P. Worby and T. C. Grenfell (2005): Surface Albedo of the Antarctic Sea Ice Zone. JOURNAL OF CLIMATE **18**: 3606–3622.

Brinkop, S. and E. Roeckner (1995): Sensitivity of a general circulation model to parameterizations of cloud-turbulence interactions in the atmospheric boundary layer. Tellus **47(A)**: 197–220.

Bromwich, D. H. (1989a): An Extraordinary Katabtic Wind Regime at Terra Nova Bay, Antarctica. Monthly Weather Review **117**: 688–695.

Bromwich, D. H. (1989b): Satellite Analyses of Antarctic Katabatic Wind Behavior. Bulletin American Meteorological Society **70**: 738–749.

Bromwich, D. H. (1991): Mesoscale Cyclogenesis over the Southwestern Ross Sea Linked to Strong Katabatic Winds. Monthly Weather Review **119**: 1736–1752.

Bromwich, D. H. and D. D. Kurtz (1984): Katabatic Wind Forcing of the Terra Nova Bay Polynya. Journal of Geophysical Research **89**: 3561–3572.

Budd, W. F. (1991): Antarctica and global change. Climatic Change **18**: 271–299, URL http://dx.doi.org/10.1007/BF00139002, 10.1007/BF00139002.

Businger, S., S. R. Chiswell, M. Bevis, R. A. Duan, Jingping Anthes, C. Rocken, R. H. Ware, M. Exner, T. VanHove and F. S. Solheim (1996): The Promise of GPS in Atmospheric Monitoring. Bulletin of the American Meteorological Society **77**.

Carrasco, J. F., D. H. Bromwich and A. J. Monaghan (2003): Distribution and Characteristics of Mesoscale Cyclones in the Antarctic: Ross Sea Eastward to the Weddell Sea. Monthly Weather Review **131(2)**: 289–301.

Carroll, J. (1982): Long-Term Means and Short-term Variability of the Surface Energy Balance Components at the South Pole. Journal of Geophysical Research **87**: 4177–4286.

Chenoli, S. N., J. Turner and A. A. Samah (2013): A climatology of strong wind events at McMurdo station, Antarctica. International Journal of Climatology **33**: 2667–2681.

Christensen, J. H., O. B. Christensen et al. (1996): The HIRHAM4 regional atmospheric climate model. DMI Sci. Rep. **96(4)**.

CPC (2011): Climate Prediction Center.

Davies, H. C. (1976): A lateral boundary formulation for multi-level prediction models. Quarterly Journal of Royal Meteorological Society **102**: 405–418.

Dee, D. P., S. M. Uppala, A. J. Simmons, P. Berrisford, P. Poli, S. Kobayashi, U. Andrae, M. A. Balmaseda, G. Balsamo, P. Bauer, P. Bechtold, A. C. M. Beljaars, L. van de Berg, J. Bidlot, N. Bormann, C. Delsol, R. Dragani, M. Fuentes, A. J. Geer, L. Haimberger, S. B. Healy, H. Hersbach, E. V. Holm, L. Isaksen, P. Kallberg, M. Köhler, M. Matricardi, A. P. McNally, B. M. Monge-Sanz, J.-J. Morcrette, B.-K. Park, C. Peubey, P. de Rosnay, C. Tavolato, J.-N. Thepaut and F. Vitart (2011): The ERA-Interim reanalysis: configuration and performance of the data assimilation system. Quarterly Journal of the Royal Meteorological Society **137(656)**: 553–597.

Dery, S. J., P. A. Taylor and J. Xiao (1998): The thermodynamic effects of sublimating, blowing snow in the Atmospheric Boundary Layer. Boundary-Layer Meteorology **89**: 251–283.

Dethloff, K., K. Glushak, A. Rinke and D. Handorf (2010): Antarctic 20th Century Accumulation Changes Based on Regional Climate Model Simulations. Advances in Meteorology **2010**.

Dorn, W. (2001): Natürliche Klimavariationen der Arktis in einem regionalen hochauflösenden Atmosphärenmodell. Ph.D. thesis, Universität Potsdam.

Feser, F. (2006): Enhanced Detectability of Added Value in Limited-Area Model Results Separated into Different Spatial Scales. Monthly Weather Review **Volume 134**: 2180–2190.

Feser, F. and H. von Storch (2005): A Spatial Two-Dimensional Discrete Filter for Limited-Area-Model Evaluation Purposes. Monthly Weather Review **Volume 133**: 1774–1786.

Fogt, R. L. and D. H. Bromwich (2006): Decadal Variability of the ENSO Teleconnection to the High-Latitude South Pacific Governed by Coupling with the Southern Annular Mode. Journal of Climate **19**: 979 – 997, doi:doi: 10.1175/JCLI3671.1.

Genthon, C., M. S. Town, D. Six, V. Favier, S. Argentini and A. Pellegrini (2010): Meteorological atmospheric boundary layer measurements and ECMWF analyses during summer at Dome C, Antarctica. JOURNAL OF GEOPHYSICAL RESEARCH **115**, doi:10.1029/2009JD012741.

Glushak, K. (2007): Atmospheric circulation and the surface mass balance in a regional climate model of Antarctica. Ph.D. thesis, Universität Potsdam.

Goldner, A., M. Huber and M. Caballero (2013): Does Antarctic glaciation cool the world? Climate of the Past **9**: 173–189.

Harangozo, S. A. (2000): A SEARCH FOR ENSO TELECONNECTIONS IN THE WEST ANTARCTIC PENINSULA CLIMATE IN AUSTRAL WINTER. INTERNATIONAL JOURNAL OF CLIMATOLOGY **20**: 663–679.

Hoinkes, H. (1960): Studies of Solar Radiation and Albedo in the Antarctic. Arch. Meteorol. Geophys. Bioklimatol. **10**: 175–181.

Holland, M. M., C. M. Bitz, E. C. Hunke, W. H. Lipscomb and J. L. Schramm (2006): Influence of the Sea Ice Thickness Distribution on Polar Climate in CCSM3. JOURNAL OF CLIMATE **19**: 2398–2414.

Horwath, M. and R. Dietrich (2009): Signal and error in mass change inferences from GRACE: the case of Antarctica. Geophysical Journal International **177(3)**: 849–864, doi:10.1111/j.1365-246X.2009.04139.x, URL `http://dx.doi.org/10.1111/j.1365-246X.2009.04139.x`.

Hoskins, B. J. and K. I. Hodges (2005): A New Perspective on Southern Hemisphere Storm Tracks. Journal of Climate **18**: 4108 – 4129.

Hoskins, B. J. and P. J. Valdes (1990): On the Existence of Storm-Tracks. Journal of the Atmospheric Sciences **47(15)**: 1854–1864.

Jaatinen, J. and Kajosaari (2000): Loran-C based windfinding in Meteorology. 29th ANNUAL CONVENTION AND TECHNICAL SYMPOSIUM OF THE INTERNATIONAL LORAN ASSOCIATION .

Jarraud, M. (2008): WMO GUIDE TO METEOROLOGICAL INSTRUMENTS AND METHODS OF OBSERVATION. Tech. Rep. 8, WMO.

Joughin, I. and S. Tulaczyk (2006): Positive Mass Balance of the Ross Ice Streams, West Antarctica. Science **295**: 476–480.

King, J. C., W. M. Connolley and S. H. Derbyshire (2001): Sensitivity of modelled Antarctic climate to surface and boundary-layer flux parametrizations. Quarterly Journal of the Royal Meteorological Society **127**: 779–794.

King, J. C. and J. Turner (1997): Antarctic meteorology and climatology .

Kistler, R., E. Kalnay, W. Collins, S. Saha, G. White, J. Woollen, M. Chelliah, W. Ebisuzaki, M. Kanamitsu, V. Kousky, H. van den Dool, R. Jenne and M. Fiorino (1999): The NCEP/NCAR 50-year Reanalysis. Tech. rep., NCEP/NCAR.

Kraus, H. (2004): Die Atmosphäre der Erde .

Krinner, G., O. Magand, I. Simmonds, C. Genthon and J. Dufresne (2007): Simulated Antarctic precipitation and surface mass balance at the end of the twentieth and twenty-first centuries. Climate Dynamics **28**: 215–230.

Kwok, R. and J. C. Comiso (2002a): Spatial patterns of variability in Antarctic surface temperature: Connections to the Southern Hemisphere Annular Mode and the Southern Oscillation. Geophys. Res. Lett. **29**: 4, doi:doi:10.1029/2002GL015415.

Kwok, R. and J. C. Comiso (2002b): Southern Ocean Climate and Sea Ice Anomalies Associated with the Southern Oscillation. JOURNAL OF CLIMATE **15**: 487–501.

Lenaerts, J. and M. van den Broeke (2012): Modeling drifting snow in Antarctica with a regional climate model: 2. Results. Journal of Geophysical Research: Atmospheres **117**: D05109/1–D05109/11.

Machenbauer, B. (1988): The HIRLAM final report, HIRLAM Technical Report 5.

Marshall, G. J. and J. C. King (1998): Southern Hemisphere circulation anomalies associated with extreme Antarctic Peninsula winter temperatures. Geophysical Research Letters **25(13)**: 2437–2440.

Massom, R. A., P. T. Harris, K. J. Micheal and M. J. Potter (1998): The distribution and formative processes of latent-heat polynyas in East Antarctica. Annals of Glaciology **27**.

Matthes, H., A. Rinke and K. Dethloff (2010): Variability of Extreme Temperature in the Arctic - Observation and RCM. The Open Atmospheric Science Journal **4**: 126–136.

Meredith, M. P. and J. C. King (2005): Rapid climate change in the ocean west of the Antarctic Peninsula during the second half of the 20th century. GEOPHYSICAL RESEARCH LETTERS **32**.

Monaghan, A. J., D. H. Bromwich and S.-H. Wang (2006): Recent trends in Antarctic snow accumulation from Polar MM5 simulations. Philosophical Transactions of the Royal Society A **364**: 1683–1708.

Nylen, T. H., A. G. Fountain and P. T. Doran (2004): Climatology of katabatic winds in the McMurdo dry valleys, southern Victoria Land, Antarctica. Journal of Geophysical Research **109**: D03114.

Peterson, R. G. and W. B. White (1998): Slow oceanic teleconnections linking the Antarctic Circumpolar Wave with the tropical El Nino-Southern Oscillation. JOURNAL OF GEOPHYSICAL RESEARCH **103**: 24573–24583.

Phillpot, H. R. and J. W. Zillman (1970): The Surface Temperature Inversion over the Antarctic Continent. J. Geophys. Res. **75**: 148–227.

Polanski, S., A. Rinke and K. Dethloff (2010): Validation of the HIRHAM-Simulated Indian Summer Monsoon Circulation, Advances in Meteorology. Advances in Meteorology **2010**: 14 pages.

Renfrew, I. A. and P. S. Anderson (2002): The surface climatology an an ordinary katabatic wind regime in Coats Land, Antarctica. Tellus **54A**: 463–484.

Rignot, E., J. L. Bamber, M. R. van den Broeke, C. Davis, Y. Li, W. J. van de Berg and E. van Meijgaard (2008): Recent Antarctic ice mass loss from radar interferometry and regional climate modelling. Nature Geosci **1**: 106–110.

Roeckner, E., K. Arpe, L. Bengtsson, M. Christoph, M. Claussen, L. Dümenil, M. Esch, M. Giorgetta, U. Schlese and U. Schlzweida (1996): The atmospheric general circulation model ECHAM-4: Model discription and simulation of present-day climate. MPI Report **218**: 90 pp.

Roeckner, E., R. Brokopf, M. Esch, M. Giorgetta, S. Hagemann, L. Kornblueh, E. Manzini, U. Schlese and U. Schulzweida (2006): Sensitivity of Simulated Climate to Horizontal and Vertical Resolution in the ECHAM5 Atmosphere Model. Journal of Climate **19**: 3771 – 3791.

Rowe, P. M., L. M. Miloshevich, D. D. Turner and V. P. Walden (2008): Dry Bias in Vaisala RS90 Radiosonde Humidity Profiles over Antarctica. JOURNAL OF ATMOSPHERIC AND OCEANIC TECHNOLOGY **25**: 1529–1541.

Schulzweida, U., L. Kornblueh and R. Quast (2009): CDO User's Guide. Tech. Rep. Version 1.3.1, MPI for Meteorology.

Simmonds, I., K. Keay and E.-P. Lim (2003): Synoptic Activity in the Seas around Antarctica. Monthly Weather Review **131(2)**: 272–288, doi:10.1175/1520-0493(2003)131¡0272:SAITSA¿2.0.CO;2.

Simmons, A., S. Uppala, D. Lee and S. Kobayashi (2007): ERA-interim: New ECMWF reanalysis products from 1989 onwards. Tech. Rep. 110, ECMWF.

Smith Jr, W. O. and L. I. Gordon (1997): Hyperproductivity of the Ross Sea (Antarctica) polynya during austral spring. Geophysical Research Letters **24**: 233–236.

Sundqvist, H. (1978): A parameterization scheme for non-convective condensation including prediction of cloud water content. Quarterly Journal of Royal Meteorological Society **104**: 677–690.

Tamura, T., K. I. Ohshima and S. Nihashi (2008): Mapping of sea ice production for Antarctic coastal polynyas. Geophysical Research Letters **35**, doi: 10.1029/2007GL032903.

Thompson, W. J., David and J. M. Wallace (2000): Annular Modes in the Extratropical Circulation. Part I: Month-to-Month Variability. Journal of Climate **13**: 1000–1016.

Troup, A. J. (1965): The southern oscillation. Quarterly Journal of the Royal Meteorological Society **91(390)**: 490–506, doi:10.1002/qj.49709139009.

Turner, J., J. C. Comiso, G. J. Marshall, T. A. Lachlan-Cope, T. Bracegirdle, T. Maksym, M. P. Meredith, Z. Wang and A. Orr (2009): Non-annular atmospheric circulation change induced by stratospheric ozone depletion and its role in the recent increase of Antarctic sea ice extent. GEOPHYSICAL RESEARCH LETTERS **36**.

Turner, J., G. J. Marshall and T. A. Lachlan-Cope (1998): ANALYSIS OF SYNOPTIC-SCALE LOW PRESSURE SYSTEMS WITHIN THE ANTARCTIC PENINSULA SECTOR OF THE CIRCUMPOLAR TROUGH. International Journal of Climatology **18**: 253–280.

Unden, P., L. Rontu, H. Jarvinen, P. Lynch, J. Calvo, G. Cats, J. Cuxart, K. Eerola, C. Fortelius, J. A. Garcia-Moya, C. Jones, G. Lenderlink, A. McDonald, R. McGrath, B. Navascues, N. W. Nielsen, V. Odegaard, E. Rodriguez, M. Rummukainen, R. Room, K. Sattler, B. H. Sass, H. Savijarvi, B. W. Schreur, R. Sigg, H. The and A. Tijm (2002): HIRLAM-5 Scienti
c Documentation.

Uppala, S., P. Kallberg, A. Hernandez, S. Saarinen, M. Fiorino, X. Li, K. Onogi, N. Sokka, U. Andrae and V. D. C. Bechthold (2004): ERA-40: ECMWF 45-year reanalysis of the global atmosphere and surface conditions 1957-2002. Tech. Rep. 101, ECMWF.

Uppala, S., P. Kallberg, A. Simmons, U. Andrae, V. da Costa Bechtold, M. Fiorino, J. Gibson, J. Haseler, A. Hernandez, G. Kelly, X. Li, K. Onogi, S. Saarinen, N. Sokka, R. Allan, E. Andersson, K. Arpe, M. Balmaseda, A. Beljaars, L. van de Berg, J. Bidlot, N. Bormann, S. Caires, F. Chevallier, A. Dethof, M. Dragosavac, M. Fisher, M. Fuentes, S. Hagemann, E. Holm, B. Hoskins, L. Isaksen, P. Janssen, R. Jenne, A. McNally, J.-F.

Mahfouf, J.-J. Morcrette, N. Rayner, R. Saunders, P. Simon, A. Sterl, K. Trenberth, A. Untch, D. Vasiljevic, P. Viterbo and J. Woollen (2005): The ERA-40 re-analysis. Quarterly Journal of Royal Meteorological Society **131**: 2961–3012.

Vaisala (2006): Vaisala Radiosonde RS92-SGP.

van den Broeke, M. R. and N. P. van Lipzig (2004): Changes in Antarctic temperature, wind and precipitation in response to the Antarctic Oscillation. Annals of Glaciology **39(1)**: 119–126, doi:doi:10.3189/172756404781814654.

van den Broeke, M. R., N. P. M. van Lipzig and E. van Meijgaard (2002): Momentum Budget of the East Antarctic Atmospheric Boundary Layer: Results of a Regional Climate Model. Journal of the Atmospheric Sciences **59**: 3117–3129.

Vey, S. (2007): Bestimmung und Analyse des atmosphärischen Wasserdampfgehaltes aus globalen GPS-Beobachtungen einer Dekande mit besonderem Blick auf die Antarktis. Ph.D. thesis, TU Dresden.

Vey, S., R. Dietrich, M. Fritsche, A. Rülke, P. Steigenberger and M. Rothacher (2009): On the homogeneity and interpretation of precitipable water time series derived from global GPS observations. Journal of Geophysical Research **114**.

Weatherhead, E. C. and S. B. Andersen (2006): The search for signs of recovery of the ozone layer. Nature **441**: 39 – 45, doi:doi: 10.1038/nature04746.

Weiss, A. I., J. C. King, T. A. Lachlan-Cope and R. S. Ladkin (2011): Albedo of the ice-covered Weddell and Bellingshausen Sea. The Cryosphere Discussions **5(6)**: 3259–3289, doi:10.5194/tcd-5-3259-2011, URL `http://www.the-cryosphere-discuss.net/5/3259/2011/`.

Wendler, G., C. Stearns, G. Weidner, G. Dargaud and T. Parish (1997): On the extraordinary katabatic winds of Adelie Land. Journal of Geophysical Research **102**: 4463–4474.

Wexler, H., M. J. Rubin, J. E. J. Caskey, R. L. Cameron and G. B. Bull (2013): The Thermal Diffusivity and Thermal Conductivity of Glacial Ice at Wilkes Station, Antarctica.

Wingham, D. J., A. Shepherd, A. Muir and G. Marshall (2006): Mass balance of the Antarctic ice sheet. Philosophical Transactions of the Royal Society A **364**: 1627–1635.

Yuan, X. (2004): ENSO-related impacts on Antarctic sea ice: a synthesis of phenomenon and mechanisms. Antarctic Science **16**: 415–425.

Eidesstattliche Erklärung

Ich erkläre, dass ich die beigefügte Dissertation selbstständig verfasst und keine anderen als die angegebenen Hilfsmittel genutzt habe. Alle wörtlich oder inhaltlich übernommenen Stellen habe ich als solche gekennzeichnet.
Ich versichere ausserdem, dass ich die beigefügte Dissertation nur in diesem und keinem anderen Promotionsverfahren eingereicht habe und, dass diesem Promotionsverfahren keine endgültig gescheiterten Promotionsverfahren vorausgegangen sind.

Acknowledgements